



EUROPEAN
COMMISSION

Community research

RECOSY

(Contract Number: FP7-212287)

DELIVERABLE (D-N°:7.6) Proceedings of the third annual workshop

Author(s): **AMPHOS**

Reporting period: e.g. 01/04/2010 – 30/03/2011

Date of issue of this report: 03/09/2011

Start date of project: 01/04/2008

Duration: 48 Months

Project co-funded by the European Commission under the Seventh Euratom Framework Programme for Nuclear Research & Training Activities (2007-2011)		
Dissemination Level		
PU	Public	X
RE	Restricted to a group specified by the partners of the RECOSY project	
CO	Confidential, only for partners of the RECOSY project	

1.





KIT SCIENTIFIC REPORTS 7603

3rd Annual Workshop Proceedings of the Collaborative Project “Redox Phenomena Controlling Systems” (7th EC FP CP RECOSY)

Marcus Altmaier, Bernhard Kienzler, Lara Duro,
Mireia Grivé, Vanessa Montoya (eds.)

Marcus Altmaier, Bernhard Kienzler, Lara Duro,
Mireia Grivé, Vanessa Montoya (eds.)

**3rd Annual Workshop Proceedings of the Collaborative Project
"Redox Phenomena Controlling Systems" (7th EC FP CP RECOSY)**

Karlsruhe Institute of Technology
KIT SCIENTIFIC REPORTS 7603

3rd Annual Workshop Proceedings of the Collaborative Project "Redox Phenomena Controlling Systems" (7th EC FP CP RECOSY)

Marcus Altmaier
Bernhard Kienzler
Lara Duro
Mireia Grivé
Vanessa Montoya
(eds.)

Report-Nr. KIT-SR 7603

The report is printed without colours. The report with the original colours in different photos, tables, figures and logos, can be downloaded from the KIT Scientific Publishing homepage.

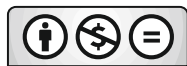
Karlsruher Institut für Technologie (KIT)
Institut für Nukleare Entsorgung

Amphos XXI Consulting S.L.
Passeig de Garcia i Faria, 49-51, 1^o-1^a
E08019 Barcelona
SPAIN

Impressum

Karlsruher Institut für Technologie (KIT)
KIT Scientific Publishing
Straße am Forum 2
D-76131 Karlsruhe
www.ksp.kit.edu

KIT – Universität des Landes Baden-Württemberg und nationales
Forschungszentrum in der Helmholtz-Gemeinschaft



Diese Veröffentlichung ist im Internet unter folgender Creative Commons-Lizenz publiziert: <http://creativecommons.org/licenses/by-nc-nd/3.0/de/>

KIT Scientific Publishing 2011
Print on Demand

ISSN 1869-9669
ISBN 978-3-86644-756-1

FOREWORD

The present document is the proceedings of the 3rd Annual Workshop of the EURATOM FP7 Collaborative Project ReCosy (Redox Phenomena Controlling System). The electronic version of this proceedings are also available in the webpage of the project (www.recosy.eu). The Workshop was hosted by SUBATECH and held in Balaruc-les-Bains (Sète - Languedoc - Roussillon, France) 21st – 24th March 2011. The project started April 2008 and has four years duration. It has 32 Contractors and presently 6 Associated Groups. Annual workshops bring together, Beneficiaries/Contractors, Associated Groups and external interested groups. The present proceedings will be followed by one additional proceedings corresponding to the Final Workshop (4th Annual Workshop) to be held in 2012. The 4th Annual Workshop will be held in Karlsruhe, Germany 23rd – 26th January 2012, organized by KIT.

The proceedings serve several purposes. The key purpose is to document and make available to a broad scientific community the outcome of the RECOSY project. For this purpose, a considerable part of the project activity reporting is done through the proceedings, together with the outcome of a large number of scientific-technical contributions and Topical Sessions on different topics, which could be important for the development of the project. In the 3rd Annual Workshop this topic focused on electrochemistry and redox processes. Additional purposes of the proceedings are to ensure ongoing documentation of the project outcome, promote systematic scientific-technical development throughout the project, and to allow thorough review of the project progress.

All Scientific and Technical papers submitted for the proceedings have been reviewed by the EUCG (End-User-Consultancy-Group). The EUCG is a group specifically set up within the project in order to represent the interests of the end users to the project and its desired outcome. To this aim, the composition of the EUCG includes organizations representing national waste management or national regulatory interests and competence.

The proceedings give only very brief information about the project structure and the different activities around the project, such as training measures and dissemination of knowledge. Such information about the project can be found in detail under www.recosy.eu.

Finally, we want to thank all those who submitted Scientific and Technical contributions for review and, especially, the Workpackage leaders who provided the summary of the different workpackages for publication in these proceedings. We also want to give a special thanks to the reviewers, whose effort and hard work reflect their commitment and dedication to the project.

TABLE OF CONTENTS

THE PROJECT	1
THE THIRD ANNUAL WORKSHOP	1
Objectives	2
RTD sessions	2
Poster presentations	5
Topical session	6
Structure of the proceedings	7
SUMMARY OF WP ACTIVITIES	9
WORKPACKAGE 2:	11
Introduction	11
Work performed by partners	11
References	26
WORK PACKAGE 3:	27
Introduction	27
Work performed by partners	27
WORK PACKAGE 4:	35
Introduction	35
WP 4.1.	36
WP 4.2.	51
WORK PACKAGE 5:	57
Introduction	57
Work performed by partners	57
WORKPACKAGE 6:	61
Introduction	61
Work performed by partners	62
References	76
S + T CONTRIBUTIONS	79
List of contributions	81
POSTER ABSTRACTS	273
List of poster abstracts	275

THE PROJECT

The EURATOM 7th EC Framework Program Collaborative Project REDox phenomena Controlling SYstems (RECOsY) started in April 2008 and extends over 4 years. Although redox is not a new geochemical issue, different questions are still not resolved. For this reason, main objectives of RECOsY project are a) the sound understanding of redox phenomena controlling the long-term release/retention of radionuclides in nuclear waste disposal, b) providing tools to apply the result to Performance Assessment/Safety Case, c) training of next generation and d) documentation and communication of the results. To this aim, the project set up a consortium of 32 Beneficiaries/Contractors and presently 6 Associated Groups. The consortium includes key European Research Institutes, Universities, National Waste Management Agencies and SMEs, from 13 EURATOM signatory states, Russia, Japan, Korea, USA and one European Joint Research Centre. The ReCosy concept is innovative in the scientific approach to the redox phenomena. It includes i) advanced analytical tools, ii) investigations of processes responsible for redox control (thermodynamically and kinetically controlled processes, surface reactions and microbial processes,...), iii) provision of required data on redox controlling processes, and iv) response to disturbances in disposal systems. The work program is structured along six RTD workpackages (WP1-6). They cover near-field and far field aspects as well as all relevant host-rocks considered in Europe. In WP1, the scientific state-of-the-art and its application to Performance Assessment/Safety Case is documented and regularly up-dated. WP2 focuses on development of redox determination methods. WP3 focuses on redox response of defined and near-natural systems. WP4 studies the redox reactions of radionuclides. WP5 focuses on Redox processes in radionuclide transport and WP6 deals with redox reactions affecting the spent fuel source-term. Specific workpackages on knowledge management, education and training (WP7) and administrative management issues (WP8) are also included in the project

The present proceedings document the outcome of the 3rd Annual Project Workshop and give an overview of the outcome of the 3rd project year.

THE THIRD ANNUAL WORKSHOP

The 3rd Annual Project Workshop was held in Balaruc-les-Bains (Sète - Languedoc - Roussillon, France) 21st – 24th March 2011. The Workshop was hosted by SUBATECH. There were 65 attendees at the workshop, representing Beneficiaries/Contractors, Associated Groups, the End-User Consultancy Group, and project external organizations. The workshop was organized in four days of oral presentations on results obtained within the project, two poster sessions, and a topical session on electrochemistry and redox processes.

Objectives

The Workshop combines different activities and meetings with the following objectives:

- Informing about the scientific progress. For this purpose, plenary sessions are used for communicating results from the different technical workpackages and poster sessions.
- Informing about the administrative status.
- Informing/agreeing upon forthcoming reporting.
- Discussing various topics of interest for the consortium.
- Agreeing upon the forthcoming work program.

Emphasis was on scientific-technical topics with administrative issues kept to the minimum necessary.

RTD sessions

Individual workpackage internal meetings were held in parallel during the 1st day of the annual workshop (21st March). The following days of the workshop included plenary sessions where the results from the different work packages were presented. Next to an overview of the achievements within the respective WP, scientific highlights were presented. The following presentations were given within the project.

WP2 session:

- M. Perdicakis. Some Practical Considerations on Potential Measurements.
- I. Ignatiadis, S. Betelu and Ch.Tournassat. Pyrite-electrode potential measurements in reference solutions versus measured and computed redox potential.
- V.G. Petrov, X. Gaona, D. Fellhauer, S.N. Kalmykov and M. Altmaier. Solubility and phase transformations of Np(V) hydroxide in NaCl solutions.
- T. Kobayashi, X. Gaona, D. Fellhauer and M. Altmaier. Redox Behavior of Tc(VII)/Tc(IV) Couple in various reducing systems.
- M. Kumke, D.Steinbrück and E. Schmäzlin. Recent developments of fiber-optical chemical sensing (FOCS).

- M. Altmaier, X. Gaona, D. Fellhauer and G. Buckau. Final Report on ReCosy ICE on redox determination methods.

WP3 session:

- K. Lázár, J. Megyeri, E. Bokori and Z. Máthé. Interaction of iron bearing minerals with dithionite in Boda Claystone samples.
- M. Perdicakis, Y. Xu, K. Lázár, Z. Máthé and L. Rouillard. Voltammetric characterization of Boda Albitic Claystone: Comparison with Mössbauer spectroscopy data.
- M. Perdicakis, L. Rouillard, C. Bouchereau and C. Malhomme. Reactivity of Callovo-Oxfordian Argillite with Soluble Iodine and Selenium Species. An Electrochemical Approach.
- F. Bardelli, M. Kang and L. Charlet. Redox reaction of pyrite with Se: mechanisms deduced from wet chemistry and XAS
- C. Domènech, L. Duro, M. Grivé, D. Arcos, I. Rojo, F. Clarens and J. de Pablo. Quantification of pyrrhotite O₂ consumption by using pyrite oxidation kinetic data.
- K. Pedersen, J. Arlinger, L. Hallbeck, S. Lydmark, J. Johansson and A. Pääjärvi. The response in redox from additions of hydrogen and oxygen to natural deep groundwater/rock systems with active microorganisms.
- J. Hadi, L. Charlet, I. Ignatiadis and C. Tournassat. Modelling the CEC variation in dioctahedral smectites as a function of iron reduction level.

WP4 session

- E. Krawczyk-Bärsch, K. Pedersen, A. Lehtinen and T. Arnold. Uranium immobilization in biofilms from a granitic nuclear waste repository research tunnel - A microscopic and spectroscopic study.
- X. Gaona, J. Tits, D. Fellhauer, K. Dardenne, E. Wieland and M. Altmaier. Redox chemistry of Np(V/VI) in alkaline conditions: aqueous speciation and solubility.
- J. Tits, X. Gaona and E. Wieland. Influence of oxidation state on neptunium uptake by calcium silicate hydrates.

WP5 session

- B. Frasca, S. Savoye, C. Wittebroodt, O. Leupin and J. L. Michelot, Speciation dependent transport properties of selenium in indurated clay rocks: the Opalinus clay (Mont Terri, Switzerland) and the Toarcian argillite.
- S. Savoye, B. Grenut, P. Meier and Th. Vercouter. Study of the diffusive behaviour of I(-I), U(VI), Se (IV) and Se (VI) through clayey hard-rocks under N₂/CO₂ conditions: Application to the Callovo-Oxfordian claystones.
- K. Lázár, J. Megyeri, Zs. Mácsik, E. Széles and Z. Mathe. Migration of uranyl ions in Boda Claystone samples.
- N. Banik, F. Huber, A. Smyrek, P. Kunze, J. Rothe, T. Schäfer, D. Schild and Ch. Marquardt. Status of the work on actinide and Tc interaction with fracture filling material, clay and magnetite nanoparticles.
- J. Suksi, A. Lehtinen and P. Pitkänen. Fracture surface U as an indicator of recent redox-front.
- O. N. Batuk S. D. Conradson, V.G. Petrov and S. N. Kalmykov. Actinide speciation and local distribution in colloids collected in organic-rich pond.

WP6 session

- P. Carbol, P. Fors, S. Van Winckel and K. Spahiu. Corrosion of spent fuel in presence of H₂.
- D.H. Wegen and A. Seibert. Studies on spent fuel in presence of corroding Fe and on thin film model systems.
- R. Pehrman, M. Trummer, C. Lousada and M. Jonsson. Redox reactivity of doped UO₂ - Effects on the reactivity towards H₂O₂.
- A. Loida, V. Metz, E. Bohnert, B. Kienzler, N. Müller, D. Schild and E. Soballa. Trapping of radionuclides/actinides onto canister (Fe) corrosion products.
- D. Cui and J. Low. Spent fuel leaching at simulated early canister failure conditions, effect of H₂ and Fe(II).
- D. Dobrev, R. Cervinka and A. Vokál. Redox Potential in Near Field of Deep Geological Repository with Carbon Steel Waste Packages.

Poster presentations

The following posters were presented during the 3rd Annual Workshop:

- M. Altmaier. ABC-Salt workshop.
- M. Altmaier. HiTAC workshop.
- N. L. Banik, C. M. Marquardt, J. Rothe, D. Schild and T. Schäfer. Sorption and redox behavior of radionuclides in natural clay rocks.
- D. Cui, P. Carbol and K. Spahiu. On the redox chemistry at the near field of repository, the influences of iron canister material and hydrogen.
- R. Druteikiene, B. Luksiene, D. Peciulyte, K. Mazeika, A. Gudelis and D. Baltrunas. Behaviour of Tc(VII) in aqueous solutions in the presence of iron oxides and microorganisms.
- N. Evans, R. Hallam, S. Jain, M. Felipe-Sotelo and N. Bryan. Effect of EDTA, ISA and Picolinic Acid on Redox Chemistry of Tc.
- X. Gaona, R. Dähn, J. Tits, C. Scheinost and E. Wieland. Uptake of Np(IV) by C-S-H phases and cement. An EXAFS study.
- M. Grivé, V. Montoya, O. Riba, L. Duro. Redox potential measurements on unirradiated UO₂(s) dissolution experiments under alkaline conditions in the presence of dithionite.
- S. Holgersson. Agreement between measured Eh and quantification of actinide oxidation states -Progress Report.
- F. Huber, P. Kunze and T. Schäfer. Tc(VII), U(VI) and Np(V) sorption/reduction kinetics under glacial melt water conditions: Comparison between batch and column migration experiments.
- R. Kay, L. Abrahamsen, N.D. Bryan, A. Stockdale. Actinide Partition in Humic Colloidal Ternary Systems.
- K. Lázár, J. Megyeri, E. Bokori and Z. Máthé. Interaction of iron bearing minerals with dithionite in Boda Claystone samples.
- K. Lázár, J. Megyeri, Zs. Mácsik, E. Széles, Z. Máthé. Migration of uranyl ions in Boda Claystone samples.
- A. Loida, V. Metz, E. Bohnert, B. Kienzler, N. Müller, D. Schild, E. Soballa. Trapping of radionuclides/ actinides onto canister corrosion products.

- J.F. Lucchini, D. Reed, M. Richmann, J. Swanson, D. Ams, H. Khaing and M. Borkowski. Actinide redox chemistry in high salinity media: a LANL/ACRSP overview.
- J. Y. Oh and J. I. Yun. Investigation of redox behaviors of iron in aqueous solutions by combination of chemical speciation and Eh measurements.
- M. Perdicakis, C. Malhomme and C. Bouchereau. An Electrochemical Approach to Study the Reactivity of Pyrite with Soluble Iodine and Selenium Specie.
- M. Perdicakis, Y. Xu, K. Lázár and Z. Máthé. Voltammetric characterization of Boda Albitic Claystone: Comparison with Mössbauer spectroscopy data.
- T. Petersmann, T. Gouder, A. Seibert, Th. Fanghänel. Electrochemical investigations on doped and undoped UO₂ spent fuel model surfaces.
- O. Riba and M. Grivé. Redox measurements of iron systems from the intercomparison exercise.
- I. Rojo, F. Clarens, J. de Pablo. Oxygen scavenger capacity.
- C. Sabater, C. Walther, G. Geipel, M. Grivé, L. Duro. Complexation study of U(VI) with phenol by TRLFS.
- T. Schrage, B. P. Bischofer and S. Hagemann. Formation of Fe(III)-hydroxo complexes in brines.
- D. Soltermann, D. Marques Fernandes, B. Baeyens, R. Dähn, M. H. Bradbury. The interaction of Fe(II) with clay minerals.
- D. Steinbrück, E. Schmälzlin and M.U. Kumke. Progress in the development of a fibre optical chemical sensor (FOCS) for the simultaneous determination of proton oxygen and chloride concentrations.

Topical session

The Topical Sessions aim at covering the key areas of redox determination methods along with the project. The Topical Session focuses on Electrochemistry and Redox Processes

Presentations within this topic were:

- N. Smart. UK radioactive waste management, Importance of sound science underpinning safety assessments.
- D. Reed. Redox Chemistry of multivalent metals and actinides in the WIPP.

- A. Seibert. The use of the electrochemical quartz crystal microbalance in corrosion investigations of spent nuclear fuel models.
- E. Silvestre. Ferrocene-mediated electron transfer between Fe(II) adsorbed onto hydrous ferric oxide (HFO) and a solid electrode.
- M. Sander. Electrochemical characterization of the redox properties of natural organic matter and iron bearing clay minerals.

Structure of the proceedings

The proceedings are divided into the following sections:

- WP activity overviews, with summaries of the Research, Technology and Development Components
- Individual Scientific and Technical Contributions, containing reviewed scientific and technical manuscripts
- Abstracts of the posters presented during the Workshop

All the Scientific-technical contributions submitted were reviewed by the EUCG members (End-User Consultancy Group).

SUMMARY OF WP ACTIVITIES

WORKPACKAGE 2: DEVELOPMENT OF REDOX DETERMINATION METHODS

M.U. Kumke

Institute of Chemistry, University of Potsdam, Karl-Liebknechtstr. 24-25, 14476
Potsdam, Germany

Introduction

The objective of WP2 is the development and testing of redox determination methods using different type of electrodes as well as optodes (optical sensors) in order to provide a broad and solid scientific-technical basis for the application of such. In combination with chemical analysis and associated thermodynamic modeling the redox state of systems (relevant for nuclear waste repositories) is assessed. The overall goals are (i) redox determination methods specifically designed for environmental applications, and (ii) a broader information base for interpretation of system conditions. The first point reflects the limitations of existing determination methods and models (and new developments) due to poisoning of electrode material, diffusion potentials in electrode bridges, drift through catalytic reactions on electrode material, drift through changes in electrolytes via diffusion, analytical difficulties in determining concentrations of redox sensitive system components or state of involved solids/minerals, and insufficient/inadequate thermodynamic data for calculation of the redox state.

In the following paragraphs a summary of the work performed during the third project year is given by each partner. Note, that originally the duration of WP2 was set to month 24 and was extended to month 42 to give some of the partners the opportunity to continue work.

Work performed by partners

The work performed by **KIT-INE** during the third project year within WP2 was focussed on the redox behaviour and thermodynamic description of Technetium and Neptunium in dilute to concentrated aqueous systems. Within activity (A), the redox behaviour of Tc(VII), e.g. redox transformations to Tc(IV) in 0.1 M NaCl, was investigated in homogenous solutions and heterogeneous suspensions and analysed in terms of pH/ E_h dependencies. The studies on Np chemistry (B) were centred on solubility studies with pentavalent Np(V) in NaCl solutions performed in cooperation with **MSU** (V. Petrov and S. Kalmykov), and (C) investigations in TMA-OH media to

constrain the stability field of hexavalent Np(VI) under strongly alkaline conditions performed in cooperation with **PSI** (J. Tits and E. Wieland).

Activity (A)

The behavior of Tc in the environment critically depends on its oxidation state. In the +VII oxidation state, Tc forms highly soluble solids and exists as an anionic TcO_4^- ion in aqueous systems. On the other hand, in +IV oxidation state, Tc is easily hydrolyzed to form sparingly soluble hydroxide solids and aqueous hydrolysis species, and considered to be relatively immobile. It is, therefore, needed to clarify the Tc(VII)/Tc(IV) redox processes and to predict the redox state distribution and respective stability fields as function of basic geochemical parameters (E_h , pH, ionic strength) under the reducing redox conditions relevant for deep geological repositories. In WP2, the redox behavior of the Tc(VII)/Tc(IV) couple in 0.1 M NaCl/NaOH solutions is investigated by **KIT-INE** in various homogeneous and heterogeneous reducing systems. The systematization of Tc redox processes in both homogenous and heterogenous systems within the established E_h /pH concept offers a robust approach and allows conclusions on main reaction mechanisms.

Aliquots of TcO_4^- stock solution was added to the sample solutions which were pre-equilibrated with different reducing agents at certain pHs in 0.1 M NaCl/NaOH solutions. The reductants used in this study were sodium anthraquinone / anthrahydroquinone disulfonate redox buffer solutions (AQDS / AH_2QDS), hydroquinone solutions, Fe(II) / Fe(III) solutions and precipitates, $\text{Na}_2\text{S}_2\text{O}_4$ solutions, Fe powder suspensions, 2-hydroxy-1,4-naphthoquinone (Lawson) redox buffer solutions, and the Sn(II) system. The initial TcO_4^- concentration after spiking the pre-equilibrated samples was set to 10^{-5} M. After given periods, pH and E_h values were measured and Tc concentrations determined in solution after 10kD (2 nm) ultrafiltration using Liquid Scintillation Counting (LSC). The detection limit was approximately 10^{-8} M. The concentrations of Tc(VII) and reduced Tc(IV) species were determined using solvent extraction technique (tetraphosphorylchloride (TPPC) extraction of TcO_4^- into chloroform).

The Tc concentrations in the aqueous phases decreased in $\text{Na}_2\text{S}_2\text{O}_4$, Sn(II), Lawson, Fe powder (neutral pH range), and AQDS / AH_2QDS (acidic pH range) systems, indicating the reduction of Tc(VII) and the formation of the expected sparingly soluble Tc(IV) solid phases. In contrast, the initial Tc concentrations did not change in the systems of AQDS/ AH_2QDS (alkaline pH), hydroquinone, Fe(II)/Fe(III) (acidic pH) and Fe powder (alkaline pH). The reaction kinetics do not show any pronounced differences related to homogenous or heterogenous system characteristics and rather suggest a dependence on overall E_h /pH conditions. The results are summarized quantitatively in the E_h -pH diagram (Figure. 1). Samples in which no Tc(VII) reduction was observed are plotted as filled symbols, samples in which Tc(VII) was reduced are plotted as open symbols. The dashed line represents the experimental borderline for the reduction, which was found to be independent of the reducing chemicals or the presence of iron solid phases. This systematic trend of the Tc(VII)/(IV) redox behaviors depending on the E_h /pH conditions agrees well with the predictions from thermodynamic calculations (Rard et al. 1999) considering a known effect of solid

phase particle size on the solubility and redox equilibria. Well defined stability fields for dominant Tc(VII) and Tc(IV) redox states can be established for the given experimental parameters indicating E_h and pH conditions.

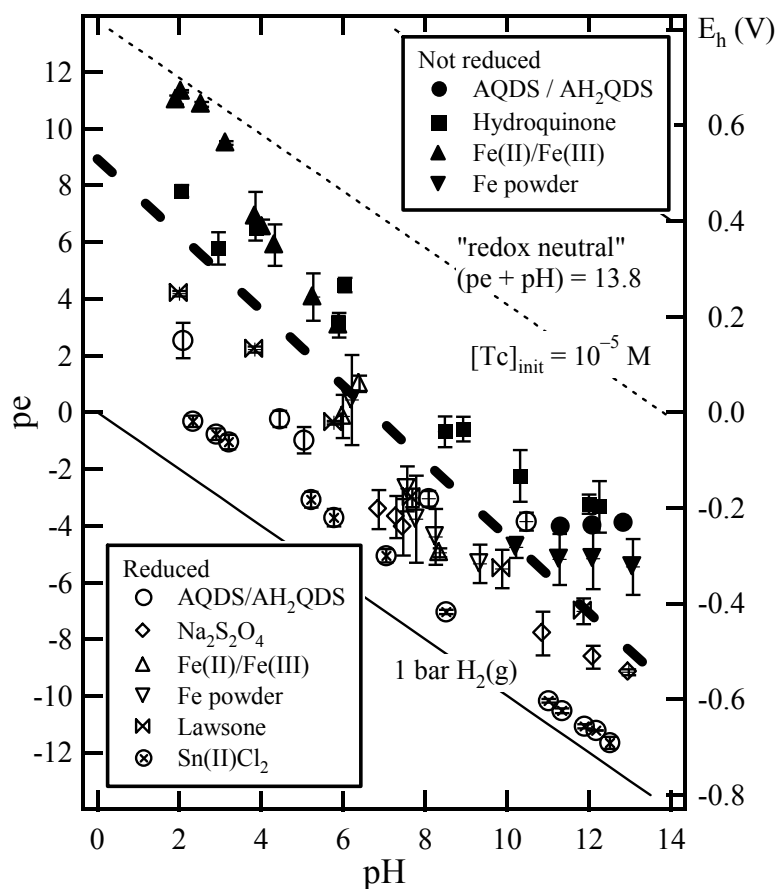


Figure 1: Reduction of Tc(VII) in 0.1 M NaCl/NaOH solutions. Open symbols indicate Tc(VII)/(IV) reduction, filled symbols indicate no Tc(VII) reduction within up to 1.5 months. The dashed line represents the experimental borderline for Tc(VII)/Tc(IV) reduction.

Activity (B)

The solubility of Np(V) was investigated in dilute to concentrated NaCl-NaOH solutions ($0.1 \text{ M} \leq I \leq 5 \text{ M}$, $10 \leq \text{pH}_c \leq 14$) with special focus on the characterization of neptunium solubility-limiting solid phases in equilibrium with supernatant solutions. Composition, stoichiometry and structure of these solid phases need to be understood as a basis for improved thermodynamic descriptions. Complementary studies in NaClO_4 were conducted to assess the effect of the background electrolyte, whilst allowing the direct comparison with previous published data (Neck et al. 1992).

Np(V) solubility data obtained in NaClO_4 solutions are consistent with previous studies (Neck et al. 1992). A very significant decrease in the solubility is observed between experimental series at 1 and 3 M NaClO_4 . This observation was previously explained as an aging effect of the forming $\text{NpO}_2\text{OH}(\text{am})$. Further characterization of

the solid phases is on-going. In NaCl, only solubility data at low ionic strength (0.1 M NaCl) were consistent with the NaClO₄ system. Under increasing ionic strength conditions, significant changes in Np solubility were observed: a pronounced drop in the solubility was observed in the pH_c region 11.5 – 12.0, which coincided with a change of solid phase colour from green to white indicating a solid phase transformation. Further increase of pH_c to strongly alkaline conditions resulted in increased neptunium solubility and another change of solid phase colour from white to light violet. XRD, XANES, chemical analysis and SEM-EDS of the solid phases show that with increasing pH_c and NaCl concentration, Np(V) hydroxide undergoes significant phase transformation to Na-Np(V) phases, which are currently not considered in thermodynamic models. Additional experiments are ongoing in order to establish more detailed solubility curves and assess the possible effect of long term kinetics on the solid phases. Based upon our systematic and comprehensive experimental approach focusing both on the aqueous phase and the solubility limiting solids, the **INE-MSU** collaboration is aiming to contribute towards a better understanding and thermodynamic description of Np(V) solubility behaviour in NaCl media.

Activity (C)

The redox chemistry of Np(V/VI) under hyperalkaline conditions was investigated in TMA-OH solutions. Despite the use of TMA-OH, the high total Np concentration ($[\text{Np}]_{\text{tot}} \sim 2 \cdot 10^{-3} \text{ M}$) gave rise to the precipitation of solid Np phases in some of the samples. The carbonate concentration (as impurity of TMA-OH) was $2\text{-}3 \cdot 10^{-3} \text{ M}$. Redox conditions were defined by the absence or presence of ClO⁻ as oxidizing agent and pH ranged between 9 and 13.5.

UV spectra obtained from the supernatant in TMA-OH solutions and in absence of ClO⁻ showed very clear Np(V) features, identified as NpO_2^+ , $\text{NpO}_2(\text{CO}_3)^-$ and $\text{NpO}_2(\text{OH})_2(\text{CO}_3)^{3-}$. XANES of these samples confirmed the predominance of Np(V). No UV features were observed within 800-1300 nm for samples with ClO⁻, even though Np(VI) is expected to occur. This different behaviour could be explained by the lower Np concentration in some of the samples, but is also indicative of the possible formation of centrosymmetric Np(VI) species (e.g. $\text{NpO}_2(\text{OH})_4^{2-}$) with lower absorption coefficients. XANES at the INE Beamline for Actinide Research at ANKA of this second set of samples confirmed the predominance of Np(VI), in accordance with reference spectra. A similar Np redox distribution was observed for the solid phases based on XANES and EXAFS measurements. EXAFS spectra indicative of $\text{Np}^{\text{V}}\text{O}_2\text{OH(s)}$ and $\text{Np}^{\text{VI}}\text{O}_3 \cdot x\text{H}_2\text{O(s)}$ were obtained for samples Np-1/Np-2 and Np-5/Np-9, respectively. The formation of a Na-Np(VI) solid phase in $5 \cdot 10^{-2} \text{ M}$ ClO⁻ and pH~12 (sample Np-8) was indicated from both EXAFS and chemical analysis.

These results confirm the relevance of Np(VI) in hyperalkaline systems even under mildly oxidizing conditions. Anionic species analogous to U(VI) are expected to form in the pH range 10-14. Indications of a Na-neptunate formation at $[\text{Na}] = 0.01 \text{ M}$ suggest the potential relevance of Na-Np(VI) (and Ca-Np(VI)) solid phases in cementitious and saline environments.

The aim of the work of **ARMINES** is to determine Se(-II) species at low level concentrations in order to use the speciation of Se(-II) as a probe for redox state determination in hyperalkaline solution. UV-visible spectrophotometry is the efficient technique for the characterisation of Se(-II) species but its sensitivity is too weak for determining concentrations lower than 10^{-4} M.

The *in fine* analytical approach is then to use a speciation technique (ion chromatography) *off line* coupled with a very sensitive analytical technique (ICP-MS).

A specific electrosynthesis of a selenide ions source (sodium selenide) was developed at the end of the previous period (2009-2010). The first characterization step by X-Ray Diffraction has shown that the synthesized product was $\text{Na}_2\text{Se} \cdot \text{H}_2\text{O}$. In the present period, this solid has been more precisely characterized by X-Ray Photoelectron Spectroscopy (XPS). Actually, the solid is kept in a glove box under inert atmosphere, the XPS technique allows then to check that those storage conditions are airtight enough to keep the solid unchanged during several months.

Selenium XPS analysis were performed a Kratos Axix Ultra XPS spectrometer at the Institut Matériaux de Nantes- Jean Rouxel (IMN, France) on a aged sodium selenide sample (*ie* : stored during 2 months in the glove box). The transfer of this sample from Subatech to IMN required the use of a specific “fully airtight transfer device” for maintaining an anoxic atmosphere. Moreover, a specific feed of ultrapur N_2 ($\text{O}_2 < 100$ ppb) was connected to the spectrometer in order to provide a residual atmosphere with the lowest O_2 level. The deconvolution of the XPS peaks shows contributions between 52 and 54.25 eV which can be assigned to Se(-II) species (3d5/2 and 3d3/2 transitions). This result proves that the storage conditions are airtight enough to keep Se(-II) samples protected against oxidation during monthly long period.

Solutions of sodium selenide ($6.2 \cdot 10^{-4}$ M) were prepared by dissolving the solid in sodium hydroxide solutions ranging from 0.5 to 8 M in order to investigate the whole range of stability of Se(-II) monomer species. UV-visible spectra were systematically acquired for all these solutions. Results show that the major specie is HSe^- ($\lambda_{\text{max}} = 245\text{nm}$) for NaOH concentrations lower than 1M and Se^{2-} ($\lambda_{\text{max}} = 274\text{nm}$) for concentrations higher than 2M. This result agrees well with literature data (Lich et al. 1995).

Speciation experiments were conducted on HSe^- solutions with a Dionex IC 2500 ion chromatograph. The redox potential of the solution is -0.655V/ESH. The separation protocol was optimized for *on line* detection of the following species (HSe^- , Se(IV) and Se(VI)) related to different redox states in order to get simultaneous informations on a potential reoxidation during the analysis. For that purpose, two different detectors (a UV-visible single wavelength detector and a conductimetric one) were coupled to an ion chromatograph for detecting HSe^- with UV-visible spectrometry at 245nm and oxidized species with conductimetry. The eluant solution (KOH = 20 mM) and all the separation apparatus were flushed continuously with ultrapur Helium for maintaining an anoxic environment during the analysis. The flow rate and temperature were set at 1mL/min and 30°C respectively.

Figure 2 shows the analysis of a HSe^- solution in NaOH 0.05 M. UV-visible detection shows only one peak at 12.6 min. which is assigned to HSe^- .

Because of the time shift related to the coupling of the two detectors, the peak at 12.3 min can then be assigned to this species in conductimetry detection.

The other peaks are assigned to Se(IV) and Se(VI) at 6.3 and 7.7 minutes respectively. The presence of those oxidized species show that, despite the precautions, some traces of O₂ were still trapped in the chromatographic system. However, this contamination remains at a low level since Se(IV) and Se(VI) concentrations were measured less than 5 and 0.2 % of the total Se concentration respectively. The additional peak at 7.0 min. is due to the presence of carbonate ions in the eluant.

As a conclusion for this period, we have succeeded in finalizing an analytical protocole aiming at measuring the reduced specie HSe⁻ at millimolar level. Setting strict anoxic experimental conditions allows to recover around 95% of Se as reduced species. In the next period, i) the efficiency of the separation at trace level will be performed by using a fraction collector and an *off line* ICP-MS analysis and ii) this protocole will be applied to other monomer (Se²⁻) or polymer species.

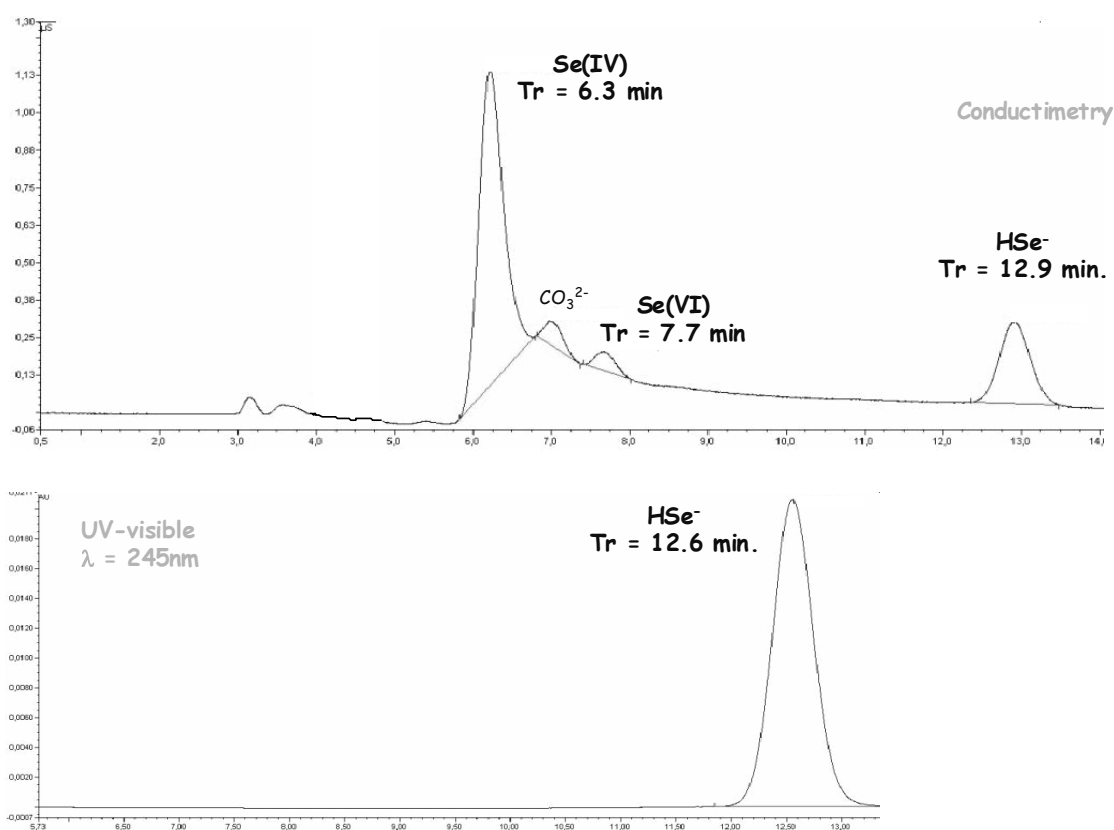


Figure 2: Chromatograms (upper: conductimetric detection; lower: UV-visible at 245nm detection) of a HSe⁻ solution in 0.05 M NaOH)

At **BRGM** one of the objectives was to carry out robust geochemical (Eh-pH) sensor concepts being able to be devoted (after adaptation or development and/or implementation) to the observation and monitoring of the underground components of a

nuclear waste storage. These sensors must answer precise specifications related to the requirements and constraints of observation and monitoring of the storage components (geological environment and associated phenomenology). In addition to the technical aspects, the major constraint seems to be the operation life, which will have to be based on the robustness and the perseverance of the principle of the sensors. Among the geochemical parameters to be followed, the most significant are temperature, pH, conductivity, redox potential, the speciation of certain elements, and measurement of H₂, O₂, CO₂ and H₂S. The inventory and the assessment of the currently available methodologies and tools for these parameters indicate that today there are not suitable geochemical sensors for monitoring nuclear waste storing systems. Based on this report, **BRGM** proposes some realistic pathways of research and development to be initiated to mitigate the lack of geochemical sensors dedicated to the underground storage of nuclear waste. For that purpose, R&D pathways will be the development and manufacture of geochemical sensors made of robust and unalterable material (gold, platinum, glassy carbon). They must possess active principles everlasting, or protected or restored easily.

Moreover, solid-state sensors fabricated with a few component of the argillaceous formations (raw Callovo-Oxfordian argillite (COx) or purified argillite K119, or pyrite) for measuring pH and redox potential can be designed for use. Response characteristics of these sensors must be tested in aqueous samples with compositions similar to those present inside an underground repository and results were compared with those obtained with commercial electrodes obtaining a good agreement between commercial and the sensors. Electrochemical methods will be in the base of the sensors assessments. These approaches will be consisted in the continuous or semi-continuous analysis of large surface electrodes (pyrite, argillite) immersed in solutions with or without oxidant (nitrate, selenate and selenite) or reducer (sulfide, Fe²⁺). The electrochemical behavior of these electrodes was compared to those of known inert and unattackable electrodes (Pt, Au, glassy carbon) positioned in the same operating conditions. Measurements realized by voltammetry (at open circuit potential and cyclic voltammetry), by Tafel polarization analysis and by electrochemical impedance spectroscopy (EIS) were used to identify, monitor and compare the electrochemical reactions and kinetics occurring during immersion, both in solution and on the surface of electrodes. The combination of chemical and electrochemical approaches appears to be an appropriate method to investigate the redox reactivity of COx components versus predicted redox perturbations.

Among other experiments, the Inter-laboratory Comparison Exercise (ICE) was an occasion to establish (together with the determination of the redox potential of reference solutions) also pyrite electrode potential measurement. **BRGM** demonstrated that measurement of free electrode potential of Pyrite and Platinum electrodes immersed in different media allow us to manufacture systems of solid and robust electrodes where the reference electrode is unnecessary. It will be also possible, provided that the potential difference between Pt and pyrite electrode is known, to deduce the pH of the solution.

The results of the Interlaboratory Comparison Exercise (ICE) confirmed, with absolute clarity, that the behaviour of pyrite is a function of the Fe(III)/Fe(II) ratio at the interface. These results are even more interesting because they lead to highlight the

double interest of pyrite electrode as both redox and pH indicator when integrated in the bunch of electrodes. In fact, in natural conditions, i.e. those of initial CO_x formation, pyrite can operate as redox electrode (its potential is similar to that of an Inert Electrode. An increase of its potential versus the potential of an Inert Electrode can be correlated to an alkaline environment: pyrite electrode can thus behave as a pH indicator. This can be applied in the case of CO_x formation during its envisaged evolution as nuclear waste repository.

Microsensor measurements were performed by **FZD** in the bacteriogenic iron oxides biofilms of the BIOS BRIC flow-cell, which is located in a cavity that has been excavated into the wall of the main access tunnel of the Äspö HRL at site 2200 A. As described in Anderson and Pedersen (2003) the groundwater for the BRIC was sourced from borehole KA2198A that intersects a water-conducting fracture behind the rock face. The predominant biomass in these biofilms is *Gallionella* stalk material (Hallbeck and Pedersen, 2005). Biofilm samples were removed from the BIOS BRIC flow-cell and exposed into a rectangular cell with an outer dimension of 121 x 42 x 15 mm. During the sensor measurements, 150 ml of the groundwater as a blank solution from the site was pumped through the cell in a closed circuit with a flow velocity of approximately 4 ml/min. For the sensor measurements a miniaturized platinum redox microelectrode, oxygen microsensor of the Clark-type and a miniaturized conventional pH electrode, each with a tip diameter of 10 µm, were used. After the values were recorded, uranium was added in ecologically relevant concentrations (4×10^{-5} M) to the groundwater solution. Microsensor measurements were recorded 20 hours after the addition of uranium. Samples of the groundwater solution were taken before and after the addition of uranium as well as at the end of the experiments. The samples were acidified in-situ and analyzed for determination of the inorganic elements by Inductively Coupled Plasma Spectrometry. The anions were determined by Ion Chromatography. The analytical data of the groundwater sample was used for the calculation of the predominance fields of different uranium species in the pH-Eh diagram for the U-S-O-H-C system at 15°C by using the geochemical speciation code “Geochemist’s Workbench” Version 8.0.8 / ACT2 Version 8.0.8.

Microsensor measurements of the oxygen concentration within the biofilms showed that the microbes of the biofilm battle the toxic effect of uranium. Before the addition of uranium the oxygen concentration is relatively high and amounts to 271 ± 4 µmol/L as an average value of several measurements. After the addition of uranium to the groundwater the concentration decreased to 250 ± 6 µmol/L after 20 hours. Although the oxygen concentration decreases in minor amounts, it indicates that the gradient of the oxygen concentration within the studied biofilms is slightly affected by the presence as well as by the concentration of uranium in the bulk solution. The addition of uranium (VI) in ecologically relevant concentrations (4×10^{-5} M) to the biofilms has induced a decrease of the oxygen concentration, which is a relatively slow. Only low oxygen consumption can be assumed due to the added uranium, which will have a low effect on the stimulation of the metabolism of *Gallionella* and, consequently, on the respiratory activity. Several microprofilings of the redox potential were performed in the biofilm sample, placed in the flow cell. Before the addition of uranium to the groundwater, with was pumped through the biofilm in a closed circle, the results

showed an average value of 704 ± 2 mV, including a correction factor of + 242 mV after Cammann and Galster (1997). After 20 hours after the addition of uranium the redox potential of the biofilm has decreased to a value of 520 ± 20 mV, indicating that the addition of uranium has strongly influenced the geochemical parameter of the biofilm.

For a better interpretation the analytical data of the bulk water was used for the calculation of the predominance fields of different uranium species in the pH-Eh diagram for the U-S-O-H-C system at 15°C by using the geochemical speciation code “Geochemist’s Workbench” Version 8.0.8 / ACT2 Version 8.0.8. By means of the equilibrium speciation model the speciation of the uranium metal can be determined and changes in the concentration of the various species with changing conditions of redox potential, pH, temperature, ionic strength, and solid mineral phases can be related to changes in the behavior of the microbe. The default database used was the thermo.dat accompanying code, supplemented by the most recent NEA database for uranium (Guillaumont et al., 2003), and by solubility data for Bayleyite from Gourman-Lewis et al. (2008). The theoretical predominance fields of solid uranium species under the ambient condition found in the contaminated groundwater are defined clearly in two geochemically different areas: The first area is characterized by a redox potential of approximately < 1 V and a pH > 4 . This area is dominated by the magnesia bearing uranyl carbonate mineral Bayleyite $[\text{Mg}_2(\text{UO}_2)(\text{CO}_3)_3 \cdot 18\text{H}_2\text{O}]$. The second area is characterized by a redox potential of approximately < 320 mV and a pH which varies between 0 and 5.8. Assuming reducing conditions, the formation of Uraninite, a uranium(IV) oxide (UO_2) mineral, was predicted. The results of the redox potential measurements of the biofilm before the addition and after 20 hours were plotted together with the pH into the calculated pH-Eh diagram for the U-S-O-H-C system. The plots appear in the area of Bayleyite, indicating that an uranium(VI) solid mineral may have been formed in the contaminated groundwater as well as in the biofilm after thermodynamically calculations. The analysis of the groundwater, which was exposed to uranium, showed significant differences between the uranium concentration at the beginning and at the end of the experiments. The initial concentration of 4×10^{-5} M has decreased during 20 hours to 1×10^{-5} M. Consequently, a substantial retention of uranium from the groundwater of approximately 70 % can be considered by the microbial community. Both, analytical data and thermodynamically calculations reveal, that during the experiments the solid U(VI) mineral Bayleyite could have been formed.

In the last project year **GRS** started to develop a thermodynamical model for iron, which includes different Fe(III) species, Fe(III)-chloro and Fe(III)-hydroxo complexes, explicitly. Therefore UV-spectra of Fe(III) in NaCl, MgCl_2 , and CaCl_2 brines were measured at different pH values. Fe(III)-chloro complexes were investigated at pH=1 and various HCl, NaCl, MgCl_2 , and CaCl_2 concentrations from 0 – 16 mol/l chloride. pH titrations were conducted for detecting Fe(III)-hydroxo complexes. These investigations were carried out in simple $\text{Fe}(\text{ClO}_4)_3$ solutions without disturbing chloride and also with NaCl and MgCl_2 concentrations constant near saturation.

First of all based on these spectra single species spectra were identified (see Figure 3). A model-free evolving factor analysis of the chloride titration at pH=1 showed that there are three Fe(III)-chloro complexes. Most probably these are $[\text{FeCl}]^{2+}$,

$[\text{FeCl}_2]^+$, and $[\text{FeCl}_4]^-$. The neutral complex $[\text{FeCl}_3]$ most likely does not exist. In NaCl solutions up to 5 mol/kg Fe^{3+} , $[\text{FeCl}]^{2+}$, and $[\text{FeCl}_2]^+$ are detected. The $[\text{FeCl}_4]^-$ occurs only in concentrated MgCl_2 or CaCl_2 solutions containing approximately more than 6 mol/kg chloride.

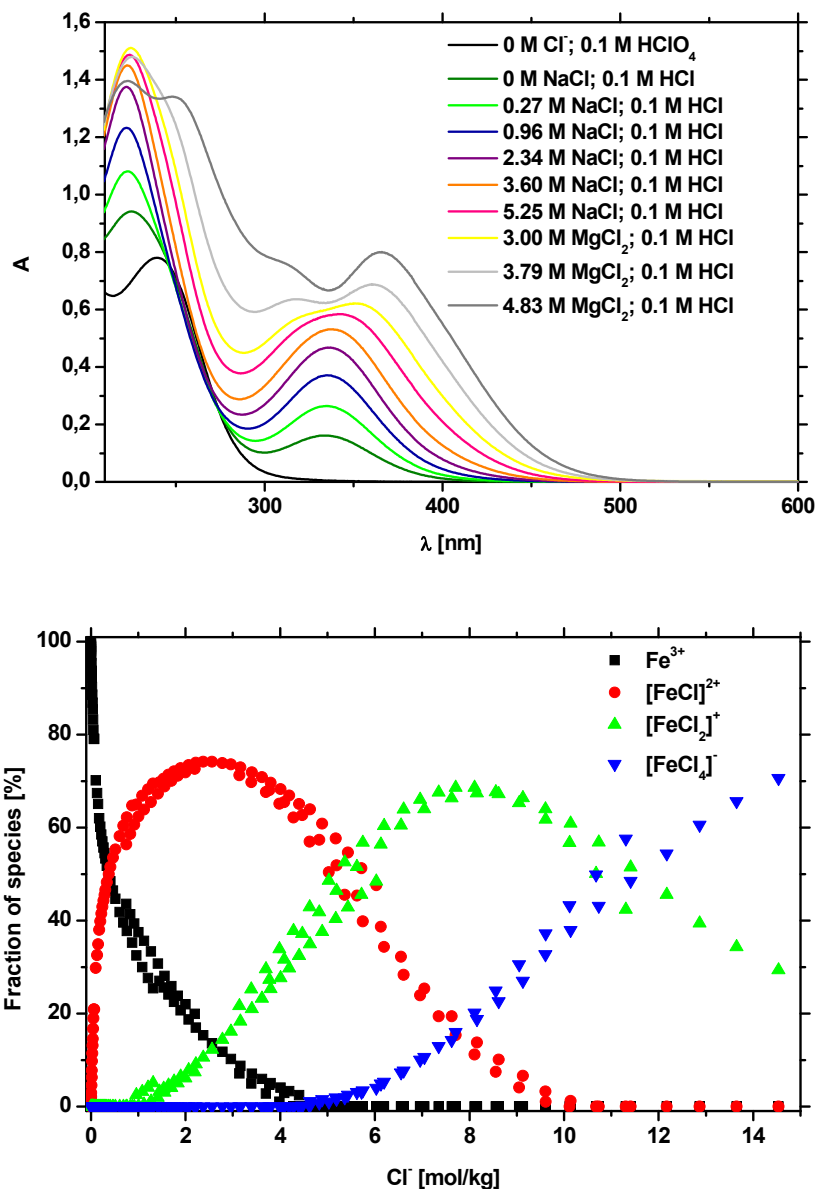


Figure 3. UV-spectra of solutions containing $2 \cdot 10^{-4}$ mol/l Fe(III) and various chloride concentrations at $\text{pC}_\text{H} = 1$ (top) and development of the Fe(III) species distribution in chloride solutions (bottom).

The single spectra of $[\text{FeOH}]^{2+}$ was identified with pH-titrations in $\text{Fe}(\text{ClO}_4)_3$ solutions between pH 1 and 4 (adjusted with HClO_4). In titrations at the same pC_H (the negative logarithm of the hydrogen ion concentration) range the hydroxo complex in solutions with 5 mol/kg NaCl was only visible from $\text{pC}_\text{H} = 3.1$. The deconvolution of these spectra by linear regression showed that it is possible to reconstruct them from the

single species spectrum of $[\text{FeOH}]^{2+}$ and a mixed spectrum of chloro complexes. That leads to the conclusion that in 5 mol/kg NaCl solutions no mixed Fe(III)-chlorohydroxo complexes exist. Hypothetical equilibria for mixed complexes at a given chloride concentration, independent from pH, would be $[\text{FeOH}]^{2+} + \text{Cl}^- = [\text{FeCl}(\text{OH})]$ or $[\text{FeOH}]^{2+} + 2\text{Cl}^- = [\text{FeCl}_2\text{OH}]$. If there is no evidence for these complexes in a solution with 5 mol/kg and a pH of 3.9, then most probably both complexes are not significant at other pH . No hydroxo complexes were detectable in 4.5 mol/kg MgCl_2 solutions up to pH 4 (see Figure 3)

The Outcome of the last project year for TUG can be divided in two different tasks.

Application of the CE-ICP-MS method to the ICE-samples

During the ICE the CE was not working at the INE-lab. Therefore the samples were stored under inert conditions and were measured in the last project year.

Figure 4 shows the calibration of iodide and iodate. Free iodine samples for calibration could not be prepared under similar conditions in the electrolyte system. Only standards in organic solvents can be prepared but the sensitivity of the ICP-MS signal is different and cannot be transferred to aqueous electrolyte systems.

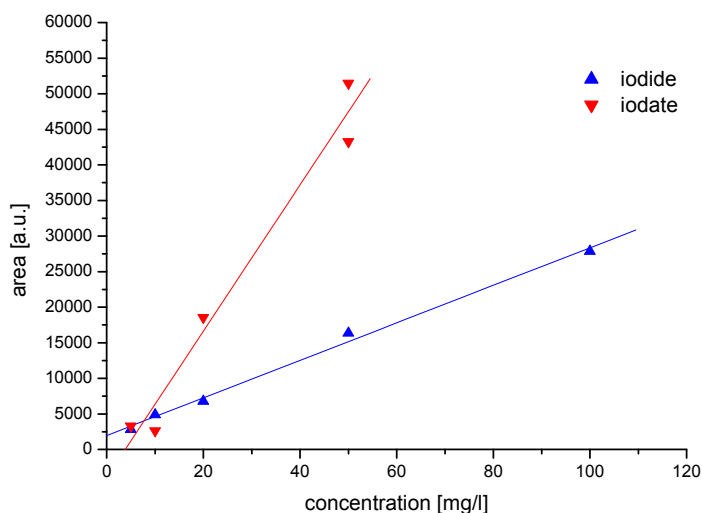


Figure 4. Calibration of iodine and iodate by CE-ICP-MS

All samples from the ICE were measured, but solely the sample Ref 3a ISe contains enough iodine to determine the content of the species (see Figure 5). From the content of 10^{-4} M iodide and iodate (12.7 mg/L) we could detect 28.3 % as iodate and a not quantifiable amount of free iodine. Iodide could not be determined.

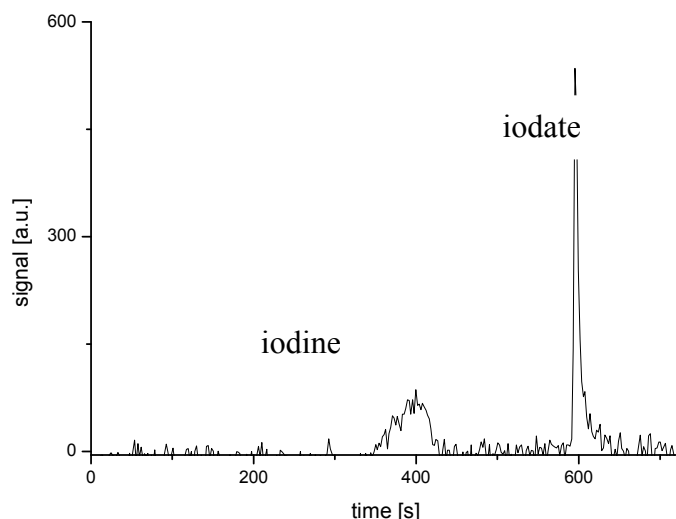


Figure 5: Electropherogram of the sample Ref 3a ISe.

Development of the IC speciation method

Ion chromatography can be used as alternative separation technique for the determination of distribution of iodine species.

In this part of project work semi-natural samples were examined. Modelling the ionic strength with NaClO_4 pH values of solutions were adjusted between 2-10. Two sets of samples were prepared. Solutions with only iodine species were compared with binary iodine species-kaolinite systems. The effect of the presence of kaolinite on the equilibrium between the iodine species was investigated over a period of 3 months.

During that time the species were stable in presence of kaolinite as well as without it. After 3 months for both species a loss of appr. 10% was measured in the samples without kaolinite. This suggests sorption on the glass, or the formation of free iodine. Losses in the binary systems were not significantly higher. Therefore, in addition to our earlier investigations, it can be assumed that the no significant sorption can be observed in the binary iodine species-kaolinite systems that could be assigned to kaolinite.

The electronic and optic components of the experimental set-up were further miniaturized by **UPPC** to improve handling in field applications. In order to increase the applicability of the set up for multiparameter sensing, the accessible modulation frequency range was increased as well. This increases the number of potential fluorescence probes to be used within the optodes.

Different chromophores can now be used in the oxygen sensor in order to address different concentration ranges with a high precision. In detailed experiments the influence of the layer thickness was characterized. The slope of the calibrations curves, as central parameter, was independent on the layer thickness and subsequently also the limit of detection (LOD). With the Pd-based probe the determined LOD for oxygen in

aqueous solution is 1 ppb and around 7 ppb for the Pt-based sensor type. For both optode types outstanding accuracies in the data acquisition were achieved. A major factor for the excellent sensitivity, accuracy and reproducibility is the fact, that the measurements were performed at two different frequencies, which significantly reduced any contribution from background luminescence and scattered light.

The fundamental aspects of pH sensing based on luminescence decay time measurements were further evaluated by testing different pH-sensitive probes and by optimizing the polymer matrix to improve the proton-selectivity and reduce cross-sensitivity for other cations. The experiments were focused on different fluorescein derivatives as probes and their potential for luminescence decay time based pH-sensing was evaluated in batch as well as fiber-based experiments. In the later case the probes were immobilized in a novel polymer, which shows very high proton permeability. For calibration purposes a series of citrate and TRIS buffer solutions with fixed pH-values were used. The phase shift at pH 1 was used as reference point and the change of the phase shift at all other pH compared to pH 1 was recorded. From these relative phase shift the change in decay time was calculated. With the current optode a pH range between one and five can be addressed.

For the integration of optically chloride sensing into the robust luminescence decay time based sensing platform, the luminescence probe lucigenin was evaluated. The luminescence decay time of lucigenin is quenched in the presence of chloride. The preliminary results show, that such an optode has a good sensitivity in the chloride concentration range up to 0.5 mol/L. Compared to measurements in aqueous solutions the sensitivity of immobilized lucigenin is slightly reduced which is most probable connected to limitations in chloride diffusion inside the polymer matrix. Here, further optimization of the polymer matrix are needed to improve the sensor performance.

During the third year of the project, the **CNRS/LCPME** activities consisted essentially in an attempt to interpret the results obtained during the intercomparison exercise. The work undertaken was both theoretical and experimental. The objects of the theoretical work were the critical analysis of the potentials determined during the ICE on the basis of the voltammetric curves that we recorded at platinum ultramicroelectrodes and a bibliographic study on the operation principle of the electronic millivoltmeters. The object of the experimental work was the measurement of the current that flows through the potentiometric electrodes in various operating conditions for a series of commercial instruments used for redox potential determinations.

The examination of the voltammetric curves that we recorded with all the solutions and suspensions for which we determined the redox potential has given valuable information on the electrochemical kinetics of the different redox systems. Moreover, the shape of these curves has allowed us to predict the possible consequences of an eventual polarization of the potentiometric electrodes on the potential measurements. We also envisaged the influence of the solutions convection on the potentiometric measurements.

The detailed analysis is included in the **CNRS** individual report for the intercomparison exercise. Among the conclusions drawn from this report probably the most important is that a possible polarization of the electrodes as well as differences on

the stirring mode of the solutions cannot explain the discrepancies existing among the measurements performed by the different participants with solutions as simple as $\text{Fe}^{3+} + \text{Fe}^{2+}$ mixtures in acidic media. Such discrepancies demonstrate the requirement of standardized protocols for the potentiometric measurements.

The analysis of the bibliographic data accumulated during this year is in progress and the conclusions will be discussed in the final report after discussion with a physicist.

The work started with the purchase of a device sensitive enough to measure the current that flows through a potentiometric electrode during its operation. Moreover, the response time of this apparatus is smaller than 1 ms. It was computer interfaced for data acquisition and control through an IEEE port connection.

After, we have undertaken the rough measurement of the current flowing through a series of pH-meters, ionometers, potentiostats and other commonly used instruments for the measurement of redox potentials. The figure below depicts shows typical diagrams that represent recordings of the current flowing through two commercial pH-meters. Figure 6 (top) corresponds to a fast acquisition frequency: one point every 0.2 ms. The diagram on the bottom is for a high accuracy measurement: each point correspond to the mean value of the data acquired for 0.2 s. In both cases current pulses with a frequency of about 1 kHz pass through the electrical circuit. In the case of the second pH-meter, the pulses intensity ranges from -6 nA to 6 nA, whereas in the case of the first one the pulses are more than two orders of magnitude lesser. When the high accuracy mode is used, the "apparent" performances of both instruments are dramatically improved: by about 60 times in the case of the second pH-meter (the offset current is not specified by the manufacturer) and by about three orders of magnitude, i.e. about 5×10^{-14} A, in the case of the first pH-meter (offset current announced by the manufacturer: $< 3 \times 10^{-13}$ A).

The comparison of our experimental data with the performances announced by the manufacturers of the different instruments showed that, at best, the announced characteristics correspond to mean currents and not to real currents that flow through the electronic circuit.

The use of pulses in the ms range is usual when transient electrochemical techniques are performed. When this kind of pulses is applied, faradaic currents flow and the electrodes are polarized. In present case, the pulses which we observed when the pH-meters are operating are sufficient to polarize more or less the potentiometric electrodes in function of the current intensity and the size of the electrodes.

Measurements were practiced with 11 commercial instruments, and the currents measured using the "fast" detection mode ranges between 5 pA and 40 nA. As the measurement of such low currents is an extremely delicate task, now, these results are checked again to verify their correctness. The experiments under way seem to confirm the earlier ones. Moreover, now amperometric measurements are carried out with various solutions and suspensions in order to determine the most suitable instrument to use for the potentiometric measurements planned in the framework of WP3.

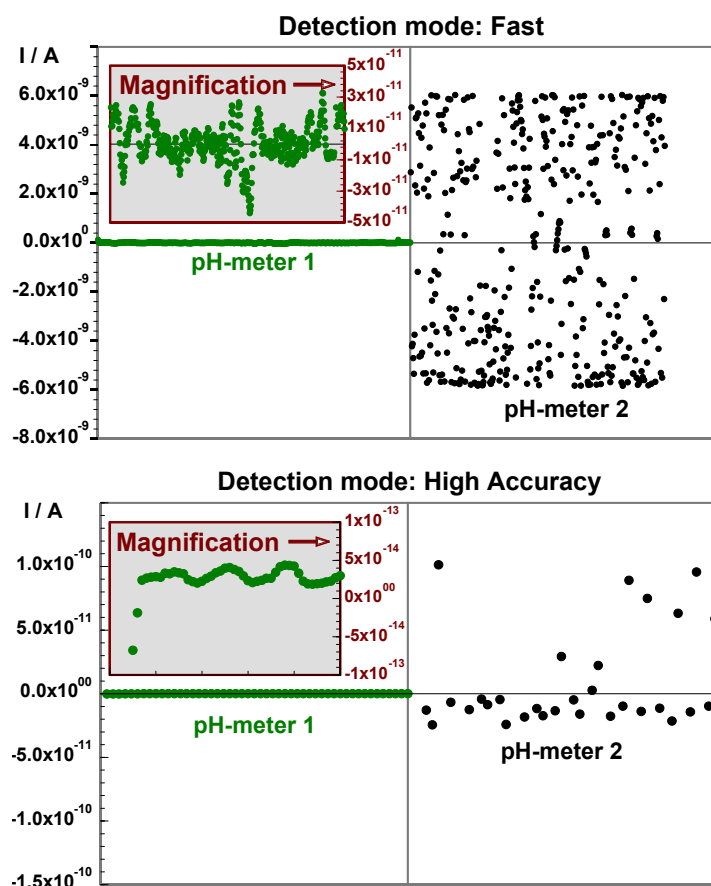


Figure 6. Comparison of the current that flows through two commercial pH-meters in function of the detection mode of the instrument used.

As in past years, contribution of **LQC** was essentially advisory to various other partners on issues in which the principal investigator in **LQC** has direct experience. As planned, no new direct actions were executed by partner **LQC** during the third year of the exercise, and activities were limited to follow-up and a general advisory role.

These included:

- oxygen sensing technologies: follow-up upon installation of Ocean Optics and TauTheta sensor systems. Communications with partners CTM and SKB continued on experimental set-up designs and interpretation of preliminary results.
- redox sensing technologies. Communications on methods and instrumentation suitable for electrochemical determination of pH and redox potential in poorly buffered media were held with various partners.
- hydrolysis studies and data processing. Constructive discussions were held with partner **KIT-INE** on the determination and interpretation of hydrolysis constant data, relevant to modeling of speciation and transport of actinides in neutral and alkaline environments.

Acknowledgements

The research leading to these results has received funding from the European Union's European Atomic Energy Community's (Euratom) Seventh Framework Programme FP7/2007-2011 under grant agreement n° 212287 (RECOSY project).

References

- Anderson C.R., Pedersen K. (2003). In situ growth of Gallionella biofilms and portioning of lanthanides and actinides between biological material and ferric oxyhydroxides. *Geobiology* 1, 169-178.
- Cabral, T., Ignatiadis, I. (2001). Mechanistic study of the pyrite-solution interface during the oxidative bacterial dissolution of pyrite (FeS₂) by using electrochemical techniques. *International Journal of Mineral Processing*, 62, 41-64.
- Cammann, K., Galster, H. (1997). *Das Arbeiten mit ionenselektiven Elektroden: Eine Einführung für Praktiker*. Springer-Verlag, Berlin, Heidelberg, New York, Barcelona, Budapest, Hongkong, London, Mailand, Paris, Santa Clara, Singapur, Tokio, , pp. 296.
- Evangelou, V. P. (1995) *Pyrite oxidation and its control*; CRC Press, Inc. Boca Raton: New York, London, Tokyo.
- Guillaumont, R.; Fanghänel, T.; Fuger, J.; Grenthe, I.; Neck, V.; Palmer, D.A.; Rand, M.H. (2003) Update on the chemical thermodynamics of uranium, neptunium, plutonium, americium and technetium. In *Chemical Thermodynamics*. OECD Nuclear Energy Agency, Ed., Elsevier, Amsterdam, Vol.5.
- Gourman-Lewis, D., Burns, C. Fein, J.B. (2008). Review of uranyl mineral solubility measurements. *J. Chem. Thermodynamics* 40, 335-352.
- Hallbeck L., Pedersen K. (2008). Characterization of microbial processes in deep aquifers of the Fennoscandian Shield. *Applied Geochem.*, 23, 1796-1819.
- Licht S., Forouzan F. (1995). Speciation Analysis of Aqueous Polyselenide Solutions. *J. Electrochem. Soc.*, 142, 1546-1551
- Neck, V.; Kim, J. L.; Kanellakopulos, B.,(1992) Solubility and Hydrolysis Behavior of Neptunium(V). *Radiochim. Acta*, 56, 25-30.
- Rard, J., Rand, M., Anderegg, G., Wanner, H. (1999) *Chemical Thermodynamics of Technetium*, Elsevier, North-Holland, Amsterdam.

WORK PACKAGE 3: REDOX RESPONSE OF DEFINED AND NEAR NATURAL SYSTEMS

Laurent Charlet

(CNRS)-Laboratoire de Géophysique Interne et tectonophysique LGIT- (UMR 5559)
Rue de la Piscine, 1381
38041/19 Grenoble
France

Introduction

The “Redox processes of defined and near-natural system” WP3 group has in Year 2 performed work on (i) Field data, (ii) Field samples, (iii) Microbiology, (iv) Sorption experiments, (v) Redox experiments and (vi) Conceptual Model. This work is summarized below.

Work performed by partners

KIT-INE studied the heterogeneous reduction of U(VI) to U(IV) by ferrous iron, which is believed to be a key process influencing the fate and transport of U in the environment.

Magnetite as stainless steel corrosion product will be one of the main Fe(II) containing mineral phases present when spent fuel corrosion occurs. Thus, an extensive laboratory program under anoxic conditions and exclusion of CO₂ as function of pH and contact time has been conducted to study the interaction of uranium with a synthetic nanoparticulate (size distribution 30-300nm) magnetite (Fe^{II}Fe^{III}O₄) applying spectroscopic techniques (XPS, XAFS) to verify the presence and amount of reduced uranium on the magnetite surface. U(VI) sorption kinetic studies revealed a fast initial sorption with > 90% magnetite associated U after 24 hours within the pH range 5-11. In contrast to earlier studies neither an uranium association at pH < 3 nor a decrease in the magnetite associated U at pH ≥ 9 could be observed.

Redox speciation on one year reacted samples by XPS and U L₃-edge XANES revealed for samples within pH 5.4 to 9.7 40-60% tetravalent U. Results from a standard U L₃ edge XANES comparative study of references with different U oxidation states and U magnetite nanoparticles previously performed at the INE-Beamline at ANKA, Germany, were inconclusive. The large core-hole lifetime broadening of the U 2p state (>7 eV), yielding broad spectral features, prevented unambiguously distinguishing between the different oxidation states in the XANES of the U-magnetite nanoparticles.

We suppressed the core-hole lifetime broadening by measuring partial fluorescence yield PFY-XANES of the U-magnetite(mag)/maghemite(magh) nanoparticles, thereby improving energy resolution and sharpening spectral features. The U_mag_pH8 spectrum shows broadening of the white line. The U_magh_pH5, 8, 11 spectra all exhibit similar spectra, with only variations in WL intensity. The spectra of both pH 5 samples have reduced signal-to-noise ratios, indicating their having relatively less sorbed U. Representatives of the general two types of spectra observed, U_mag_pH8 and U_magh_pH11, are compared to U(IV), U(V) and U(VI) reference spectra. The WL for the U_mag_pH8 sample resembles the broad WL exhibited by the U(IV) reference; however, its energy position coincides with the WL energies of the spectra for U_magh_pH11 and the U(VI) references. The broad energy distribution of 6d states, leading to the WL broadening, combined with the observed WL energy position, suggests that a U(IV) and U(VI) mixture is present in the U_mag_pH8 sample. The similarity of the other U-magnetite/maghemite nanoparticle spectra with the U(VI) reference PFY-XANES indicates that these samples contain predominantly U(VI). The fact that the PFY-XANES features of the U(V) reference spectrum differ from those of the U-nanoparticle spectra, notably its lower energy position, is a clear indication that no U(V) oxidation state species is present in any of the samples. We conclude that this advanced spectroscopic study allows us to exclude the presence of U(V) in the investigated set of U-magnetite/maghemite nanoparticles, in contrast to earlier published results. If U(V) species were at all formed, the kinetics of the redox reaction leading to its formation must be faster than a few days timescale, which is again in contrast to previous published results by Ilton and co-worker. Thermodynamic calculations based on the experimentally determined pe/pH values corroborate the spectroscopic findings and predict U(IV) as the predominant redox state in our studies.

In order to cross and overcome certain limits by improvement in the knowledge, **BRGM** proposed to complete the description of the Callovian-Oxfordian (COx) formation by investigating the redox (potential and reactivity) of its various mineral components. The main objective was to retrieve the electrochemical kinetics of the COx system in contact with different plausible redox perturbations by jointly using: i) specific electrodes built out of COx rock samples and individual redox reactive minerals that constitute the COx, and ii) diverse electrochemical techniques. Entire exploitation of the ICE measurement realized by **BRGM** with not only results on the redox measurements (by conventional electrodes), but also on how to make a generic pH electrode by using pyrite electrode potential measurements coupled to Pt electrode.

Particular equipment has been purchased and methodology has been developed and/or adapted for the investigation, including the design of various specific electrodes and the use of diverse electrochemical techniques, in order to explore the electrochemical kinetics of the COx system in contact with different plausible redox perturbations. Material under investigation includes massive and/or paste claystone rock samples (COx) as well as individual mineral contributors to the redox reactivity already identified in the media, provided we could meet the necessary conductivity limits (e.g. pyrite, clay paste).

CTM and **AMPHOS** objectives for Year 3 were to:

- Continue the kinetic oxygen studies with natural pyrrhotite in 0.1 M NaClO₄ media so as to measure sulphate, tiosulphate and iron concentrations in solution.
- Study the kinetic oxygen capacity of a natural pyrite, and compare the results with the experiments with pyrrhotite.
- Study the kinetic oxygen capacity of two different fracture filling materials (from Äspö and Grimsel) provided by **KIT-INE**.
- Characterization of solids by SEM, EDX, XPS and XRD techniques.

They have thus evaluated the oxygen scavenger capacity of four different minerals: two natural iron sulphides, pyrrhotite and pyrite, and two fracture filling materials (FFM) from Äspö and Grimsel. Experiments were performed with an initial oxygen concentration of 10⁻³M in 0.1M NaClO₄ media. The oxygen uptake capacity for each material was measured as rate of oxygen consumption in solution. No conclusions could be derived from direct measurements. Currently, raw data is being analyzed to take into account parallel reactions like secondary phase formation.

In parallel, the mineral dissolution has been monitored. In the experiments with pyrrhotite and pyrite the aqueous concentrations of Fe_{total}/SO₄²⁻/S₂O₃²⁻ increase with time, the same behavior is observed for Ca²⁺/NH₄⁺/SO₄²⁻/Si/Al/trace metals in the Äspö FFM experiment. Due to electrolyte diffusion from the pH/redox electrodes used, in all experiments a linear increase of K⁺ concentration in solution has been observed.

Mineral changes have been characterized at the end of the experiments by XRD. New crystalline phases of α -S₈, biothite and goethite have been identified in the pyrrhotite experiment and clinocllore in the final FFM Äspö solid. Other solids are being characterized.

Their main outcomes are thus the following for Year 3:

- In all kinetic studies, mineral dissolution has been observed. Experiments with pyrrhotite and pyrite shows Fe, sulphate and tiosulphate aqueous concentrations increase with time. Experiment with Äspö fracture filling material shows dissolution of Ca²⁺/NH₄⁺/SO₄²⁻/Si/Al/trace metals.
- SEM images and EDX measurements show oxide crystals that have grown on both oxygen treated iron sulphide minerals.
- XPS spectra of oxygen treated pyrrhotite results in an increase in the concentration of elemental sulphur and components assigned to tiosulphate, sulphate and components belonging to ferric ions. These results are coherent with the new crystalline phases (α -S₈, biothite and goethite) identified by XRD in the oxygen treated pyrrhotite.
- Further oxygen data analysis is needed to understand the direct oxygen measurements in solution for the different experiments performed before deriving a rate of oxygen consumption for each material studied.
- Continuous pH and redox measurements with commercial combined electrodes create a contamination of the reaction solution due to the internal KCl electrolyte diffusion.

CNRS main outcomes were the following.

Clays: reactivity of U(VI) with Fe(II) in presence of Fe-free clays.

The influence of surface-bound Fe(II) on uranium oxidation state and speciation was studied as a function of time (6 min- 72 h) and pH (6.1-8.5) in a U(VI)-Fe(II)-montmorillonite (Camontmorillonite, MONT) system under CO₂-free, anoxic (O₂ <1 ppmv) conditions. The results show a rapid removal of U(VI) from the aqueous solution within 1 h under all pH conditions. U LIII-edge X-ray absorption near-edge structure spectroscopy shows that 96% of the total sorbed U(VI) is reduced at pH 8.5. However, the extent of reduction significantly decreases at lower pH values as specifically sorbed Fe(II) concentration decreases. The reduction kinetics followed by X-ray photoelectron spectroscopy during 24 h at pH 7.5 demonstrates the presence of partially reduced surface species containing U(VI) and U(IV). Thermodynamically predicted mixed valence solids like U₃O₈/ U₃O₇/U₄O₉ do not precipitate as verified by transmission electron microscopy and extended X-ray absorption fine-structure spectroscopy. This is also supported by the bicarbonate extraction results. The measured redox potentials of Fe(II)/Fe(III)-MONT suspensions are controlled by the Fe(II)/hydrous ferric oxide [HFO(s)] couple at pH 6.2 and by the Fe(II)/lepidocrocite [γ -FeOOH(s)] couple at pH 7.5. The key finding of our study is the formation of a sorbed molecular form of U(IV) in abiotic reduction of U(VI) by sorbed Fe(II) at the surface of montmorillonite.

Sulfide minerals: reaction of pyrite (FeS₂) with selenium(IV).

Selenium solubility largely depends on redox conditions: Se(IV) and Se(VI) prevail as very mobile aqueous oxyanions, while the oxidation states 0, -I, and -II are solids with low solubility. Due to the weak adsorption of Se(IV) and Se(VI) on natural minerals, and in particular on granite or claystone minerals, chemical reduction is considered to be the most effective way to immobilize ⁷⁹Se. On the other hand, pyrite (FeS₂) is the most frequent sulfide mineral and is also present in geological barriers of nuclear waste repositories. Its strong reducing capacity and its stability under anoxic condition make it a good candidate for the immobilization of redox-sensitive radionuclides, like ⁷⁹Se. Many works have focused on the identification of the reduced form of selenium when reacted with pyrite, but reported conflicting results. Therefore **CNRS** performed a systematic study where they investigate the effects of the reaction of Se(IV) and Se(VI) with pyrite in several different experimental conditions. Experiments were conducted at pH 5.05, 5.65, 6.1, 7.0, and 8.5, reaction times of 7, 24, 36, and 48 days, and, at pH 7.0 and 8.5, with and without the addition of extra Fe²⁺ (10⁻⁴ mol/l). ICP-OES measurements were used to monitor the iron and Se concentrations and showed a decreasing trend of Se and increasing iron as a function of time. XAFS spectroscopy was used to unravel the selenium speciation. At pH 5.05 and 5.65 Se(0) was found to be the main reaction product, while at pH > 5.65, in addition to Se(0), XANES suggested the formation of iron selenides (Se -I or -II), in an amount which increased with the reaction time. The presence of iron selenides is further supported by Mössbauer spectroscopy clearly showing two different environments for Fe²⁺ in pyrite reacted with

Se. The results carried out in this study suggest that pyrite can significantly attenuate the mobility of ⁷⁹Se through chemical reduction.

Voltametric and spectroscopic characterization of Cox and Boda clays

The voltammograms recorded in acidic media with different samples that have been previously characterized by Mössbauer spectroscopy pointed out the voltammetric signals for all the iron containing species, i.e. Fe²⁺ and Fe³⁺ ions associated with clays pyrite and hematite. Moreover, the measurements have allowed to clear up an uncertainty that remained after the Mössbauer determinations about the presence of pyrite in two samples. Along this study, we were quite bothered by the evolution of the iron (II) containing samples. The evolution of the i-E curves relative to the pyrite containing samples with time is impressive: the amount of iron (II) progressively increases, whereas the signal of pyrite decreases and finally disappears into the peak for iron (II) oxidation. Anyway, the electrochemical behaviour of pyrite in Boda Clays is complex and two target experiments must be conducted to test the hypotheses that we proposed.

The COx particles that have reacted with soluble species of iodine or selenium were voltammetrically characterized in acidic chloride media (1 M KCl, pH 1) after their mechanical immobilization on the cross section of a graphite rod that acted as a current collector (Voltammetry of MicroParticles technique¹). To transfer and to immobilize the particles on the graphite surface, typically some µg of the sample were placed on a filter paper, and then the electrode was pressed onto the particles and gently moved. The voltammograms recorded for COx samples conditioned with elemental iodine are quite different from the others. Today, the detailed analysis of the voltammetric data is in progress, and some experiments are conducted again in order to confirm certain results.

Solution analyses: The interpretation of the chromatographic analysis data for aliquots sampled during the conditioning of COx was disturbed for a long time by unexpected matrix phenomena. Moreover, there was an interference during the determination of iodine species because of an unknown species released by the filtering cartridges that has the same retention time as iodate ions. Six different cartridges have been tested without any significant improvement and as the rinsing does not eliminate the problem, but sometimes it increased it the filtration was replaced by centrifugation.

Anaerobic conditioning of COx samples with soluble iodine and selenium species (s/l = 0.5% w:w).

Solution aliquots were sampled during the conditioning and analyzed by ICP-AES, ion chromatography and UV-visible spectroscopy. After reaction, the COx particles were separated from the liquid phase, rinsed, dried and then characterized voltammetrically. Sorption experiments were performed in the dark, at room temperature and under argon atmosphere with 0.5% (w:w) solid/liquid ratio. COx lumps, instead of powder, were used in order to limit the oxidation of the clay by the atmospheric oxygen. The suspensions were stirred by means of a come and go movement shaker. The conditioning of COx suspensions has been performed at 'natural' pH and without pH

control in the following conditions: $[I^-] = [IO_3^-] = [SeO_3^{2-}] = [SeO_4^{2-}] = 1$ or 0.1 mM; with elemental iodide, we used a saturated I_2 solution (solid I_2 was always present) or the liquid phase sampled from an iodine suspension in 1 mM I^- . After reaction, the solid particles were taken out, washed with deaerated osmosed water, filtered or centrifuged, and then characterized by different techniques.

The objectives for the past project year for **UNIZAR** were:

- Compilation of different types of information related to the study of redox parameters in crystalline systems based on the experience within the Swedish site characterization program.
- Comparison and integration of the results obtained during this second year, with the rest available data (mineralogical and microbial data) in order to produce an integrated conceptual model for these systems.
- Preliminary evaluation of uncertainties

The **UNIZAR** main obtained results in Year 3 suggest that the redox features in the groundwater system of the Swedish candidate sites (Forsmark and Laxemar) are fully consistent with the existence of presently active processes of stable bacterial sulphate reduction in both studied sites, as indicated by the potential presence (according to speciation-solubility calculations) of metastable amorphous iron monosulphides not yet recrystallized to ordered or crystalline mackinawite or pyrite. Moreover, the existence of equilibrium situations with respect to ferrous iron monosulphides also indicates the presence of a source of dissolved Fe(II), without which the concentrations of dissolved sulphide in the groundwaters would be much higher. This interpretation has important implications for performance assessment, since high sulphide concentrations are known to affect very negatively to the safety of canisters owing to corrosion processes.

II-HAS studied Boda Claystone samples originated from different boreholes which were exposed to treatment with sodium dithionite. The hematite content of samples was converted to a new solid phase component, containing iron in ferrous state. The mineral components containing iron originally in ferrous form (e.g. in chlorite) were not affected.

The **MICANS** main outcomes were:

- The effect of varying concentrations of hydrogen and acetate on microbial sulphate reduction was documented and quantified.
- The influence of microbial activity as a function of the hydrogen load on oxygen reduction was demonstrated to be significant
- Microbial populations appear to have a strong redox buffering capacity.
- Modeling of the microbial processes have been initiated with a program denoted Microbe

Biological life systems are non-equilibrium systems and in most cases, they will never reach equilibrium. The overall influences of microbial activity on the Eh are complex and dependent on availability of sources of energy and carbon, either inorganic or organic compounds, and the nature of these. In the work performed last year, pressure resistant Pt and Ag/AgCl reference electrodes were constructed and installed into pressurized (2 MPa) circulation systems. Investigations of the relations between Eh and microorganisms growing with different electron donors (lactate or hydrogen) and electron acceptors (nitrate or sulphate) were performed. The influence of pulses of oxygen on the redox stability under different growth conditions was analysed. It became clear that microbial activity was very important for how the Eh developed in the studied systems. Microbial lactate and hydrogen oxidation, sulphide production and oxygen reduction occurred and the effect from introduction of oxygen on Eh was mitigated by microbial activity. The presence and activity of microorganisms consequently have a great influence on Eh in natural water systems.

WORK PACKAGE 4: REDOX REACTIONS OF RADIONUCLIDES

¹M. Perdicakis, ²S. Allard, ²S. Holgersson, ³N. Brian, ³R.R. Kay, ³N. Li, ³A. Stockdale,
⁴D. Baltrunas, ⁴G. Lujanienė, ⁵Th. Schäfer, ⁵Ch. Marquardt, ⁶N. Evans, ⁶R. Hallam, ⁶P.
Warwick, ⁷M. Grivé, ⁸X. Gaona, ⁸J. Tits, ⁸E. Wieland, ⁹E. Krawczyk-Bärsch

¹Laboratoire de Chimie Physique et Microbiologie pour l'Environnement, Nancy-
Université, CNRS -54600 VILLERS-LES-NANCY (FR)

²Chalmers University of Technology, SE-412 96 Gothenburg, (SE)

³University of Manchester, Centre for Radiochemistry Research, School of Chemistry,
Manchester, M13 9PL, (UK)

⁴Institute of Physics of Lithuania, LT-02300 Vilnius, (LT)

⁵Karlsruhe Institute of Technology, Institute for Nuclear Waste Disposal, Karlsruhe
(DE)

⁶Loughborough University, Department of Chemistry, Loughborough, Leics, LE11
3TU, (UK)

⁷AMPHOS 21 Consulting, S.L., Passeig de Garcia i Faria, 49-51, E08019 Barcelona,
(ES)

⁸Paul Scherrer Institut, Laboratory for Waste Management, CH-5232 Villigen-PSI (CH)

⁹Helmholtz-Zentrum Dresden-Rossendorf, Institute of Radiochemistry Dresden (DE)

Introduction

The goal of the activities within work package 4 is to provide fundamental process understanding of the redox behaviour of radionuclides in solution and in solid matrices, including the question of equilibrium / disequilibrium with the system redox conditions. The objectives of this work package result from gaps in the knowledge identified from previous projects dealing with redox processes involving radionuclides.

The work package is divided in 2 parts:

4.1. Chemical and redox behaviour of the investigated radionuclides in the different systems.

1. Interactions of radionuclides with pyrite
2. Interactions of radionuclides with far-field solids
3. Redox processes under hyperalkaline conditions

4.2. Chemical and redox behaviour of the investigated radionuclides in the different systems through microbial mediated processes.

WP 4.1.

CHEMICAL AND REDOX BEHAVIOUR OF THE INVESTIGATED RADIONUCLIDES IN THE DIFFERENT SYSTEMS

Work performed by partners

4.1.1. Interactions of radionuclides with pyrite

During the third year of the project, the CNRS/LCPME activities consisted in the anaerobic conditioning of pyrite micrometric grains (40-80 μm) with soluble species of iodine and selenium (s/l = 0.5% w:w). Solution aliquots were sampled during the conditioning and analyzed by ICP-AES, ion chromatography and UV-visible spectroscopy. After reaction, the pyrite microparticles were separated from the liquid phase, rinsed, dried and then characterized by voltammetry, impedancemetric and XPS measurements.

Pyrite grains conditioning

The pyrite samples were dry ground in air in a porcelain mortar just before use in order to limit their oxidation by the atmospheric oxygen. Surface analyses by XPS of ground pyrite indicated essentially pure material with no evidence of surface oxidation products. Only the particles between 40 and 80 μm (surface area $\sim 0.1 \text{ m}^2/\text{g}$) were selected. Sorption experiments were performed under argon atmosphere at room temperature by stirring the conditioning containers in the dark by means of a come and go movement shaker. The solution pH was adjusted to 3.0 at the beginning of the experiment with nitric or hydrochloric acid. After reaction, the sulphide grains were taken out, washed with deaerated osmosed water, filtered or centrifuged, and then characterized by the different techniques. The conditioning of pyrite suspensions has been performed using a 0.5% (w:w) solid/liquid ratio in the following conditions: $[\text{I}^-] = [\text{IO}_3^-] = [\text{SeO}_3^{2-}] = [\text{SeO}_4^{2-}] = 1$ or 0.1 mM ; with elemental iodide, we used a saturated I_2 solution (solid I_2 was always present) or the liquid phase sampled from an iodine suspension in 1 mM I^- .

Voltammetric measurements

The pyrite grains conditioned beforehand with soluble species of iodine or selenium were voltammetrically characterized in acidic chloride media (1 M KCl , pH 1) after their mechanical immobilization on the cross section of a graphite rod that acted as a current collector (Voltammetry of MicroParticles technique (Scholtz and Meier, 1998). To transfer and to immobilize the particles on the graphite surface, typically some μg of

the sample were placed on a filter paper, and then the electrode was pressed onto the particles and gently moved.

Two different kinds of determinations were performed as a function of the scan rate used for the voltammetric records: i) voltammograms recorded with the classic scan rate of 5 mV/s and ii) voltammograms recorded at 0.1 mV/s (Figure 1) that allow the complete transformation of the immobilized electroactive material. The voltammograms recorded at 0.1 mV/s are very promising; however, the duration of a voltammetric sweep, that is about 12 hours, seriously increases the time required for the interpretation of the results.

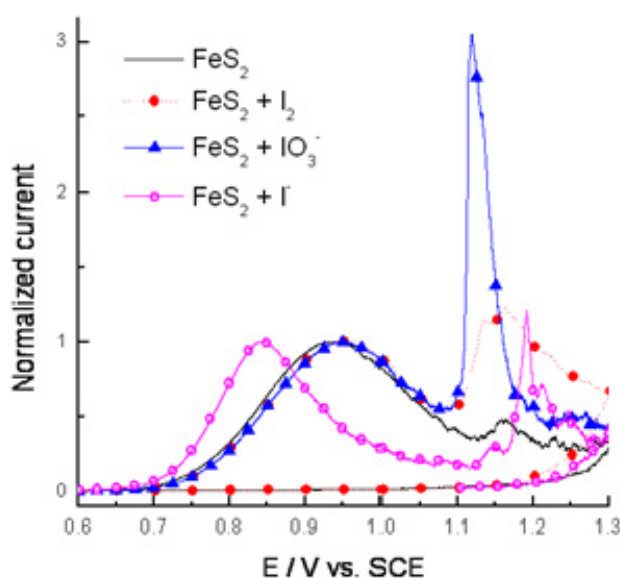


Figure 1. Voltammograms recorded at 0.1 mV/s

Impedancemetric measurements

The pyrite grains that have reacted beforehand with soluble species of iodine or selenium were characterized as they were or in the presence of solutions in the 0.4-100 MHz range. The raw complex impedance (Z^*) data acquired were processed in order to determine the real part Z' , that correspond to the resistance, and the imaginary part Z'' as well as the dielectric permittivity ϵ' (dielectric constant) and the dielectric loss ϵ'' of the samples. The analysis of these results is in progress.

Solution analyses

The interpretation of the chromatographic analysis data for aliquots sampled during the conditioning of pyrite particles was disturbed for a long time by unexpected matrix phenomena. Moreover, there was an interference during the determination of iodine species because of an unknown species released by the filtering cartridges that has the same retention time as iodate ions. Six different cartridges have been tested without any

significant improvement and as the rinsing does not eliminate the problem, but sometimes it increased it the filtration was replaced by centrifugation.

4.1.2. Interactions of radionuclides with far-field solids

The work performed within this topic is focused on obtaining fundamental process understanding of the interaction of redox sensitive radionuclides such as Tc, U, Np and Pu with various far-field minerals.

The contribution of **CHALMERS** to ReCosy WP4 consists of an investigation of redox reactions and states of selected redox sensitive elements with relevance to a crystalline rock environment (Äspö, Sweden).

The investigations are basically divided into two parts:

1. Bulk water measurements
2. Groundwater with crushed minerals measurements ("batch" experiments)

In both parts it is intend to look into aspects of the Eh agreement between the redox couple Fe(II)/Fe(III) and e.g. Tc(IV)/Tc(VII), U(IV)/U(VI), Np(IV)/Np(V), Pu(IV)/Pu(VI) in ionic media of varying type with ionic strength < 0.1, including natural Äspö groundwater. The aim is to perform these studies under both oxic and anoxic conditions. Measurements with commercial redox electrodes as well as analysis and quantification of elemental oxidation states will be examined over time and discrepancies between these will be looked into.

Geological material and groundwater recipe are taken from the Äspö LTDE-project (Long Term Diffusion Experiment) where results for in-situ adsorption of radionuclides onto rock surface, both for transport in fractures and fracture zones, and in-diffusion into the rock matrix is compared with laboratory results with crushed material.

During 2010 the experiments have continued with:

- 1) Production of An(IV) from An(VI) (An=U, Np) by catalytic reduction with H₂/Pt.
- 2) Spectroscopic measurement of purity of 0.1-1mM solutions of An(IV) from An(VI) and its stability over time in inert atmosphere (glove-box).
- 3) Separation of An(IV) from An(VI) by solvent extraction, using Thenoyltrifluoroacetone (TTA) or Dibenzoylmethane (DBM) for the purpose of quantification of ²³³U and ²³⁷Np in tracer concentrations (<1 µM).
- 4) Testing a method for quantification of An oxidation states of tracers added to some artificial redox systems, i.e. Fe(II)/Fe(III) in electrolytes and synthetic groundwater of the LTDE type.

The reduction and solvent extraction experiments look promising but a final method for rapidly determining the oxidation states of An has yet to be devised. The intention is to use reduced An(IV) tracers as an addition to the aqueous system of interest and then, after a period of time, take samples for extraction and measurements

with alfa/beta discriminating Liquid Scintillation Counting for determining the concentration of the An(IV) and An(VI). The method is intended to be used in inert gas glove-boxes.

UMANCH is investigating the interactions between surfaces, humic acids (HA) and redox sensitive radionuclides in ternary systems, with the aim of developing a mathematical model to predict actinide chemistry and solid/solution partition.

During 2010 the partition of radionuclides between solid and solution phase has been studied in humic/quartz sand ternary systems. Data have been recorded under ambient (air) and inert (O₂ and CO₂ free) atmospheres. For Eu(III) and Th(IV), the systems show simple behaviour, with sorption decreasing (and mobility increasing) in the presence of humic, whilst for uranyl, the behaviour is more complex, with the humic enhancing sorption and reducing mobility. There is also evidence that the sorbed humic has an enhanced affinity for the uranyl, which is probably due to fractionation of the humic. Data have also been obtained for the U(IV) ion. A simple mathematical model has been developed to predict the behaviour of both metal ion and humic acid. The model performs well in predicting the partition of the humic and that of the metal ions in the systems that show simpler ternary behaviour.

The experimental procedures used this period are described in the S and T contribution from the University of Manchester in this workshop proceedings.

Full details of the model are also given in the S and T contribution, but brief details are given here. The interaction of metal ions with the humic is described using two components, with initial uptake to an exchangeable fraction which is assumed to be instantaneous. Subsequent transfer to and from the non-exchangeable fraction is a first-order kinetic (slow) process. The interaction of metal ion with the quartz surface is described with a single kinetic reaction with forward and backward rate constants. For the sorption of the humic itself, the model assumes that the surface is the source of the heterogeneity. There is a single type of humic species in solution and two surface sites. Kinetic reactions with separate forward and backward rate constants are used to describe humic sorption.

Examples of the experimental data that have been produced thus far are shown in the figures. Because of space restrictions it is not possible to show all of the data (more is available in the S and T contribution). The data are plotted as the natural log of C/C_0 , where C is the concentration in solution at any point, and C_0 is the concentration of metal in solution before exposure to the mineral surface.

Figure 2 shows the results of the experiment for the Th(IV) 'in air' system. Th(IV) is showing simple ternary system behaviour in this system (solution phase Th concentration increasing with [HA]). As the concentration of the humic increases, the amount of Th sorbed to the mineral surface decreases. Hence, in this system, the main effect of the humic is to act a competing solution phase ligand, which holds it in solution. In this system, the model performs reasonably well. Figure 2 shows the results of the analogous experiment for the uranyl system. In this case, the effect of the humic is very different: the presence of the humic actually increases the sorption of uranyl. This can happen in systems where the interaction of the metal ion with the mineral surface is weak compared to that with the humic. In that case, ternary surface complex

formation is particularly favourable for the metal, and the presence of humic enhances sorption. However, the situation is more complex than that. In a system where the humic binding strength dominates, if it behaves like a simple homogeneous ligand, then the metal ion should ‘follow’ the humic: that is the solid/solution partition of the metal should approach that of the humic. The lines in Figure 2 show the behaviour of the humic (calculated using the model) in this system. The fact that the solution concentration is depressed in the presence of humic shows that ternary complexes are significant, whilst the difference between the humic partition and that of the uranyl shows that the humic on the surface has different interaction to that in solution.

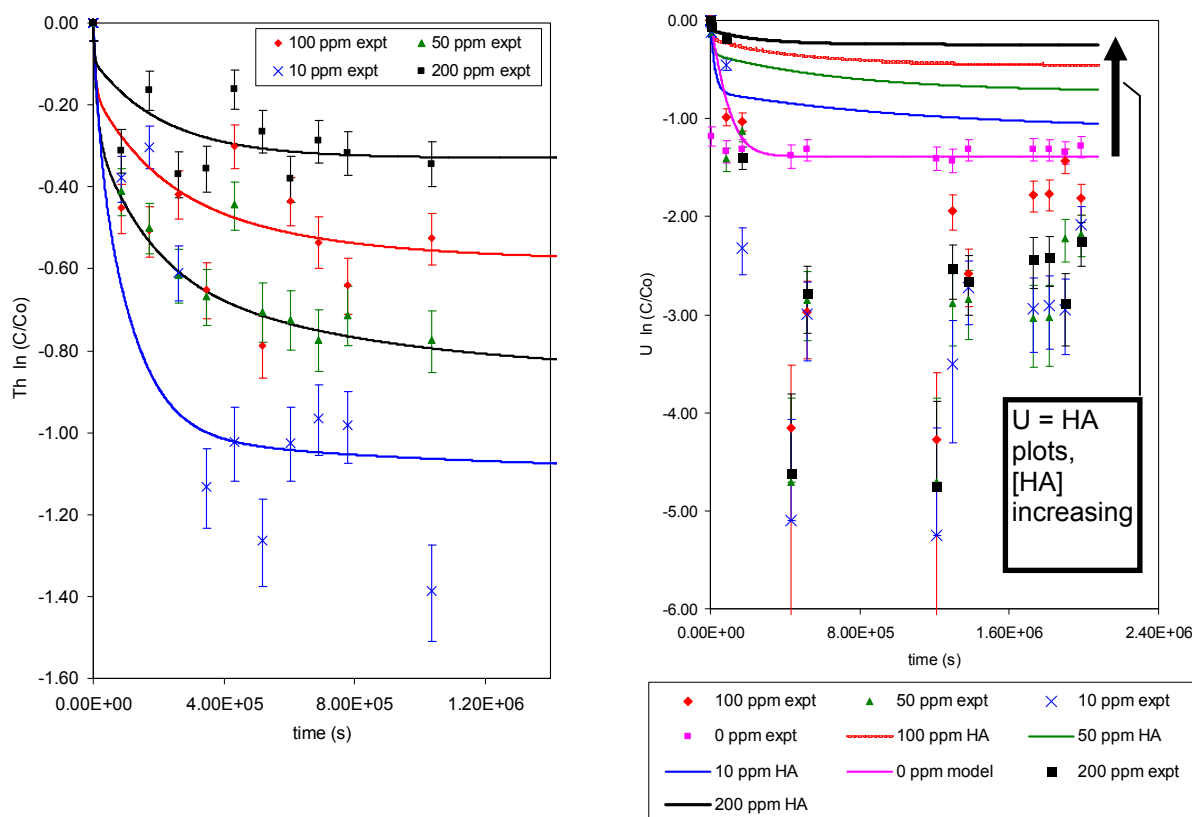


Figure 2: (a): results for Th sorption in ternary humic acid/quartz sand system, $[M_T] = 188 \text{ Bq l}^{-1}$, $I = 0.1$, $\text{pH} = 6$, in air, as a function of humic acid concentration: experimental data (points) and model fits (lines). (b): results for UO_2^{2+} sorption in ternary humic acid/quartz sand system, $[M_T] = 100 \text{ Bq l}^{-1}$, $I = 0.1$, $\text{pH} = 6$, in air, as a function of humic acid concentration: experimental data (points) and the behaviour of the U if it followed the humic (lines).

The experiments have also shown that the ternary system behaviour is very different in the presence and absence of air, because of the influence of carbon dioxide and dissolved (hydrogen)carbonate. For Th(IV), the behaviour becomes more complex in the absence of carbonate, with behaviour intermediate between that shown in Figures 1 and 2. The U(IV) behaviour in ternary systems (inert atmosphere) has also been studied. The U(IV) shows similar behaviour to that of Th(IV), as would be expected.

More recently, the Pu behaviour in ternary systems has been studied. Preliminary experiments with Pu(IV) and Pu(VI) sorption have been performed and also some experiments where the oxidation state of the Pu is changed during the experiment.

KIT – INE carried out sorption and redox speciation studies of Np, Pu and on crushed OPA and COx clay rocks with artificial pore water. The batch experiments were performed at pH 7.6 for OPA and pH 7.2 for COx under argon atmosphere (<1 ppm O₂) with 1% CO₂ conditions at room temperature. Four different solid to liquid ratio, S/L (10, 20, 50, 200) at constant ionic strength (0.1 M NaCl), and with contact times up to 4 months have been studied. Three series with initial concentration of Np(V), Pu(V) and Tc(VII) in solution of 3.0×10^{-4} , 3.0×10^{-7} and 1.0×10^{-8} M have been probed. The pH and the E_h values have been monitored over the experimental period. The pH was constant over the period of one year, whereas the E_h decreased from about 230 mV to about -100 mV. It was observed that the sorption of the radionuclides increases with increasing clay amounts and with increasing contact time. In the low concentration range 10^{-8} – 10^{-7} M more than 80 % of Np and Pu were sorbed on the clay whereas only 35 % of Tc was bound on OPA and COx after 4 months contact time. The preliminary K_d values for batch experiments of OPA and COx are listed in Table 1 and 2, respectively. The log K_d values are almost independent on the S/L ratios at S/L higher than 20.

Table 1: K_d values and percentage sorption of RN on COx (pH 7.2) in pore water at 3×10^{-7} M after 4 months contact time.

Solid to liquid ratio, [g/L]	K _d [mL/g] & sorption [%] of Np	K _d [mL/g] & sorption [%] of Pu	K _d [mL/g] & sorption [%] of Tc
10	5.4/76	5.5/71	0.04/19
20	0.9/81	3.2/88	0.02/20
50	0.3/84	0.8/89	0.02/28
200	0.1/87	0.3/93	0.01/53

Table 2: K_d values and percentage sorption of RN on OPA (pH 7.6) in Pore water at 3×10^{-7} M after 4 months contact time

Solid to liquid ratio, [g/L]	K _d [mL/g] & sorption [%] of Np	K _d [mL/g] & sorption [%] of Pu	K _d [mL/g] & sorption [%] of Tc
10	5.5/83	6.3/84	0.05/28
20	1.0/81	3.0/86	0.03/28
50	0.7/86	1.3/88	0.01/36
200	0.1/88	0.3/89	0.01/65

The redox state of the metal cations in the samples was characterized by EXAFS, UV-Vis absorption, X-ray photoelectron spectroscopy, and liquid-liquid extraction (PMBP, TTA). The speciation of Np, Pu, Tc in solution and on the solid phase is separately studied at various contact times. EXAFS spectroscopy on Tc has been performed at the INE-KIT beamline in a first time. By measuring Tc(IV) and Tc(VII) references, the XANES showed that Tc in the clay suspension was still in the heptavalent oxidation state after one week contact time. Also neptunium remained as Np(V), whereas plutonium was reduced in the clay suspension to Pu(IV). The reduction of Pu to Pu(IV) was confirmed by XPS as it is shown in Figure 3. Here, the OPA was

measured as a wet paste. For Np the results were not clear. Np(V) and Np(IV) have similar binding energies of the 4f elemental lines and conclusions concerning the valence state of Np are solely derived from the positions of 4f satellites if present. However, satellites were not observed in the spectra.

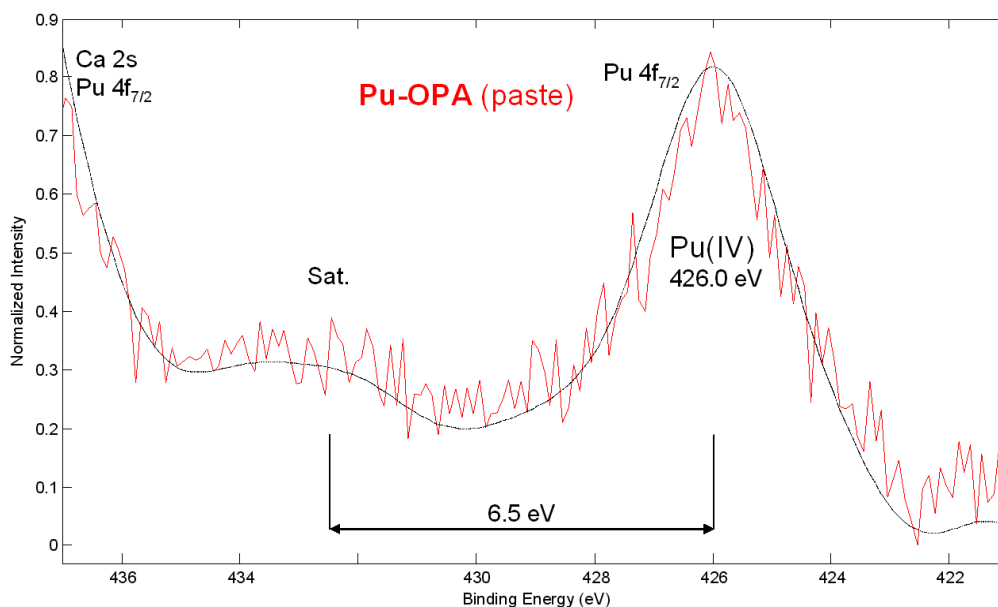


Figure 3: XPS measurement of plutonium sorbed on Opalinus clay after a reaction time of 7 days. 3×10^{-4} M Pu(V) was added to Opalinus clay (S/L 50) at pH 7.6 (Pu 4f_{7/2} spectrum, Al K α mono x-ray excitation, charges referenced C1s (CxHy): 284.8 eV)

In contrast to the high concentrations series, small amounts of Np(IV) and Tc(IV) were detected in the clay solution at low concentrations by liquid-liquid extraction. The amount of the tetravalent oxidation state of both elements increased with the reaction time up to 4 months. The plutonium maintained in the tetravalent oxidation state. To be aware of the uncertainty of the liquid-liquid extraction method, capillary electrophoresis (CE) coupled on ICP-MS was introduced as a second redox speciation method. Unfortunately, first experiments clarified that the injection system of the commercial CE is not optimal for very oxygen sensitive species. But these experiments also showed that speciation of Np(V) and Np(IV) was semi-quantitatively achieved at very low concentrations of about 10^{-9} M. However, it is mandatory to develop a new injection system running under argon atmosphere to stabilize the oxygen-sensitive redox states.

4.1.3. Redox processes under hyperalkaline conditions

The work performed within this topic aims to provide an understanding of the redox behaviour of redox-sensitive radionuclides such as Tc, U, Np under hyperalkaline conditions.

The contribution of **ULOUGH** to the Recosy WP4 consists of an investigation of the effect of EDTA, ISA and Picolinic Acid on the Redox Chemistry of Technetium. The current UK option for the management of ILW is to store it in a deep geological disposal facility (GDF). This may then be backfilled with a cementitious material. The GDF will develop highly alkaline porewater for *ca.* 10^5 years. Corrosion of steel canisters will lead to reducing conditions, so the chemistry of Tc in the waste must be understood in the context of this chemistry. The aqueous chemistry of technetium is likely to be dominated by the highly mobile pertechnetate anion in aerobic waters, and by $\text{TcO}_2(\text{am})$, in anaerobic.

Organic complexing agents will be present in ILW, including decontamination agents such as EDTA and picolinic acid, as well as polyhydroxylated carboxylic acids like α -isosccharinic acid (ISA). Such ligands are often highly complexing and can cause significant increases in radionuclide solubility, especially at high pH. The GDF will not be homogenous so there will be areas of reducing and oxidising potential, which could mean both Tc(VII) and Tc(IV) are present. If TcO_4^- migrates into an area of reducing conditions, the organics may complex with Tc during reduction to form water-soluble species. Also of relevance, is the possibility of increased solubility when organics are in contact with reduced Tc. In other words, does the presence of organics affect the reduction of Tc(VII) to Tc(IV)? Studies were undertaken in which TcO_4^- was reduced in the presence and absence of the three ligands, to determine whether there was an increase in Tc solubility when TcO_2 was contacted with the ligand.

Experiments were conducted in an N_2 glove box. Solutions were boiled, N_2 sparged and kept in presence of Fe filings to maintain reducing conditions. The ligands were added to $\text{NaOH}(\text{aq})$ in the form of solids at pH 13.3, to give concentrations between 0.4 and $0.001 \text{ mol dm}^{-3}$. NH_4TcO_7 was added and pH and Eh measured. Reduction was achieved by 3 methods, the addition of 0.7 g of SnCl_2 or FeCl_2 or electrochemically. Five replicates were used. Control experiments showed that reducing conditions were maintained for the required periods of time and that 14 days was sufficient for steady state to be established.

The red data points in figures 1, 2 and 3 show the effect of EDTA, ISA and picolinic acid concentration on Tc(IV) solubility. The slopes of close to unity for ISA and picolinate indicate that the increase in solubility of Tc is being controlled by the formation of a 1:1 Tc(IV)-ligand complex. It is difficult to interpret the slope of 1.76 for EDTA. Crystallisation and characterisation of these complexes is ongoing in collaboration with the University of Nevada (Las Vegas).

TcO_4^- reduction in presence of ligands

In the presence of ISA, a lowering of $[\text{Tc}](\text{aq})$ took place, showing that ISA did not prevent reduction taking place (Figure 4). If this reduction was to Tc(IV), then the final $[\text{Tc}](\text{aq})$ should be the same as that produced by the addition of ISA to Tc(IV) solution, i.e. the Tc(IV)-ISA complex would again be formed, but by 2 different routes at steady state. For ISA, this would seem to be the case. The presence of EDTA inhibited the reduction of pertechnetate by all three methods tried, i.e. SnCl_2 , Fe(II) and electrochemically, (figure 5). The presence of PA again inhibited the reduction of pertechnetate by all three reduction methods tried, (Figure 6).

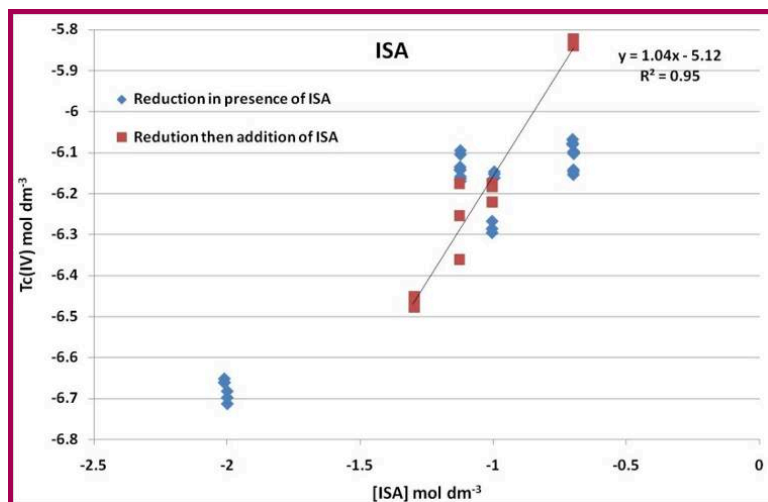


Figure 4. Comparison of final [Tc] in presence of ISA at pH 13.3, starting from TcO_4^- and Tc(IV).

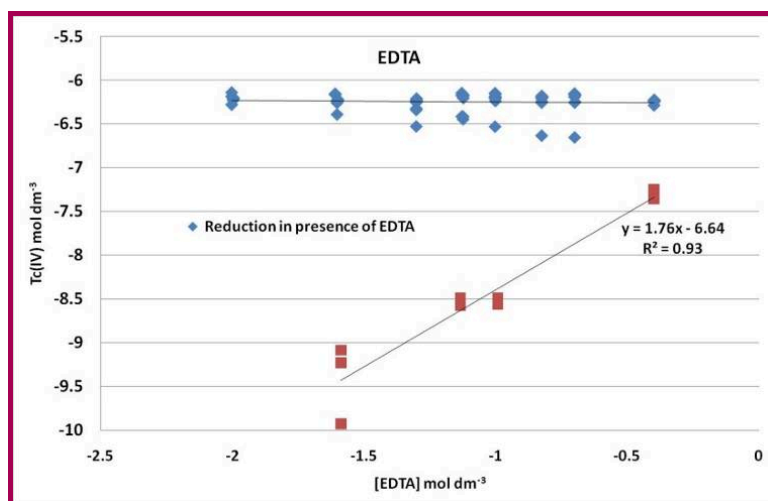


Figure 5. Comparison of final [Tc] with EDTA at pH 13.3, starting from TcO_4^- and Tc(IV)

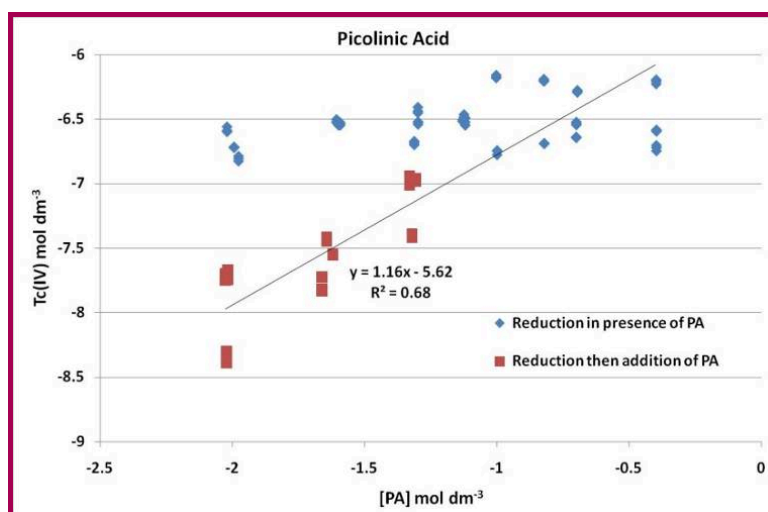


Figure 6. Comparison of final [Tc] with of PA at pH 13.3, starting from TcO_4^- and Tc(IV)

AMPHOS aims at providing an understanding of the redox behaviour of the uranium system under alkaline conditions by performing solubility experiments in the presence of H₂(g) or using a reducing agent (Na-dithionite) to keep reducing conditions. During the second year of the project Amphos studied the UO₂ solubility in the presence of H₂(g). The experimental data suggested a poor capability of H₂(g) to keep reducing conditions in the absence of a catalyst. For this reason, the use of Na-dithionite as a reducing agent has been used in this third year of the project, in order to avoid the oxidative dissolution of UO₂(am) under alkaline conditions.

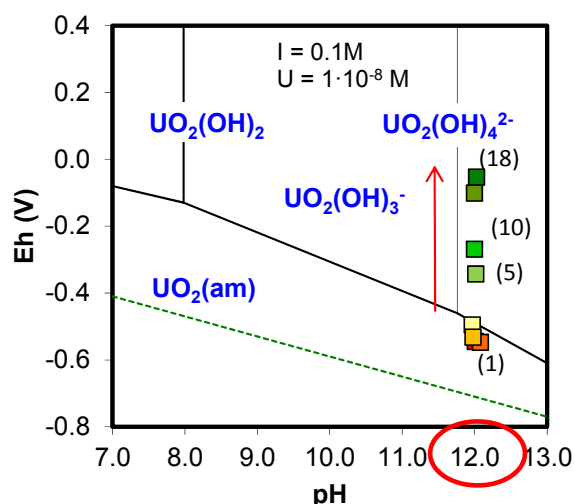
Solubility of freshly prepared UO₂(am) solid has been measured at pH = 10, 11 and 12 at ionic strengths of 0.1 M (NaClO₄) and using two different dithionite concentrations (0.001 and 0.01 M). All the solubility experiments have been performed in a glove box under N₂ atmosphere.

Both, pH and E_h have been measured in the experiments inside the reactor. In all the cases, experiments show an increase of the measured redox potential with time (see Figure 6). A decrease on the pH with time has also been observed and the pH of the system has been periodically adjusted using NaOH when needed. This evolution of the pH and Eh measurements with time indicated that under the experimental conditions, the systems seem not to be in thermodynamic equilibrium.

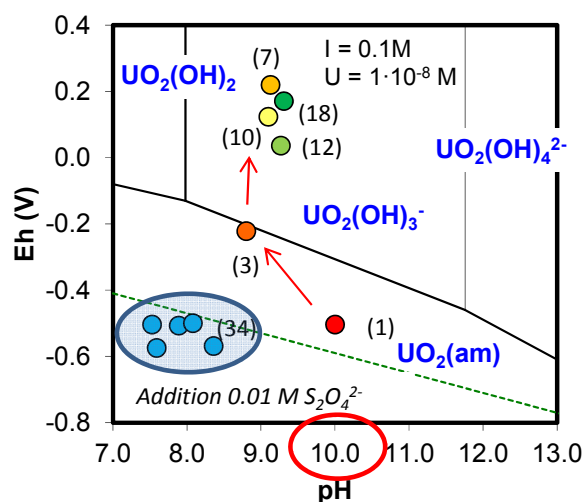
At the measured E_h and pH, uranium concentrations have also been measured by ICP-MS after being filtered with 0.22 µm pore filter size and acidified. The measured uranium concentrations of all the experiments correspond to those expected from the reaction (1) where no oxidation of uranium has occurred (see Figure 7). The measured concentrations are also in agreement with other solubility experiments previously performed and reported in the literature where no oxidation of uranium is described (Ryan and Rai, 1983; Rai et al., 1990; Yajima et al., 1995; Ollila, 2002; Carbol et al., 2005).



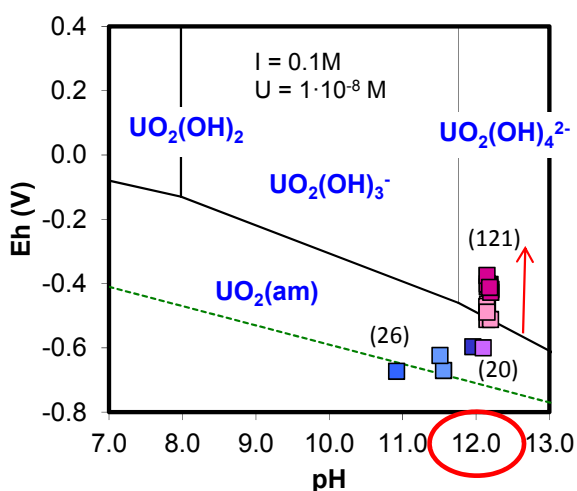
These results evidenced that despite the high E_h measured at the end of the experiments where UO₂(s) would be expected to oxidize (see Figure 6) giving high uranium concentrations in solution (see Figure 7), the measured uranium concentrations are characteristic of U(IV) species in equilibrium with UO₂(s).



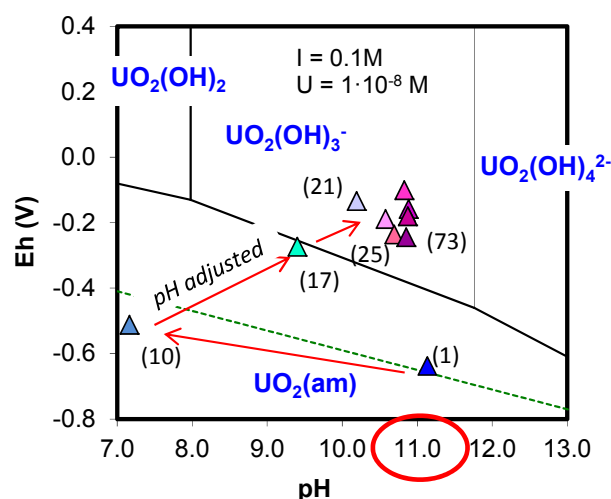
A) Initial dithionite = 0.001 M, pH = 12



B) Initial dithionite = 0.001 M, pH = 10



C) Initial dithionite = 0.01 M, pH = 12



D) Initial dithionite = 0.01 M, pH = 11

Figure 6. Eh/pH predominance diagram of uranium at uranium concentration of $1 \cdot 10^{-8}$ M and $I = 0.1$ M. The green dashed line stands for the water reduction at $P_t = 1$ atm. Symbols account for measured Eh and pH for experiments initially set up at a) pH 12 and $[S_2O_4^{2-}] = 0.001$ M b) pH 10 and $[S_2O_4^{2-}] = 0.001$ M, symbols inside the circle indicate addition of 0.01 M $S_2O_4^{2-}$ c) pH 12 and $[S_2O_4^{2-}] = 0.01$ M, d) pH 11 and $[S_2O_4^{2-}] = 0.01$ M. In brackets is expressed the reaction time in days.

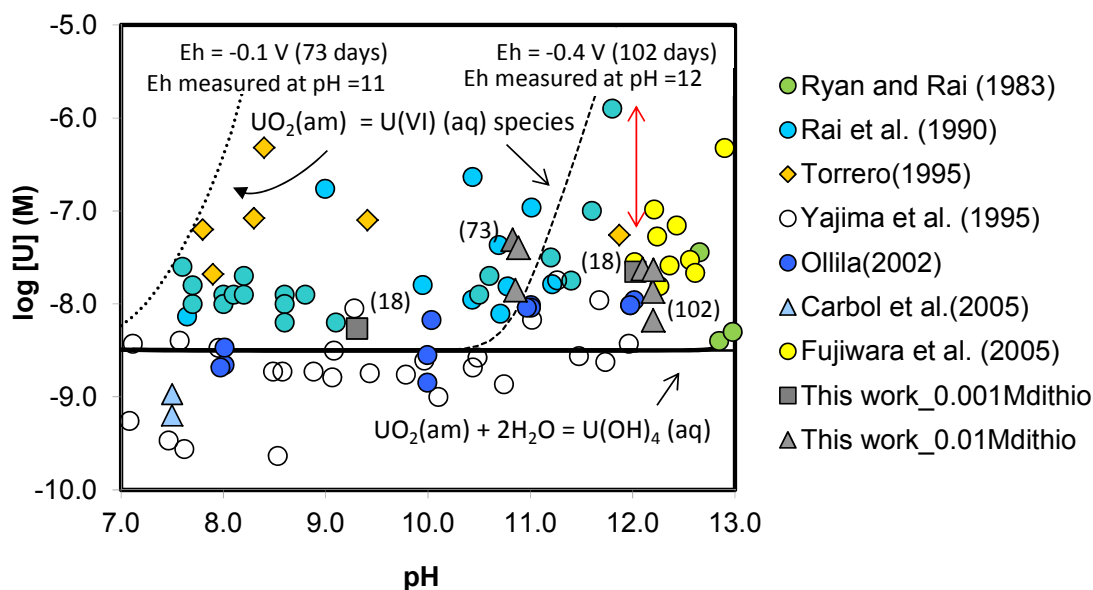


Figure 7. Solubility of $\text{UO}_2(\text{am})$ (black solid line) versus pH at $I = 0.1$ (SIT corrected) when no oxidation of uranium is taking place. Dashed line: solubility of $\text{UO}_2(\text{am})$ at $E_h = -0.1 \text{ V}$ (measured E_h after 73 days for experiments set up a pH 11) and -0.4 V (measured E_h after 102 days for experiments set up a pH 12). Symbols: $\text{UO}_2(\text{am})$ solubility data reported in the literature and measured in this work. In brackets are expressed the reaction time in days.

The contribution of **PSI** to WP4 focuses on the influence of redox conditions on the immobilization of Neptunium in highly alkaline cementitious environments.

Neptunium is commonly believed to exist in oxidation states +IV and +V in a cementitious environment under reducing, respectively oxidizing conditions. However, the possible formation of anionic Np(VI) species ($\text{NpO}_2(\text{OH})_3^-$ and $\text{NpO}_2(\text{OH})_4^{2-}$) under oxidizing hyperalkaline conditions, in analogy to U(VI) , may significantly limit the stability field of Np(V) in favour of Np(VI) species. Whereas experimental data concerning the sorption of Np(V) by cementitious materials are scarce, sorption data concerning Np(IV) and Np(VI) are non-existing in the literature. In many sorption databases these gaps are filled by proposing estimates for the missing sorption data based upon chemical analogies (e.g. $\text{Th(IV)} - \text{Np(IV)}$ or $\text{U(VI)} - \text{Np(VI)}$) or based upon the electrostatic interaction energy (expressed by the effective charge, Z_{eff}) implying increasing sorption values in the series $\text{Np(V)} (Z_{\text{eff}}=2.2) < \text{Np(VI)} (Z_{\text{eff}}=3.0) < \text{Np(IV)} (Z_{\text{eff}}=4.0)$ (e.g. Wieland & Van Loon, 2002). The PSI contribution to WP4 aims at validating these assumptions.

During the first 2 years of Recosy, emphasis was mainly put on the determination of the Neptunium redox speciation under hyperalkaline conditions and on the development of experimental procedures to control the redox conditions and measure the Np redox state during solubility and sorption experiments. In addition the sorption of Np(V) on cementitious materials was investigated in detail. These latter studies showed that sorption distribution ratios (R_d values) measured for the Np(V) sorption onto C-S-H phases are surprisingly high ($R_d = (6 \pm 4) \cdot 10^5 \text{ L kg}^{-1}$) (see Figure 12) compared to R_d values for Th(IV) ($R_d = (4 \pm 2) \cdot 10^5 \text{ L kg}^{-1}$) and U(VI) ($10^3 \text{ L kg}^{-1} < R_d <$

10^5 L kg^{-1}) measured in our laboratory on the same C-S-H phases in the same experimental conditions. This observation is in contradiction with the assumption postulated above that R_d values increase with increasing Z_{eff} . Np(V) sorption kinetics and redox measurements suggested that a reduction of the Np(V) on the surface of the cement phases might take place.

The investigations during the third year of Recosy focussed on the determination of R_d values for Np(IV/V/VI) on C–S–H phases with varying C:S ratios in the pH range between 10.0 and 13.3 and a comparison of the R_d values obtained for these three redox states with R_d values obtained on the same C–S–H phases with Th(IV) and U(VI). Dithionite, at a concentration of $5 \cdot 10^{-3} \text{ M}$, was applied as a reducing agent to stabilize Np(IV) whereas $5 \cdot 10^{-3} \text{ M}$ hypochlorite was applied to stabilize Np(VI) in the C–S–H suspensions. The results of the experiments are discussed in detail in a scientific contribution in the present proceedings. In summary sorption values were found to be very high for all actinides (An(IV): $R_d = (5 \pm 3) \cdot 10^5 \text{ L kg}^{-1}$, An(V): $3 \cdot 10^5 \text{ L kg}^{-1} < R_d < 3 \cdot 10^6 \text{ L kg}^{-1}$, An(VI): $6 \cdot 10^2 \text{ L kg}^{-1} < R_d < 10^6 \text{ L kg}^{-1}$). The oxidation state analogy appears to be valid for the sorption on cementitious materials in the case of the tetravalent actinides, while this is not strictly true in the case of the hexavalent actinides. The postulated correlation of the actinides sorption on C–S–H phases with electrostatic interaction energy was found to be invalid.

In addition X-ray absorption spectroscopy investigations were carried out with the aim to obtain a mechanistic understanding of the sorption of Np(IV) on C–S–H phases and hardened cement paste (HCP). EXAFS measurements were carried out on the ROBL beamline at the European synchrotron radiation facility (ESRF), Grenoble, France. The results of this study are described in detail in (Gaona et al., 2011).

Principal Component Analysis (PCA) indicated that only two components are needed to explain the whole set of Np(IV) EXAFS data collected; these components were identified afterwards by Iterative Target Factor Analysis (ITFA) as Np(IV) in C-S-H 0.75 and Np(IV) in C-S-H 1.65. All remaining spectra could be fitted as linear combinations of these two “ende members”. This showed that, first, Np(IV) uptake by C-S-H phases is only affected by the C:S mol ratio of C-S-H and, secondly, that the local coordination environment of Np(IV) in HCP corresponds to that of Np(IV) in C-S-H phases, i.e. Np(IV) in HCP is predominantly taken up by a C-S-H phase with a C:S = 1.65.

Experimental data and fits of the EXAFS spectra of Np(IV)-C-S-H 0.75 and Np(IV)-C-S-H 1.65 are shown in Figure 8. The structural parameters are summarized Table 3. Fitting was performed by assuming Np–O, Np–Si, Np–Ca1 and Np–Ca2 back scattering pairs. The high Si-coordination numbers (N_{Si}) obtained for both Np(IV)/C-S-H systems (5.0 ± 1.5 and 3.6 ± 0.7) indicate the incorporation of Np(IV) into the C-S-H structure. If surface complexation were the dominant uptake process, then the number of neighbouring Si atoms would be significantly lower. The number of neighbouring Ca atoms (N_{Ca}) is higher in the Np(IV) loaded C-S-H phase with C:S = 1.65 compared to the Np(IV) loaded C-S-H phase with C:S = 0.75, which is consistent with the larger number of Ca atoms bound in the interlayer in C-S-H with C:S = 1.65

Table 3: EXAFS structural parameters determined for Np(IV) taken up by C-S-H 0.75 and C-S-H 1.65.

Sample	Np-O	Np-Si	Np-Ca	Quality of the fit
Np(IV)/C-S-H 0.75	$N_{O1} = 6.8 \pm 0.8$ $r_{O1} = 2.27 \pm 0.01 \text{ \AA}$ $\sigma^2 = 0.010 \pm 0.002$	$N_{Si-1} = 5.0 \pm 1.5$ $r_{Np-Si1} = 3.57 \pm 0.03 \text{ \AA}$ $\sigma^2 = 0.009 \pm 0.004$	$N_{Ca-1} = 2.2 \pm 0.9$ $r_{Np-Ca1} = 4.05 \pm 0.05 \text{ \AA}$ $\sigma^2 = 0.006^*$ $N_{Ca-2} = 2.1 \pm 1.0$ $r_{Np-Ca2} = 4.22 \pm 0.05 \text{ \AA}$ $\sigma^2 = 0.006^*$	$\Delta E = 5.8 \pm 0.7 \text{ eV}$ R-factor = 6.8 %
Np(IV)/C-S-H 1.65	$N_O = 7.7 \pm 1.2$ $r_O = 2.27 \pm 0.01 \text{ \AA}$ $\sigma^2 = 0.009 \pm 0.003$	$N_{Si} = 3.6 \pm 0.7$ $r_{Np-Si} = 3.59 \pm 0.03 \text{ \AA}$ $\sigma^2 = 0.009^*$	$N_{Ca-1} = 4.3 \pm 1.1$ $r_{Np-Ca1} = 4.12 \pm 0.03 \text{ \AA}$ $\sigma^2 = 0.006^*$ $N_{Ca-2} = 3.3 \pm 1.2$ $r_{Np-Ca2} = 4.28 \pm 0.05 \text{ \AA}$ $\sigma^2 = 0.006^*$	$\Delta E = 5.5 \pm 1.0 \text{ eV}$ R-factor = 9.0 %

* parameters fixed in the fit

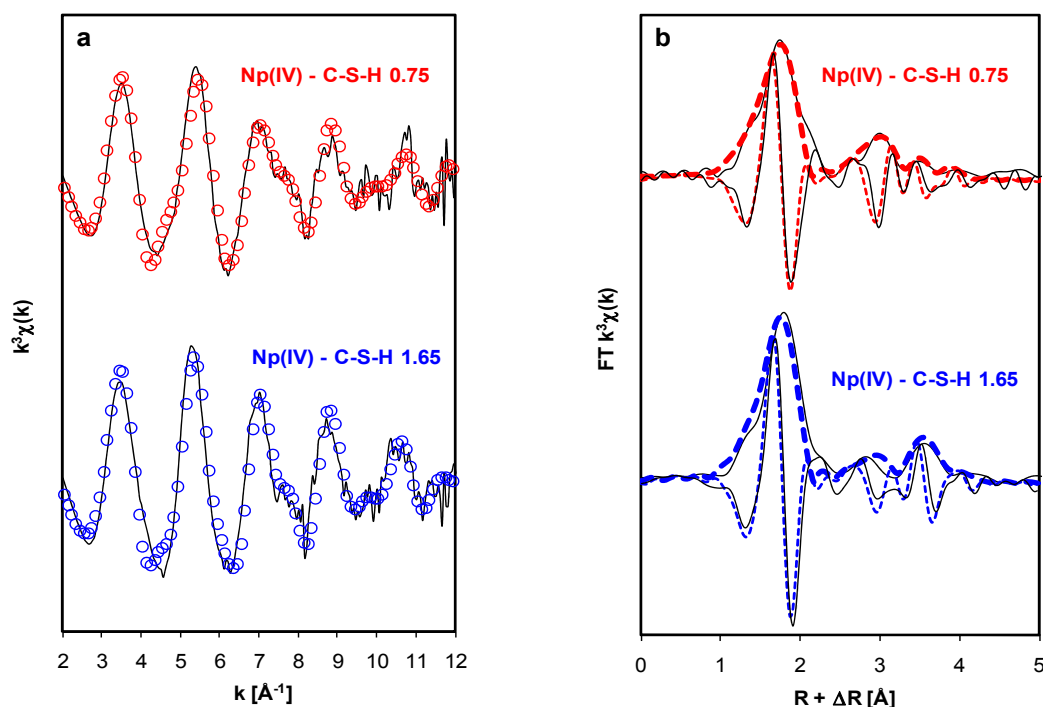


Figure. 8: Experimental (solid lines) and fits (circles and dashed line) of a) k^3 -weighted Np L_{III} -edge EXAFS spectra and b) the corresponding Fourier transforms (modulus and imaginary parts) for Np(IV) taken up by C-S-H with C:S = 0.75 and 1.65.

Acknowledgements

Manchester university would like to thank the United Kingdom Engineering and Physical Sciences (DIAMOND Universities Consortium) and Natural Environment (BIGRAD Consortium) Research Councils for funding this work.

References

- Carbol, P., Cobos-Sabaté, J., Glatz, J.-P., Ronchi, C., Rondinella, V., Wegen, D.H., Wiss, T., Loida, A., Metz, V., Kienzler, B., Spahiu, K., Grambow, B., Quiñones, J. and Martínez-Esparza, A. (2005) The effect of dissolved hydrogen on the dissolution of ^{233}U doped $\text{UO}_2(\text{s})$, high burn-up spent fuel and MOX fuel. SKB Technical Report TR-05-09.
- Fujiwara, K., Yamana, H., Fujii, T., Kawamoto, K., Sasaki, T., Moriyama, H. (2005) Solubility of uranium(IV) hydrous oxide in high pH solution under reducing conditions. *Radiochim. Acta.*, 93, 347-350.
- Gaona, X., Dähn, R., Tits, J., Scheinost, A., and Wieland, E. (2011). Uptake of Np(IV) by C–S–H phases and cement: an EXAFS study. *Environ. Sci. Technol.*, Submitted.
- Ollila K. (2002) Uranium solubility. In: Nuclear Waste Managements in Finland. Finalreport of Public Sector's Research Programme, JYT 2001 (Ed. K. Rasilainen), Ministry of Trade and Industry, Helsinki, Finland, pp. 77-79.
- Rai, D., Felmy, A. R., Ryan, J. L. (1990) Uranium (IV) hydrolysis constants and solubility product of $\text{UO}_2 \cdot x\text{H}_2\text{O}(\text{am})$. *Inorg. Chem.*, 29, 260-264
- Ryan, J. L., Rai, D. (1983) The solubility of uranium(IV) hydrous oxide in sodium hydroxide solutions under reducing conditions. *Polyhedron*, 2, 947-952.
- Scholz, F., Meyer, B. (1998). Voltammetry of solid microparticles immobilized on electrode surfaces. In: *Electroanalytical Chemistry, A Series of Advances* (A.J. Bard, I. Rubinstein, ed.) Marcel Dekker, Vol. 20, pp. 1-86.
- Torrero, M. E. (1995) Estudio de la disolución del UO_2 como análogo Químico de la matriz del combustible nuclear gastado. Influencia de los principales parámetros fisicoquímicos que definen los repositorios en medios salino y granítico. Universidad de Barcelona, Thesis, Barcelona, Spain.
- Wieland, E. and van Loon, L. R. (2002). Cementitious Near-Field Sorption Data base for performance Assessment of an ILW Repository in Opalinus Clay. PSI Report. Nr. 03-06, Paul Scherrer Institute, Villigen-PSI, Switzerland and Nagra Technical Report NTB 02-20, Nagra, Wettingen, Switzerland
- Yajima, T., Kawamura, Y., Ueta, S. (1995) Uranium(IV) solubility and hydrolysis constants under reduced conditions. *Sci. Basis Nucl. Waste Management XVIII, Symp. Proceedings*, 353, 1137-1142

WP 4.2.

CHEMICAL AND REDOX BEHAVIOUR OF THE INVESTIGATED RADIONUCLIDES IN THE DIFFERENT SYSTEMS THROUGH MICROBIAL MEDIATED PROCESSES

Introduction

Within WP 4.2 the participating institutes are focusing their work on the study of the microbial impact (**IPL**) and on the uranium redox state in-situ in biofilms with emphasis on biologically mediated redox processes (**HZDR**). The studies are carried out on isolated microorganisms as well as on biofilms. Biofilms are composed of bacteria, fungi, algae, protozoa, exopolymeric substances (EPS), corrosion products and 50–95% water. They are ubiquitous and have to be considered as an important factor in natural biogeochemical processes influencing the redox state of radionuclides. They show a multiplicity of interactions with metals and contribute to metal mobility or immobilization.

Work performed by partners

The activities of **HZDR** during the third year of ReCosy were focused on biologically mediated redox processes of biofilms growing in the nuclear waste repository research tunnel ONKALO (Finland), which will be part of the nuclear waste repository in the future.

Introduction

Since most surface and subsurface environments are inhabited by microorganisms, natural microbial communities (= biofilms) are considered, along with minerals, as an important factor influencing the transport of radionuclides in the environment. Microsensor measurements of the oxygen concentration, redox potential and pH are helpful in interpreting in-situ microbial metabolic processes in biofilms. Since microbial processes are sensitive to metals and their speciation, the bioavailability of the metals changes with redox potential, pH, and oxygen in a complex manner. Massive biofilms are growing next to a fracture zone in a granitic rock environment. at site 777 m of the tunnel. They were described by Pedersen et al. (2008) as a pink and solid slime, consisting of *Pseudomonas anguilliseptica*, *Arthrobacter bergeri*, *Hydrogenophaga sp.*, *Methylobacter tundripaludum*, *Rhodoferrax ferrireducens*, and *Haliscomenobacter hydrossis*.

Experimental

Biofilm samples were removed from the tunnel wall at the 777 m position and exposed into a rectangular cell with an outer dimension of 121 x 42 x 15 mm. During the sensor measurements, 150 ml of the groundwater as a blank solution from the site was pumped through the cell in a closed circuit with a flow velocity of approximately 4 mL/min. For the sensor measurements a miniaturized platinum redox microelectrode, oxygen microsensor of the Clark-type and a miniaturized conventional pH electrode, each with a tip diameter of 10 µm, were used. After the values were recorded, uranium was added in ecologically relevant concentrations (4×10^{-5} M) to the groundwater solution. Microsensor measurements were recorded 22 and 42 hours after the addition of uranium. Samples of the groundwater solution were taken before and after the addition of uranium as well as at the end of the experiments. The samples were acidified in-situ and analyzed for determination of the inorganic elements by Inductively Coupled Plasma Spectrometry. The anions were determined by Ion Chromatography. The analytical data of the groundwater sample was used for the calculation of the predominance fields of different uranium species in the pH-Eh diagram for the U-S-O-H-C system at 15°C by using the geochemical speciation code “Geochemist’s Workbench” Version 8.0.8 / ACT2 Version 8.0.8. For Energy-filtered Transmission Electron Microscopy (EF-TEM) and by electron energy loss spectroscopy (EELS) studies a biofilm sample was fixed in-situ with 1 % (vol/vol) glutardialdehyde at the end of the experiments and prepared afterwards following the routine embedding protocol with minor modifications as described by Lünsdorf et al. (2001). EF-TEM offers the possibility to systematically study and analyse the ultrastructure and elemental composition of nanoscale mater by electron energy loss spectroscopy (EELS).

Results

Several microprofilings of the redox potential and pH were performed in the biofilm sample, placed in the flow cell. Before the addition of uranium to the groundwater, which was pumped through the biofilm in a closed circle, the results showed an average value of $+70 \pm 2$ mV, including a correction factor of + 239 mV after Stumm and Morgan (1996) and a pH of 5.37. The values measured in the groundwater differed significantly. The results showed a pH of 8.68 and a redox potential of +491 mV. The redox potential of the groundwater is approximately 420 mV lower than in the biofilm. The difference of the pH amounts more than 3.5 units. These results clearly demonstrate that the geochemistry inside a biofilm is totally different compared to the surrounding water/environment. With regard to the migration and the retention of radionuclides these differences are of great importance. In uranium contaminated waters the formation of possible uranium species are dependent on the redox potential and the pH. Changes of these parameters will have the consequence of the formation of solid uranium(IV) and uranium(VI) species as precipitates in the determined biofilm. In our experiments microsensor measurements were performed 42 hours after the addition of uranium, showing a significant change of the parameters. The redox potential within the biofilm decreased to -164 mV with an increase of the pH at the same time to 7.27. The low redox potential indicates that reducing conditions are present, probably catalyzed by microorganisms. For a better interpretation a pH-Eh diagram for the U-S-O-H-C system at 15°C was constructed by using the geochemical speciation code “Geochemist’s

Workbench” Version 8.0.8 / ACT2 Version 8.0.8. The analytical data of the uranium contaminated groundwater was used for the calculation of the predominance fields of different uranium species. The default data base used was the thermo.dat accompanying code, supplemented by the most recent NEA database for uranium (Guillaumont et al., 2003), and by solubility data for Bayleyite from Gourman-Lewis et al. (2008). The theoretical predominance fields of solid uranium species under the ambient condition found in the contaminated groundwater are defined clearly in geochemically different areas: The first area is characterized by a redox potential of approximately $< 1V$ and a $pH > 4.0$. This area is dominated by the solid uranyl carbonate Rutherfordine $(UO_2)CO_3$ and the magnesia bearing uranyl carbonate mineral Bayleyite $[Mg_2(UO_2)(CO_3)_3 \cdot 18(H_2O)]$ at a $pH > 4.2$. The second area is characterized by a redox potential of approximately $< +320$ mV and a pH which varies between 0 and 5.8. Assuming reducing conditions, the formation of Uraninite, a uranium(IV) oxide (UO_2) mineral, was predicted. The results of the redox potential measurements of the biofilm 42 hours after the addition of uranium to the groundwater were plotted together with the pH into the calculated pH-Eh diagram for the U-S-O-H-C system. As shown in Fig. 3, the plots appear in the area of Bayleyite, indicating that an uranium(VI) solid mineral may have been formed in the contaminated groundwater. For great importance is the localization of the measured biofilm plotted into the eh-pH diagram. Due to the fact that after the addition of uranium the redox potential inside the biofilm decreased and the pH increased the formation of a solid uranium(IV) mineral within the biofilm seems possible after thermodynamically calculations.

The retardation of uranium in the biofilm was determined by Energy-filtered Transmission Electron Microscopy (EF-TEM) and Electron Energy Loss Spectroscopy (EELS). Elongated particles of high electron density were observed in the cytoplasm of some rod shaped gram negative bacteria, which were often found associated with large rod shaped bacteria. Analysis of the elongated particles by EELS provided spectroscopic evidence for the presence of uranium immobilization, showing unequivocally uranium ionization intensity peaks of O4,5- and N6,7-edges. Distribution analysis of uranium, phosphorus and calcium clearly showed, that a solid uranium mineral has formed intracellular, which indicates the presence of a solid U-phosphate mineral similar to Autunite $(Ca[UO_2]_2[PO_4]_2 \cdot 10-12H_2O)$.

The scientific activities of **IPL** during the third year within ReCosy comprised the behaviour of $^{99}Tc(VII)$ in the system iron-bearing mineral-Na brine-microorganism under aerobic conditions. In order to estimate the effect of minerals/mineral surface on redox, sensitive radionuclide (technetium) sorption has been studied. To explore the interactions of Tc with iron-bearing minerals, series of laboratory batch-type experiments were carried out. The effect of pH on the radionuclide transport/retention was taken into consideration as well as the exposure time and the microbial activity. The composition of two powdered iron oxides (purchased from FSU) was verified using Mössbauer spectroscopy. Mössbauer spectra indicated the presence of hematite (Fe_2O_3) (first sample) and wustite and magnetite (second sample). For wustite, Fe(II) and Fe(III) components of Mössbauer spectra in the ratio 18:82 were detected in agreement with wustite formula $Fe_{(1-x)}O$. Two subspectra, which are attributed to tetrahedral and octahedral sublattices are characteristic of magnetite. The ratio of area of magnetite

subspectra is 45:55. Tetrahedral sublattice of magnetite is occupied by Fe(III) ions while octahedral is occupied by Fe(II)+Fe(III) ions. Thus, Fe(II) may be found either in magnetite and wustite.

For the batch experiments under ambient conditions, 0.1 g of mineral hematite (ms) and 0.2 g of mixture of wustite and magnetite (resuspended in 0.08 M Na brine solution) were used. The colloidal mineral suspensions were obtained by adding the volume (V) of 5 mL of Na-brine solution to hematite. The volume to mass ratio was 50 in the series of experiments (V/ms=50) with hematite. The solution volume to mass ratio (V/ms=250) was 250 in the experiments with mineral wustite/magnetite. After addition of ammonium pertechnetate to the suspension pH values reached 7.5 ± 0.5 . Bacteria and fungi, isolated from groundwater of two different boreholes and from soil of known physical-chemical properties, were tested under different conditions. Microbes (*Streptomyces sp.*, *Aspergillus niger*, *Arthrobacter globiformis*, *Cellulomonas cellulans*, *Bacillus mycoides*, *Fusarium oxysporum*, *Penicillium sp.*, *Rhodococcus sp.*, *Spicaria sp.*) were selected for batch-type experiments because of their more pronounced peculiarities: ability to reduce nitrate, H₂S formation, organic acid production and resistance to different pH values. The ability of selected microorganisms to participate in adsorption processes of ⁹⁹Tc(VII) on hematite and wustite/magnetite was investigated by batch experiments. Results of the combined effect of microorganisms and iron-bearing minerals on Tc(VII) sorption peculiarities using batch-type experiments have shown that bacteria isolated from fluidized soil *Arthrobacter globiformis* and *Cellulomonas cellulans* practically did not have any influence on Tc(VII) sorption onto hematite under aerobic conditions, while *Micromicete Fusarium Oxysporum* of the same substrate altered sorption to approximately 85% compared to that in the system without microorganisms. Differences in Tc(VII) sorption processes onto hematite due to microbial activity of microorganisms isolated from the groundwater borehole were observed as well. Presence of microorganisms *Penicillium sp.*, *Rhodococcus sp.* and *Streptomyces sp.* in the tested system induced Tc(VII) sorption onto hematite up to 80-85%. The effect of microbial activity of *Bacillus mycoides*, *Aspergillus niger* and *Spicaria sp.* on Tc(VII) sorption onto hematite was lower 60%, 27% and 17%, respectively. Thus, we can state that mineral hematite at neutral or slightly alkaline pH under aerobic conditions is attributed to minerals which do not adsorb Tc(VII). Stimulation of Tc(VII) sorption onto hematite is achieved because of presence of specific microorganisms.

References

- Guillaumont R., Fanghänel T, Fuger J, Grenthe I, Neck V, Palmer DA, Rand MH (2003): Update on the chemical thermodynamics of uranium, neptunium, plutonium, americium and technetium. Chemical Thermodynamics Vol. 5 (OECD Nuclear Energy Agency, ed.), Elsevier, Amsterdam.
- Nguyen AN, Silvac RJ, Weed HC, Andrews JW (1992) Standard Gibbs free energies of formation at the temperature 303.15 K of four uranyl silicates: soddyite, uranophane, sodium boltwoodite, and sodium weeksite. Journal of chemical thermodynamics, Vol. 24 (4), 359-376.

Pedersen K, Arlinger J, Eriksson S, Hallbeck M, Johansson J, Jägevall S, Karlsson L. "Microbiology of Olkiluoto Groundwater". Results and Interpretations 2007. POSIVA Working Report 2008-34. Olkiluoto, Finland.

Stumm W and Morgan JJ. Aquatic Chemistry, Chemical Equilibria and Rates in Natural Waters. 3rd ed. John Wiley & Sons, Inc., New York, 1996.

WORK PACKAGE 5: REDOX PROCESSES IN RADIONUCLIDE MIGRATION

Juhani Suksi

University of Helsinki, Department of Chemistry, Laboratory of Radiochemistry,
Finland

Introduction

WP5 studies the behaviour of redox-active radionuclides Tc, Np, U, Pu, I and Se with an aim to determine the redox impact on their transport. Redox impact is studied in different redox-milieus anticipated in and around planned waste repositories. The target of the study is to clarify the role of redox reactions in radionuclide transport and retardation in particular. The transport has been studied in diffusion and sorption experiments in different experimental designs with clay and fracture surface materials. In addition to laboratory experiments redox impact has been studied directly in nature examining transport observations of natural U at the selected disposal site in Finland and in and around a phosphogypsum stack in Cyprus. Moreover, the transport of artificial radionuclides released into the environment has been studied at the contaminated site in Mayak, Russia. In all above mentioned cases retardation of radionuclides has been observed but whether the redox-state of the system has affected oxidation states of radionuclides is not yet clear. The status of the investigations was presented by the partners in the 3rd ReCoSy AWS in Balaruc-les-Bains, France. The investigations are high-lighted below.

Work performed by partners

Near natural laboratory experiments

KIT-INE has performed reduction kinetic experiments of Tc(VII), U(VI) and Np(V) in natural groundwater from the Grimsel Test Site (GTS, Switzerland) in presence of fracture filling material simulating low ionic strength glacial melt water intrusion conditions (pH 9,6; ionic strength ~1mM). This groundwater was also used throughout the Inter Comparison Exercise (ICE) under the reference number NAT 3. The batch-type studies show a decreasing E_H from +25mV to -70mV (pH 9.6 - 9.1) over the experimental duration of 7500h. Comparison with thermodynamic calculations reveal a stability of U(VI) species and no sorption could be observed, whereas the pe/pH

conditions are close to the borderline of the $\text{TcO}_4^-/\text{TcO}_{2(s)}$ transition. Observed slightly lower ^{99}Tc distribution coefficients for fracture filling material (FFM) from Grimsel compared to Äspö can be correlated to the FFM Fe(II) inventory. In the case of $^{237}\text{Np(V)}$, a decrease in concentration after ~ 300 h can be explained by a slow reduction to Np(IV) and subsequent sorption to mineral surfaces in accordance with the evolution of pe/pH. The batch sorption/reduction data was compared with distribution coefficients re-calculated from column migration studies on an over cored natural fracture from Äspö (Sweden) having the full 3D geometry reconstruction through computer tomography (CT) data and thereby determined connected porosity of 0.68%. The $\log(K_d)$ values of -1.8 to -2.7 determined for ^{237}Np in the column migration studies are within the analytical uncertainty comparable to the batch-type studies with $\log(K_d)$ of -2.0 to -2.5 determined under the same contact time.

CEA continued investigations on behaviour of U and long-lived redox active fission products Se and I in contact with Callovo-Oxfordian (CO_x) argillite samples. Through-diffusion and batch experiments were performed in N_2/CO_2 glove box in physico-chemical conditions as close as possible to those prevailing *in situ*. The initial redox states of the elements were I(-I), Se(IV,VI), and U(VI). A special care was paid to monitor possible changes in the redox state, especially for I and Se, using an anion chromatographic technique. The experiments with U(VI) showed that diffusion into the rock sample would occur mainly as oxyanions with carbonate and calcium complexes evidenced by TRLFS in the high-concentration container without significant retardation but with strong steric and anion exclusions. Even though in batch experiments no clear I(-I) affinity towards CO_x was observed, in contrast in through- and out-diffusion experiments low but significant retardation was observed with respect to $^{36}\text{Cl}^-$, a non-reactive anion, for initial I(-I) concentrations less than or equal to 10^{-4} mol/L, and both with and without the presence of a reducing species, $\text{S}_2\text{O}_3^{2-}$. Despite the reducing conditions Se (VI) diffused more or less like $^{36}\text{Cl}^-$, with no change of its redox state, as previously was shown in the Boom Clay case. On the other hand, Se (IV) exhibited a strong affinity towards the CO_x , in inverse ratio to its initial concentration, until suspected precipitations in more reduced forms, at a concentration of 10^{-6} mol/L, both in batch and diffusion experiments.

Natural system studies

UH continued investigations on U decay series disequilibrium in fracture surface material (calcite, kaolinite, chlorite and clays) from groundwater infiltration area in Olkiluoto. U series disequilibrium was studied to outline infiltration induced mobilisation of U and to find fractures where U can be seen to immobilise. Both phenomena can be easily shown by observations of U movement relative to the immobile U series ^{230}Th . Because of the long half-life of ^{230}Th ($T_{1/2}=75200$ y) the influence of glacial melt water infiltration and related redox-front can be studied. New and repetition samples including outcrop samples were analysed. Outcrop samples are important because they represent the most oxidising part of the redox-front. In most of the samples measured disequilibria were shown to have formed in steady-state flow field. Part of the samples showed disequilibrium which is not possible in steady-state

flow, i.e. infiltration different from currently occurring one may have taken place (probably melt water intrusion) and caused U remobilisation modifying U series nuclide distribution. U remobilisation is possible if flow conditions change which in turn may cause changes in redox-conditions thus explaining U mobilisation. U series disequilibria obtained in the outcrop samples clustered in the model diagram in the upstream side of the redox-front as was expected. An interesting observation was that U mobilisation was observed in fractures where pyrite was present. Collaboration was started with the University of Cyprus on uranium occurrence in natural organic material sampled from suboxic phosphogypsum. An objective was to utilise the results from U bearing Tertiary sediments in Ruprechtov natural analogue study site (Czech Republic) where collaboration between UH, GRS and NRI is underway (not financed by ReCoSy). Reductive U retardation is studied by analysing U oxidation states in U accumulated in the sediment. Analysis of the U isotopic results is underway.

II-HAS has investigated reduction driven retention of I, Tc and U in a redox gradient in clay rock. Experimental design consists of break-through diffusion cells where a redox gradient is established by different redox conditions in the respective ends of the cell. The cell was equilibrated with radionuclides keeping redox conditions constant along the clay sample. In the last year c.a 4 years long uranium break-through experiments performed on Boda Claystone samples were evaluated. In particular, measuring cells were disassembled, and bore core discs were analysed by laser ablation ICP-MS to determine the distribution of uranium along the migration path. $\text{Fe}^{2+}/\text{Fe}^{3+}$ ratios in the surface layers of the bore cores were also analysed by Mössbauer spectroscopy to determine whether any redox change has taken place in the iron containing minerals during the experiments. LA-ICP-MS measurements attested that uranyl ions had a strong sorption, by penetrating through only ca. 4 mm into the bore core sample, and the uranium concentration shows an exponential decrease perpendicular to the surface. The Mössbauer analysis showed that redox processes had not taken place in the iron containing minerals in the c.a. 2 mm thick surface layers of the sample discs. The apparent interpretation of these results is that redox $\text{Fe}^{2+} \rightleftharpoons \text{Fe}^{3+}$ redox processes do not play primary role in the strong sorption of uranium. Collaboration with UH on further post-mortem analyses has been started.

UCYPRUS continued investigations to assess the impact of redox conditions on the stability of the phosphogypsum stack (e.g sulfate reduction) and U(VI). The redox conditions are correlated with the distribution and mobility of redox sensitive radionuclides. Samples were collected directly from the phosphogypsum stack and from fluids from three different sub-areas of the phosphogypsum stack. The solid samples were investigated by TGA, XRF and XRD regarding their water content and composition. The stack fluids have been analyzed regarding pH, EC, Eh, the main constituents and uranium concentration in solution. In addition to *in situ* measurements pH, E_H and solubility experiments were performed also in simulated laboratory systems. Generally, in the open phosphogypsum stack oxidizing conditions predominate stabilizing sulphur and uranium in their hexavalent oxidation state. After the application of a soil/vegetative cover and in the presence of natural organic matter, anoxic

conditions prevail ($E_H < -70$ mV) probably resulting in S(VI) and U(VI) reduction to S(-II) and U(IV), respectively.

UCYPRUS and **UH** started collaboration to study the redox-state of U in the samples. The measurements have shown that uranium chemistry differs in phosphogypsum without natural organic matter (NOM) contamination and phosphogypsum containing relatively large amounts of NOM (1-3%). The $^{238}\text{U}/^{234}\text{Th}$ -ratio in NOM-containing phosphogypsum is significantly higher than in non-contaminated phosphogypsum, indicating similar chemical behaviour of uranium and Th and hence possible reduction of U(VI) to U(IV) by NOM. However, almost no reduced U(IV) was found in the extracted uranium from the NOM-containing phosphogypsum. This was ascribed to possible U(IV) oxidation by atmospheric oxygen during sampling and storage of the sample.

MSU has investigated actinide speciation in samples collected at the Mayak site by the combination of alpha track analysis, SEM-EDX and various synchrotron based methods with microfocusing beam, i.e. μ -XAFS, μ -XRF. Local distribution of U and Pu in organic rich pond bottom sediments does not match which suggests differences in their speciation. Uranium is present in various oxidation states that indicates the formation of both chemisorbed U(VI) species and kinetically stable U(IV) oxide particles. The nano-SIMS measurements are planned in near future to obtain high resolution elemental maps.

WORKPACKAGE 6: REDOX PROCESSES AFFECTING THE SPENT FUEL SOURCE- TERM

D. H. Wegen^{1*}, P. Carbol¹, A. Seibert¹, T. Gouder¹, T. Petersmann¹, R. Pehrman²,
M. Trummer², C. Lousada², M. Jonsson², A. Loida³, N. Müller³, V. Metz³, E. Bohnert³,
B. Kienzler³, D. Cui⁴, K. Spahiu⁶, D. Dobrev⁵, R. Červinka⁵, A. Vokál⁵

¹ Institute for Transuranium Elements (ITU), (DE)

² KTH Chemical Science and Engineering, Nuclear Chemistry, Royal Institute of
Technology, (SE)

³ Institut für Nukleare Entsorgung (INE), KIT, (DE)

⁴ Studsvik Nuclear AB, (SE)

⁵ Nuclear Research Institute Řež plc (NRI), (CZ)

⁶ Svensk Kärnbränslehantering AB (SKB), (SE)

Introduction

The source term from spent fuel dissolution is subject to considerable uncertainties, both with respect to the presence and extent of oxidative dissolution processes of the spent fuel itself and the coupling with processes associated with the iron canister. Related problems to be examined in this work package are the representativeness and reliability of laboratory data with respect to the impact of unavoidable minor concentrations of oxygen also in inert-gas boxes used, the potential reactivity and its outcome of hydrogen from container corrosion in combination with high burn-up spent fuel, possible galvanic coupling of spent fuel and container material and the retention of redox sensitive radionuclides by relevant minerals, especially by steel container corrosion products.

A set of investigations has been conducted with the aim of getting better insight into redox processes determining spent fuel and iron canister corrosion. **ITU** reports on studies on spent fuel in presence of corroding Fe, on corrosion of spent fuel in presence of H₂ and on fuel corrosion studies on thin film model systems. The redox reactivity of doped UO₂ in view of effects on the reactivity towards H₂O₂ has been studied at **KTH**. The reductive trapping of actinides in container corrosion products during spent fuel corrosion is investigated by **INE**. **Studsvik** reports on the redox chemistry at the near field of repository and the influences of iron canister material and hydrogen. Redox conditions near waste packages were studied by **NRI**.

Work performed by partners

Studies on spent fuel in presence of corroding Fe and on thin film model systems

Last year experiments with a new developed electrochemical cell for thin film applications start were started (Buckau et al. 2010). This cell is connected to the vacuum system of a XPS/UPS spectrometer. The construction allows a transfer of electrodes from the cell into the spectrometer without any exposure to air. A further advantage is the low resistance of thin UO_2 films. On the other hand is there a risk of O_2 inleakage because it is not installed inside a glove box.

Special manufactured carbon steel supports were fully or partially coated with UO_2 by reactive sputtering and then used as electrodes. The stoichiometry of the films was checked by XPS analysis before and after the experiments. After 2 minutes pre-cathodisation at -1.3 V open circuit potentials (OCP) were measured over 20 hours on uncoated, partially coated and fully coated carbon steel specimen in 10 mM NaCl solution under Ar-purging at 19°C-22°C (Figure 1).

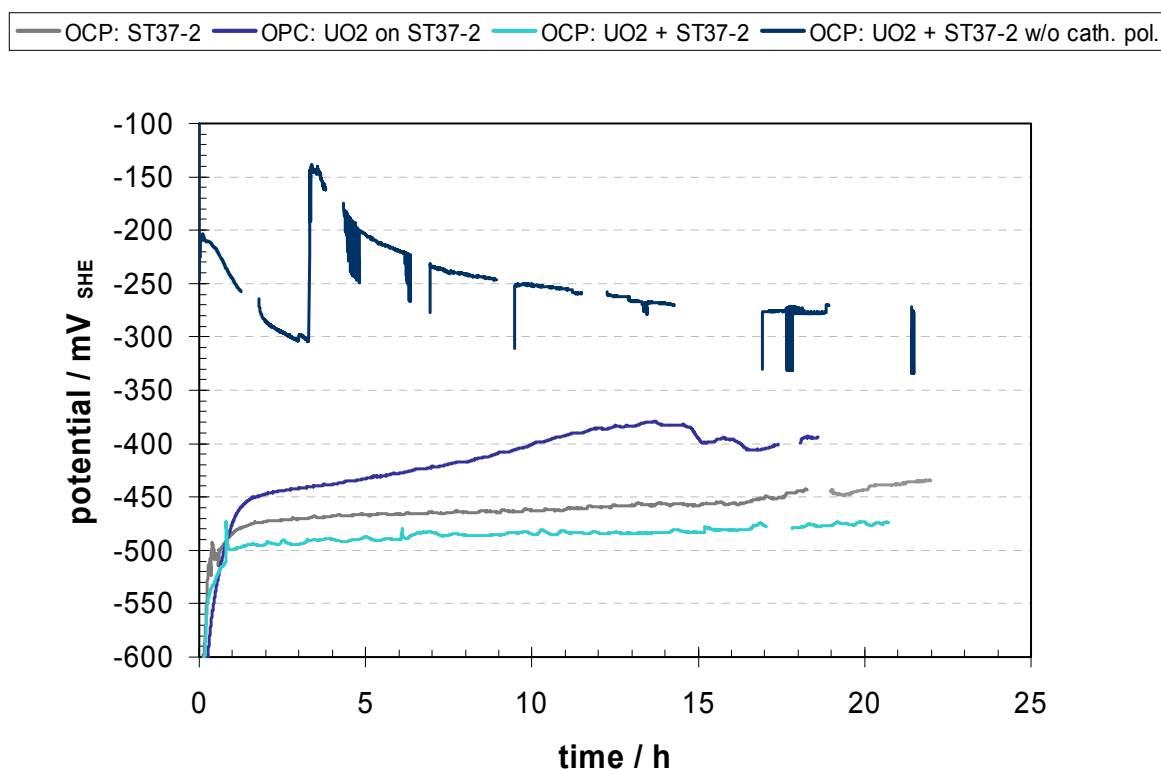


Figure 1: Open circuit potentials (OCP) measured on carbon steel and on fully and partially UO_2 coated carbon steel in Ar-purged 10 mM NaCl solution at RT with and without pre-treatment (cathodic polarisation). Curves from bottom to top: OCP of partially UO_2 coated carbon steel; OCP of carbon steel; OCP of fully UO_2 coated carbon steel; OCP of fully UO_2 coated carbon steel without cathodic polarisation before measurement.

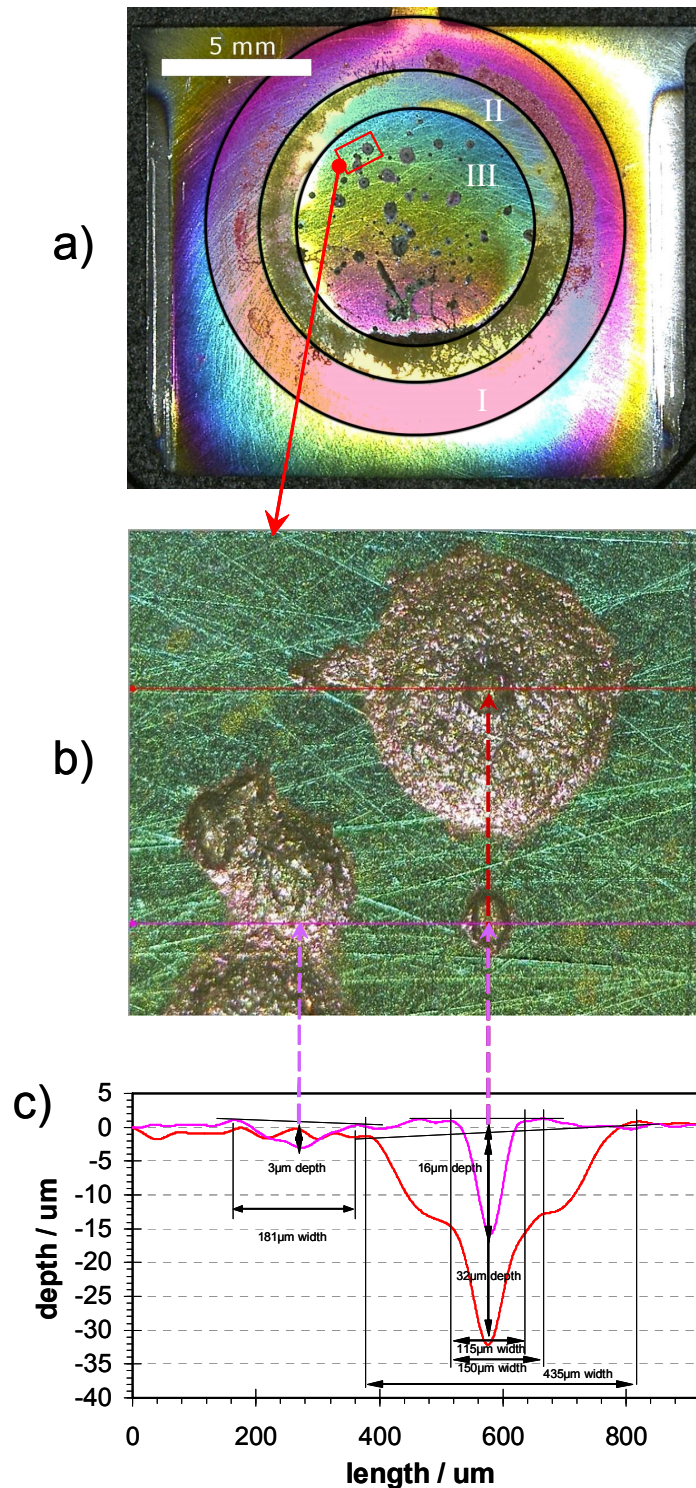


Figure 2: Optical microscopy of the UO_2 coated carbon steel after the experiment (a). The outer reddish zone I marks the area where the sealing (O-ring) touched the sample surface. In the second yellowish zone II a crevice was formed between the cell and the sample surface. The inner ring III shows the area where the surface was in direct contact with the solution. The macrograph b) shows pits which have formed and the related depth profile in c).

XPS measurements on the uranium oxide surface showed that UO_{2+x} was reduced to UO_2 after the experiment. It could not be distinguished if this reduction occurred during the pre-cathodisation or due to the galvanic coupling with iron. Therefore the experiment was repeated with a fully UO_{2+x} covered carbon steel sample without pre-cathodisation. The measured OCP is shown in Figure 1 (upper curve). The OCP is 150 to 200 mV higher than in the former measurements. An air inleakage occurred after ~3.5 hours and results in a sharp increase of the potential. After 4 hours the potential became instable and showed scattered data. This was a first hint for ongoing localised corrosion processes. During the time where the OCP curves show gaps impedance measurements were performed. They show pseudo inductive behaviour of the corroding sample which is also a sign for localised corrosion. The final proof was the optical examination after the experiment (Figure 2). There are three zones which also reflect the influence of the experimental set-up on the corrosion processes. In the outer zone I the sample surface was touched by the sealing (O-ring) of the measurement cell. In the 12 to 3 o'clock position slight crevice corrosion is visible which occurred in the very narrow gap between the inner part of the O-ring and the sample surface. The next inner zone II is characterised by a gap formed between the acrylic glass of the cell and the sample (some tenth millimetres) with much more pronounced crevice corrosion. Depth profiles show here a loss of 3 – 5 μm . In the central zone III contact between surface and solution is not hindered. Here localised pitting corrosion occurred with pit depth up to 40 μm .

ICP-MS and ICP-OES analysis shows much more iron than uranium in solution. This means that the ongoing processes and also the OCP are governed by steel corrosion. The measured OCP is in all cases below the potential of surface oxidation for UO_2 (of around -0.150 V_{SHE}).

Table 1: Solution analysis results obtained by ICP-OES and ICP-MS from experiments with fully UO_2 covered carbon steel samples.

	ICP-MS	ICP-OES	
	[U]	[U]	[Fe]
Covered with cathodisation		< 5 $\mu\text{g/l}$	0.1 mg/l
Covered w/o cathodisation	4 $\mu\text{g/l}$	< 5 $\mu\text{g/l}$	21.5 mg/l

XPS measurements were carried out on the UO_{2+x} film on steel before and on the sample surface after the experiment (without pre-cathodisation). Iron oxides and stoichiometric UO_2 could be identified. The slightly oxidised uranium oxide layer was reduced.

The experiments have shown that the corrosion processes are ruled by iron corrosion and in contact with iron is a reduction of UO_{2+x} to UO_2 possible.

Corrosion of spent fuel in presence of H_2

The corrosion experiments of the high burn-up structure zone of commercial spent nuclear fuel in presence of 4.1 MPa hydrogen gas pressure, i.e., a dissolved H_2 concentration of 33 mM, has continued as planned at ITU. A detailed description of the fuel, the inventory and the initial corrosion results for the first 60 days is given in Buckau et al. (2009). Results obtained in the period 502 to 1435 days are summarized in the following text. Detailed information of the experiment can be found in Fors et al. (2009).

Sampling

Leachates were sampled 10 times throughout the corrosion experiment; during filling (5 hours after wetting the fuel), and after 1, 7, 62, 63, 138, 265, 313, 316, 319, 329, 502 and 1435 days. The sampling sequence consisted of one rinse and two samples.

The long time-period of 933 days (day 502 to 1435) was required to study the long-time corrosion of the fuel after the rinse action. The rinse action, on day 313, was specifically made to decrease the concentration of all non-redox sensitive elements in the leachate making it possible to detect small concentration changes and thereby a small spent fuel corrosion rate. This strategy makes it possible to determine a reliable long-term spent fuel corrosion rate.

Sampling, analysis and evaluation of high burn-up rim UO_2 fuel leachate

The leachate from the HBU autoclave was sampled 1435 days after start of the experiment. The leachate sampling was performed according the procedure outlined in the 2nd AWS S+T report (Buckau et al. 2010). The first leachate sampled, the rinse sample, had an unusual light green colour. Also the second leachate, the pre-sample, had a weakly green colour, less pronounced in comparison with the rinse sample. These colour changes has not been observed during earlier samplings. The samples were taken out of the hot cell within 1 hour. The samples were extracted into new containers and sub-samples prepared (diluted, acidified and spiked with internal standard) for HR-ICP-MS analysis, within 19 days after sampling (ICP-MS was not available earlier). Additionally, sub-samples were prepared for γ -spectrometry measurements.

The leachates were analysed by HR-ICP-MS twenty days after sampling. The standard measurement and evaluation procedure, as described in the 2nd AWS S+T contribution (Bukau et al. 2010), was followed for HR-ICP-MS measurements, as well as, for γ -spectrometry.

E_h measurement

Redox potential measurements were made at each leachate sampling of the HBU corrosion experiment. The values were recorded but made no sense as they showed strongly positive potentials (in the range of +500 mV) which in no case corresponded with the low U concentrations and the relatively high concentration, $\sim 10^{-7}$ M, of Fe (as Fe^{2+}) in the leachate.

Having discovered that the second sampling valve had been opened during a time period of 1122 days, (in air hot cell) and that the E_h increased during the last

leachate sampling it was clear that the polarity of the E_h electrode had been switched. After inversion of the observed E_h values and correction with +221 mV (vs. SHE, at 21°C) all values for the complete experimental period of 0-1435 days made sense.

Results

The results of the measured redox potential, E_h , during the complete experimental period are shown in Figure 3. Only in two cases, on day 265 and 1435, no stable E_h values could be obtained during the leachate sampling. Since the E_h measurement occurs only during sampling, when the leachate passes the E_h measurement cell, the time is short (1-2 min) and might result in non-stable reading.

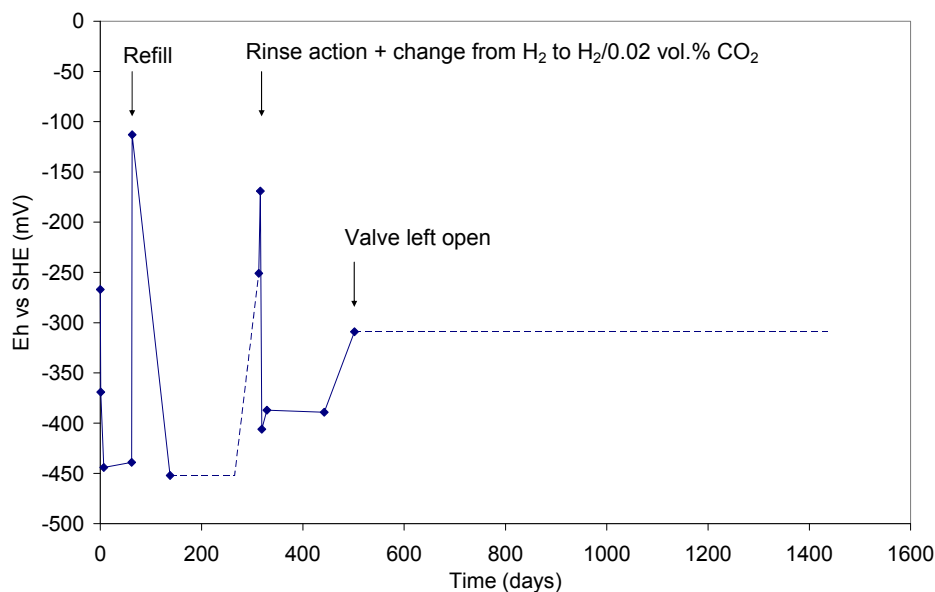


Figure 3: Redox potential measured during leachate sampling.

For comparison, in Figure 4 the concentration of the redox sensitive elements: Fe, Mo, U and Pu are shown together with the non-redox sensitive element Cs. It can be seen that the E_h correlates with the U concentration, meaning that when E_h is decreasing (more reducing conditions) the U concentration decreases as a consequence of U(VI) reduction to U(IV) and precipitation as $U(OH)_4(s)$. The uranium precipitation occurs, most probably, on the spent fuel surface.

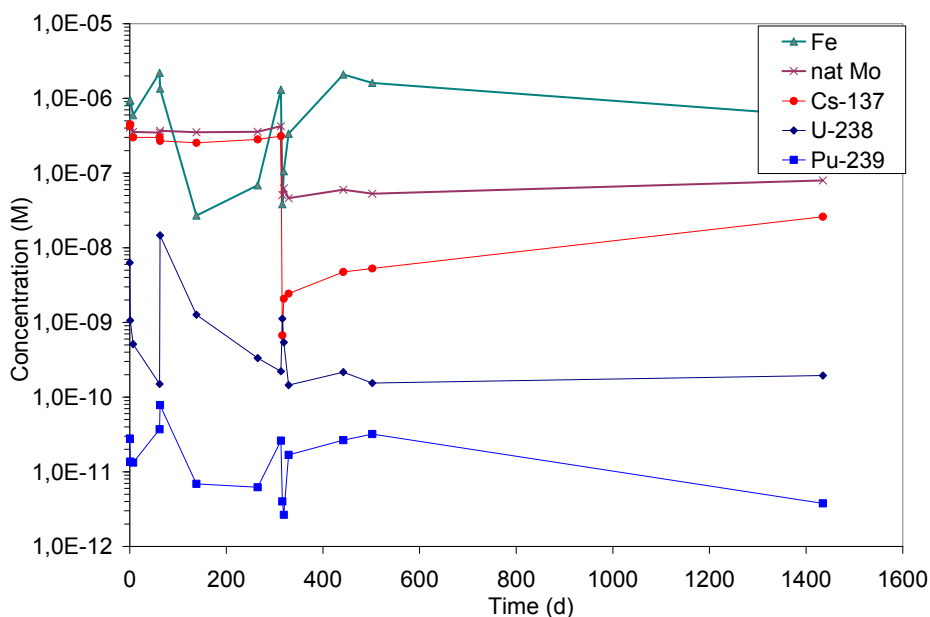


Figure 4: Concentration of elements and radionuclides in HBU-leachate as a function of corrosion time.

Disturbances in this mechanism occur when oxygen un-avoidably enters the autoclave during leachate refilling (day 63) and rinse action (day 313). After lowering the leachate concentration of radionuclides through the rinse action a small change in fuel corrosion could be monitored. The change of the gas composition from H_2 to $H_2/0.02 \text{ vol.}\% CO_2$ increased the HCO_3^- concentration by a factor of 10. It can be seen that during 933 days, period 502-1435 days, during which the second sampling valve was open (see section E_h measurements);

- $[^{137}Cs]$ increased about 5 times from $5.3 \cdot 10^{-9} \text{ M}$ to $2.6 \cdot 10^{-8} \text{ M}$
- $[^{238}U]$ changed slightly from $1.5 \cdot 10^{-10} \text{ M}$ to $1.9 \cdot 10^{-10} \text{ M}$
- $[^{239}Pu]$ decreased an order of magnitude from $3.1 \cdot 10^{-11} \text{ M}$ to $3.8 \cdot 10^{-12} \text{ M}$

While, during the same time period, the concentration of the inactive redox sensitive elements (Fe, Mo) in the leachate changed as follows:

- $[Fe]$ decreased about 3 times from $1.6 \cdot 10^{-6} \text{ M}$ to $5.8 \cdot 10^{-7} \text{ M}$
- $[Mo]$ changed from $5.3 \cdot 10^{-8} \text{ M}$ to $8.0 \cdot 10^{-8} \text{ M}$

The changes are significant in relation to measurement uncertainty, but not in respect to the possible experimental errors during sampling and especially in relation to the open sampling valve letting tiny amounts of oxygen intruding the autoclave. Anyhow, the increased concentration of Cs and U, period 502-1435 days, indicate an oxidation of virgin UO_2 matrix. The slightly oxidative conditions are evident by the increased natural $[Mo]$. A decrease of $[Fe]_{\text{total}}$ also confirm slightly oxidising conditions inside the autoclave, through oxidation of Fe^{2+} to Fe^{3+} which, due to the low solubility of $Fe(OH)_3(s)$, precipitates. A decreased $[Pu]$ by one order of magnitude can only be explained by a co-precipitation of Pu with $Fe(OH)_3(s)$.

Conclusions

The fuel corrosion experiments give a consistent picture between the changes of the redox potential and the co-variation of the redox sensitive elements. In this experiment the E_h measurement function as an oxygen sensor. It could be concluded that a change of the HCO_3^- concentration by a factor of 10 did not affect the corrosion of the high burn-up UO_2 fuel.

Even though, there was an intrusion of O_2 into the autoclave, during the period 502-1435 days (a period of 933 days), the following conclusions can be made:

- [Cs] was only doubled
- [U] increased by 25%, to $2 \cdot 10^{-10}$ M
- [Pu] decreased 10-fold, to $6 \cdot 10^{-12}$ M
- $^{239}\text{Pu}/^{238}\text{U}$ in the leachate was found to be 0.019 while $(^{239}\text{Pu}/^{238}\text{U})_{\text{fuel}}$ is 0.007

The ratio $(n_{\text{Cs-137}}/n_{\text{U-238}})_{\text{leachate}}$ was found to be 134 while $(n_{\text{Cs-137}}/n_{\text{U-238}})_{\text{fuel}}$ is 0.003. This divergence of a factor of $5 \cdot 10^4$ indicate a mechanism that reduces the amount of pre-oxidised (start of experiment) and oxidised (radiolytically and through O_2 -intrusion) uranium during the experiment. Of course, the UO_2 grain boundaries contain a higher caesium to uranium ratio, but not by a factor of $5 \cdot 10^4$. A comparison with corrosion of spent UO_2 fuel with a burn-up of 53 MWd/kg U in a flow-through reactor under oxidising conditions gave a $(n_{\text{Cs-137}}/n_{\text{U-238}})_{\text{leachate}}$ of 5.

Fuel corrosion studies on thin film model systems

ITU has prepared thin films of uranium oxides with fission product (fp) inclusions by sputter deposition from uranium metal, palladium and molybdenum metal targets in the presence of O_2 . These thin films can serve as model systems for spent nuclear fuel (Stumpf et al. 2009, 2010).

The corrosion processes and the influence of the Pd inclusions (as single model element for ϵ -particles) in these processes are investigated by open circuit potential (OCP) measurements under different gas atmospheres (air, Ar, Ar/ H_2). Samples with varying Pd concentration (0 – 30 %) are investigated.

Under oxic conditions (air) open circuit potentials above the threshold of UO_2 oxidation are obtained for all samples. With increasing the amount of Pd in the UO_2 matrix the OCP shifts from 0.260 V (UO_2) to 0.408 V (UO_2/Pd 30 %) and up to 0.505 V for the pure Pd-system. These values are comparable to literature data. The measurements under Argon show lower values which are anyhow still above the UO_2 oxidation threshold for all Pd doped systems and pure UO_2 .

Under Ar/ H_2 conditions the potential of both UO_2 and UO_2/Pd films is decreased. For UO_2 the OCP values are comparable to those under Ar, so the decrease is just due to the absence of oxidants. The presence of Pd leads to a much stronger decrease of the OCP, below the threshold of the surface oxidation of UO_2 , therefore fuel corrosion should be inhibited.

Switching between anoxic and reducing conditions shows that the UO_2/Pd system reacts on the presence and absence of H_2 . By now it is not clear if it is a completely reversible system: In the time scale of the measurement switching from Ar to Ar/ H_2 it was not possible to reach the OCP value determined in the experiment where Ar/ H_2 was applied without a pre-oxidation.

Further electrochemical investigations (like cyclovoltammetry) on the UO_2/Pd systems are ongoing.

In addition Mo doped films are produced. Molybdenum is also used to represent the ϵ -Phase. It is the majority component of the ϵ -Phase and it is conceivable that it shows catalytic activity similar to Pd (Zellner et al. 2005). In a first step it was possible to prepare UO_2/Mo films with Mo metal content by sputter co-deposition. Due to the high oxidation affinity of Mo (forming stable oxides like MoO_2 and MoO_3) oxygen pressure during sputter deposition was a key parameter. By controlling the oxygen partial pressure UO_2/Mo , UO_2/MoO_2 , $\text{UO}_2/\text{MoO}_{2+x}$ (with Mo content between 5 to 30 %) are prepared. Molybdenum oxides are not part of the ϵ -phase in spent fuel they appear in an oxide phase or as solid solution in the fuel matrix (Bruno and Ewing, 2006). Still the oxides are interesting as they also show catalytic activity towards hydrogen forming active molybdenum hydrogen bronze $\text{H}_x\text{MoO}_2/\text{H}_x\text{MoO}_3$ (Khyzhun et al. 2004, Al-Kandari et al. 2008).

Next steps are the structural and morphological characterisation of the UO_2/Mo model systems and investigations by open circuit potential measurements under the same conditions already used for UO_2/Pd .

Redox reactivity of doped UO_2 - Effects on the reactivity towards H_2O_2

In the last year studies at KTH have shown that Y_2O_3 doped UO_2 pellets are significantly less reactive towards H_2O_2 than pure UO_2 pellets (Buckau et al. 2010). These studies have been continued to clarify this effect.

Background

H_2O_2 can react with UO_2 by catalytic decomposition and by oxidizing U(IV) to U(VI). Recent experiments have shown that the dissolution yield, i.e. the amount of dissolved uranium per consumed H_2O_2 varies dramatically between different UO_2 -based materials. It has not been clear whether this variation can be attributed to changes in redox reactivity or in the catalytic ability of the material. To elucidate this we have studied the reactivity of a number of oxidants towards doped UO_2 materials. In parallel we have studied the catalytic formation of hydroxyl radicals (upon reaction with H_2O_2) on the doped UO_2 materials.

Reactivity of H_2O_2 towards doped UO_2

The consumption of H_2O_2 and the production of OH on UO_2 powder are illustrated in Figure 5. It can clearly be seen that the consumption of H_2O_2 is accompanied by production of OH. However, for UO_2 powder, the dissolution yield is relatively high (80

%). OH production for doped pellets varies by less than a factor of four (UO₂, SIMFUEL, Y₂O₃ doped UO₂, Pd-doped UO₂ and Y₂O₃/Pd-doped UO₂).

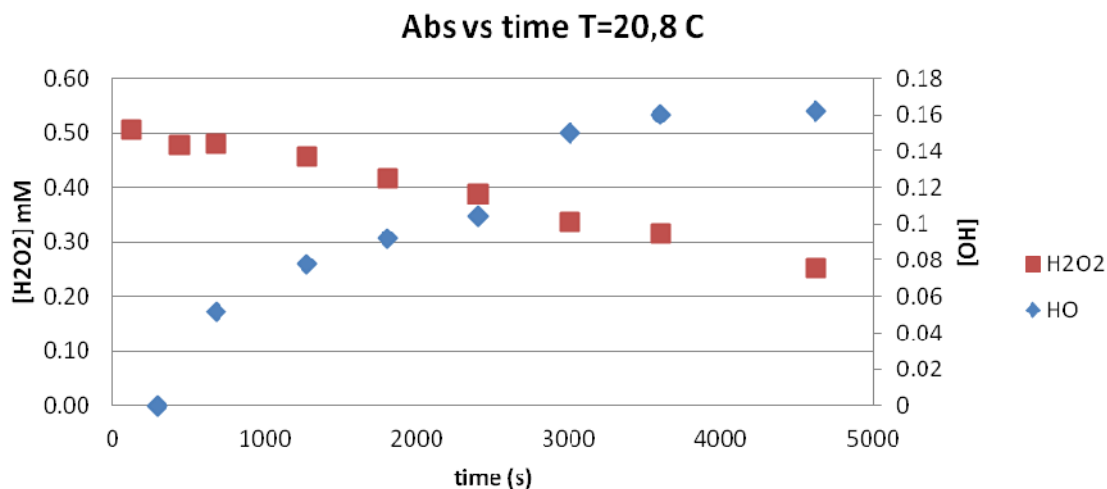


Figure 5: Consumption of H₂O₂ and production of OH on UO₂ powder.

Redox reactivity of doped UO₂

IrCl₆²⁻ and MnO₄⁻ were used as oxidants to monitor the redox reactivity of the doped UO₂ materials. In Figure 6 and Figure 7 the reactivity of the different pellets towards these oxidants can be seen.

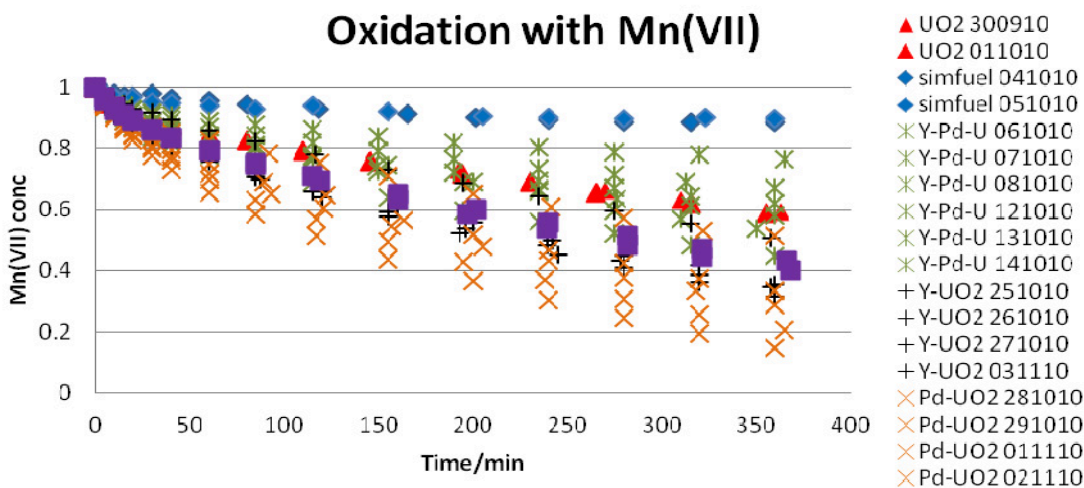


Figure 6: Oxidation of different doped and undoped UO₂ pellets and SIMFUEL by Mn(VII).

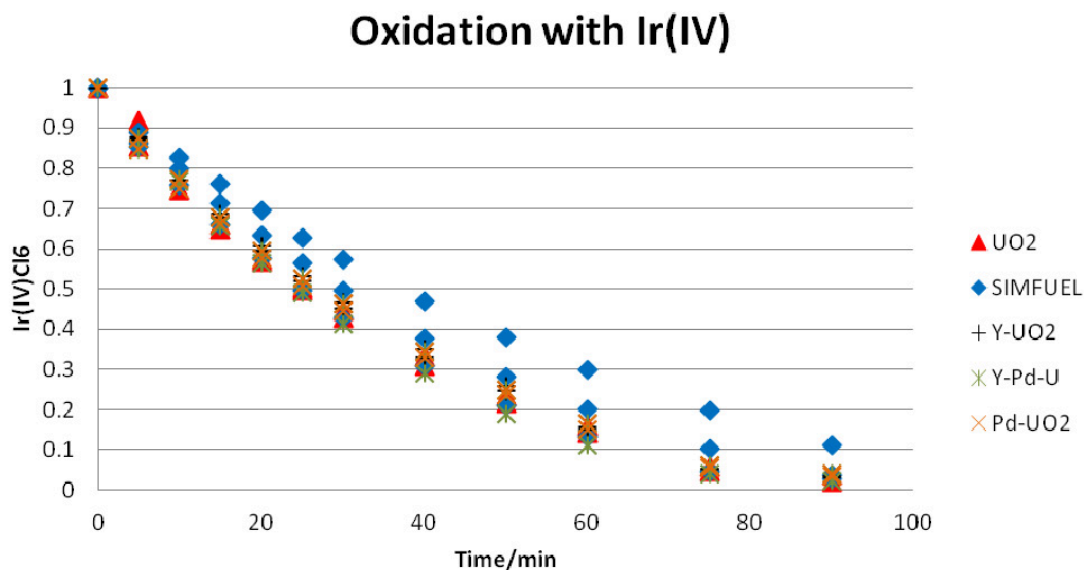


Figure 7: Oxidation of different doped and undoped UO_2 pellets and SIMFUEL by Ir(IV).

What can clearly be seen here is that the redox reactivity of the doped materials differs significantly for the weaker oxidant (MnO_4^-). The reaction with IrCl_6^{2-} is much faster and the difference between the doped materials is also less pronounced. The experiments show that the activation energy for oxidation of UO_2 by MnO_4^- is lower than the activation energy for oxidation of SIMFUEL by MnO_4^- .

Conclusion

The observed difference in dissolution yield between different doped UO_2 materials can mainly be attributed to differences in the redox reactivity (i.e. activation energy for oxidation). The difference in the ability to catalyze H_2O_2 decomposition is fairly small for the materials studied here.

Reductive Trapping of Actinides in Container Corrosion Products during Spent Fuel Corrosion

Introduction

The source term from spent nuclear fuel (SNF) dissolution is highly dependent on oxidative dissolution of the fuel matrix. Various experimental data on the dissolution behaviour of the spent fuel matrix itself and in some cases in presence of container material (initially metallic iron) as well, and the associated releases of radioelements were already obtained by extensive laboratory test programs and reported e.g. in (Schoesmith, 2000, Ferry et al. 2005, Loida et al. 1996). The capacity of iron phases formed by corrosion of metallic canister materials to incorporate radionuclides is under investigation within the European Collaborative Project “ReCosy”. The stable corrosion product of steel canister material under reducing disposal conditions is magnetite.

In the present study, **KIT-INE** investigates reductive trapping of actinides by Fe-oxide corrosion products in the presence of spent nuclear fuel corroding in NaCl solution. The effect of a magnetite rich Fe-oxide powder on the radionuclide release was measured in a spent nuclear fuel leaching experiment (denoted as “K14Mt”) for almost 10 years. At a final stage of the leaching experiment a relatively high concentration of dissolved U, $\sim 1 \cdot 10^{-4}$ M, accompanied with a considerable CO₂ content of 0.8 vol.-% in the gas phase were observed.

Fe-oxide powder and the fuel pellet, recovered from the leaching experiment, were analyzed by means of optical microscopy (SNF sample, Fe-oxide powder), SEM/EDS (Fe-oxide powder), XPS (Fe-oxide powder) and Raman spectroscopy (Fe-oxide powder). Additionally, the untreated Fe-oxide powder was mineralogically and chemically analyzed. Based on the solution and solid phase analyses, the distribution of radioelements between the magnetite rich Fe-oxide, container wall and the aqueous phase was determined.

Experimental

The corrosion experiment was performed by using a pellet sized segment of high burn-up SNF (50 MWd/kg U, linear power 260 W/m), 6.6 g fuel, and 10 mm in length together with commercial available “Fe₃O₄” powder (Alfa Aesar 012962, 99.997% purity, grain size ~ 5 μ m). SNF sample and the Fe-oxide powder were immersed simultaneously in 5 mol/L NaCl solution (initial volume 200 ml, under Ar-atmosphere), using a glass vessel. During the initial phase of the experiment, the leachant was replaced entirely by fresh solution for four times until total 65 days. This procedure reduced effectively the “initial release fraction (IRF)”, such as the fast released fraction of ¹³⁵Cs, ¹³⁷Cs and fission gases. Afterwards the experiment was continued without replacing the solution (static), lasting over 3562 days. The gas phase and solution were sampled at 78, 215, 349, 771, 1895 and 3562 days after start of the static phase. The analytic procedures are described in Loida et al. 2010, Grambow et al. 1996). After termination of the experiment, fractions of the magnetite rich Fe-oxide were recovered and analyzed. Various analytical methods have been applied: SEM/EDX, XRD, Raman spectroscopy, XPS, digestion in HCl, stripping by HNO₃ and radiochemical analyses of the dissolved sample.

Phase composition of the used Fe-oxide powder

To determine the phase composition of the untreated Fe-oxide “Fe₃O₄” and the Fe-oxide recovered from the SNF leaching experiment, aliquots of these samples were analyzed using XRD and Raman spectroscopy. Diffraction patterns of the untreated Fe-oxide and powder recovered from the leaching experiment show essentially the same reflexes. In both samples magnetite (Fe₃O₄) and hematite (α -Fe₂O₃) are detected as major phases. Though weak reflexes at 33.9°, 47.2° and 59.8° 2 θ indicate traces of an unidentified phase, no reflexes of a Fe-carbonate mineral are observed. Using Raman spectroscopy, only hematite was identified in both samples.

Acid digestion of the untreated Fe-oxide powder

In order to detect the carbon source of the SNF leaching experiment “K14Mt”, an aliquot of the untreated “Fe₃O₄” was treated with diluted HCl. An amount of 5 g of the untreated Fe-oxide was given to 30 ml HCl (30%) in an autoclave under initially Ar-atmosphere. During the acid treatment magnetite was completely dissolved. Analyzes of the gas atmosphere after 74 days revealed a decrease of Ar to 33 vol.-%, an increase of H₂ up to ~67 vol.-% and CO₂ up to 0.1 vol.-%. The CO₂ content of 0.1 vol.-% corresponds to a mass fraction of 0.02 wt.-% CO₂ impurities in the Fe-oxide sample. Such a trace concentration of carbonate or another carbon bearing phase is below the XRD detection limit. However, the CO₂ gas content released from the Fe-oxide powder in the inactive autoclave experiment is in the range of CO₂ measured in the SNF leaching experiment “K14Mt”. It is considered as the sole CO₂ source in experiment “K14Mt”.

Radioelement distribution

The amounts of retained radionuclides upon the Fe-oxide sample recovered from the SNF leaching experiment and the walls of the glass vessel were obtained after dissolution of 230 mg Fe-oxide in 30% HCl and acid stripping of the vessel wall (5M HNO₃) followed by radiochemical analysis of related aliquots. The results show that the total release of Cs, Sr and Tc (in solution + on the vessel wall + on the Fe-oxide) were measured at $1.48 \cdot 10^{-6}$ M, $3.04 \cdot 10^{-7}$ M and $1.52 \cdot 10^{-7}$ M, where fractions of 95%, 99% and 98.5 % of the respective radionuclides were found in the aqueous phase. U was released in total at $5.07 \cdot 10^{-5}$ M, whereof 70% was found upon the recovered Fe-oxide. The total measured amount of Am was determined to be $3.56 \cdot 10^{-8}$ M, where a percentage of 95% upon the Fe-oxide was encountered. The Pu release was measured to be $2.3 \cdot 10^{-8}$ Mol, whereof 90% was re-immobilized upon the Fe-oxide. The retention of radionuclides upon the glass vessel wall does not play a significant role.

Concluding remarks

The gas composition in the SNF leaching experiment “K14Mt” changed significantly over almost 10 years observation period. Due to the unexpected elevated concentrations of CO₂ the U concentration in solution increased up to $\sim 1 \cdot 10^{-4}$ M. The considerable CO₂ content in the gas phase at the end of the corrosion experiment is related to the carbon / CO₂ content of the “Fe₃O₄” powder used in the leaching experiment. In spite of the significant release of U (due to carbonate complexation), considerable amounts of actinides were retained upon the magnetite rich Fe-oxide. With respect to Am, Pu, U and Np about 95, 87, 71 and 39 % of the released measured amounts were found to be re-immobilized upon the Fe-oxide powder.

On the redox chemistry at the near field of repository, the influences of iron canister material and hydrogen

Np-Pu reductive immobilization by iron canister material

The Pu(VI) –Fe(0) redox experiment was restarted after adopting a method of oxidising Pu(IV) by fuming HClO₄ to Pu(VI) and then adding it to a carbonate solution. At room temperature, oxidation reactions by ClO₄⁻ are generally kinetically slow and should not have significantly influence on the reducing capacity of Fe(0). To substantiate this statement a separate experiment was made to study the reaction of ClO₄⁻ with Fe(0).

Anyhow, to minimize the potential effect of excess ClO₄⁻ on the simulated near field reducing conditions, after oxidizing Pu(IV) to Pu(VI) and diluting it in a 2 mM HCO₃⁻ solution, KCl was added to precipitate most ClO₄⁻ left in the solution. The solubility of KClO₄ is 1.5 g/l. In a solution containing ppm-level of Pu(VI) most of the Pu was found to be immobilized on the iron surface and the oxidation state of the precipitated Pu on the iron surface will be analysed by XANES and re-evaluated.

Mechanisms of the hydrogen influence on radionuclide migration by D/H isotope exchange method

- a) It was observed that isotope exchange between D in D₂ gas (11 bar) and H in water solution does slowly occur with the presence of SIMFUEL pellet, (a spent fuel simulator containing UO₂ and noble metal fission product) particles through the reaction $D_2 + H_2O \Rightarrow D_2O + H_2$, but not significant occurs in the blank experiment.
- b) An increase of N₂/O₂ ratio in the gas mixture of air and D₂ in autoclave containing water solution and the SIMFUEL pellet, but not in blank experiment without SIMFUEL.
- c) The D/H ratio in water solution that interacted with a 11.3 bar gas mixture of D₂ + 0.14% O₂ with the presence of SIMFUEL pellet for 2 months was found to be (7157 dD per mil) 1270 ppm (isotopic ratio). It is about three times higher than the calculated value according to the O₂ added in the system. It proves that beside the deoxygenation reaction, $2D_2 + O_2 \Rightarrow 2D_2O$, there should be an isotope exchange reaction $D_2 + H_2O \Rightarrow D_2O + H_2$.

Redox conditions near waste packages

In the previous work carried out by **NRI** in the RECOSY project, it was found that the redox potential of bentonite water decreased significantly by the addition of an iron powder into reaction vessels, but after a while the potential started to increase. This apparent increase of the redox potential (E_h) of bentonite water measured continuously by platinum and gold electrodes was caused mainly by the formation of corrosion product layers on the surface of the electrodes. Nevertheless a slight increase of the E_h was also observable in discontinuous measurements after careful cleaning of the electrodes. It was assumed that this increase was affected by diffusion of oxygen into the reaction vessels. Therefore our experiments have now been carried out in an anaerobic box to prevent inleakage of oxygen. Most of the experiments have been

carried out with carbon steel plates, but some of the experiments have been carried out with an iron powder of high surface with the main aim to increase the extent of corrosion reactions and consequently the effect of corrosion on the change of E_h . This enables also a comparison of the behaviour of carbon steel and pure iron in bentonite water under anaerobic conditions.

The corrosion system consisted of 1 or 10 carbon steel plates or 30 g of the iron powder in 2 litre of synthetic bentonite pore water, which was put into the anaerobic box with an oxygen concentration below 0.1 ppm 14 days before the experiments begun. Two independent electrodes, made of platinum and gold, were used to measure the redox potential continuously in the corrosion system with carbon steel and bentonite water. The experiments were carried out at various temperatures. The concentration of Fe^{3+} and the total iron concentration in solution after the experiments were measured by UV/Vis spectroscopy and by atomic absorption spectroscopy, respectively. Corrosion products on the carbon steel plates after finishing experiments were measured by Raman spectrometer LabRam with two lasers (He – Ne and Ar), by X-ray diffraction (Philips-Xpert PRO) and by ESCA Probe P Omikron Nanotechnology in CAE mode. The extent of corrosion was determined by measuring the amount of hydrogen generated during anaerobic corrosion of iron.

The results obtained showed that the evolution of E_h and pH is different whether carbon steel plates or an iron powder were used in experiments. The E_h was continuously increasing after a fast decrease in the beginning of the corrosion reaction in experiments with carbon steel samples. In experiments with the iron powder no increase of E_h after a very quick decrease was observed. In all the experiments with carbon steel plates the pH decreased, but in experiments with iron powder it remained constant. The difference between the behaviour of carbon steel plates and of iron powder is possible to explain by the formation of protecting corrosion layers on the surface of carbon steel samples. It was found that the nature of these layers is dependent on the temperature at which the experiment is carried out. While at 40 °C no corrosion layer was detected by Raman spectroscopy, such a layer was detected on samples corroded at 60 or 70 °C. Using an ESCA probe, it was found that in comparison to non-corroded samples, the firmly adhering, protective corrosion layers containing high amount of oxygen were formed during corrosion of carbon steel plates in the bentonite water under anaerobic conditions. It was also shown that the temperature affects the corrosion rate and consequently the development of E_h in the system. The higher the temperature, the higher is an initial decrease of E_h .

It was also shown that the surface to volume ratio of carbon steel plates in solution affects significantly the development of E_h in the system. The higher this ratio is the higher is the initial decrease of E_h in bentonite water solution due to faster accumulation of ferrous ions in the system. In the system with 1 carbon steel sample, the E_h decreased quickly from positive values to values ranging from -100 to -300 mV, depending on the temperature and in the system with 10 samples to values between -200 to -350 mV, again depending on the temperature. After 30 days duration of experiments, however, E_h slightly increased in both systems to the values -100 to -250 mV. This suggests that the E_h in solution will be strongly affected by the nature of precipitated solids. In the experiment with the iron powder E_h very quickly decreased from positive

values to values less than -500 mV and remained practically constant for the whole duration of the experiment.

A simple approach was chosen to simulate the E_h evolution during the corrosion process. First, the corrosion process was simulated by adding iron into the bentonite porewater solution in steps according to the measured corrosion rate. On the basis of speciation in solution and Fe(II)/Fe(III) activities the E_h was calculated. Second, the solution was equilibrated with Fe-bearing minerals (magnetite, $Fe(OH)_2$) and E_h was calculated again. These calculations were performed for both experiments (with carbon steel plates and iron powder) using geochemical code PHREEQC version 2.15.07 with OECD NEA database. The following processes were taken into account in the calculations: trace concentration of oxygen in the anaerobic box (< 0.1 ppm), reduction of sulphate to sulphide and precipitation of corrosion products, which are not in equilibrium with the solution. Reduction of carbonate to methane was not allowed in the model calculations, because of kinetic constraints. Sulphate to sulphide reduction was partly allowed, because of a specific sulphide smell occurrence after experiments. The sulphide concentration was below detection limit of the measurement technique (< 0.1 mg/l).

The results achieved clearly suggest that the development of E_h in the near field of deep geological systems with carbon steel is not easily predictable, because it depends on a large number of various factors such as temperature, ratio of surface of metal to water contacting carbon steel or composition of water, let alone physical constraints to migration of corrosion products due to compacted bentonite surrounding carbon steel waste packages. The experiments clearly showed that replacing carbon steel by pure iron powder in simulations of near field conditions in deep geological repository can lead to highly misleading results. This is because carbon steel can after immersion into anaerobic water be quickly covered by a passive layer, which protects the steel against further corrosion and affects also the geochemical conditions in the near field of deep geological repository with carbon steel waste packages. Unfortunately, rather short-term, 30 day experiments carried out in our work do not enable an easy prediction of the further behaviour of corrosion layers of carbon steel. Much longer-term experiments under conditions approaching the conditions in a repository will have to be carried out to obtain a more reliably estimate of geochemical conditions evolving in deep geological repositories.

References

- Al-Kandari, H. Al-Kharafi, F. Katrib A. (2008): Catalytic activity-surface structure correlation of molybdenum-based catalysts, *J. Molecular Catalysis A*, 287, 128.
- Bruno J. and Ewing R. C. (2006): Spent Nuclear Fuel, *Elements*, 2, 343-349.
- Buckau G., Kienzler B., Duro L., Grivé M., Montoya V. (eds.) (2010): 2nd Annual Workshop Proceedings of the Collaborative Project “Redox Phenomena Controlling Systems” (EC 7th FP CP RECOSY), Karlsruhe Institute of Technology, KIT Scientific Reports 7557, Germany.

Buckau G., Kienzler B., Duro L., Grivé M., Montoya V. (2009): Collaborative Project “Redox Phenomena Controlling Systems” - 1st Annual Workshop Proceedings, Forschungszentrum Karlsruhe, Wissenschaftliche Berichte, FZKA 7466, Karlsruhe 2009, pp.51.

Ferry C., Poinssot C., Broudique V., Cappelaere C., Desgranges L., Garcia P., Jegou C., Lovera P., Marimbeau P., Piron J. P., Poulesquen A., Roudil R., Gras J-M-, Bouffieux P. (2005): Synthesis of the Spent Fuel Long-Term Evolution, Rapport CEA-R-6084.

Fors P., Carbol P., Van Winckel S., Spahiu K. (2009): Corrosion of high burn-up structured UO₂ fuel in presence of dissolved H₂. J. Nucl. Mater., 394 (2009) 1-8.

Grambow, B. Loida, A. Dressler, P. Geckeis, H. Gago, J. Casas, I. de Pablo, J., Gimenez, J. Torrero M.E. (1996): Long-Term Safety of Radioactive Waste Disposal: Chemical Reaction of Fabricated and High Burnup Spent UO₂ Fuel with Saline Brines, Wissenschaftliche Berichte FZKA 5702, März 1996.

Khyzhun, O. Yu., Strunskus, T. Solonin Yu. M. (2004): XES, XPS and NEXAFS studies of the electronic structure of cubic MoO_{1.9} and H_{1.63}MoO₃ thick films, J. Alloys and Compounds, 366, 54.

Loida, A. Grambow B., Geckeis H. (1996): Anoxic corrosion of various high burnup spent fuel samples. J. Nucl. Mater., 238, 11-22.

Loida, A. Bohnert, E. Kienzler, B. Müller, N. Plaschke, M. Schild, D. Soballa E. (2010): Release and retention of radionuclides during 10 years corrosion of Spent Nuclear Fuel (SNF) in presence of magnetite, in: G. Buckau, B. Kienzler, L. Duro, M. Grivé, V. Montoya (eds.), 2nd Annual Workshop Proceedings of the Collaborative Project “Redox Phenomena Controlling Systems” (EC 7th FP CP RECOSY), Karlsruhe Institute of Technology, KIT Scientific Reports 7557, Germany (2010).

Serrano-Purroy, D., F. Clarens, J.-P. Glatz, D. Wegen, B. Christiansen, J. de Pablo, J. Giménez, I. Casas and A. Martínez-Esparza (2009): Leaching of 53 MWd/kgU spent nuclear fuel in a flow-through reactor, Radiochim. Acta, 97, 491–496.

Shoesmith D.W. (2000): Fuel corrosion processes under waste disposal conditions, J. Nucl. Mater., 282, 1-31.

Stumpf, S. Seibert A., Gouder T., Huber F., Wiss T., Römer J. (2009): Development of fuel-model interfaces: Investigations by XPS, TEM, SEM and AFM. J. Nucl. Mater., 385, 208.

Stumpf S., Seibert A., Gouder T., Huber F., Wiss T., Römer J., Denecke M. A. (2010): Development of fuel-model interfaces: Characterization of Pd containing UO₂ thin films. J. Nucl. Mater., 397, 19.

Zellner, M. B., Goda, A. M., Skoplyak, O., Barteau M.A. and Chen J.G. (2005): Trends in the Adsorption and Decomposition of Hydrogen and Ethylene on Monolayer Metal Films: A Combined DFT and Experimental Study, Surface Science, 583, 281.

S + T CONTRIBUTIONS

List of contributions

Progress in the development of a fibre optical chemical sensor (FOCS) for the simultaneous determination of proton, oxygen and chloride concentrations <i>D. Steinbrück, E. Schmälzlin, M. U. Kumke</i>	83
Migration of uranyl ions in Boda Claystones samples <i>K. Lázár1, J. Megyeri1, Z. Mácsik, É. Széles, Z. Máthé</i>	91
Redox potential in the near field of a deep geological repository containing carbon steel waste packages <i>D. Dobrev, R. Červinka, A. Vokál</i>	99
The application of microsensors for the determination of redox processes in biofilms from uranium contaminated acidic mine drainage waters <i>E. Krawczyk-Bärsch, T. Arnold, E. Eisbein, V. Brendler, U. Jenk, U. Zimmermann</i>	117
XAFS investigations of Np(V/VI) redox speciation in hyperalkaline TMA-OH solutions <i>X. Gaona, J. Tits, K. Dardenne, E. Wieland, M. Altmaier</i>	123
Systematic evaluation of Tc(VII)/Tc(IV) redox processes in 0.1 M NaCl solutions <i>T. Kobayashi, X. Gaona, D. Fellhauer, M. Altmaier</i>	137
Study of the diffusive behaviour of selenite and selenite through the Callovo-Oxfordian Claystones (France): effect of the initial selenite concentration <i>S. Savoye, B. Frasca, A. Fayette, B. Grenut, J. Radwan</i>	147
Influence of the redox state on the neptunium sorption by cementitious materials <i>J. Tits, X. Gaona, A. Laube, E. Wieland</i>	163
Actinide partition in humic colloidal ternary systems: experiments and preliminary modelling <i>R. Kay, L. Abrahamsen, A. Stockdale1, K. Smith, N.D. Bryan, P. Warwick, N. Evans</i>	177
Behaviour of Tc(VII) in aqueous solutions in the presence of iron oxides and microorganisms <i>R. Druteikienė, B. Lukšienė, D. Pečiulytė, K. Mažeika, A. Gudelis, D. Baltrūnas</i>	187

The response in redox from additions of hydrogen and oxygen to natural deep groundwater/rock systems with active microorganisms <i>K. Pedersen, J. Arlinger, L. Hallbeck, S. Lydmark, J. Johansson, A. Pääjärvi</i>	197
Sorption and redox behaviour of radionuclides in natural clay rocks <i>N. L. Banik, C.M. Marquardt, D. Schild, J. Rothe, T. Schäfer</i>	205
Quantification of pyrrhotite O ₂ consumption by using pyrite oxidation kinetic data. <i>C. Domènech, L. Duro, M. Grivé, D. Arcos, I. Rojo, F. Clarens, J. de Pablo</i>	219
Electrochemical investigations on doped and undoped UO ₂ spent fuel model surfaces <i>T. Petersmann, A. Seibert, D.H. Wegen, T. Gouder, S. Stumpf, Th. Fanghänel</i>	231
Redox reactivity of doped UO ₂ - Effects on the reactivity towards H ₂ O ₂ <i>R. Pehrman, M. Trummer, C. Lousada, M. Jonsson</i>	241
Redox-controlling processes for multivalent metals and actinides in the WIPP <i>D. Reed, M. Borkowski, J. Swanson, M. Richmann, H. Khaing, J. F. Lucchini, D. Ams</i>	251
Trapping of radionuclides/actinides in the canister corrosion product magnetite <i>A. Loida, V. Metz, E. Bohnert, B. Kienzler, N. Müller, D. Schild, E. Soballa</i>	265

PROGRESS IN THE DEVELOPMENT OF A FIBRE OPTICAL CHEMICAL SENSOR (FOCS) FOR THE SIMULTANEOUS DETERMINATION OF PROTON, OXYGEN AND CHLORIDE CONCENTRATIONS

Dörte Steinbrück, Elmar Schmäzlin and Michael U. Kumke*

Institute of Chemistry, University of Potsdam (GER)

* Corresponding author: kumke@uni-potsdam.de

Abstract

Our recent developments of an improved FOCS system for the determination of dissolved oxygen in ppb range, the pH-value, in a limited pH range (~ 1 to 4), and first results for the optical determination of chloride concentrations up to 0.5 M are discussed. In contrast to commercially available intensity-based systems for the determination of only single parameters, the novel FOCS system is fully based on the determination of the luminescence decay times.

Introduction

Depending on the system under investigation fibre-optical chemical sensing (FOCS) has been proven to be a powerful alternative to electrochemical-based techniques for sensing of analytes such as oxygen or pH. Using novel fluorescence dyes which change their emission properties in the presence of certain ions (e.g., chloride), the optical-based simultaneous sensing of different chemical parameters can be envisaged. A major challenge to be tackled is the cross-sensitivity of the luminescence probes for ions. When the probe is embedded in a tailored polymer-matrix, this matrix can enhance the selectivity. The polymer matrix can be designed in a way that it will be permeable only for specific ions, which subsequently are the ones that interact with the sensor dye.

Currently available optical sensors for ions often use alterations in the luminescence intensity of spectral shifts for the qualitative and quantitative determination of the analytes. However, intensity-based measurements are prone to aging effects of the sensor and require a tedious calibration procedure (often using additional dyes as internal reference). Therefore, sensing schemes that are based on measurements of the luminescence decay time are preferred because such drawbacks are minimized.

Our current research is focused on the evaluation and integration of decay-time based optical sensing schemes for the simultaneous determination of different chemical

parameters. In this contribution we present the progress made in the development of a combined optical sensor for the simultaneous determination oxygen, chloride and pH.

Experimental

In the FOCS measurements phase-modulation spectroscopy was applied. This frequency-domain spectroscopy (FD-S) method combines the advantage of real time monitoring and low cost equipments. In reference experiments time domain spectroscopy (TD-S) measurements using the method of time correlated single photo counting (TCSPC) were also carried out.

In the FD-S measurements the phase shift ϕ between the modulated excitation and luminescence is determined. With equation 1 the luminescence decay time τ can be calculated (Lakowicz, 2006):

$$\tan(\phi) = 2\pi f \cdot \tau \quad (1)$$

The modulation frequency f has to be adjusted to the respective decay time range of the sensitive dye. In order to establish the simultaneous detection of different analytes a multi frequency approach is employed. Moreover, the probes should have different luminescence decay times for a good separation of the signals. The three luminescence probes discussed in this report have decay times in three different time ranges (for oxygen $\tau_0 = 700 \mu\text{s}$; for pH $\tau_0 = 4.5 \text{ ns}$; for chloride $\tau_0 = 20 \text{ ns}$).

In principle, the dyes can be excited with same excitation wavelengths in the spectral range of $405 \text{ nm} < \lambda_{\text{ex}} < 470 \text{ nm}$.

For the detection of the emission in the MHz range (pH and chloride sensing) we used a photomultiplier tube (Hamamatsu, H6780-20) with signal amplification (Femto, model DHPCA-100). The determination of the phase shift was performed using a Lock-In Amplifier from Stanford Research Systems (model SR844). The excitation light was modulated using the DynaLase-C system (ELOVIS electronics-optics-solutions).

Some experiments (e.g., the characterisation of the oxygen optode) were performed with a dual-frequency phase modulation approach (d-FD-S) to eliminate contributions of background luminescence signals (Schmälzlin et al. 2005, Löhmansröben and Schmälzlin, 2007). For the detection an in-lab built multiplexer with an integrated photo multiplier tube was used.

The oxygen optode is based on a fluorinated polymer with a high permeability for oxygen. The dye used for oxygen detection is Pd(II)-tetrapentafluorophenylphorphyrin (Pd-TPFPP; further we used the same dye with Pt as central ion, Pt-TPFPP).

The new pH-optode consists of an advanced polymer, which we obtained from the Fraunhofer IGB (Fraunhofer Institute for Interfacial Engineering and Biotechnology) Stuttgart (Prof. Dr. Thomas Hirth) (Roelofs et al., 2009). For pH measurements we embedded the dye 6-Carboxyfluorescein (6-CF).

The optode for chloride determination consists of the Poly(2-hydroxypropyl)methacrylat (PHPMA) as polymer matrix and Lucigenin (bis-*N*-methylacridinium nitrate) as chloride sensitive dye.

In the experiments the temperature of the samples was controlled by a thermostat. In the oxygen concentration measurements an in-line optical temperature sensor was used in order to directly account for any temperature shifts (Schmälzlin et al. 2005, Löhmansröben and Schmälzlin, 2007).

Optimization and sensitivity enhancement of the oxygen-sensitive optode

The electronic and optic components of the experimental set-up were further miniaturized to improve handling in field applications. In order to increase the applicability of the set up (for future multiparameter sensing) the accessible modulation frequency range was increased as well. Depending on the concentration range of interest different chromophores can be applied in the oxygen sensor. In Figure 1 calibration curves for different optodes using a Pd-based probe are shown. It is shown that the absolute value of the measured decay time is influenced by the layer thickness, but the slopes of the calibrations curves are (almost) independent on it – which can be also be seen from the values of the limit of detection (LOD) individually determined for each sensor. With the Pd-based probe the determined LOD for oxygen in aqueous solution is 1 ppb and around 7 ppb for the Pt-based sensor type. In both cases outstanding accuracies in the data acquisition were achieved, e.g., the standard deviation in the determination of τ_0 was as low as 2 μ s. A major factor for the excellent sensitivity, accuracy and reproducibility is the fact, that the measurements were performed at two different frequencies, which significantly reduced any contribution from background luminescence and scattered light

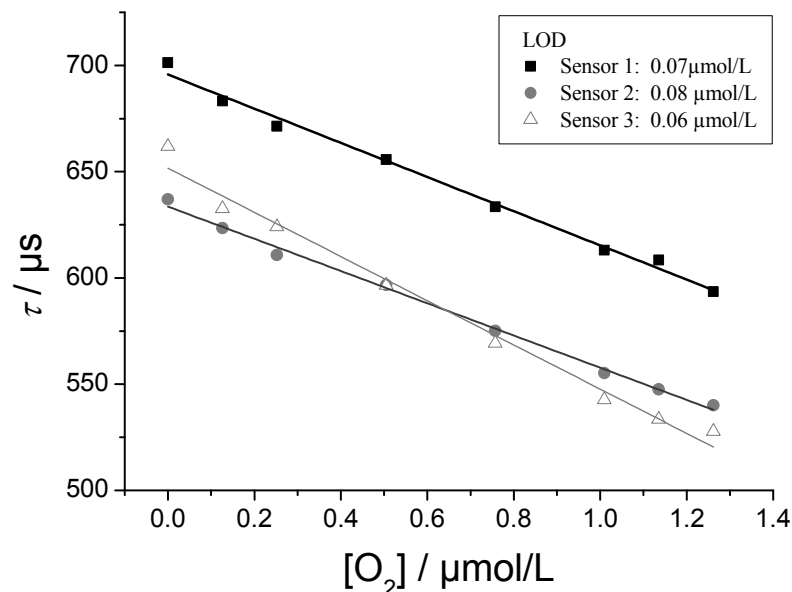


Figure 1: Calibration curves of the Pd-based optode in water in low μ mol concentration range of oxygen. A limit of detection (LOD) of 1 ppb for oxygen dissolved in water was determined. The difference of the (λ_{ex0}) values are a result of varying coating thickness of the optode ($\lambda_{ex} = 405$ nm; ($\lambda_{em} > 600$ nm).

Characterisation of the novel luminescence decay time based pH-optode

Optical determination of pH based on spectral shifts or intensity changes are well established. On the other hand pH measurements using an alteration of the luminescence decay time is at its infancy. Therefore, the fundamental aspects of pH sensing based on luminescence decay time measurements were evaluated: i) testing of pH-sensitive probes and ii) optimization of the polymer matrix to achieve an optimum in proton-selectivity and reduce cross-sensitivity for other cations.

In the experiments different fluorescein derivatives were tested as probes for their potential in luminescence decay time based pH-sensing. The probes were immobilized in a novel polymer, which shows very high proton permeability. In Figure 2 the calibration curves of the pH-optode are presented. The preliminary FD-S measurements were performed using a microscope based set up. The luminescence of the optode was excited at $\lambda_{\text{ex}} = 450 \text{ nm}$, collected with the objective and disposed by a dichroic mirror to a photomultiplier, which is connected to a lock-in amplifier for the determination of the phase shift.

For calibration purposes a series of citrate and TRIS buffer solutions with fixed pH-values were prepared as described in Rauscher et al. (1977). The phase shift at pH 1 was set to zero and the change of the phase shift at all other pH compared to pH 1 was recorded. From these relative phase shift the relative change in decay time were calculated using equation (1), assuming that the tan function shows a linear relationship in the relevant pH-range. From Figure 2 it can be seen that with the current optode a pH range between one and five can be addressed, which is nicely found in frequency as well as in time domain measurements.

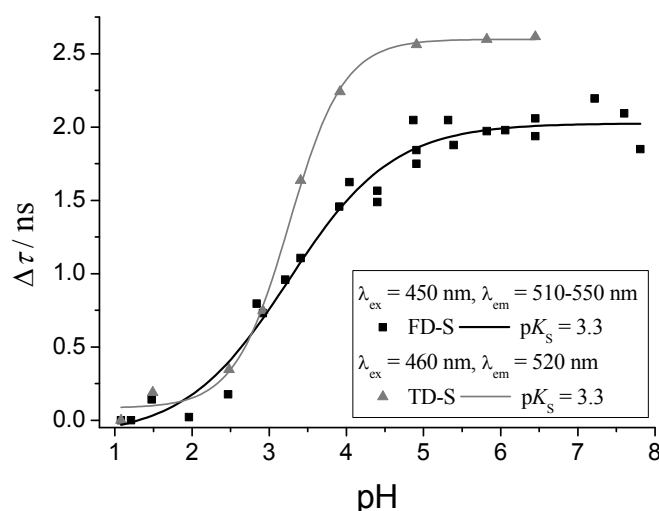


Figure 2: Comparison of calibrations for a decay time based pH-optode obtained with different detection methods using embedded 6-CF. The pH of the buffer solutions were controlled with a regular pH electrode and were prepared freshly for all calibration.

Characterization of the novel chloride-optode

In many redox processes, such as corrosion or in physiological processes, chloride ions play a central role. Because of the high potential for on-line sensing and for miniaturization, optically-based chloride ion sensing is very attractive. For the integration of optically chloride sensing into the robust luminescence decay time based sensing platform, the luminescence probe lucigenin was evaluated. The luminescence decay time of lucigenin is quenched in the presence of chloride. In Figure 3 the preliminary results of TD-S measurements of lucigenin embedded in PHPMA for different chloride concentrations are shown. The Stern-Volmer plot was performed by using the average decay times:

$$\tau_{av} = \frac{A_1 \cdot \tau_1^2 + A_2 \cdot \tau_2^2 + A_3 \cdot \tau_3^2}{A_1 \cdot \tau_1 + A_2 \cdot \tau_2 + A_3 \cdot \tau_3} \quad (2)$$

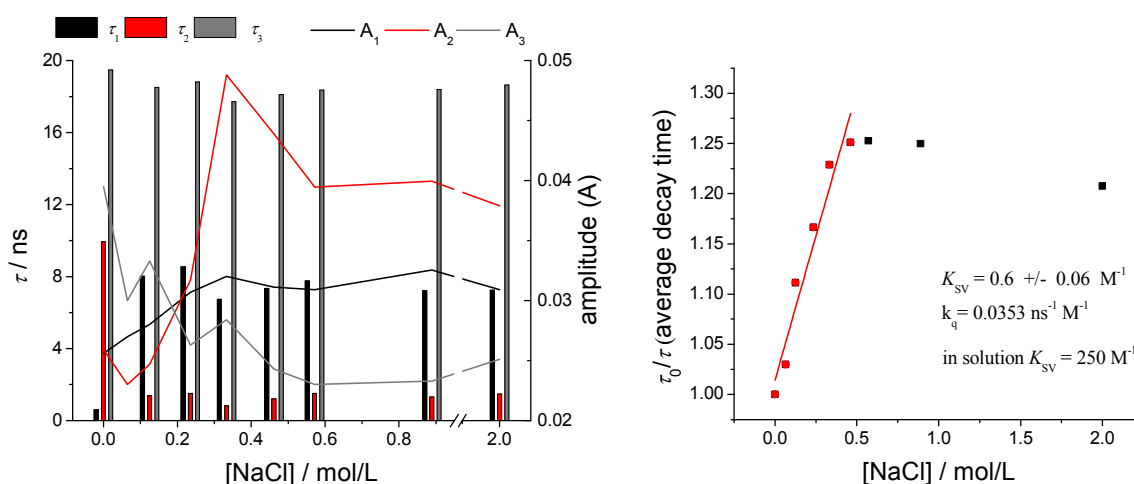


Figure 3: Optical determination of chloride concentration. Left: Experimental luminescence decay times measured in TD-S measurements. Right: Stern-Volmer plot of the calculated average decay times (equation 2) for the determination of the optode sensitivity for chloride ($\lambda_{ex} = 420$ nm).

The results show, that such an optode has a good sensitivity in the chloride concentration range up to 0.5 mol/L. Higher concentrations do not lead to a further increase of the quenching effect. Compared to measurements in aqueous solutions the sensitivity is slightly reduced which is most probable connected to limitations in chloride diffusion inside the polymer matrix. Here, further optimization of the polymer matrix will improve the sensor performance. Promising candidates are “interpenetrating network” polymers (Xu et al. 2010, Myung et al. 2008). These polymers have in their micro structure different regions of polarity and the permeability of chloride ions will be much higher than in the used PHPMA.

Summary / Conclusions

The optical determination - based on luminescence decay time quenching - of three different chemical parameters was evaluated using FD-S and TD-S. Based on the changes in the luminescence decay time (measured as phase shift) the concentration of oxygen, protons (pH), and chloride was determined. The current pH-Sensor is optimized for the low pH-range up to five, but using other pH-sensitive probes other pH ranges are in principle accessible. In the experiments, central experimental parameters such as excitation wavelength, emission wavelength, and modulation frequency range were tailored in order to set up a combined optical detection platform for multiparameter sensing. All optodes can be operated using excitation wavelengths in the range 450 nm $<\lambda_{\text{ex}}<$ 470 nm. Integration and optimization of multi frequency phase modulation will further improve the detection and discrimination of luminescence signal from the different optodes by splitting the luminescence signals in the frequency domain and evaluating different frequencies specifically optimized for each probe. Furthermore, the emission wavelength of the oxygen sensor is spectrally well separated from the luminescence emission of the other dyes, which are in green spectral range.

The future challenges to be met are i) to combine and integrate the different optodes into a single set up and ii) to further optimize the polymer matrices for the different sensing applications in order to increase the selectivity and further reduce the potential of cross sensitivities. Moreover the leaching of the dye from the matrix to the solution must be circumvented. First steps for permanently immobilisation of a sensitive dye were done and improved the sensing device remarkably.

Acknowledgment

The research leading to these results has received funding from the European Union's European Atomic Energy Community's (Euratom) Seventh Framework Programme FP7/2007-2011 under grant agreement n° 212287 (RECOSYproject). For experimental assistance we thank Franziska Ebert and Julia Prinz (Institute of Chemistry, University of Potsdam (Ger)).

References

- Lakowicz J. R. (2006): Principles of fluorescence spectroscopy, Berlin: Springer Science and Business Media. Chapter 5, pp.158-161.
- Löhmansröben H.-G., Schmälzlin E. (2007): Minimally invasive fiber probes for optical in-vivo oxygen measurements with integrated optical thermometer, Proceedings SPIE Vol. 6770, 67700V.
- Myung D., Waters D., Wiseman M., Duhamel, P.E, Noolandi, J. Ta C.N., Frank, C.W (2008): Progress in the development of interpenetrating polymer network hydrogels, Polym. Adv. Technol., 19, 647–657.
- Schmälzlin E., van Dongen, J. T., Klimant, I., Marmodee, B., Steup, M., Fisahn, J. Geigenberger, P. Löhmansröben, H.-G. (2005): An optical multifrequency phase modulation method using microbeads for measuring intracellular oxygen concentrations in plants, Biophysical Journal, 89, 1339–1345.

Rauscher K., Voigt J., Wilke I. (1977): Chemische Tabellen und Rechentafeln für die analytische Praxis, VEB Deutscher Verlag für Grundstoffindustrie, Leipzig, Chapter 9.4, pp. 140-145.

Roelofs K.S., Kampa A., Hirth T., Schiestel T. (2009): Behavior of Sulfonated Poly(ether ether ketone) in Ethanol-Water Systems, J. of Appl. Polymer Science, 111, 2998-3009.

Xu L. Q., Yao F., Fu G. D., Kang E. T. (2010): Interpenetrating Network Hydrogels via Simultaneous “ClickChemistry” and Atom Transfer Radical Polymerization, Biomacromolecules, 11, 1810–1817.

MIGRATION OF URANYL IONS IN BODA CLAYSTONE SAMPLES

Károly Lázár^{1*}, János Megyeri¹, Zsuzsanna Mácsik¹, Éva Széles¹, Zoltán Máthé²

¹ Institute of Isotopes, Hungarian Academy of Sciences (HU)

² Mecsekérc Environmental Plc. (HU)

* Corresponding author: lazar@iki.kfki.hu

Abstract

Migration of UO_2^{2+} through Boda Claystone borecore disc samples was studied by using saturated uranyl acetate solutions in break-through cells. LA-ICP-MS was used to analyse the distribution of uranium in the bore core discs stored in the cells for ca. 1900 days. $\text{Fe}^{2+}/\text{Fe}^{3+}$ ratios were monitored in the mineral components of clay before and after the experiments by Mössbauer spectroscopy. Strong accumulation of uranium in a few mm thick surface layer was detected. This process was not accompanied with any noticeable change in the $\text{Fe}^{2+}/\text{Fe}^{3+}$ ratio of minerals. Thus as for the accumulation of uranium under the recent conditions, coupled redox $\text{Fe}^{2+} \Rightarrow \text{Fe}^{3+}$ processes cannot be considered.

Introduction

Uranium species may take part in redox processes which may influence their migration properties in geological media. For instance, mobile U(VI) (uranyl, UO_2^{2+}) can be converted to immobile U(IV) (uranium oxide) if a simultaneous reverse redox process proceeds in the neighbouring medium, in our case in the minerals of a host rock matrix.

The Boda Claystone Formation is considered as a possible host rock for future high level nuclear waste disposal in Hungary. Some of the mineral components of the stone contains iron as well, in some minerals as Fe^{3+} (eg. in hematite), and some other layered clay mineral may contain both Fe^{2+} and Fe^{3+} , e.g. in chlorite (Árkay et al. (2000), Varga et al. (2005)). The conditions can simply be illustrated on the Pourbaix diagram of the uranium by considering the region where the possible Eh-pH values occur in the rock under the natural conditions (Figure 1). It is shown that both $\text{Fe}^{2+} \Leftrightarrow \text{Fe}^{3+}$ and $\text{U(VI)} \Leftrightarrow \text{U(IV)}$ ($\text{UO}_2^{2+} \Leftrightarrow \text{UO}_2$) may proceed in the mentioned particular region.

Therefore, three different techniques were combined to obtain information on the possible role of the redox processes. First, the migration properties were followed in a break-through cell, which can be used for determination of effective diffusion constants. In our former studies diffusion constants of $^{125}\text{I}^-$, $^{99}\text{TcO}_4^-$, $\text{H}^{14}\text{CO}_3^-$ anions were determined in various Boda Claystone samples (Mell, et al. (2006), Lázár et al. (2009)). The second technique used was the Mössbauer spectroscopy which is able to distinguish

between the Fe^{2+} and Fe^{3+} states of iron present in various minerals of Boda Claystone (Burns (1994)). The third technique applied was laser ablation inductively coupled plasma mass spectrometry (LA-ICPMS). This method provides a mean to determine the isotopic composition in a 20 - 100 micron diameter spot, providing thereby a very sensitive tool to determine the spatial distribution of the studied isotope or element. The experiments were composed from the three parts accordingly: first the break-through measurements were carried out for a long period, (ca. 1900 days), then the cells were dismantled, the distribution of the uranium was determined along the diffusion path in the bore core cells, and additionally, prior to and after the measurements the $\text{Fe}^{2+}/\text{Fe}^{3+}$ ratios were determined in the surface layers of the sample discs by Mössbauer spectroscopy, whether any trace of $\text{Fe}^{2+} \Rightarrow \text{Fe}^{3+}$ transition could be evidenced.

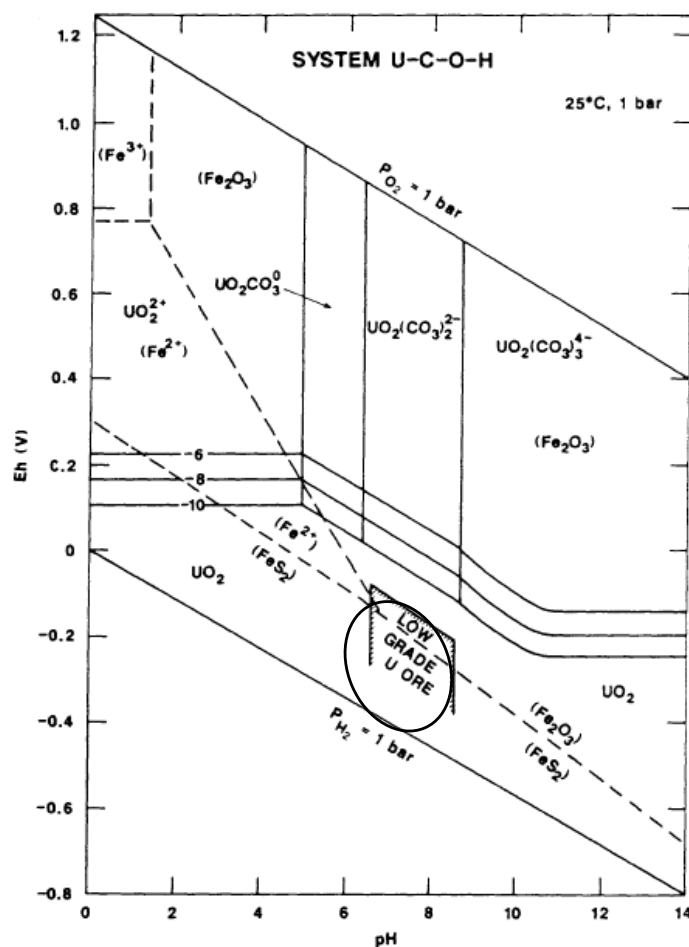


Figure 1. The Eh-pH Pourbaix diagram for uranium (from Brookins(1988)). The shaded area shows the estimated equilibrium conditions in the geological medium

Experimental

Samples

Samples were obtained from the deep region of Boda Claystone (- 1050 m) from horizontal boreholes Delta-5 (~ 80 m) – sample 1, and Delta-6 (~ 144 m) – sample 2. The rock is a claystone with albitic nests. The main constituents of sample 1 are: illite-

muscovite, albite, calcite-dolomite, hematite, quartz and chlorite (37, 22, 22, 8, 8 and 3 per cents, respectively). The mineral composition of sample 2 is similar.

For the break-through measurements ca. 10 mm thick discs were cut from the 47 mm diameter borecores.

Break-through measurements

These measurements were performed in the conventional arrangement: one compartment of the cell was filled with the saturated uranyl acetate solution (7.7 g uranium salt / 100 ml, using synthetic ground water), the other ca. 100 ml volume compartment was filled with plain ground water. The two compartments were separated with the ca. 10 mm thick sample discs. Small quantities (5 ml) of solutions were taken out from the two compartments in regular time intervals, the activities were measured with a scintillation counter, then the solutions were filled back to the cell (Figure 2.) Four parallel measurements were carried out, two with discs from sample 1, two other from sample 2.

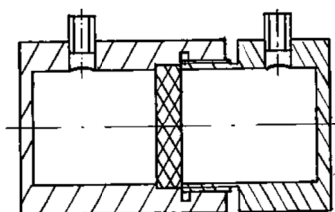


Figure 2. Scheme of the break-through measuring cell

LA-ICP-MS

Element 2 ICP-MS (Thermo Electron Corp., Germany) with magnetic sector field and single electron multiplier was used, equipped with UP-213 laser ablation system (New Wave Research, USA) with a Nd:YAG laser at a wavelength of 213 nm. The borecore samples were cut, then the 10 mm thick cross sections were analysed in perpendicular direction to their original surface plane with 10 micron s⁻¹ speed. The diameter of the evaporating laser beam was 95 micron, the frequency of shots was 10 Hz with energy of 0.08 mJ. On the total path 650 data points were analysed.

Mössbauer spectroscopy

A KFKI spectrometer was used in constant acceleration mode. The isomer shift parameters are relative to that of metallic alpha-iron. The spectra were decomposed to Lorentzian shape. The accuracy of positional parameters is ca. 0.03 mm/s.

Results

Break-through measurements

Figure 3 shows the results of break-through measurements carried out for c.a. 1900 days. The relative activity (a/a_0) is plotted against the elapsed time (a is the activity in the solution, a_0 is the activity at the very beginning, at $t = 0$). The top curve was recorded on samples taken from the compartment filled with the saturated solution of uranyl acetate. It is shown that in the early stage a certain drop had taken place in the amount of the uranium present in the solution, a/a_0 drops to ca. 75 per cent. (This can probably be attributed to the reactions of the saturated uranium solution with the ground water.) Later on, this state had been stabilized for a long while (ca. one year). Then a permanent decrease is seen – during further 4 years ca. half of the original amount of the uranyl ions disappeared from the solution. Surprisingly, on the other, “inactive” side of the measuring cell the uranium does not appear in detectable amount even after 1900 days (bottom curve, Figure 3).

For comparison, it might be mentioned that anions of $^{125}\text{I}^-$, $^{99}\text{TcO}_4^-$, $\text{H}^{14}\text{CO}_3^-$ were able to cross the sample discs in much shorter periods, break-through was observed in detectable extents under similar experimental conditions within already a month (Mell et al. (2006), Lázár et al. (2009)).

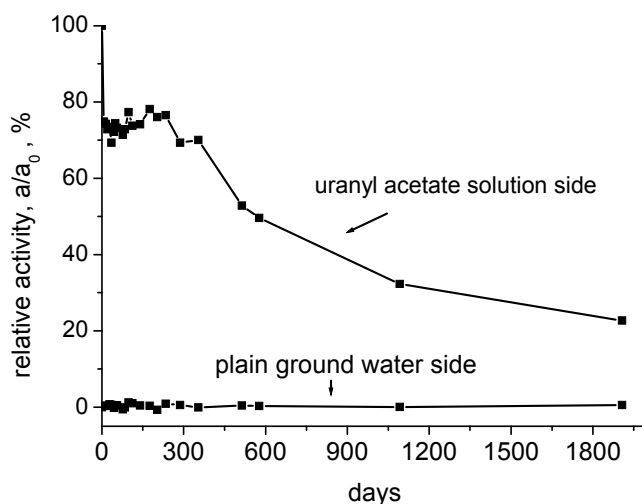


Figure 3. The decrease of the concentration of the uranium in the uranyl acetate solution (top curve), and the lack of break-through to the other compartment (bottom curve).

LA-ICP-MS measurements

The experiments were concluded after having ca. 1900 days elapsed. The distribution of the uranium was measured across the discs. Figure 4 shows typical distributions of ^{238}U (top curve) and ^{235}U isotopes (bottom) in logarithmic plot for the same sample which is shown in Figure 3. The method is very sensitive, the natural ^{238}U and ^{235}U contents of the original untreated sample are also seen as a constant low intensity background. As shown, the uranium from the uranyl acetate solution was able to migrate only to ca. 4

mm depth into the sample. In a first approximation a straight line can easily be drawn to the logarithmic plot, ie. with a first empirical approximation the distribution of the concentration can simply be described as:

$$C = C_0 e^{-kx} \quad , \quad \text{Eq. (1)}$$

where C is the concentration of uranium inside, C_0 is at the surface, x is the distance from the surface of sample and k is an empirical constant. The values can easily be determined from the plot (using for $(C/C_0)_{\text{surf}} / (C/C_0)_{x=4 \text{ mm}} \sim 40$), k will be approximately - 1.387 in mm^{-1} units. It can be visualized in other way as well, namely, that each mm corresponds to 2.5 times decrease in the concentration of uranium, as proceeding from the surface into the bulk sample. The distribution of the uranium in four samples have been measured all of them exhibited the same exponential distribution.

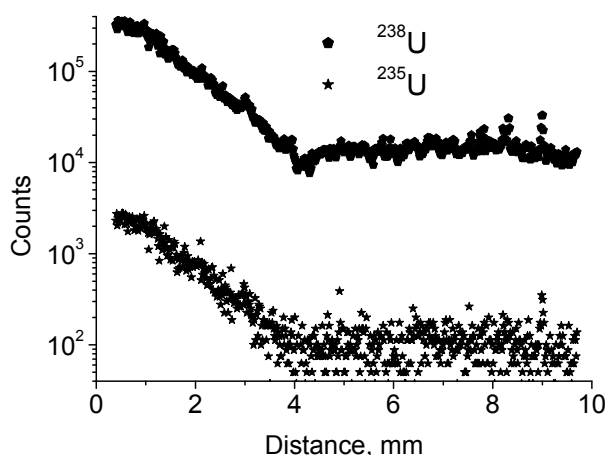


Figure 4. Distribution of uranium along the cross section perpendicular to the surface of the 10 mm thick disc of sample 2. The contact with the uranyl acetate solution was at 0 mm on the scale. The intensities of ^{238}U (top) and ^{235}U (bottom) are shown in logarithmic scale.

Mössbauer spectroscopy

Figure 5 shows spectra collected in wide (± 12 mm/s) and in narrow (± 4 mm/s) velocity ranges. In the wide range the full spectrum of hematite (Fe_2O_3) is shown (sextet), whereas in the narrower spectrum only the central part of hematite appears (two lines only). The clay minerals can be analysed with better resolution in the low velocity range. The Fe^{2+} and Fe^{3+} components can be distinguished both in the narrow and in the wide ranges.

For the identification of the ferrous component in the low velocity spectra, isomer shift (IS) and quadrupole splitting (QS) 1.13 mm/s and 2.62 mm/s values were used respectively, complemented with the two lines of hematite located at - 0.79 and 1.77 mm/s.

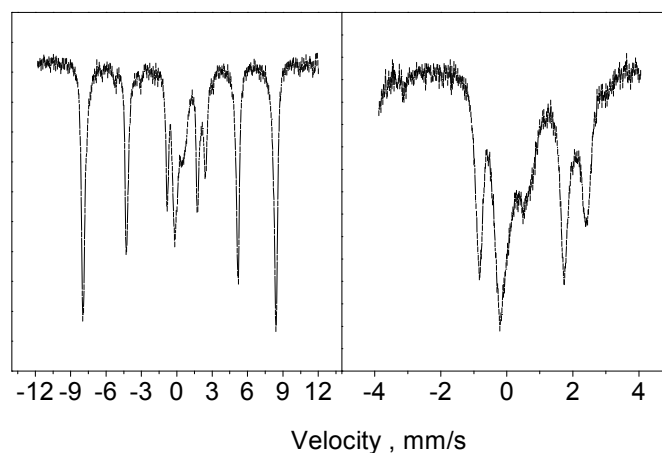


Figure 5 . Mössbauer spectra of sample 2 collected in wide (± 12 mm – left) and in narrow (± 4 mm/s – right) velocity ranges. On the left spectrum the whole contribution of hematite is shown, the right spectrum shows only the central part.

Table 1. Relative contributions of Fe^{2+} and Fe^{3+} components to spectra of sample 2, in per cent.

Experiment	1		2	
	in contact with U	inactive side	in contact with U	inactive side
Fe^{2+}	35	34	34.5	34
Fe^{3+} (hematite)	28	29	30	28
Fe^{3+}	37	37	35	38

In the same manner, similar values can be calculated from the high velocity range spectra of the slices taken from the outer slices of samples either having contacted with the uranyl solution or being in contact only with the “inactive” ground water. Furthermore, it is important to note, that these spectra are also very similar to those of the original claystone samples without any contact with any solution. (Further description and interpretation of Mössbauer spectra of the Boda Claystone samples can be found e.g. in Lázár et al. (2010).)

In short, for the present aspect the important informations are that Fe^{2+} and Fe^{3+} forms coexist in the samples, and the contact with uranium does not influence the $\text{Fe}^{2+}/\text{Fe}^{3+}$ distributions.

Discussion and Summary

From the combination of the three types of measurements it can be supposed that the presumed coupled $\text{Fe}^{2+} \Rightarrow \text{Fe}^{3+}$ redox processes are not dominant. To confirm this statement it is worth to consider additionally the mass balances of uranium and iron in the clay. The amounts of uranium and iron are comparable. In more detail, as for the uranium, from the 100 ml of the saturated uranyl acetate solution ca. 2/3 was absorbed

by the claystone. This amount is equivalent with ca. 10 mmol. With an overestimation of the amount of Fe^{2+} present in the 4 mm thick layer of the 47 mm diameter borecore sample it corresponds only 2.5 mmol. Thus, as for stoichiometry, the amount of sorbed uranium exceeds by far the amount of ferrous iron. And, as the Mössbauer experiments attested, no change in the Fe^{2+} contents were detected. Thus, it can be concluded that the simultaneous combination of the coupled redox processes, mentioned in the Introduction ($\text{Fe}^{2+} \rightleftharpoons \text{Fe}^{3+}$ and $\text{U(VI)} \rightleftharpoons \text{U(IV)}$) had not taken place. Instead, most probably sorption or other processes (e.g. precipitation) can be considered as prevailing in the accumulation of uranium.

The analysis and interpretation of the value obtained for the empirical constant k in Eq (1) may provide further information on the processes which take place, this work is in progress recently.

Acknowledgement

The research leading to these results has received funding from the European Union's European Atomic Energy Community's (Euratom) Seventh Framework Programme FP7/2007-2011 under grant agreement FP7 212287 CP (ReCosy) project.

References

- Árkai P., Balogh K., Demény A., Fórizs I., Nagy G., Máthé Z. (2000) Composition, diagenetic and post-diagenetic alterations of a possible radioactive waste repository site: the Boda Albitic Claystone Formation, southern Hungary. *Acta Geologica Hungarica* 43, 351-378.
- Brookins, D.G., (1988) Eh-pH diagrams for Geochemistry, Springer. 153.
- Burns, R.G., (1994) Mineral Mössbauer spectroscopy: Correlations between chemical shift and quadrupole splitting parameters, *Hyperfine Interactions*, 91, 739-745.
- Lázár K., Megyeri J., Parneix, J-C. Máthé Z., Szarvas T. (2009) Diffusion of anionic species ($^{99}\text{TcO}_4^-$, $\text{H}^{14}\text{CO}_3^-$) and HTO in Boda Claystone borecore samples. 4th Annual Workshop Proceedings, Eds: G. Buckau et al., *Wissenschaftliche Berichte FZKA 7461* 199-204.
- Lázár K., Máthé Z., Földvári M. (2010) Various redox conditions in Boda Claystone as reflected in the change of $\text{Fe}^{2+}/\text{Fe}^{3+}$ ratio in clay minerals. *Journal of Physics: Conference Series*, 217, 012053.
- Mell P., Megyeri J., Riess L., Máthé Z., Hámos G., Lázár K., (2006) Diffusion of Sr, Cs, Co and I in argillaceous rock as studied by radiotracers. *Journal of Radioanalytical and Nuclear Chemistry* 268, 411-417.
- Varga R.A., Szakmány Gy, Raucsik B., Máthé Z., (2005) Chemical composition, provenance and early diagenetic processes of playa lake deposits from the Boda Siltstone Formation (Upper Permian), SW Hungary. *Acta Geologica Hungarica* 48, 49-68.

REDOX POTENTIAL IN THE NEAR FIELD OF A DEEP GEOLOGICAL REPOSITORY CONTAINING CARBON STEEL WASTE PACKAGES

David Dobrev, Radek Červinka, Antonín Vokál*

Nuclear Research Institute Rez (Czech Republic)

* Corresponding author: voa@ujv.cz

Abstract

This article presents the results of an investigation into the effects of the corrosion of thin wire and plates of carbon steel and iron powder on the evolution of the redox potential (Eh) in bentonite water. All the experiments were carried out in an anaerobic box to limit the effect of oxygen on corrosion reactions. The Eh and pH were measured discontinuously to avoid the impact of corrosion product layers from the corrosion of carbon steel or iron powder precipitated on the surface of electrodes on the results of measurements. The extent of the corrosion was determined by measuring hydrogen generated during anaerobic corrosion of iron. The nature of corrosion layers formed on the surface of carbon steel plates was determined using X-ray diffraction, Raman spectroscopy and analyses of the elemental composition of carbon steel surface layers using ESCA electron spectroscopy. It was shown that the Eh of the bentonite solution measured by a Pt electrode decreased very slowly in an anaerobic box without the presence of iron and settled at values above 0 mV. Only after carbon steel or iron samples were immersed did it start to decrease to negative values. The results obtained showed that the evolution of Eh and pH differs depending on whether carbon steel or iron powder was used in experiments. In experiments with carbon steel the Eh after an initial, great decrease, started to continuously increase in the following days, in experiments with iron powder no increase of Eh after a very fast decrease was observed. In all the experiments with carbon steel plates the pH decreased during the 30-day experiments, but in experiments with iron powder it remained constant. It was shown that the corrosion temperature affects the corrosion rate and consequently the evolution of Eh in the system. The higher the temperature, the higher the initial decrease of Eh. Also the ratio of the surface of the carbon steel plates to the volume of solution significantly affects the evolution of Eh in the system. The higher this ratio the higher the initial decrease in Eh. The difference between the behaviour of carbon steel plates and iron powder may be due to the formation of protecting, passive corrosion layers on the surface of carbon steel samples. It was shown that the nature of these layers depends on the corrosion temperature. In the experiment carried out at 40 °C no corrosion product layer was detected by Raman spectroscopy but this layer was detected on samples corroded at 60 or 70 °C. Using an ESCA probe, it was found that the firmly adhering corrosion product layers containing a high amount of oxygen were formed during the corrosion of carbon steel plates in the bentonite water under anaerobic

conditions. Geochemical calculations were carried out for the experiments with carbon steel plates and iron powder using the PHREEQC geochemical code. For experiments with carbon steel plates the modelled values (Eh, pH) showed large differences from the experimental data, but the results for experiments with iron powder were much closer.

Introduction

Conditions in the near field of deep geological repositories with carbon steel waste packages could be strongly affected by the reactions of iron with groundwater penetrating through the clay buffer to the surface of the waste packages. A number of studies have been therefore devoted to investigating iron reactions in repository conditions (Marsch and Taylor, 1988, Beverskog and Puigdomenech, 1996, Johnson and Smith, 2000, Peat et al., 2001, Smart et al., 2002, Wersin et al., 2003, Xia et al., 2005, Carlson et al., 2007), but only the work of Peat et al., 2001 deals with the experimental investigation of the effect of the corrosion of carbon steel wires on the change of Eh and pH in anoxic water. The experiments of Peat et al., 2001 were conducted in artificial bentonite-equilibrated water, at a pH of more than 10.4 at 30 °C. They observed a decrease of both Eh and pH after immersing carbon steel wires in anoxic bentonite-equilibrated water.

In the experiments published earlier by the authors of this paper (Dobrev et al., 2009) the corrosion system was simulated by carbon steel plates immersed in synthetic, bentonite water with and without the addition of iron powder. The redox potential and the pH of bentonite water in closed reaction vessels were measured with platinum and gold electrodes. It was found in Dobrev et al., 2009 that the Eh of bentonite water decreased significantly by the addition of iron powder into the reaction vessels and it remained constant for the time of the experiments. But in the experiments without iron powder, the Eh started to increase after a while. It was assumed in Dobrev et al., 2009 that this apparent increase of Eh of the bentonite water was most probably caused by the formation of precipitated iron corrosion product layers from the corrosion of carbon steel or iron powder on the surface of the platinum or gold electrodes. Nevertheless some increase of Eh was also observable, if it was measured discontinuously after carefully cleaning the electrodes before measuring (Dobrev et al., 2009). It was assumed that this increase was affected by the diffusion of oxygen in reaction vessels. Therefore our additional experiments presented in this paper have been carried out in an anaerobic box, with oxygen below 0.1 ppm, to prevent oxygen penetrating into reaction vessels.

One of the experiments presented in this paper was also carried out with a high surface iron powder with the main aim of increasing the extent of the corrosion reaction and consequently the effect of iron corrosion reactions on the Eh change. Iron powder has been used in a number of works before (Lantenois, et al., 2005, Wilson et al., 2006, Perronet et al., 2007, de Combarieu et al., 2007, Osacky et al., 2010) to model the effect of iron corrosion on the conditions evolved in a repository, and particularly on the change of bentonite surrounding waste packages. Iron instead of carbon steel has also been used in papers on modelling the effect of canister materials on the conditions evolved in a repository (Bildstein, 2006, de Combarieu, 2007). A comparison of the effect of carbon steel and iron powder on the evolution of the Eh and pH of bentonite water presented in this paper can thus contribute to a deeper understanding of the

differences between the impact of these materials on the conditions evolved in the near field of a deep geological repository.

Experimental

The first corrosion system consisted of a thin 2 mm diameter carbon steel wire immersed 5 cm in 800 ml of synthetic bentonite water, the second system of 1 or 10 carbon steel plates in 2 L of synthetic bentonite pore water and the third system of 30 g of iron powder in the same amount of water. The carbon steel both as wire and plates correspond to the Czech standard ČSN ISO 11321 with a carbon concentration of approximately 2.74 % (the plate is 70x70x1 mm with an 8 mm diameter circle cut out in the centre). The iron powder was Alfa Aesar A Johnson Matthey Company (< 10 micron, 99.9+% (metal basis), surface 0.205 m²/g). Before the experiment the carbon steel wire and plates were polished with grid 600 sandpaper and washed with ethanol. The surface of the carbon steel plates was 99.7 cm²/plate.

The synthetic bentonite pore water was prepared according to the proposal of Brudbury and Bayens, 2003. The composition of this water and the quantity of chemicals used in preparing it is given in Table 1. The pH of this water was 7.5, conductivity 2100 mS.m⁻¹, and ionic strength 0.29 mol.l⁻¹.

Table 1. Compositions and chemicals for preparing synthetic bentonite water

Salt	m [g.l ⁻¹]	ion	m [mol.l ⁻¹]
NaCl	0	Na ⁺	0.2
KCl	0.2013	K ⁺	0.0036
MgCl ₂ .6H ₂ O	1.5491	Mg ²⁺	0.0190
MgSO ₄ .2H ₂ O	0.5438	Ca ²⁺	0.0087
CaCl ₂ .2H ₂ O	0	Cl ⁻	0.065
CaSO ₄ .2H ₂ O	1.5842	SO ₄ ²⁻	0.1
SrCl ₂ .6H ₂ O	0.0216	F ⁻	0.0003
Na ₂ SO ₄	12.843	HCO ₃ ⁻	0.0008
NaHCO ₃	0.0748		
NaF	0.0092		

This water should correspond to the composition of sodium bentonite Volclay KWK 20-80 with a density of 1600 kg.m⁻³. The synthetic bentonite water was put into the anaerobic box 14 days before the experiments began to remove the oxygen trapped in the solution. It was found that after approximately 14 days the Eh of the bentonite water almost did not decrease (see Fig. 2).

Two independent electrodes, a 1 mm diameter platinum wire electrode 20 mm long (Beckman Instruments, USA) and a 1 mm diameter gold wire electrode 50 mm long (Safina, Czech Republic), were used to continuously measure the redox potential in the corrosion system with carbon steel and bentonite water. The redox potential was measured between the work electrode (platinum, gold) and reference Ag/AgCl electrodes. These reference electrodes were prepared by coating Ag wire with silver

chloride in our laboratory. During the experiments precipitated corrosion products were cleaned from the working and reference electrodes with hydrochloric acid. A combined platinum electrode ORC 103–BAZ (Theta '90, Czech Republic, a 4 mm diameter platinum disc) was also used to measure Eh in the system with steel plates (measuring period 1 day). The same platinum electrode and an additional XCL 101 XB2 platinum electrode (Gryf HB, Czech Republic, 2 mm diameter platinum disc) were used to measure the redox potential in the corrosion system with iron powder. An HC 113 electrode (Theta '90, Czech Republic) was used to measure pH and in the system with iron powder also a pH PCL 321 XB2 electrode (Gryf HB, Czech Republic). Electrodes from Gryf HB were also used for measuring in the carbon steel wire system.

The experiments were carried out at various temperatures controlled by a TDC 2 Temperature Controller (Gamry Instruments Inc, USA) with a Series 988 PID control unit (Watlow Controls, USA). The concentration of Fe^{3+} and S^{2-} ions in the solution after the experiments was measured with a UV/Vis spectrometer Specord 205 – 222A358 (Analytic Jena Co., Germany), Fe^{3+} by a modified ferozzine method (Viollier et al., 2000) and for sulphide detection a Spectroquant test kit (No. 167, Merck) was used. The total iron concentration in the solution was measured with an atomic absorption spectroscope Varian SpectrAA 200 (Varian, U.S.A).

Corrosion products on the carbon steel plates after the experiments were measured by Raman spectrometer LabRam (Horiba - Jobin Yvon, France) with two lasers (He – Ne and Ar), by X-ray diffraction Philips-Xpert PRO (PANalytical, Netherlands) and by ESCA Probe P (Omikron Nanotechnology, Germany) in the CAE mode (Constant Analyser Energy).

The rate of corrosion was determined by measuring the hydrogen evolved from corroding iron using equipment developed in NRI (Figure. 1).

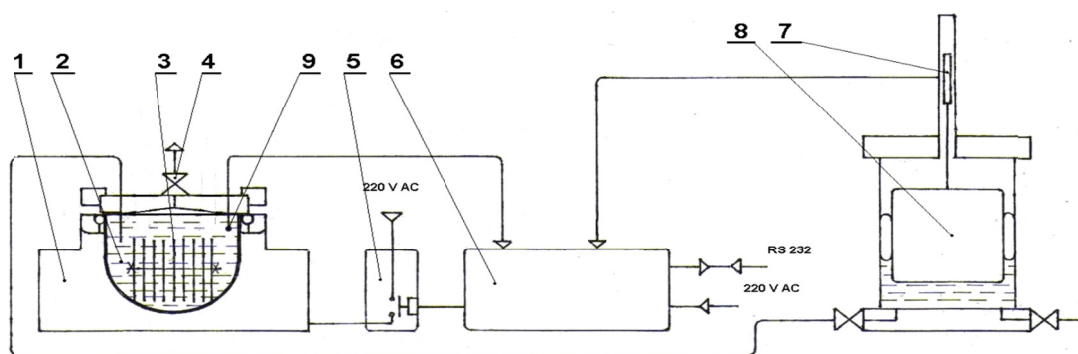


Figure 1. Hydrogen evolution measurements device. 1 – Heater, 2 – Constant pressure chamber, 3 – Sample, 4 – Gas sampling valve, 5 – Temperature regulator, 6 – Data acquisition equipment, 7 – Volume change detector, 8 – Source of constant pressure, 9 – Temperature sensor

This device enables hydrogen evolution to be measured continuously at different temperatures and at a constant water pressure. The pressure source is a heavy piston, moving in mutually interconnected pressurized cylindrical vessels with a rolling

membrane (Brůha and Pelech, 1989). The volume measurement is based on detecting the piston position, which depends on the medium volume.

Results and Discussion

Figure 2 shows the change of Eh and pH of synthetic bentonite water before immersing and immediately after immersing the carbon steel wire in a synthetic bentonite solution.

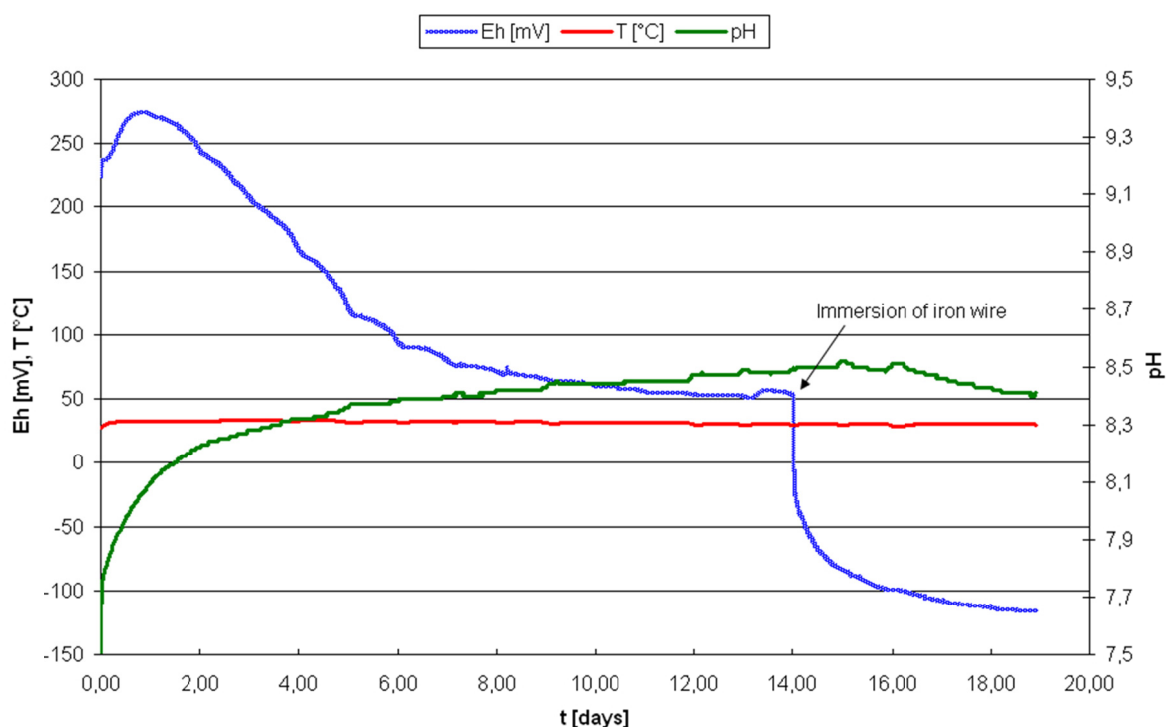


Figure 2. Eh, pH and the temperature of bentonite water before the experiments and immediately after immersing a thin iron wire in the solution

It can be seen that despite very low oxygen values in the anaerobic box the Eh of the bentonite water solution is positive before immersing the iron. Only after the carbon steel wire is immersed in the solution does the Eh quickly decrease to negative values and settle at values corresponding to the steady state of chemical reactions of corrosion and precipitation of iron proceeding in the reaction vessel.

The dependence of the change of Eh over time after immersing one carbon steel plate in 2L of bentonite water solution is shown in Fig. 3. It can be seen that the higher the corrosion temperature the higher the initial decrease of Eh, but it seems that in the long term Eh will almost level out, no matter what the corrosion temperature is, if the temperature is above 40 °C. The resulting Eh after 30 days from all experiments with one carbon steel plate was in the range of –100 to –250 mV.

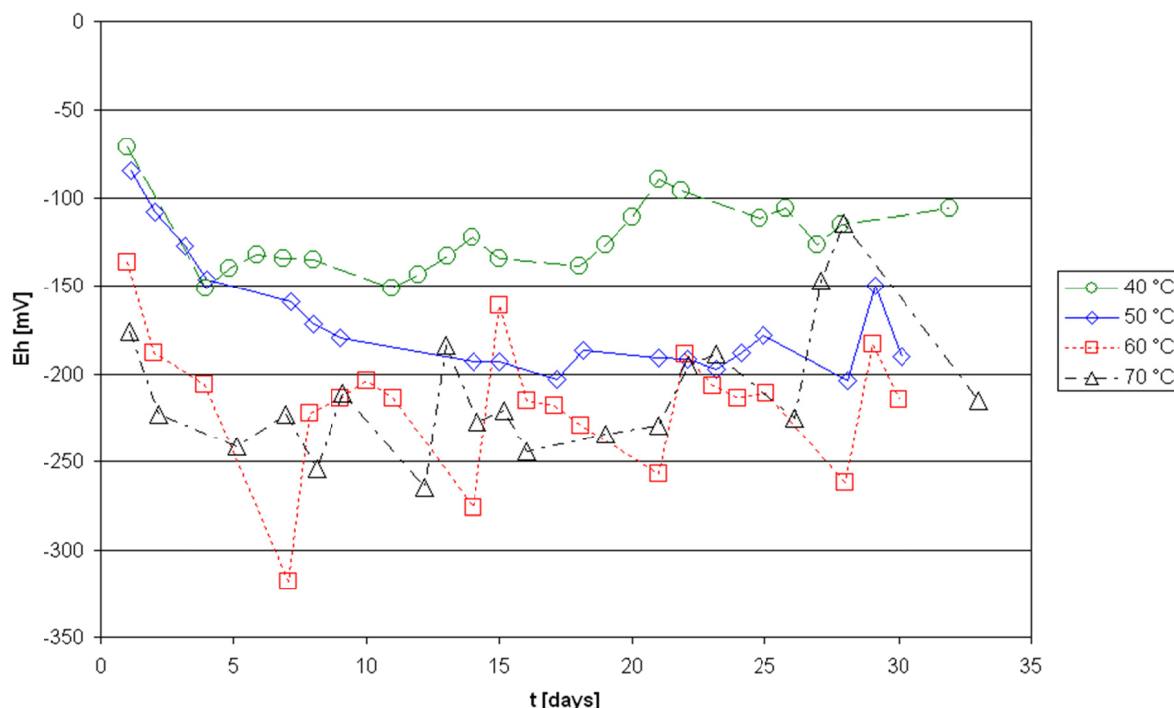


Figure 3. Change of Eh potentials of bentonite water due to the corrosion of one carbon steel plate at various temperatures.

The pH solution change after immersing one carbon steel plate in 2L of bentonite solution is shown in Fig. 4. It can be seen that the pH decreased during the 30 days of the experiments from values slightly below 8 to values below 7. Similar results have already been obtained in the work of Peat et al, 2009, where the pH decreased in 15 days from 10.4 to 9.8. But contrary to this work they also observed a decrease of pH before immersing carbon steel wires in the water.

The change of Eh in the system with ten carbon steel plates in 2 L of bentonite water at various temperatures is shown in Fig. 5. The initial values of Eh are lower compared to previous experiments conducted with one plate. Again the results show that the higher the corrosion temperature the higher the initial decrease of Eh, but after a very short time the Eh starts to increase to values which approach the values obtained in previous experiments with one carbon steel sample. The resulting Eh is in the same range as that of the experiments with one carbon steel plate.

The decrease of pH in the system with ten carbon steel plates is more evident here (Figure 6) than in the previous case with one carbon steel plate.

In another experiment, 30 g of iron powder was used instead of carbon steel samples. The ratio between the surface of the samples and the volume of the solution in the corrosion system was $(1 \text{ cm}^2)/(20 \text{ mL})$ with one carbon steel plate, and $(1 \text{ cm}^2)/(2 \text{ mL})$ with ten carbon steel plates, but in the experiment with iron powder it was $(30 \text{ cm}^2)/(1 \text{ mL})$. The results in the change of Eh with iron powder are shown in Figure 7. The Eh decrease was much greater than in previous experiments with carbon steel plates, the resulting Eh being approximately -500 mV .

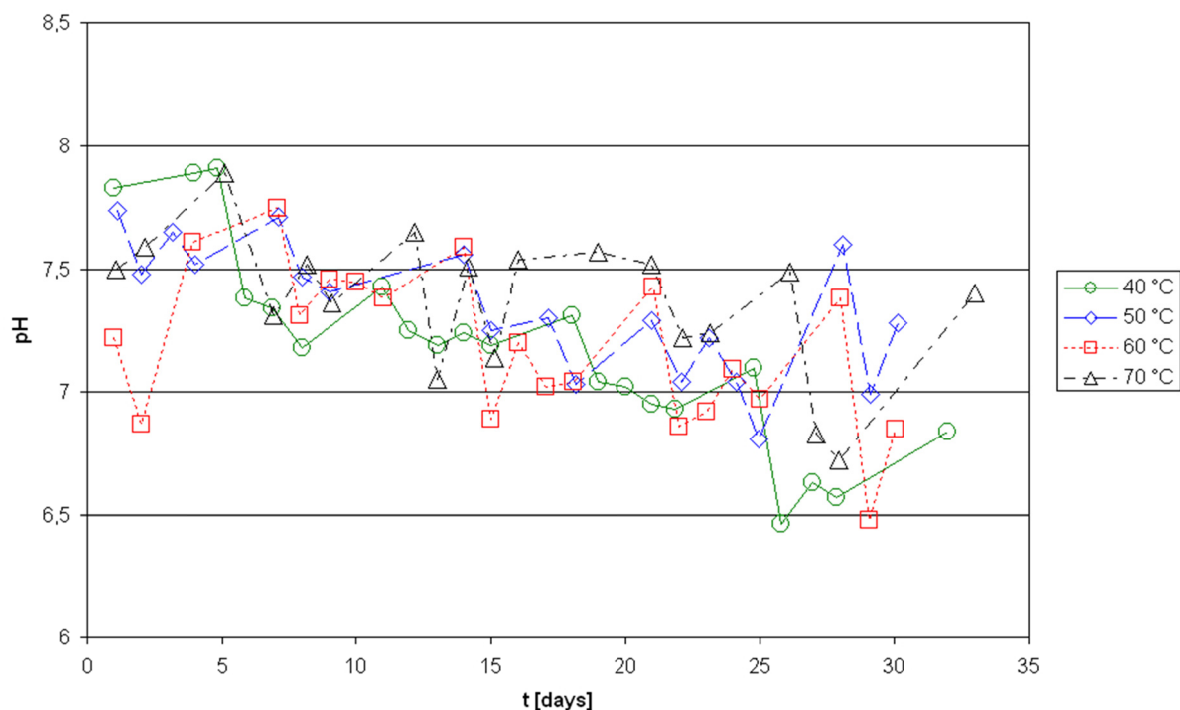


Figure 4. pH change of bentonite water due to the corrosion of one carbon steel plate at various temperatures.

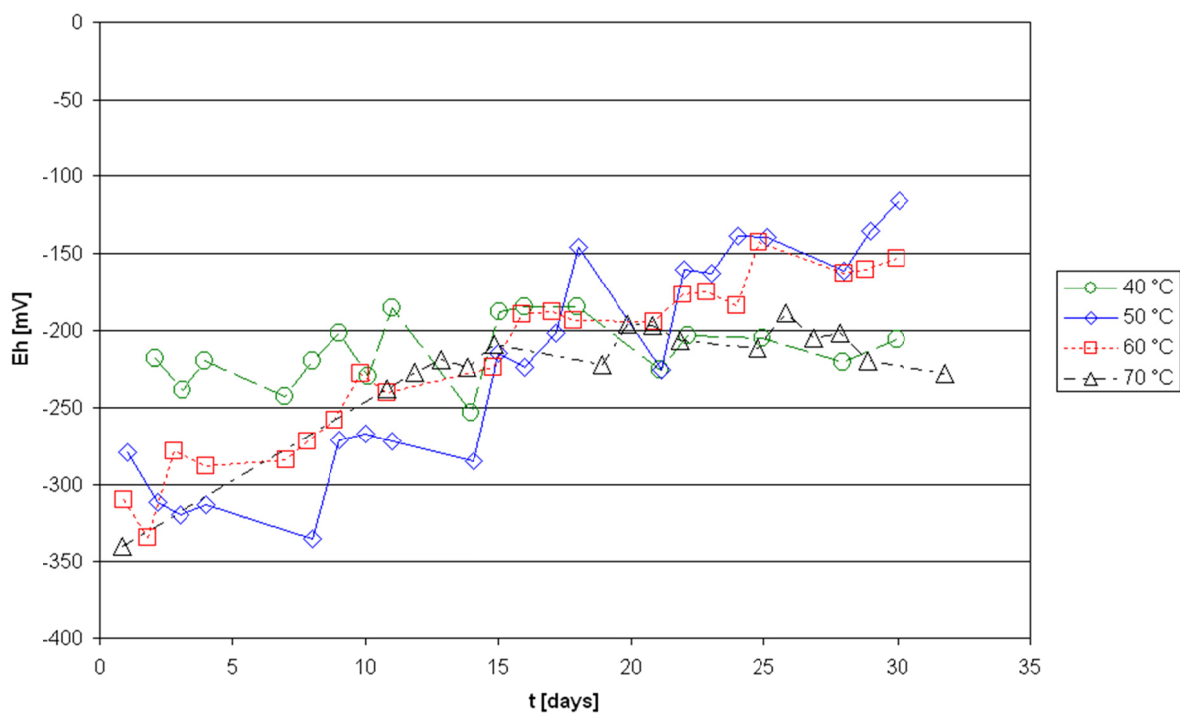


Figure 5. The redox potential change in the system with 10 samples of carbon steel in 2 l of synthetic water.

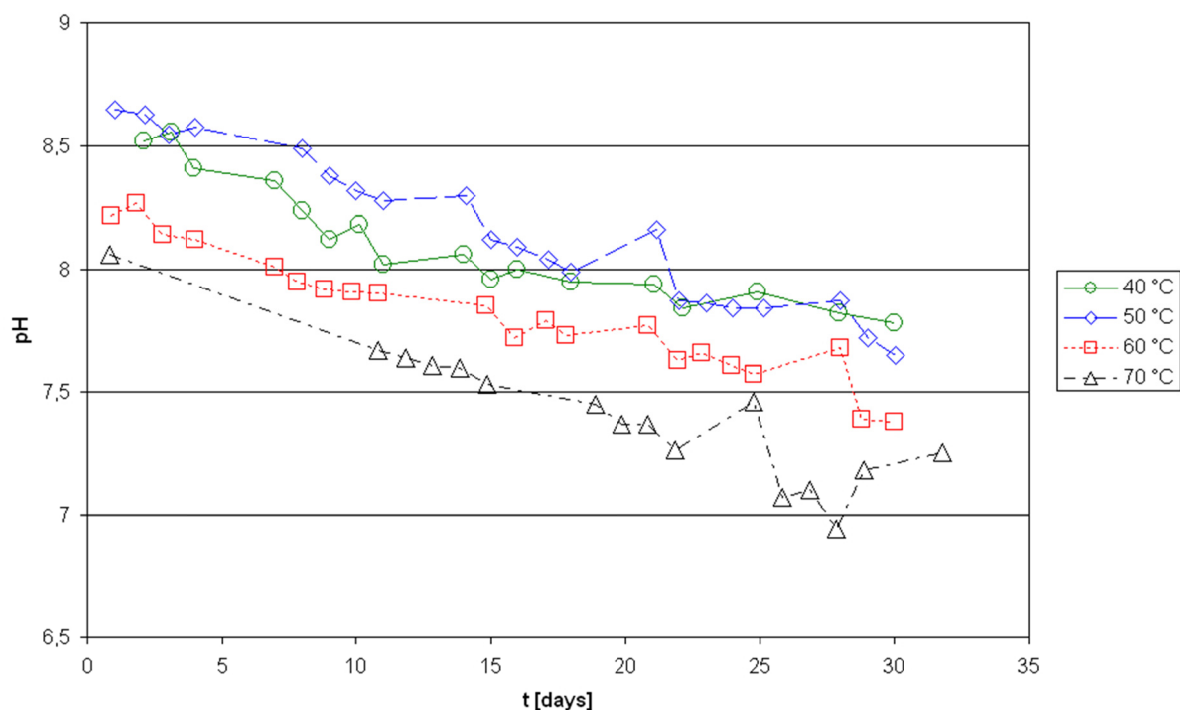


Figure 6. The pH change in the system with 10 samples in 2 L of synthetic water.

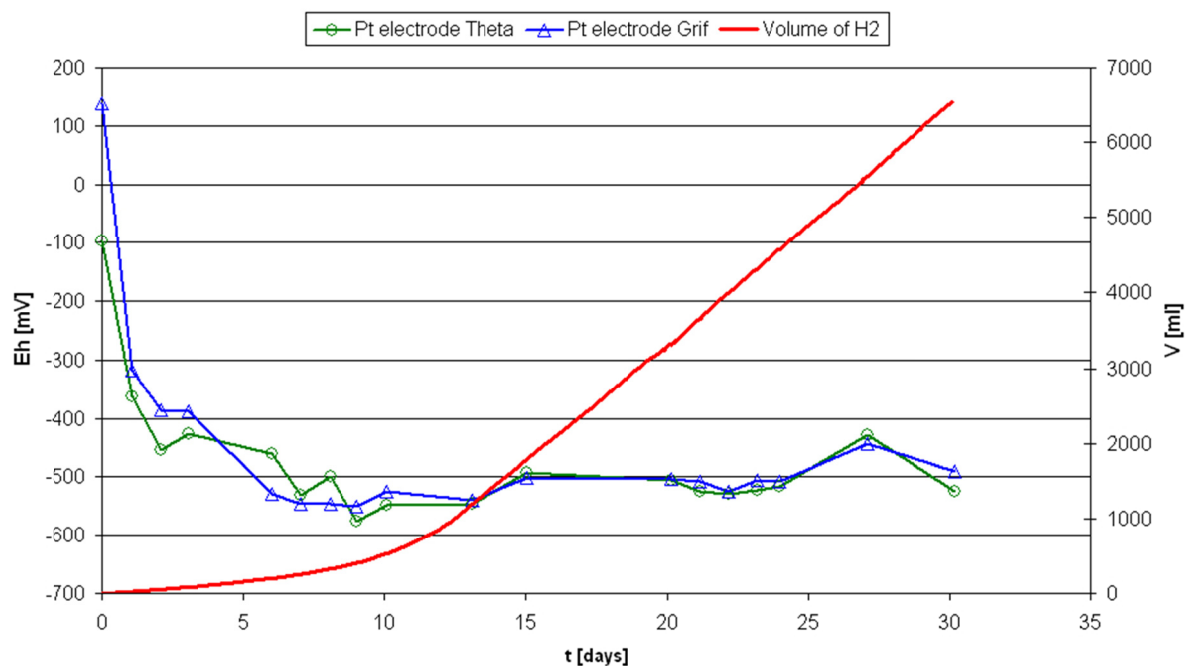


Figure 7. The redox potential in corrosion system with iron powder at 70 °C

Contrary to the systems with carbon steel plates, the pH almost did not change during the 30-day experiment (Fig. 8).

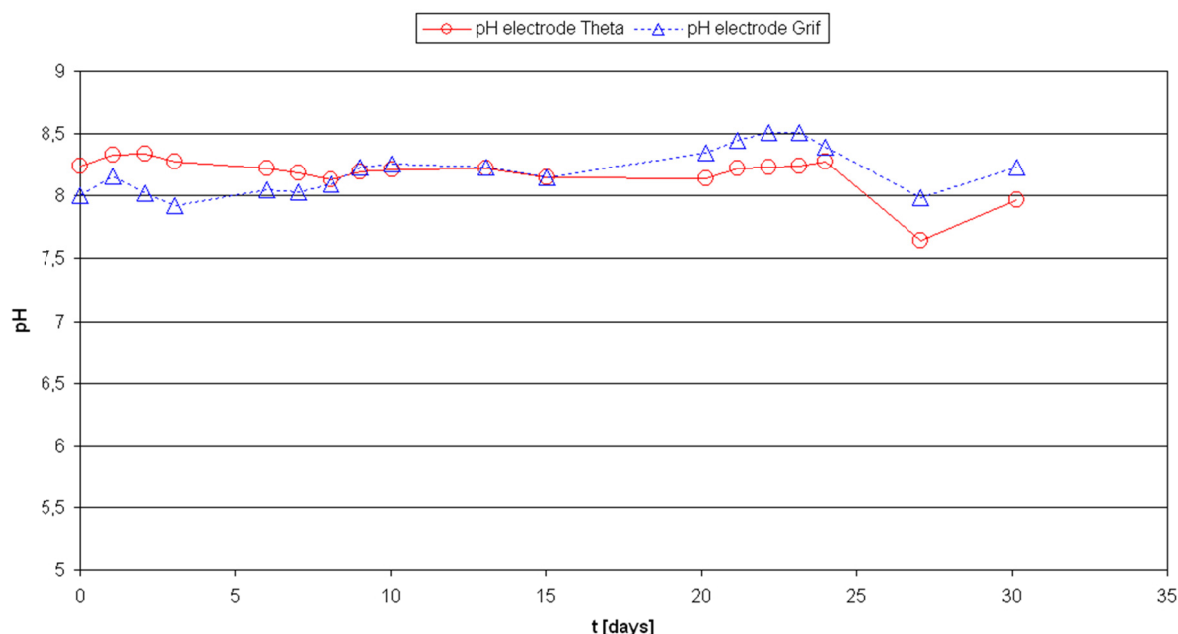
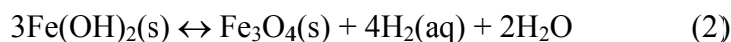
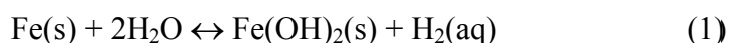


Figure 8: The pH in a corrosion system with iron powder at 70 °C.

The amount of hydrogen accumulated in the system was measured by measuring the hydrogen evolution rate using the methodology described in the experimental part. The rate of hydrogen accumulation in an anaerobic, corrosion system can be described by the following reactions (Appelo, Postma, 1999):



The linear character of hydrogen evolution accumulation after approximately 10 days of corrosion (red line in Fig. 7) of iron powder indicates that a stable corrosion rate of iron, corresponding approximately to a rate of 5.2 $\mu\text{m/year}$, was reached.

There is a great difference in the character of the hydrogen evolution curves between the one shown in Fig. 7 for iron powder and those for carbon steel plates in Fig. 9. The rate of hydrogen generation in all the experiments with carbon steel plates was very fast at the beginning of the corrosion, but after a relatively short time it decreased to much lower values. A greater decrease in corrosion rates after an initial increase was observed for the system with 10 plates presented in our previous paper (Dobrev et al., 2009). In agreement with the work of Marsh and Taylor, 1988, it is assumed that Fe(OH)_2 or Fe_3O_4 corrosion products could accumulate on the metal surface producing partially protective layers that limit the corrosion rate, the corrosion rate being thus relatively constant in the pH range 5 – 10, because the electrolyte contacting the metal surface becomes saturated with Fe(OH)_2 which buffers the pH at ~ 9.5 . But it must be also taken into account that under some circumstances oxygen may exert a beneficial effect on the corrosion of iron and steel by facilitating the formation of a truly passivating surface layer. When this occurs the rate of general corrosion is reduced to typically 0.1

– 1 $\mu\text{m year}^{-1}$ (Marsh and Taylor, 1988). This could also explain the character of the hydrogen evolution curves shown in Fig. 9.

It is often assumed that passive iron corrosion product layers are composed of a cubic spinel structure of a defective, inner layer of Fe_3O_4 (magnetite) and outer layer of $\gamma\text{-Fe}_2\text{O}_3$ (maghemite) (Kruger, 1989, Johnson and Smith, 2000, Lu and Macdonald, 2008), the thickness of these passive layers depending on the potential of the solution. Lu and Macdonald, 2008 determined that the thickness of the passive layer was in the range of 0.5 – 2 nm for iron corroding in a borate buffer solution at pH 8.4, with an applied potential of 0.2V to 0.6V. The lower the potential, the lower the thickness of the passive layer. The nature of corrosion product layers was investigated by Raman spectroscopy, X-ray diffraction and ESCA Probe P described in the experimental part of this paper.

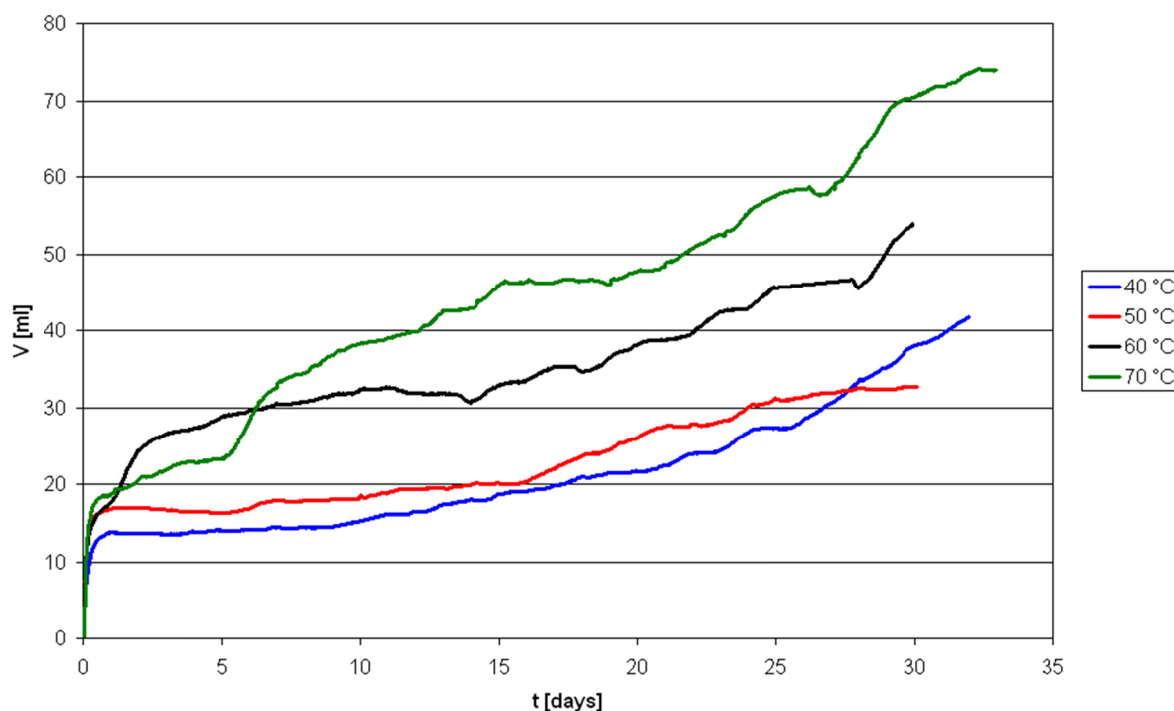


Figure 9. The evolution of hydrogen in a system with one carbon steel plate.

Corrosion product layers on the surface of the samples from experiments with one carbon steel plate conducted at 40 °C and 50 °C were under the detection limit of Raman spectroscopy and X-ray diffraction. This suggests that the thickness of these layers was very thin. Probably an increase of the corrosion rate of the sample corroded at 40 °C after approximately 20 days shown in Fig. 9 could indicate that it might lose its protective character.

The corrosion product layer of the sample from the experiment carried out at 60 °C and 70 °C was also under the detection limit of X-ray diffraction but by Raman spectroscopy magnetite/maghemite (band 676 cm^{-1}), maghemite (1430 cm^{-1}) and hematite (band 220 cm^{-1}) were detected (Figure 10 and Figure 11). The thickness of the corrosion layer on these samples was also under the detection limit of X-ray diffraction.

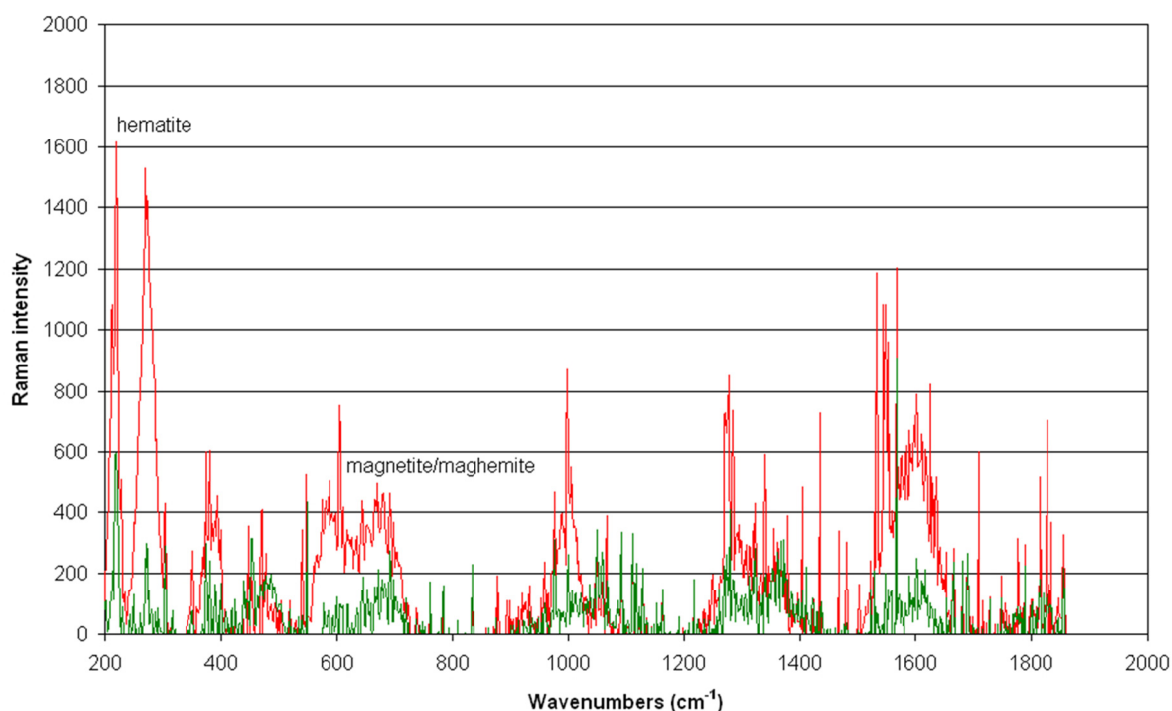


Figure 10: Raman spectrum from different carbon steel plate places at 60 °C.

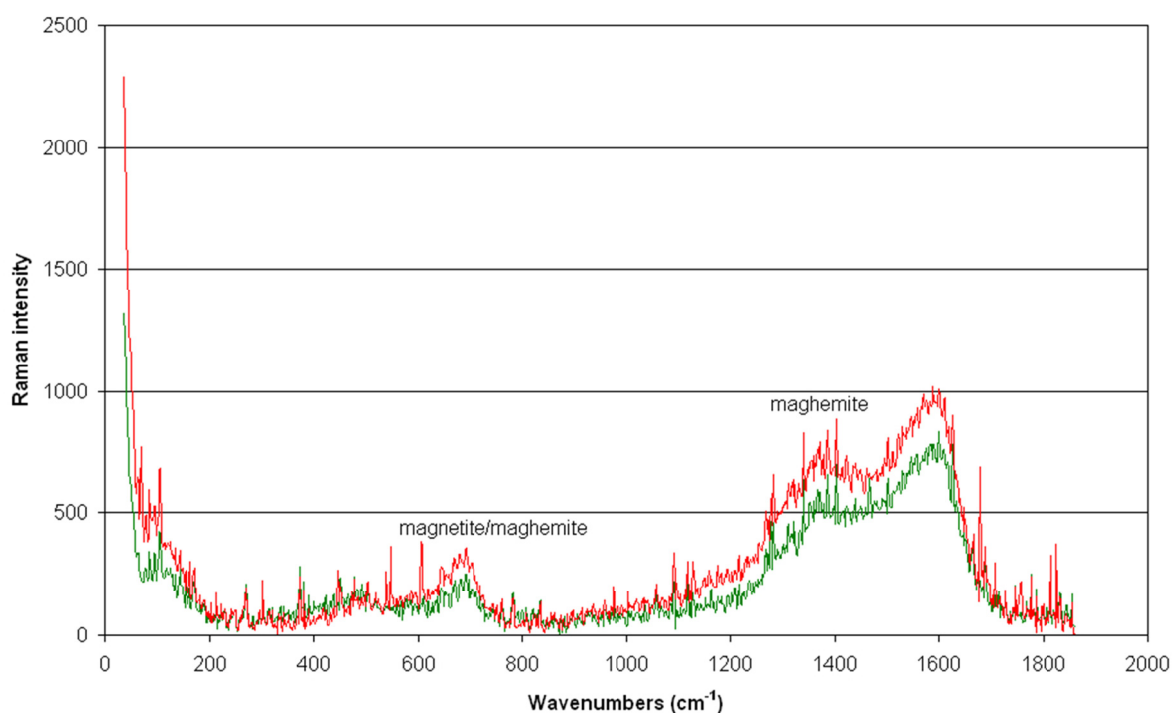


Figure 11: Raman spectrum from different carbon steel plate places at 70 °C.

One of the most interesting results that emerged from our experiments was achieved by analyzing the elementary composition of the corrosion layers by ESCA. A relatively

large number of elements were detected, but with very low percentages, so that only the 3 most important elements: C, O, and Fe are shown in Tables 2 and 3. Table 3 shows the results after etching (evaporation) a very thin surface layer (thickness nm) by an electron beam. It can be seen that after removing the first layer affected by atmospheric corrosion, the percentage of iron on the surface of a non-corroded sample is much higher than on the surfaces of corroded samples. The oxygen content in surface layers increases with the corrosion temperature. Therefore we can say that this method provided evidence that an adhering corrosion layer of non-negligible thickness was formed on the surface of carbon steel during anaerobic corrosion at 60 and 70 °C, protecting carbon steel against further fast corrosion. The oxygen content in the surface layers of samples corroded at 60 °C and 70 °C, is, however, higher than the stoichiometric ratio of Fe/O in magnetite or maghemite so that the results suggest that the composition of passive corrosion products layers is not only formed by an inner layer of magnetite and outer layer of maghemite as proposed in previous papers (Kruger, 1989, Lu and Macdonald, 2008).

Table 2: Corrosion layer composition measured at different temperatures. Number 0 means a sample without a corrosion layer.

<i>0m</i>	sample/temperature, °C				
At%	0	40	50	60	70
C 1s	49.37	64.33	37.4	29.2	50.27
O 1s	34.72	23.07	44.77	47.7	35.92
Fe 2p	9.89	1.47	4.21	5.33	2.75

Table 3: Corrosion layer composition after evaporating (etching) a thin surface layer by an electron beam. 0 is a sample without a corrosion layer.

<i>etching</i>	sample/temperature. °C				
At%	0	40	50	60	70
C 1s	7.44	53.2	19.74	4.89	12.95
O 1s	6.41	19.47	33.56	52.67	50.10
Fe 2p	86.15	9.77	26.04	21.14	14.57

After the experiments the solution was acidified and the iron content (III) was measured using UV spectroscopy and the total iron content in the solution by AAS. The results of the measurements are shown in Tables 4 – 6.

Table 4: Iron concentration in the solution during the experiment with 1 carbon steel plate.

t [°C]	c(Fe) mol.l ⁻¹	c(Fe ³⁺) mol.l ⁻¹
40	7.63×10^{-4}	1.43×10^{-7}
50	5.34×10^{-4}	1.79×10^{-7}
60	-	1.43×10^{-7}
70	6.02×10^{-4}	0.72×10^{-7}

Table 5. Iron concentration in the solution during the experiment with 10 carbon steel plates.

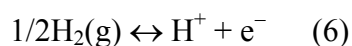
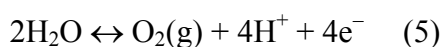
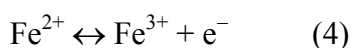
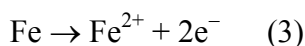
t [°C]	c(Fe) mol.l ⁻¹	c(Fe ³⁺) mol.l ⁻¹
40	5.66×10 ⁻⁴	3.58×10 ⁻⁸
50	6.60×10 ⁻⁴	2.51×10 ⁻⁸
60	5.16×10 ⁻⁴	4.30×10 ⁻⁸
70	6.68×10 ⁻⁴	5.37×10 ⁻⁸

Table 6. Concentration of iron ions in the solution during the experiment with iron powder

Day	c(Fe ²⁺) mol.l ⁻¹	c(Fe ³⁺) mol.l ⁻¹	c(Fe) mol.l ⁻¹
15	1.59×10 ⁻⁴	8.38×10 ⁻⁶	1.67×10 ⁻⁴
20	1.61×10 ⁻⁴	Under detection limit	1.61×10 ⁻⁴
27	1.74×10 ⁻⁴	Under detection limit	1.74×10 ⁻⁴
30	3.16×10 ⁻⁴	1.12×10 ⁻⁴	4.28×10 ⁻⁴

The results confirm that a significant amount of ferric ions are formed under strong anaerobic conditions during corrosion experiments. The rather low concentration of ferrous ions detected indicates that most of the ferrous ions were precipitated from the solution (from the amount of hydrogen generated it was calculated that in the experiment with iron powder almost 15 g of 30 g of iron was consumed).

We can assume that in these relatively simple carbon steel/iron/bentonite water systems, the Eh is mainly determined by the reactions of iron and iron species with water:



Before immersing iron in the bentonite water solution the Eh of the solution is associated with a partial pressure of H₂ and O₂ as shown in reactions (5) and (6) (Stumm and Morgan, 1981). After immersing iron in the solution the concentration of Fe²⁺ will start to control the Eh according to equations (3) and (4). It can be assumed that after corrosion product layers are formed on the surface of the carbon steel plates the resulting Eh will be determined by the nature of the corrosion products layers and their homogeneity and porosity affecting the migration rate of Fe²⁺ ions through them. The long-term evolution of the Eh and pH will depend on a number of factors that cannot be easily predicted using somewhat short term experiments, which are affected

by the kinetics of chemical reactions. Geochemical codes can be used to compare theoretical hypotheses and after validation for predicting the further development of geochemical conditions in repositories. A simple approach was chosen to simulate Eh evolution during the corrosion process. First the corrosion process was simulated by adding iron to the bentonite pore water solution in steps according to the measured corrosion rate. Based on speciation in the solution and Fe(II)/Fe(III) activities the Eh was calculated. Second, the solution was equilibrated with Fe-bearing minerals (magnetite, Fe(OH)₂) and the Eh was calculated again. These calculations were carried out for both experiments (with carbon steel plates and iron powder) using PHREEQC geochemical code version 2.15.07 (Parkhurst and Appelo, 1999) with the OECD NEA database (TDB NEA 17, 2005).

The following processes were taken into account in simulations: the trace concentration of oxygen in the anaerobic box (< 0.1 ppm), the reduction of sulphate to sulphide and the precipitation of corrosion products that are not in equilibrium with the solution.

The input data for the model is summarised below:

- Volclay KWK 20-80 porewater was used (Table 1).
- The temperatures were 40, 50, 60, 70 °C and the stability constants (log K) were recalculated to this temperature based on the reaction enthalpy (ΔH_r^0) and Van't Hoff equation by PHREEQC itself. We assumed that the reaction enthalpy is a constant for the involved species and phases.
- Additions of Fe (as Fe²⁺) to the solution were simulated kinetically according to the experimental corrosion rate.
- The reduction of carbonate to methane was not allowed in the model calculations, because of kinetic constraints. Otherwise, this reaction is of course thermodynamically possible and very often microbially mediated. The sulphate to sulphide reduction was partly allowed ($8e^- + 9H^+ + SO_4^{2-} = HS^- + 4H_2O$, log K = -8), because of a specific sulphide smell occurring after the experiments. However the sulphide concentration was under the detection limit of the spectrophotometric measurement technique (<0.1 mg/l).
- The evolution of Eh reflected the main redox couple Fe(II)/Fe(III).

Generally, for experiments with carbon steel plates the modelled and measured values (Eh, pH) showed great differences from the experimental data. Because other considered processes (oxygen trace, sulfate to sulphide reduction, corrosion products kinetics) did not evidently clarify these discrepancies, the explanation can be caused by passive corrosion product layers forming on the surface of the carbon steel plates, which cannot be represented by pure minerals. However with iron powder, the experimental and simulated data was in close agreement (see Fig. 12). Similar results were obtained in the work of de Combarieu et al. 2007.

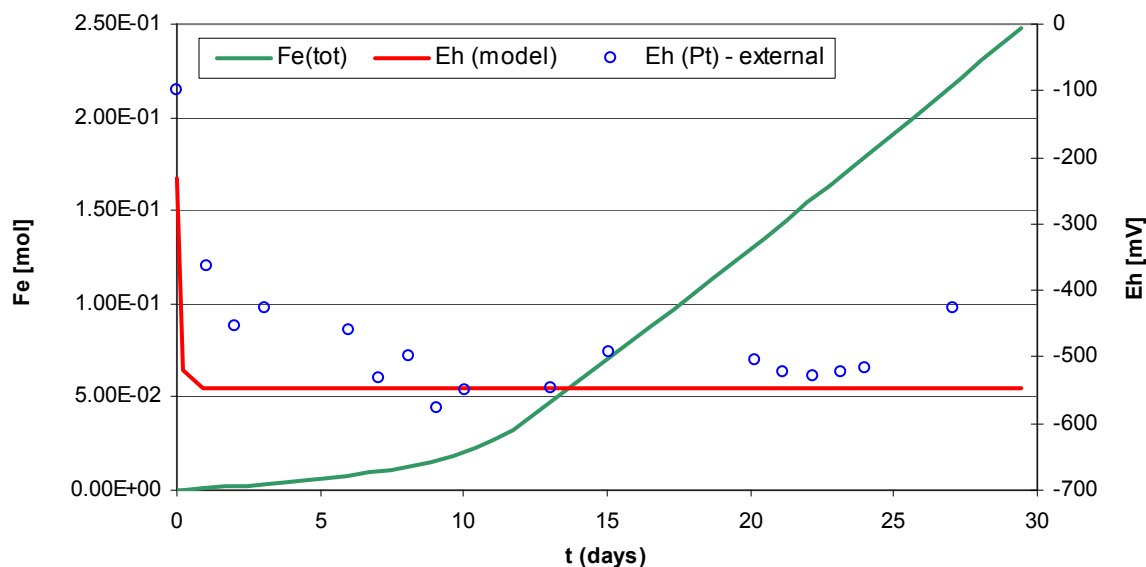


Figure 12. Comparison of the calculated and measured redox potential values in the iron powder corrosion system at 70 °C.

Summary and Conclusions

The achieved results clearly suggest that the development of Eh in the near field of deep geological systems with carbon steel is not easily predictable because it depends on a great number of factors such as temperature, the ratio of metal surface to the water contacting carbon steel and the composition of the water, let alone the physical migration constraints of corrosion products due to the compacted bentonite surrounding carbon steel waste packages. But it seems that the major problem is that the passive corrosion products layer is formed with a composition on the surface of carbon steel plates that does not correspond to the common minerals used in geochemical calculations.

The experimental data obtained here also shows a great difference between experiments with carbon steel plates and iron powder. With carbon steel the Eh, after an initial decrease, started to increase, with iron powder it decreased and settled at a relatively constant value. With carbon steel plates the pH decreased throughout the duration of the experiment but with iron powder the pH was relatively constant throughout the 30-day experiment. The experiments thus clearly showed that replacing carbon steel with iron in simulating near field conditions in a deep geological repository can lead to highly misleading results.

It was shown that the higher the corrosion temperature the greater the initial decrease of Eh after immersing the carbon steel plates in the solution, but at the end of 30-day experiments the Eh was almost level and no great temperature effect was noticeable. The ratio of the surface of the samples to the volume of the water solution had a significant effect. The higher this ratio, the higher the initial decrease of Eh, but again in

the long term the Eh and pH developed in the near field of a repository will level out, depending mainly on the nature of the corrosion layers formed.

The nature of the corrosion layers formed on carbon steel samples depends on a number of factors. First, it was seen that the corrosion temperature had a great effect. In experiments carried out at 40 or 50 °C the corrosion layers were very thin, almost undetectable by X-ray diffraction or Raman spectroscopy methods, however these layers could be detected by these methods on samples from experiments carried out at 60 and 70 °C. By determining the element composition it followed that the corrosion layers formed at these temperatures have a much higher oxygen content and lower iron content than the layers of non-corroded samples or samples corroded at 40 °C.

Unfortunately, the somewhat short-term, 30-day experiments conducted in this work do not enable the further behaviour of corrosion product layers formed on the surface carbon steel plates to be easily predicted. Much longer experiments under conditions approaching the conditions in a repository will have to be carried out to obtain a more reliable estimate of the geochemical conditions evolved in the near field of deep geological repositories. Another problem, which will be studied in an additional period of the RECOSY project, is the effect of bentonite minerals on iron reactions in repository conditions.

Acknowledgement

The research leading to these results has received funding from the European Union's European Atomic Energy Community's (Euratom) Seventh Framework Programme FP7/2007-2011 under grant agreement no. 212287 (RECOSY project). This work was also partly funded by the Ministry of Education, Youth and Sports of the Czech Republic. We would also like to thank to M. Člupek and P. Sajdl from the Department of Analytical Chemistry, ICT Prague for analysing the corrosion products.

References

- Appelo C.A.J., Postma D. (1999) Geochemistry, groundwater and pollution. A.A. Balkema/Rotterdam/Brookfield.
- Beverkog B., Puigdomenech I. (1996). Revised Pourbaix diagrams for iron at 25-300°C. Corrosion Science. 38, 2121-2135.
- Bildstein O., Trotignon L., Perronnet M., Jullien M. (2006) Modelling iron-clay interactions in deep geological disposal conditions, Physics and Chemistry of the Earth 31. 618-625.
- Bradbury M.H., Baeyens B. (2003) Porewater chemistry in compacted re-saturated MX-80 bentonite. Journal of Contaminant Hydrology 61. 329-339.
- Brůha P., Pelech I. (1989) Czechoslovak patent no. 259785, Int. Cl. F 16 J 3/00.
- Carlson L., Karnland O., Oversby V.M., Rance A.P., Smart N.R., Snellman M., Vahanen M., Werme L.O. (2007) Experimental studies of the interaction between

anaerobically corroding iron and bentonite. *Physics and Chemistry of the Earth*. vol. 1578, pp. 334-345.

de Combarieu G., Barboux P., Minet Y. (2007) Iron corrosion in Callovo-Oxfordian argillite: From experiments to thermodynamic/kinetic modelling, *Physics and Chemistry of the Earth* 32. 346-358.

Dobrev D., Bruha P., Vokal A. (2009): The effect of iron corrosion on conditions inside waste packages, KIT Report FZKA 7466, p. 93.

Johnson L.H., Smith P.A. (2000) The interaction of radiolysis products and canister corrosion products and the implications for spent fuel dissolution and radionuclide transport in a repository for spent fuel, Nagra Technical Report 00-04.

Kruger J. (1989) The nature of the passive film on iron and ferrous alloys, *Corrosion Science*. 29, 149-162.

Lantenois S., Lanson B., Muller F., Bauer A., Jullien M., Plancon A. (2005) Experimental study of smectite interaction with metal Fe at Low temperature: 1. smectite destabilization, *Clays and Clay Minerals*, Vol. 53, No. 6, 597-612.

Lu Z., Macdonald D.D. (2008) Transient growth and thinning of the barrier oxide layer on iron measured by real-time spectroscopic ellipsometry, *Electrochimica Acta* 53, 7796-7702.

Marsh G.P., Taylor K.J. (1998) An assessment of carbon steel containers for radioactive waste disposal. *Corrosion Science*, 28, 289-320.

Osacký M., Šucha V., Czímerová A., Madejová. (2010) Reaction of smectites with iron in a nitrogen atmosphere at 75 °C. *Applied Clay Science*. 237-244

Parkhurst D.L., Appelo C.A.J. (1999): User's guide to PHREEQC (version 2). A computer program for speciation, batch-reaction, one-dimensional transport and inverse geochemical calculations. USGS. Water resources investigations report. 99-4259. U.S. Geol. Survey. Denver. Colorado.

Peat R., Brabon S., Fennel P.H.H., Rance A.P., Smart N.R. (2001) Investigation of Eh, pH and corrosion potential of steel in anoxic groundwater. SKB Technical report TR-01-01.

Perronet M., Villiér F., Jullien M., Razafitianamahotovo A., Raynal J., Bonnin D. (2007) Towards a link between the energetic heterogeneities of the edge faces of smectites and their stability in the context of metallic corrosion, *Geochimica et Cosmochimica Acta*, 71, 1463-1479.

Savoye S., Legrand L., Sagon G., Lecomte S., Chausse A., Messina R., Toulhoat P. (2001) Experimental investigations on iron corrosion products formed in bicarbonate/carbonate-containing solutions at 90 °C, *Corrosion Science* 43, 2049-2064.

Smart N.R., Blackwood D.J., Werme L. (2002) Anaerobic Corrosion of Carbon Steel and Cast Iron in Artificial Groundwaters: Part 1 - Electrochemical Aspects, *Corrosion*, 58, 547.

Smart N.R., Blackwood D.J., Werme L. (2002) Anaerobic Corrosion of Carbon Steel and Cast Iron in Artificial Groundwaters: Part 2 - Gas Generation, *Corrosion*, 58, 627.

Smart N.R., Fennell P.A.H., Peat R., Spahiu K., Werme L. (2000) Electrochemical Measurements during the Anaerobic Corrosion of Steel, Mat. Res. Soc. Symp., Vol. 663, MRS 2001. p. 487, Sci Basis XXIV, Sydney.

Stumm W., Morgan J.J. (1981) Aquatic Chemistry, An Introduction Emphasizing Chemical Equilibria in Natural Water, 2nd edition, John Wiley & Sons Inc.

Viollier E., Inglett P.W., Hunter K., Roychoudhury A.N., Van Cappellen P. (2000) The ferrozine method revisited: Fe(II)/Fe(III) determination in natural waters, Applied Geochemistry, 15, 785-790.

Wersin P., Johnson L.H., Schwyn B., Berner U., Curti E. (2003) Redox Conditions in the Near Field of a Repository for SF/HLW and ILW in Opalinus Clay, Nagra Technical Report 02-13.

Xia X., Idemitsu K., Arima T., Inagaki Y., Ishidera T., Kurosawa S., Iijima K., Sato H. (2005) Corrosion of carbon steel in compacted bentonite and its effect on neptunium diffusion under reducing condition, Applied Clay Science 28, 89-100.

THE APPLICATION OF MICROSENSORS FOR THE DETERMINATION OF REDOX PROCESSES IN BIOFILMS FROM URANIUM CONTAMINATED ACIDIC MINE DRAINAGE WATERS

Evelyn Krawczyk-Bärsch ^{1*}, Thuro Arnold ¹, Emanuel Eisbein ², Vinzenz Brendler ¹,
Ulf Jenk ³, Udo Zimmermann ³

¹ Helmholtz-Zentrum Dresden-Rossendorf e.V., Institute of Radiochemistry, P.O. Box
510119, 01314 Dresden (D)

² TU Bergakademie Freiberg, Institute of Physical Chemistry, Akademiestraße 6, 09596
Freiberg (D)

³ Wismut GmbH, Jagdschaenkenstr. 29, D-09117 Chemnitz (D)

* Corresponding author: E.Krawczyk-Baersch@hzdr.de

Abstract

Microsensors were used in order to perform profiles of redox potential and pH within biofilms, which have formed uranium contaminated acidic mine drainage (AMD) waters in small drainage channels at an underground uranium mine in Saxony (Germany). The results clearly showed significant differences between the redox potential and pH of the AMD water in comparison to the measured values in the biofilm, indicating that the biofilms have built up their own microenvironment. The redox potential inside the biofilm, $E_h = +921 \pm 17$ mV was approximately 200 mV higher than in the surrounding water. The pH of the biofilm was characterized by a pH of 1.9 ± 0.1 , whereas the pH of the AMD water showed a higher pH of 2.6 ± 0.1 . The results were plotted into the pH- E_h diagram for the U-S-O-H-C system, which was constructed by using the analytical data of the drainage water for the calculation of the predominance fields of different uranium species. It clearly shows that an aqueous uranium(VI) sulfate complex exists in the biofilm as well as in the water under the ambient conditions. Laboratory experiments, simulating the first state of flooding of the uranium mine by increasing the pH of the AMD water, showed the influence of the *Ferrovum myxofaciens* dominated biofilms on the migration of uranium. Due to homeostatic mechanisms the microbes maintain their intracellular pH even when the pH of the water is increased. Consequently, an immobilization of uranium as biosorption or biorecipitation with the formation of Uranophane is inhibited in the biofilms as well as in the AMD water as long as *Ferrovum myxofaciens* will be the dominant bacteria of the biofilms.

Introduction

Several mechanisms of interactions of microorganisms with actinides under aerobic conditions are known, e.g. biosorption (Pons and Fuste, 1993), interactions with S-layers (Merroun et al., 2005) or bioprecipitation (Macaskie et al., 2000). Some of them have the potential of a substantial retention of actinides, like uranium. However, little is known about the retention processes of microbial community, such as biofilms. Since bacteria do not usually occur as single individual cells in nature but as multicellular communities, we have to draw our attention on these biofilms. Biofilms are known as populations of microorganisms that are immobilized at surfaces and are defined as matrix-enclosed bacterial populations (Costerton et al., 1995). They can be found in soils, groundwater and surface water environments and even in extreme environments (Flemming, 1995). They are characterized by building up their own microenvironment, which can differ significantly from that of the bulk solution with the consequence that biofilms are becoming more important in potential retention processes for actinides. For a better understanding of these processes the in-situ microbial metabolic processes have to be studied since these processes are sensitive to metals and their speciation and changes of redox potential, pH and oxygen will have an effect on the bioavailability of the metals. To characterize these geochemical parameters the application of microsensors is useful and has been described in recent years by a number of authors (e.g. de Beer, 2000; Revsbech, 2005; Kühl, 2005; Krawczyk-Bärsch et al., 2008) for microbial ecology studies. Since microsensors with a sensor tip of a few micrometers allow the measurements of fine scale, they have become an important method for recording chemical gradients in heterogeneous or homogeneous natural environments.

Within the framework of our studies, microsensors were used in order to obtain profiles of redox potential, pH and oxygen within biofilms from an underground uranium mine in Saxony (Germany), which is currently in the process of being flooded. In small drainage channels of uranium contaminated acidic mine drainage (AMD) water, thick biofilms have formed and occur as gelatinous filaments described in the literature as “macroscopic streamers” (Hallberg et al., 2006). Stalactite-like biofilms were hanging from the ceiling of the galleries. They consisted of a solid mineral basis whereas the most part appeared to be mucilaginous. Mine water was dripping from the ceiling and percolating the biofilms. The bacterial diversity of the streamers and the stalactite-like biofilms were described by Brockmann et al. (2010). The identification on the basis of 16S rDNA sequences showed a dominance of *Ferroplasma myxofaciens*, an acidophilic, autotrophic, iron oxidizing bacteria, which belongs to the *Betaproteobacteria*.

Experimental

Microsensor measurements were performed in the biofilms from the drainage channel on-site and in the laboratory by using redox potential and pH electrodes, each with a tip diameter of 10 µm. For redox potential measurements a miniaturized platinum electrode from Unisense (Aarhus, Denmark) was connected via a high-impedance millivoltmeter to a reference electrode, a simple open-ended Ag/AgCl electrode with a gelstabilized electrolyte. After the measurements the obtained values were corrected using a correction factor after Stumm and Morgan (1996), which is dependent on the temperature and the molar concentration of the electrolyte of the reference electrode. Measurements of pH were performed by a miniaturized conventional pH electrode from

Unisense (Aarhus, Denmark). The pH electrode was connected via a high-impedance millivoltmeter to a reference electrode as described before and calibrated by using commercially available buffers. The redox potential and pH sensors were fixed in a holder on a motor-driven micromanipulator stage, connected with a motor controller for a precise small-scale positioning and for automated measurements in 50 μm steps within the biofilms. A number of microprofilings were performed in the biofilm, starting the measurements at the biofilm/water-air interface and becoming progressively immersed into deeper zones of the biofilm towards the centre of the streamers and the stalactite-biofilms.

Additionally, biofilm samples were taken from the drainage channel and prepared for sensor measurements in the laboratory by positioning the biofilms in a self-constructed rectangular flow cell with an outer dimension of 121×42×15 mm. During the measurements the AMD water was pumped through the flow cell in a closed circuit with a flow velocity rate of 4 mL/min, simulating the condition on-site. In further experiments the first phase of flooding was simulated by increasing the pH of the AMD water to a neutral pH of approximately 6.8 by adding controlled amounts of 1 M NaOH, while the water was pumped in a closed circuit through the biofilm. The pH of the water was measured two times a day during 95 hours and was readjusted to 6.45 – 6.80 since it decreased often < 4 . Redox potential and pH measurements were performed in the biofilm and in the AMD water twice after 20 and 95 hours, respectively.

AMD water from the channels was sampled for anions and cations analysis. The analytical data of the water was used for the calculation of the predominance fields of different uranium species in the pH-Eh diagram for the U-S-O-H-C system at 15°C by using the geochemical speciation code “Geochemist’s Workbench” Version 8.0.8/ACT2 Version 8.0.8.

Results and discussion

Microprofilings started at the biofilm/water interface of the streamers. The first measuring point was depicting a redox potential of the bulk solution, $E_h = +718 \text{ mV} \pm 8 \text{ mV}$, which was confirmed by separated measurements in the collected AMD waters. Between the first and the second point a transition zone between water and the biofilm with a thickness of approximately 50 μm is shown. It could be described like a diffusive boundary layer, where dissolved material is transported away from the water into the biofilm. In this layer the redox potential is increasing quickly. As soon as the electrode penetrates into the biofilm the redox potential gets stabilized showing a value of $+866.1 \pm 0.9 \text{ mV}$. Finally, in the centre of the biofilm a high redox potential of $+921 \pm 17 \text{ mV}$ was detected. Additionally, the biofilm was characterized by a pH of 1.9 ± 0.1 , whereas the pH of the AMD water showed a higher pH of 2.6 ± 0.1 . The results of the microsensor measurements clearly show a difference between the redox potential and pH of the AMD water in comparison to the measured values in the biofilm. The redox potential inside the biofilm is approximately 200 mV higher than in the surrounding water.

The calculated theoretical predominance stability fields of the solid uranium species found in the AMD water under the ambient condition are shown in the constructed pH-Eh diagram (Fig. 1). The area of $\text{pH} > 4.8$ and $E_h < +960 \text{ mV}$ is defined by the stability

field of the solid U(VI) mineral Uranophane $[\text{Ca}(\text{UO}_2)_2(\text{SiO}_3\text{OH})_2 \cdot 5\text{H}_2\text{O}]$. At more reducing conditions, the formation of the U(IV) mineral Coffinite $[\text{U}(\text{SiO}_4)_{1-x}(\text{OH})_{4x}]$ is possible in the area of $\text{pH} > 0$ and $\text{Eh} < +300$ mV. The plotted redox potential and pH values measured in the AMD water and in the biofilm appear in the area of aqueous solution, indicating that an aqueous uranium(VI) sulfate complex exists under these conditions in the biofilm as well as in the AMD water. In fact, the highly mobile aquatic uranium sulfate species $\text{UO}_2\text{SO}_{4(\text{aq})}$ was determined in previous TRLFS studies (Arnold et al., 2011).

Under the ambient conditions there is no immobilization of uranium neither by the biofilm nor by the AMD water. Since the uranium mine is currently in the process of being flooded the local geochemical conditions are changing in particular caused by the inflow of water and the closure of the galleries. The pH of the water will increase, accompanied by a decrease of the redox potential and oxygen concentration. The geochemical condition shown in the pH-Eh diagram will change with the possible consequence of potential immobilization processes of uranium by removal from the aqueous phase with the subsequent formation of solid uranium(IV) or uranium(VI) species. In laboratory experiments the first state of flooding of the mine was simulated in flow cells by neutralization of the AMD water. The results revealed the influence of the *Ferrovum myxofaciens* dominated biofilm. Although the pH was adjusted to a neutral pH during 95 hours, the pH of the AMD water decreased often. It may be suggested that pH homeostatic mechanisms, e.g. active proton pumping (Michels and Bakker, 1985) and release of protons by efflux (Tyson et al., 2004) are used by the microbes to maintain their living condition. The results of the microsensor measurements, which were performed after 20 and 95 hours, are found again in the area of aqueous solution (Fig. 1) with a trend towards the calculated predominance fields of uranium minerals.

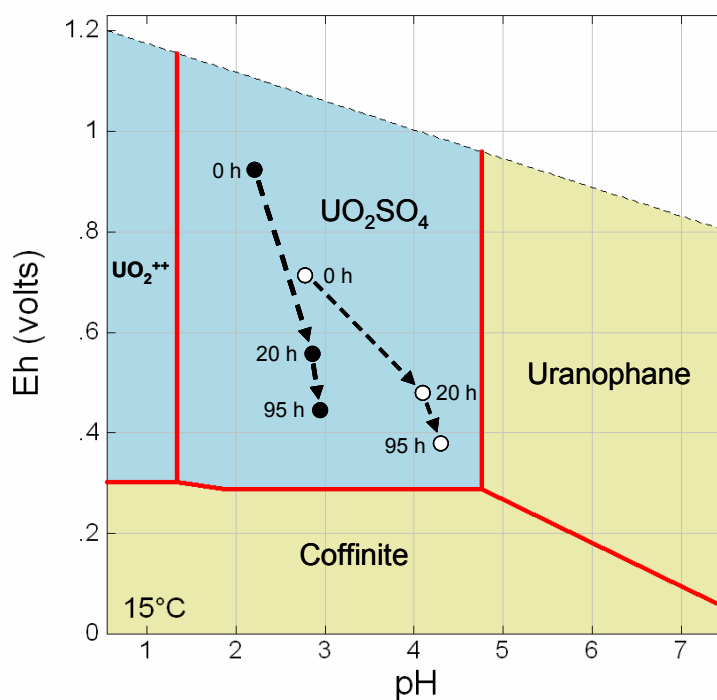


Figure 1: Calculated pH-Eh diagram for U-S-O-H-C system at 15 °C. Eh and pH data of the macroscopic streamers (●) were plotted in comparison to the AMD solution (○) before, 20 and 95 hours after the increase of the pH of the AMD water.

Summary and Conclusions

Microsensor measurements of the redox potential and the pH within the biofilms and the AMD water revealed that the retention of uranium from the AMD water by forming solid uranium(VI) or uranium(IV) species in the biofilms and in the AMD water is inhibited. We suggest that bioremediation and immobilization of uranium will be delayed as long as *Ferrovum myxofaciens* is the dominant bacteria of the biofilms. A substantial retention of uranium can be considered when basic changes of the geochemical conditions of the underground situation occur during a later phase of the flooding process, e.g. inflow of water and anaerobic conditions. As a consequence, the microbial diversity will change and the pH of the AMD water and in any evolved biofilms will increase to > 4.8.

Acknowledgement

The European Atomic Energy Community Seventh Framework Programme [FP7/2007-2013] under grant agreement n° 212287, Collaborative Project ReCosy is thanked for financial support. U. Schaefer and C. Eckardt are thanked for analysis.

References

- Arnold T, Baumann N, Krawczyk-Bärsch E, Brockmann S, Zimmermann U, Jenk U, Weiß S, Wobus A, Zirnstein I. (2011). Identification of the uranium speciation in an underground acid mine drainage environment analysed by laser fluorescence spectroscopy. *Geochimica et Cosmochimica Acta* 75, 2200-2212.
- Brockmann S, Arnold T, Schweder B, Bernhard G. (2010). Visualizing Acidophilic Microorganisms in Biofilm Communities Using Acid Stable Fluorescence Dyes. *Journal of Fluorescence*, 20, 943-951.
- Costerton JW, Lewandowski Z, Caldwell DE, Korber DR, Lappin-Scott HM (1995) Microbial biofilms. *Ann. Rev. Microbiol.* 49, 711-745.
- de Beer D (2000). Potentiometric microsensors for in situ measurements in aquatic environments. In: "In Situ Monitoring of Aquatic Systems". Buffle, J.; Horvai, G. Eds.; Wiley, Chichester, 161–194.
- Flemming H-C (1995). Sorption sites in biofilms. *Wat. Sci. Tech.*, 32, 27-33.
- Hallberg KB, Coupland K, Kimura S, Johnson DB (2006). Macroscopic streamer growths in acidic, metal-rich mine waters in north Wales consist of novel and remarkably simple bacterial communities. *Appl. and Environmental Microbiology*, 72, 2022–2030.
- Krawczyk-Bärsch E, Grossmann K, Arnold T, Hofmann S, Wobus A (2008). Influence of uranium (VI) on the metabolic activity of stable multispecies biofilms studied by oxygen microsensors and fluorescence microscopy. *Geochimica et Cosmochimica Acta*, 72, 5251–5265.

Kühl M. (2005). Optical microsensors for analysis of microbial communities. In: Environmental Microbiology, vol. 397 (ed. J. R. Leadbetter). Methods in Enzymology, 166–199.

Macaskie LE, Bonthron KM, Yong P, Goddard DT (2000). Enzymically mediated bioprecipitation of uranium by a *Citrobacter* sp.: a concerted role for exocellular lipopolysaccharide and associated phosphatase in biomineral formation. Microbiology, 146, 1855–1867.

Merroun ML, Raff J, Rossberg A, Hennig C, Reich T, Selenska-Pobell S (2005). Complexation of uranium by cells and S-layer sheets of *Bacillus sphaericus* JG-A12. App. Environ. Microbiol., 71, 5532–5543.

Michels M, Bakker EP (1985). Generation of a large, protonophore-sensitive proton motive force and pH difference in the acidophilic bacteria *Thermoplasma acidophilum* and *Bacillus acidocaldarius*. J. Bacteriol., 161, 231–237.

Pons MP, Fusté MC (1993). Uranium uptake by immobilized cells of *Pseudomonas* strain EPS 5028. Appl. Microbiol. Biotechnol., 39, 661–665.

Revsbech NP (2005). Analysis of microbial communities with electrochemical microsensors and microscale biosensors. Methods in Enzymology, 397, 147–166.

Stumm W and Morgan JJ (1996). Aquatic Chemistry, Chemical Equilibria and Rates in Natural Waters. 3rd ed. John Wiley & Sons, Inc., New York, 1996.

Tyson GW, Chapman J, Hugenholtz P, Allen EE, Ram RJ, Richardson PM, Solovye VV, Rubin EM, Rokhsar DS, Banfield JF (2004). Community structure and metabolism through reconstruction of microbial genomes from the environment. Nature, 428, 37–43

XAFS INVESTIGATIONS OF Np(V/VI) REDOX SPECIATION IN HYPERALKALINE TMA-OH SOLUTIONS

Xavier Gaona^{1*}, Jan Tits², Kathy Dardenne¹, Erich Wieland², Marcus Altmaier¹

¹ Institut für Nukleare Entsorgung, Karlsruhe Institute of Technology (DE)

² Laboratory for Waste Management, Paul Scherrer Institut (CH)

* Corresponding author: xavier.gaona@kit.edu

Abstract

The redox chemistry of Np(V/VI) was investigated in tetramethylammonium hydroxide (TMA-OH) solutions with $9 \leq \text{pH} \leq 13.5$. Redox conditions were defined by the absence or presence of ClO^- as oxidizing agent (Na-salt, $5 \cdot 10^{-3} \text{M}$ and $5 \cdot 10^{-2} \text{M}$). The high total Np concentration ($[\text{Np}]_{\text{tot}} (\sim 2 \cdot 10^{-3} \text{M})$) lead to the precipitation of solid phases in some of the samples. Carbonate concentration (as impurity of TMA-OH) was $2\text{-}3 \cdot 10^{-3} \text{M}$.

UV spectra obtained from the supernatant in TMA-OH solutions and absence of ClO^- showed very clear Np(V) features, identified as NpO_2^+ , $\text{NpO}_2(\text{CO}_3)^-$, $\text{NpO}_2(\text{OH})(\text{CO}_3)^{2-}$ and $\text{NpO}_2(\text{OH})_2(\text{CO}_3)^{3-}$. XANES of these samples confirmed the predominance of Np(V). No UV features were observed within $800 \text{ nm} \leq \lambda \leq 1300 \text{ nm}$ for samples with ClO^- , whereas XANES of this second set of samples confirmed the predominance of Np(VI) in accordance with reference spectra (Liu et al., 2009). A similar Np redox distribution was observed for the solid phases based on XANES and EXAFS measurements. EXAFS spectra indicative of $\text{Np}^{\text{V}}\text{O}_2\text{OH(s)}$ and $\text{Np}^{\text{VI}}\text{O}_3 \cdot x\text{H}_2\text{O(s)}$ were obtained for samples in absence and presence of ClO^- , respectively. The formation of a Na-Np(VI) phase in $5 \cdot 10^{-2} \text{M}$ ClO^- and $\text{pH} \sim 12$ was also indicated from the EXAFS and chemical analysis.

The results presented in this contribution support the hypothesis that Np(VI) aqueous species and solid compounds prevail far below the oxidation border of water in alkaline solutions and also far below the E_{H} border calculated with the current NEA data selection (Guillaumont et al., 2003).

Introduction

The chemical behaviour of neptunium is of special concern for the safe disposal of radioactive waste because of its long half life ($t_{1/2} = 2.14 \cdot 10^6$ years), its radiotoxicity and its redox sensitivity. In the early stages after the repository closure when reducing conditions have not yet been established, and according with the current NEA thermodynamic data selection, Np(V) is expected to dominate.

The chemistry of Np(VI) under alkaline conditions remains largely unknown. In the aqueous phase, the formation of anionic species (e.g. $\text{NpO}_2(\text{OH})_3^-$ and $\text{NpO}_2(\text{OH})_4^{2-}$)

has been proposed, although no thermodynamic data are currently selected in the NEA reviews (Lemire et al., 2001; Guillaumont et al., 2003). In analogy to U(VI), the formation of Na- and Ca-neptunates can be expected. The chemical behaviour of these aqueous species and solid compounds can be relevant in cementitious systems and NaCl/CaCl₂-dominated saline environments.

This study focuses on the aqueous and solid phase speciation of Np(VI) in alkaline solutions in order to constrain the stability field of Np(VI). The work is part of a comprehensive study on the solubility of Np(V/VI) in dilute to concentrated NaCl and CaCl₂ solutions.

Thermodynamic Background

Only very few studies are available on the aqueous speciation of Np(VI) in hyperalkaline conditions. Ermakov et al. (1977) measured the potentials of the Np(V/VI) and Pu(V/VI) couples in aqueous LiOH solutions (2.5 M to 4.0 M). The review of these data by Lemire et al. (2001) provided upper limits for $\log^*\beta^{\circ}_{1,3}$ and $\log^*\beta^{\circ}_{1,4}$, to be used only in scoping calculations ($\log^*\beta^{\circ}_{UL-NEA}$ in Table 1).

The hydrolysis of actinides is known to correlate with the effective charge (Z_{eff} , Neck and Kim, 2001). Z_{eff} is the charge that a ligand approaching the actinide ion interacts with. For An(III) and An(IV), Z_{eff} is directly the charge of the cation (+3 and +4, respectively). In the case of actinyl cations (AnO_2^+ and AnO_2^{2+}), the covalent bonding between the actinide and the two oxygen atoms enhances the charge of An in the equatorial plane, effectively resulting in 2.3 and 3.3, respectively (Choppin 1999). Accordingly, and because of the similarities in their ionic radii, actinides with the same redox state tend to have similar hydrolysis constants. The linear correlation $\log^*\beta^{\circ}_{1,n}$ ($n=1-4$) - Z_{eff} provided in Figure 1 for Np, U, Pu and Am was considered to estimate $\log^*\beta^{\circ}_{1,3}$ and $\log^*\beta^{\circ}_{1,4}$ for Np(VI) ($\log^*\beta^{\circ}_{Correl}$ in Table 1). Table 1 also provides $\log^*\beta^{\circ}_{1,3}$ and $\log^*\beta^{\circ}_{1,4}$ reviewed and selected in Grenthe et al. (1992) and Guillaumont et al. (2003) for U(VI). These are accurate and well-defined stability constants, mostly selected from solubility experiments.

Table 1: Reaction and $\log^*\beta^{\circ}$ values for the formation of $NpO_2(OH)_3^-$ and $NpO_2(OH)_4^{2-}$, as upper limits proposed in Lemire et al. (2001), calculated in the present work from correlations with Z_{eff} , and selected in Guillaumont et al. (2003) for U(VI).

Reaction	$\log^*\beta^{\circ}_{UL-NEA}$	$\log^*\beta^{\circ}_{Correl.}$	$\log^*\beta^{\circ}_{U(VI)}$
$NpO_2^{2+} + 3H_2O = NpO_2(OH)_3^- + 3H^+$	≤ -19	-19.6	-20.25 ± 0.42
$NpO_2^{2+} + 4H_2O = NpO_2(OH)_4^{2-} + 4H^+$	≤ -33	-31.6	-32.40 ± 0.68

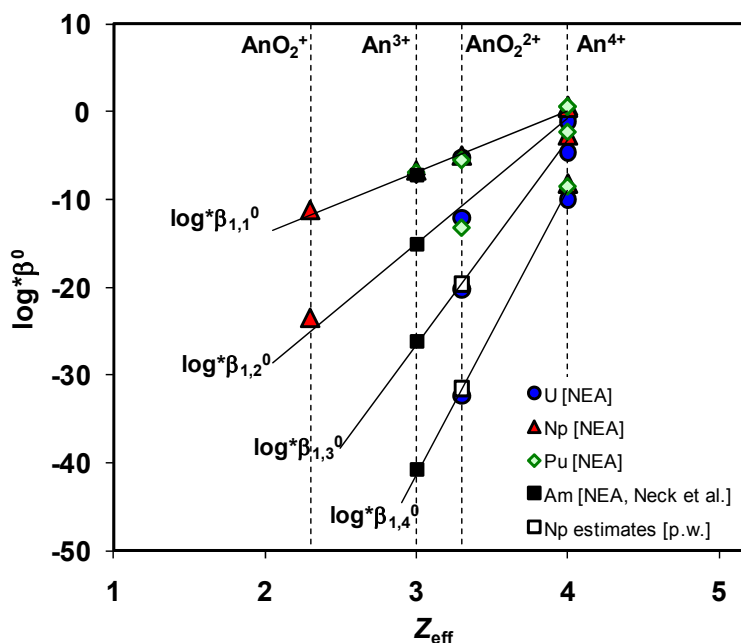


Figure 1: Linear correlation of An hydrolysis [$\log^*\beta_{1,n}^0$ ($n=1-4$)] with Z_{eff} for An = Np, U, Pu and Am. All thermodynamic data as reported in Guillaumont et al. (2003), except for $\text{Am}(\text{OH})_4^-$ (Neck et al., 2009). White squares used for Np(VI) data estimated in this work.

The relevance of the species $\text{NpO}_2(\text{OH})_3^-$ and $\text{NpO}_2(\text{OH})_4^{2-}$ is assessed in Figure 2, where the predominance diagram of Np for $-1\text{V} \leq E_{\text{H}} \leq +1\text{V}$ and $10 \leq \text{pH} \leq 14$ has been calculated (a) in accordance with the current data selection of NEA, and (b) including the third and fourth hydrolysis species of Np(VI) in analogy with U(VI). A significantly different picture is obtained when disregarding or including $\text{NpO}_2(\text{OH})_3^-$ and $\text{NpO}_2(\text{OH})_4^{2-}$. The latter case suggests a considerably smaller stability field of Np(V) under hyperalkaline conditions.

Carbonate species of Np(V) and Np(VI) are expected to form in the conditions of the experiment (see section 3.1). In addition to the Np(V/VI)-OH-CO₃ species currently selected in the NEA thermodynamic data reviews, Neck et al. (1997) reported the formation of the Np(V) species $\text{NpO}_2(\text{OH})(\text{CO}_3)^{2-}$ and $\text{NpO}_2(\text{OH})_2(\text{CO}_3)^{3-}$ (only $\log\beta$ for $I = 3\text{M NaClO}_4$ provided). Although not selected in the NEA review, Lemire et al. (2001) recommend the use of this $\log\beta_{121}$ for scoping calculations. The stability constants reported in Neck et al. (1997) have been recalculated in this work to $I = 0$ by SIT (see Table 2), using the $\varepsilon(\text{Na}^+, \text{ML}^n)$ estimates reported in Hummel (2009). These species have also been considered for thermodynamic calculations in section 4.

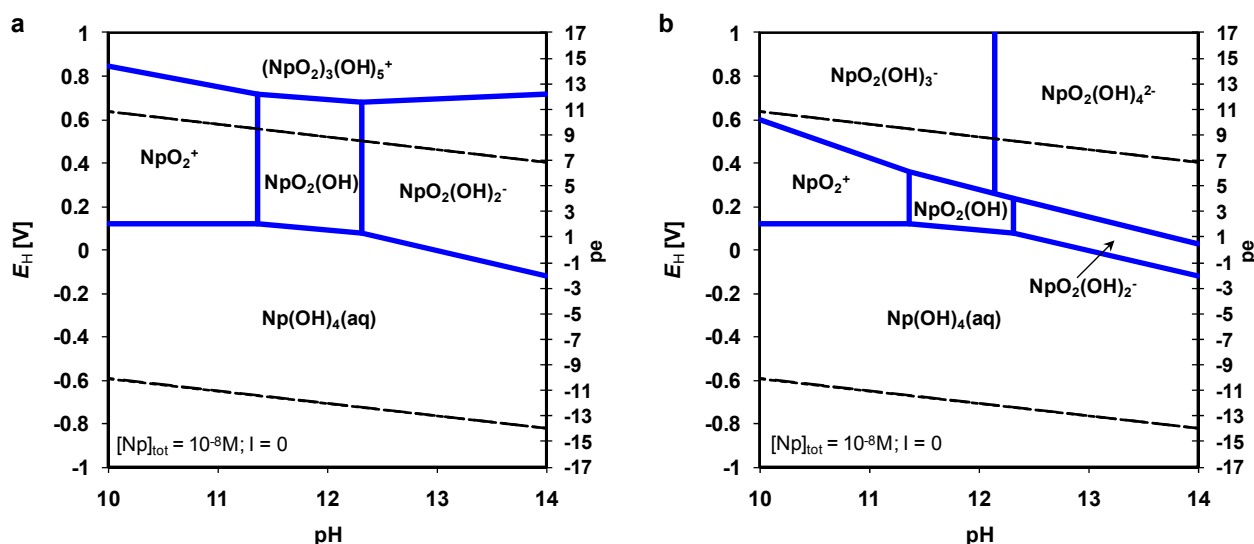


Figure 2: Predominance diagrams of Np for $-1V \leq E_H \leq +1V$ and $10 \leq \text{pH} \leq 14$, (a) calculated in accordance with the current thermodynamic data selection of NEA (Guillaumont et al., 2003); (b) including also $\text{NpO}_2(\text{OH})_3^-$ and $\text{NpO}_2(\text{OH})_4^{2-}$ species in analogy with U(VI). Only aqueous species shown.

Table 2: Reaction and $\log\beta$ values for the formation of $\text{NpO}_2(\text{OH})(\text{CO}_3)^{2-}$ and $\text{NpO}_2(\text{OH})_2(\text{CO}_3)^{3-}$ as reported in Neck et al. (1997), and recalculated to $I = 0$ in this work.

Reaction	$\log\beta_{1\text{nm}} (I = 3\text{M NaClO}_4)$	$\log\beta^\circ_{1\text{nm}}$
$\text{NpO}_2^+ + \text{OH}^- + \text{CO}_3^{2-} = \text{NpO}_2(\text{OH})(\text{CO}_3)^{2-}$	7.6 ± 0.3	7.0 ± 0.3
$\text{NpO}_2^+ + 2\text{OH}^- + \text{CO}_3^{2-} = \text{NpO}_2(\text{OH})_2(\text{CO}_3)^{3-}$	9.56 ± 0.15	7.66 ± 0.15

Experimental

Wet chemistry and UV

Samples were prepared in a tetramethylammonium hydroxide matrix (TMA-OH) to avoid the quantitative precipitation of Na-neptunates and retain sufficient Np in solution to allow for XANES analysis of Np oxidation state distribution. A solution of TMA-OH 1M was neutralized in three different aliquots with HCl (1M and 0.01M) to achieve pH values of ~ 13.5 , ~ 12 and ~ 9 . Carbonate was ubiquitous in all samples as impurity of TMA-OH (quantified as $4 \pm 1 \cdot 10^{-3}\text{M CO}_3^{2-}$ in 1M TMA-OH). Three series of samples were prepared, accounting for three different redox conditions: absence of ClO^- , $5 \cdot 10^{-3}\text{M ClO}^-$ and $5 \cdot 10^{-2}\text{M ClO}^-$.

About 2.2 mL of a radiochemically pure and well characterised Np(V)-237 stock solution $4.6 \cdot 10^{-2}\text{M}$ (287 kBq/mL) were used for the preparation of the samples. The Np(V) redox purity of the stock solution was confirmed by UV. The pH of the stock (originally in 0.1 M HCl) was adjusted to $\text{pH} \sim 4$ by addition of TMA-OH 0.01M. The pH adjusted stock was added to the 9 matrices described above to give a final total Np concentration of $\sim 2 \cdot 10^{-3}\text{M}$ in the samples. The pH and E_H were measured after the

addition of the tracer. The formation of a precipitate was observed in some of the samples after the addition of Np.

Samples were centrifuged at 4020 g in the glovebox, and a UV spectrum from the supernatant of each sample recorded between $800 \text{ nm} \leq \lambda \leq 1300 \text{ nm}$. The aqueous concentration of Np was measured by liquid scintillation counting (LSC) after 10 kD ultrafiltration after 4 and 7 days (see also Tits et al., 2011). An aliquot of each solid was washed in triplicate with ethanol to remove matrix solution and dissolved in 2% HNO₃. Neptunium and sodium in the resulting solutions were quantified by LSC and ICP-OES, respectively.

Synchrotron measurements

All samples (both aqueous and solids) for synchrotron measurements were prepared in small centrifuge vials (2 mL). In the case of solid samples, a suspension containing 1-2 mg of material was transferred to the vial and centrifuged for 10 minutes at 4020 g. The centrifuge vials were then fixed in a gas-tight cell inside the Ar-glovebox and transported to the beamline. A continuous flow of Ar was flushed through the cell during the synchrotron measurements.

The Np L_{III}-edge (17610 eV) EXAFS/XANES spectra were recorded at the INE-Beamline for Actinide Research at ANKA. Data were collected at room temperature in fluorescence mode using a five-element Ge-LE Canberra detector and Ar-filled ionization chambers for transmission. All spectra were energy calibrated using the first inflection point in the K-edge spectrum of a zirconium metal foil (17998 eV).

EXAFS data reduction and analysis were performed with the ATHENA/ARTEMIS package following standard procedures (Webb 2005, Ravel and Newville 2005, Newville 2001). Structural information was obtained by following a multi-shell approach for EXAFS data fitting. Theoretical single scattering paths (SS) for the fit of Np(V) samples were calculated with FEFF8.4 (Rehr et al., 1991; Rehr and Albers, 2000) using the structure of Np₂O₅ (Forbes et al., 2007). Theoretical SS paths for the fit of Np(VI) samples were calculated using the structure of UO₃ (Loopstra et al., 1977), where the central U atom was substituted by Np and paths recalculated using the Atoms routine in Artemis. The amplitude reduction factor, S_0^2 , was fixed to 1.0 in all fits.

Results and Discussion

Wet chemistry and UV

Figure 3 summarizes the pH and E_H measurements for all samples, plotted in the predominance diagram of Np for $8 \leq \text{pH} \leq 14$ and $-1\text{V} \leq E_H \leq +1\text{V}$. The diagram was calculated in accordance with the TDB and experimental conditions described in sections 2 and 3, respectively.

As shown in the figure, samples Np-1 to Np-3 fall within the stability field of Np(V) and Np(IV). However, the E_H measurements for these samples are rather uncertain, because they were redox-unbuffered and 5 minutes equilibration was not sufficient to obtain stable and reliable E_H readings. Despite the qualitative character of the predominance diagram, Figure 3 shows that predominance of Np(VI) aqueous species can be expected for samples Np-4 to Np-9.

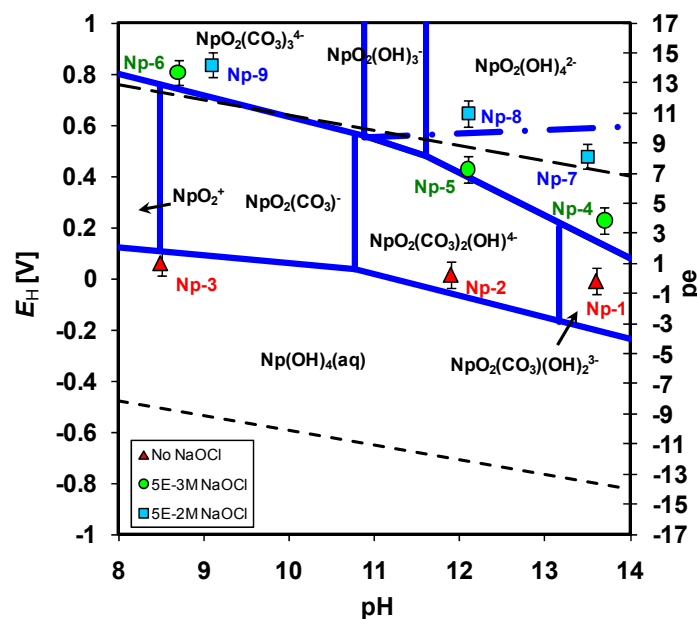


Figure 3: Predominance diagram of Np aqueous species, including experimental pH and E_H measurements. Calculations done with Np TDB described in section 2, considering $[Np]_{tot} = 1 \cdot 10^{-4} M$; $[CO_3]_{tot} = 2.5 \cdot 10^{-3} M$; $I = 0.6 M$. I corrections by Debye-Hückel. Dashed blue line: border Np(V)/Np(VI) for the conditions of the experiment, as calculated with the NEA-TDB.

The concentration of Np in the supernatant determined by LSC after 10kD ultra-filtration and the visual description of the solid phases formed are given in Table 3, together with the ratio Np:Na determined for the solid phases. As shown in the table, a very different behaviour was observed in the absence (samples Np-1 to Np-3) and presence of ClO^- (samples Np-4 to Np-9). Two types of solids were found to form: the greenish solid phase precipitating in the absence of ClO^- was (very likely) $NpO_2OH(am, fresh)$ while the brownish-purple phase corresponded to $NpO_3 \cdot xH_2O$ or to a Na-Np(VI) phase, considering the colour expected for Np(VI) (purple, see Ikeda-Ohno et al., 2008) as well as the spectroscopic observations discussed below.

UV spectra were obtained for the supernatant of samples Np-1 to Np-9 (Figure 4). Very clear features were observed for samples without ClO^- . Hence, Np-1 and Np-3 show peaks identified as NpO_2^+ , $NpO_2(CO_3)^-$, $NpO_2(OH)(CO_3)^{2-}$ and $NpO_2(OH)_2(CO_3)^{3-}$ (Neck et al., 1997). No UV features were observed within $800 \text{ nm} \leq \lambda \leq 1300 \text{ nm}$ for samples Np-4, Np-5, Np-7, Np-8 and Np-9, despite the high Np concentration in some of these samples ($\sim 2 \cdot 10^{-3} M$ in Np-4 and Np-7). This result supports the hypothesis that none of the Np(V) species observed in samples Np-1 to Np-3 exist in the presence of ClO^- . We postulate that the formation of (centro-)symmetric species (e.g. $NpO_2(OH)_4^{2-}$) and the resulting forbidden f-f transitions might have led to a significant decrease of the extinction coefficients (ϵ) for Np(VI) species under the given conditions.

Table 3: Concentration of Np in the supernatant of samples Np-1 to Np-9 (after ultra-filtration) for $t = 7$ days. In case of solid phase formation, visual description and ratio Np:Na provided.

Sample	C_{Np} [M]	Solid phase	Np:Na in solid
Np-1	$1.65 \cdot 10^{-4}$	Yes, greenish	not measured
Np-2	$4.06 \cdot 10^{-5}$	Yes, greenish	1:0.02
Np-3	$1.36 \cdot 10^{-3}$	No	
Np-4	$1.74 \cdot 10^{-3}$	No	
Np-5	$2.81 \cdot 10^{-4}$	Yes, brownish-purple	1:0.02
Np-6	$1.02 \cdot 10^{-4}$	Yes, brownish-greenish	1:0.04
Np-7	$1.70 \cdot 10^{-3}$	No	
Np-8	$8.20 \cdot 10^{-6}$	Yes, brownish-purple	1:0.77
Np-9	$1.63 \cdot 10^{-5}$	Yes, brownish-purple	1:0.13

A small peak at $\lambda = 990$ nm (corresponding to NpO_2^+) was observed in the UV of sample Np-6. The concentration of NpO_2^+ calculated from this feature was significantly lower than the total Np concentration determined after ultrafiltration for this sample, thus indicating the presence of additional species. In line with the thermodynamic calculations and the experimental pH and E_H values shown in Figure 3, the presence of the species $NpO_2(CO_3)_3^{4-}$ is to be expected, therefore resulting in an aqueous mixture of Np(V) and Np(VI) in sample Np-6.

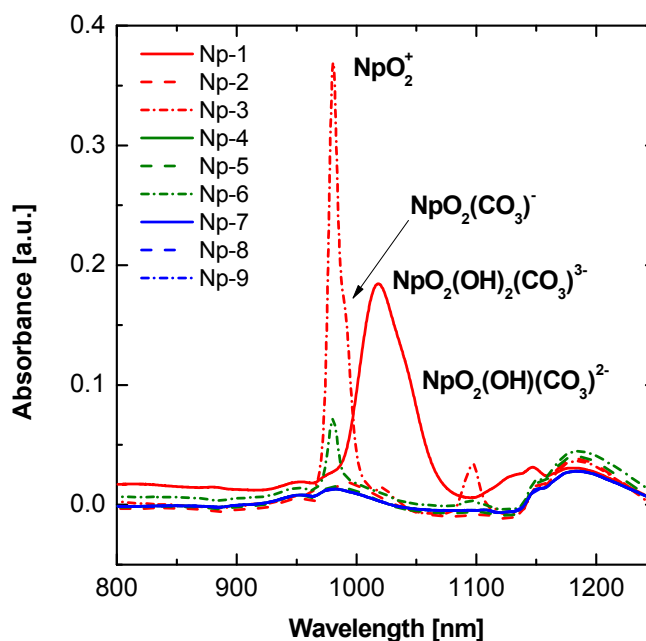


Figure 4: UV spectra of supernatant solutions from samples Np-1 to Np-9. Wavelengths for Np(V) species as reported in Neck et al. (1997).

XANES of aqueous samples

XANES spectra of aqueous samples Np-1, Np-3, Np-4, Np-5 and Np-7 are shown in Figure 5a. Two groups of samples with a well-defined difference in energies for the edge jump can be identified. In accordance with previously published Np XANES reference spectra (Liu et al., 2009; Brendebach et al., 2009), these groups correspond to Np(V) and Np(VI) species. The difference in energy is 1 - 2 eV in the inflection point and 3 - 5 eV in the white line (Table 4, reference data also included for comparison). These results represent a very good agreement with the Np(V/VI) redox border calculated including the species $\text{NpO}_2(\text{OH})_3^-$ and $\text{NpO}_2(\text{OH})_4^{2-}$ (see Figure 3).

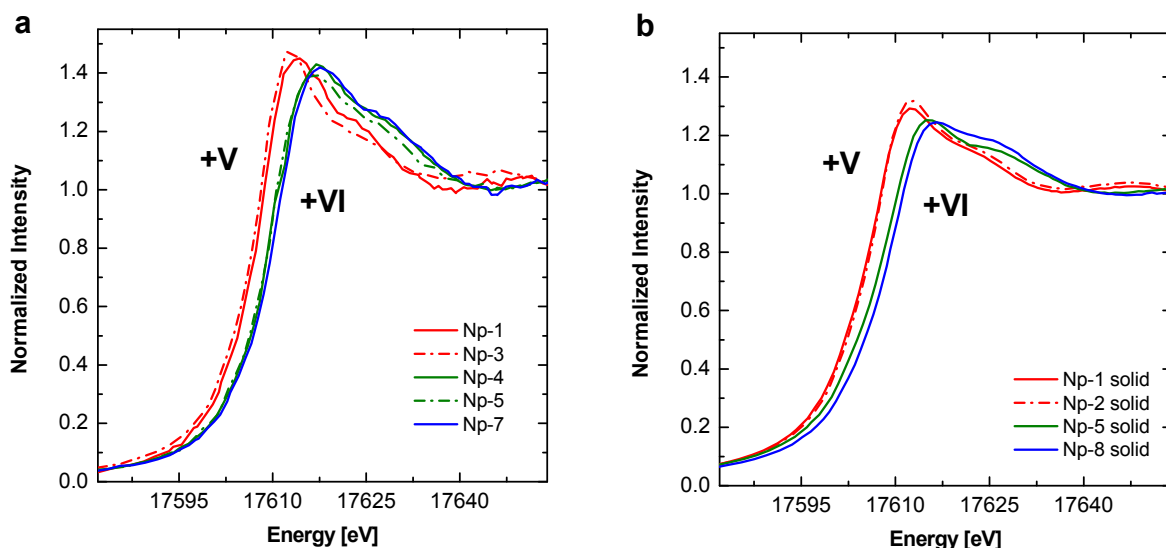


Figure 5: Experimental Np L_{III} XANES spectra: (a) for aqueous supernatant of samples Np-1, Np-3, Np-4, Np-5 and Np-7, (b) for solid phases from samples Np-1, Np-2, Np-5 and Np-8.

Table 4: Energy at the inflection point and white line for XANES spectra of aqueous samples Np-1, Np-3, Np-4, Np-5, Np-6 and Np-7, after energy calibration and normalization. XANES reference data for Np(V) and Np(VI) (in 1M HClO_4 or 1M HCl) are provided for comparison.

Sample	Inflection point [eV]	White line [eV]	Redox state
Np-1	17608.7	17614.2	+V
Np-3	17608.4	17612.4	+V
Np-4	17610.7	17616.9	+VI
Np-5	17609.9	17616.6	+VI
Np-7	17610.2	17617.5	+VI
Np-6	17609.9	17614.7	+V and +VI?
Reference Np(V) ^a	17609.1	17614.0	+V
Reference Np(VI) ^b	17611.7	17616.0	+VI

a. after Brendebach et al. (2009)

b. Rothe, personal communication

XANES-EXAFS of solid phases

XANES spectra of solid samples Np-1, Np-2, Np-5 and Np-8 are shown in Figure 5b. As for the aqueous species, two groups can be clearly identified based on the XANES spectra of the solid phases (Table 5, reference data also included for comparison). These groups show a moderate agreement with Np(V) and Np(VI) data (both for inflection point and white line) determined for the aqueous samples. A significantly lower intensity of the white line was obtained for the solid phases compared to the aqueous species, in agreement with previous experimental observations made on Np(IV) samples (Denecke et al., 2005). The decrease in the intensity of the white line is probably the reason for the slight differences with the aqueous species in terms of inflection point and white line.

Table 5: Energy at the inflection point and white line for XANES spectra of solid samples Np-1, Np-2, Np-5 and Np-8, after energy calibration and normalization. XANES reference data for Np(V) and Np(VI) (in 1M HClO₄ or 1M HCl) are provided for comparison.

Sample	Inflection point [eV]	White line [eV]	Redox state
Np-1	17607.4	17612.7	+V
Np-2	17607.9	17612.7	+V
Np-5	17609.3	17615.5	+VI
Np-8	17610.2	17616.6	+VI
Reference Np(V)^a	17609.1	17614.0	+V
Reference Np(VI)^b	17611.7	17616.0	+VI

Experimental and theoretical k^3 -weighted Np L_{III}-edge EXAFS spectra, as well as the corresponding Fourier transforms are shown in Figure 6. Structural parameters resulting from the fits are listed in Table 6. Distances Np-O_{ax} and NpO_{eq} in agreement with NpO₂OH(s) were determined for the solid samples Np-1 and Np-2. Significantly shorter Np-O_{ax} and Np-O_{eq} distances resulted for the samples Np-5 and Np-9, clearly indicating the predominance of Np(VI).

No satisfactory multi-shell EXAFS fits were obtained for the sample Np-8, which could be explained by the presence of a mixture of solids (i.e. NpO₃·H₂O and Na₂Np₂O₇). On the other hand, single-shell fits of the feature at $R+\Delta R = 3.1\text{\AA}$ strongly suggested the presence of Na in the coordination sphere of Np. This observation is in line with the chemical analysis reported in Table 3.

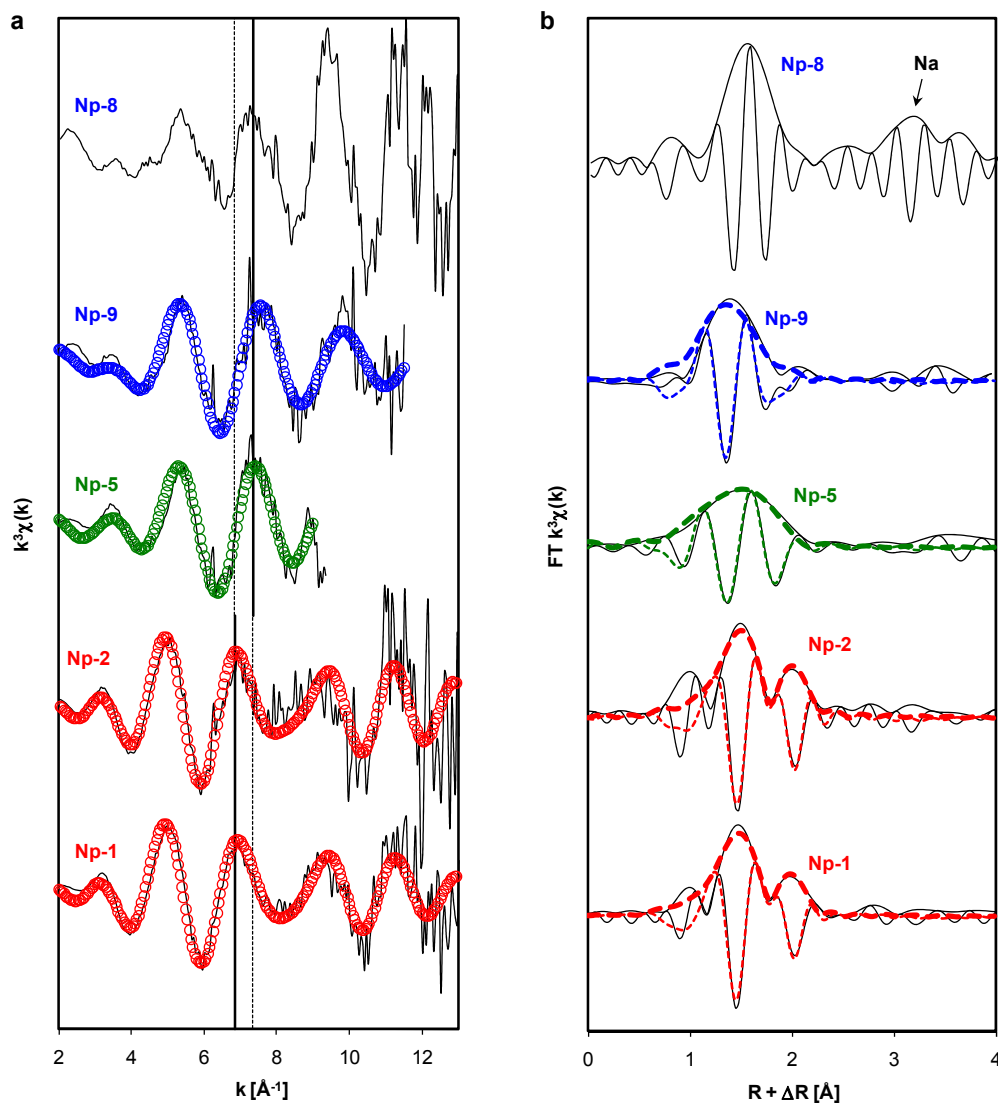


Figure 6: (a) Experimental and theoretical k^3 -weighted Np LIII-edge EXAFS spectra, and (b) Fourier transforms (modulus and imaginary parts) for solid phases in samples Np-1, Np-2, Np-5, Np-8 and Np-9.

Table 6: Structural parameters determined for Np(V/VI) solids prepared in TMA-OH solutions. [*parameters fixed in the fit]

Sample	Shell	N	R [Å]	σ^2 [Å ²]	ΔE^0 [eV]	R-factor
Np-1	O _{ax}	2*	1.86 ± 0.02	0.005 ± 0.002	5	0.011
	O _{eq1}	1*	2.19 ± 0.04	0.002 ± 0.005		
	O _{eq2}	4*	2.40 ± 0.04	0.008 ± 0.003		
Np-2	O _{ax}	2*	1.87 ± 0.05	0.005 ± 0.005	6	0.005
	O _{eq1}	1*	2.19 ± 0.06	0.002 ± 0.010		
	O _{eq2}	4*	2.40 ± 0.10	0.006 ± 0.006		
Np-5	O _{ax}	2*	1.78 ± 0.05	0.008 ± 0.007	2	0.012
	O _{eq}	4*	2.20 ± 0.09	0.009 ± 0.008		
Np-9	O _{ax}	2*	1.76 ± 0.03	0.005 ± 0.002	6	0.041
	O _{eq}	4*	2.19 ± 0.06	0.016 ± 0.006		

Summary and Conclusions

New wet chemistry and spectroscopic studies on the Np speciation in alkaline TMA-OH solutions confirm the relevance of Np(VI) in hyperalkaline systems even under mildly oxidizing conditions. Anionic species analogous to U(VI) are expected to form in the pH range 10-14. Indications of a Na-neptunate formation at [Na] = 0.01M suggests the potential relevance of Na-Np(VI) (and Ca-Np(VI)) solid phases in cementitious and NaCl/CaCl₂-dominated saline environments. Additional experimental series in carbonate free NaCl/NaOH and alkaline CaCl₂ are in progress with the aim of identifying the solubility limiting solid phases and determining the stoichiometry and stability of the aqueous Np(VI) species in order to develop a comprehensive thermodynamic model.

Acknowledgement

D. Fellhauer and V. Petrov are kindly acknowledged for the help in sample preparation and UV measurements. We also thank the staff at INE-Beamline (ANKA) for their technical assistance. JT, EW and XG acknowledge the funding of NAGRA. The research leading to these results has received funding from the European Union's European Atomic Energy Community's (Euratom) Seventh Framework Programme FP7/2007-2011 under grant agreement n° 212287 (RECOSYproject). The study was partly funded by ACTINET-i3 Integrated Infrastructure Initiative.

References

- Brendebach, B., Banik, N.L., Marquardt, C.M., Rothe, J., Denecke, M.A., Geckeis, H. (2009). X-ray absorption spectroscopic study of trivalent and tetravalent actinides in solution at varying pH values. *Radiochim. Acta*, 97, 701–708.
- Choppin, G.R. (1999). Utility of oxidation state analogs in the study of plutonium behaviour. *Radiochim. Acta*, 85, 89-95.
- Denecke, M.A., Dardenne, K., Marquardt, C.M. (2005). Np(IV)/Np(V) valence determinations from Np L3 edge XANES/EXAFS. *Talanta*, 65, 1008–1014.

- Ermakov, V. S., Peretrukhin, V. F., Krot, N. N. (1977). Redox potentials of the couples Np(VI)-Np(V) and Pu(VI)-Pu(V) in LiOH solutions. *Sov. Radiochem.*, 19, 212–213.
- Forbes, T.Y., Burns, P.C., Skanthakumar, S., Soderholm, L. (2007). Synthesis, Structure, and Magnetism of Np₂O₅. *J. Am. Chem. Soc.*, 129, 2760-2761.
- Grenthe, I., Fuger, J., Konings, R.J.M., Lemire, R.J., Muller, A.B., Nguyen-Trung, C., Wanner, H. (1992). *Chemical Thermodynamics 1. Chemical Thermodynamics of Uranium*. NEA OECD, Elsevier.
- Guillaumont, R., Fanghänel, J., Neck, V., Fuger, J., Palmer, D.A., Grenthe, I., Rand, M.H. (2003). *Chemical Thermodynamics 5. Update on the Chemical Thermodynamics of Uranium, Neptunium, Plutonium, Americium and Technetium*. NEA OECD, Elsevier.
- Hummel, W. (2009). Ionic strength corrections and estimation of SIT ion interaction coefficients. PSI Report TM-44-09-01.
- Ikeda-Ohno, A., Hennig, C., Rossberg, A., Funke, H., Scheinost, A.C., Bernhard, G., Yaita, T. (2008). Electrochemical and Complexation Behavior of Neptunium in Aqueous Perchlorate and Nitrate Solutions. *Inorganic Chemistry*, 47, 8294-8305.
- Lemire, R. J., Fuger, J., Nitsche, H., Potter, P. E., Rand, M. H., Rydberg, J., Spahiu, K., Sullivan, J. C., Ullman, W. J., and Vitorge, P., Wanner, H. (2001). *Chemical Thermodynamics 4. Neptunium and Plutonium*. NEA OECD, Elsevier.
- Liu, X., Banik, N.L., Brendebach, B., Dardenne, K., Rothe, J., Marquardt, C.M., Denecke, M.A. (2009). Neptunium redox speciation in perchloric acid by in situ XANES/EXAFS using a newly developed spectro-electrochemical cell. ANKA - Annual Report 2009. Karlsruhe Institute of Technology.
- Loopstra, B.O., Taylor, J.C., Waugh, A.B. (1977). Neutron powder profile studies of the gamma uranium trioxide phases. *Journal of Solid State Chemistry*, 20, 9-19.
- Neck, V., Altmaier, M., Rabung, T., Lützenkirchen, J., Fanghänel, T. (2009). Thermodynamics of trivalent actinides and neodymium in NaCl, MgCl₂ and CaCl₂ solutions: Solubility, hydrolysis, and ternary Ca-M(III)-OH complexes. *Pure Appl. Chem.*, 81, 1555-1568.
- Neck, V., Fanghänel, Th., Kim, J.I. (1997). Mixed hydroxo-carbonate complexes of Neptunium(V). *Radiochimica Acta*, 77, 167-175.
- Neck, V., Kim, J.I. (2001). Solubility and hydrolysis of tetravalent actinides. *Radiochimica Acta*, 89, 1-16.
- Newville, M. (2001). EXAFS analysis using FEFF and FEFFIT. *J. Synchrotron Rad.*, 8, 96-100.
- Ravel, B., Newville, M. (2005). ATHENA, ARTEMIS, HEPHAESTUS: data analysis for X-ray absorption spectroscopy using IFEFFIT. *J. Synchrotron Rad.*, 12, 537-541.
- Rehr, J.J., Mustre de Leon, J., Zabinsky S.I., Albers, R.C. (1991). Theoretical X-ray absorption fine structure standards. *J. Am. Chem. Soc.*, 113, 5135-5140.
- Rehr, J.J., Albers, R.C. (2000). Theoretical approaches to X-ray absorption fine structure. *Rev. Mod. Phys.*, 72, 621-653.

Tits, J., Gaona, X., Laube, A., Wieland, E. (2011). Influence of the redox state on the neptunium sorption by cementitious materials. This conference.

Webb, S. M. (2005). Sixpack: A graphical user interface for XAS analysis using IFEFFIT. Phys.Scr., T115, 1011-1014.

SYSTEMATIC EVALUATION OF Tc(VII)/Tc(IV) REDOX PROCESSES IN 0.1 M NaCl SOLUTIONS

Taishi Kobayashi^{1,*}, Xavier Gaona¹, David Fellhauer^{1,2}, Marcus Altmaier¹

¹. Karlsruhe Institute of Technology, Institute für Nukleare Entsorgung (DE)

². European Commission, Joint Research Centre, Institute for Transuranium Elements (DE)

* Corresponding author: taishi.kobayashi@kit.edu

Abstract

The reduction of $1 \cdot 10^{-5}$ mol/dm³ (M) Tc(VII) solutions in various reducing systems (homogeneous solutions with inorganic and organic reductants and heterogeneous suspensions containing Fe(II)/Fe(III) precipitates and Fe powder) was investigated in the pH range 2 – 13 in 0.1 M NaCl/NaOH at 22°C under Ar atmosphere. The results were systematized according to E_h /pH conditions in solution and a general borderline for the reduction of Tc(VII) to Tc(IV) regardless the reducing systems was obtained according to the reaction $(\text{TcO}_4^- + 4\text{H}^+ + 3\text{e}^- = \text{TcO}_2(\text{coll,hyd}) + 2\text{H}_2\text{O})$. This experimental borderline was (about 100 mV) lower than the equilibrium line for the reduction of Tc(VII) ($\log [\text{Tc(VII)}]_{\text{tot}} = -5.0$) calculated from reported standard redox potential of $\text{TcO}_2(\text{s})$ prepared electrochemically. This possibly implies the existence of more soluble solid phases such as small Tc(IV)oxyhydroxide particles under the given conditions. Reaction kinetics are also discussed and correlated to the measured redox potentials and the reduction borderline.

Introduction

Safety assessment for nuclear waste repositories requires a reliable prediction of radionuclide solubility limits. ⁹⁹Technetium is one of the most important radionuclides because of its long half life ($2.1 \cdot 10^5$ y) and environmental mobility. In geological systems, Tc will be either present in +VII or +IV oxidation state. In +VII oxidation state, Tc exists as anionic TcO_4^- ion which is highly soluble and mobile in the environment. On the other hand, Tc in +IV oxidation state is easily hydrolyzed to form sparingly soluble Tc(IV)-oxyhydroxide solid phases. The Tc migration behavior thus primarily depends on its oxidation state.

The redox potential of the Tc(VII)/Tc(IV) couple has been investigated in many studies by measuring the electrode potential. Meyer et al. (1991) reduced Tc(VII) to Tc(IV) solids ($\text{TcO}_2 \cdot 1.6\text{H}_2\text{O}$) electrochemically in acidic solution, and determined the standard potential of $\text{TcO}_4^- / \text{TcO}_2(\text{s})$ according to $(\text{TcO}_4^- + 4\text{H}^+ + 3\text{e}^- = \text{TcO}_2 \cdot 1.6\text{H}_2\text{O}(\text{s}) + 0.4\text{H}_2\text{O})$ to be $E^\circ = 0.747 \pm 0.004$ V using a defined Tc(IV) solid phase and known concentration of TcO_4^- solution. This value is in good agreement with

the values reported from other potential measurements. The standard potential of $\text{TcO}_4^- / \text{TcO}_2(\text{s})$ was conclusively evaluated in the NEA-TDB (Rard et al. (1999)).

On the other hand, numerous studies on redox behavior and kinetic effects have been reported on the Tc(VII)/Tc(IV) couple in natural systems and laboratory systems, considering various homogeneous and heterogeneous reducing systems. Extremely slow kinetics was reported on the Tc(VII) reduction with the aqueous Fe(II) ion in acidic solutions, while rather fast reduction was observed when Fe(II) precipitate was used under higher pH conditions (Cui et al. (1996), Ben Said et al. (1998), Zachara et al. (2007)). It was shown that the reduction kinetics are depending on pH, initial Tc concentration, concentration of reductants (Fe(II) concentration and $\text{Fe(II)} / \text{Fe(III)}$ ratios). The rather fast reduction of Tc(VII) to Tc(IV) was also often observed when $\text{Na}_2\text{S}_2\text{O}_4$ and tin(II) chloride were used. In order to understand and predict the redox behavior of Tc(VII) to Tc(IV) in various reducing systems, it is important to quantify the redox processes in terms of thermodynamics.

In the present study, the redox behavior of the Tc(VII)/Tc(IV) couple in 0.1 M NaCl/NaOH solutions was investigated in various kinds of homogeneous (anthraquinone, hydroquinone, 2-hydroxy-1,4-naphthoquinone, and $\text{Na}_2\text{S}_2\text{O}_4$ systems) and heterogeneous reducing systems ($\text{Fe(II)} / \text{Fe(III)}$, Fe powder, Sn(II) systems). The results are systematised according to E_h/pH conditions in solution and compared to those expected from thermodynamic calculation. The reaction kinetics were also assessed for each system and correlated to the measured redox potentials.

Experimental

The technetium samples with initial Tc(VII) concentration ($[\text{TcO}_4^-]_{\text{init}} = 10^{-5} \text{ M}$) were prepared by adding 57 μl of 2.6 mM NaTcO_4 stock solutions (pH 3) to 15 ml 0.1 M NaCl/NaOH pre-equilibrated with the following reducing agents (p.a. grade chemicals):

- $3.0 \cdot 10^{-3} \text{ M}$ sodium anthraquinone / anthrahydroquinone disulfonate; homogeneous solutions ($\text{AQDS} / \text{AH}_2\text{QDS} = 1:3$); oxidized form from Fluka; partly reduced with $\text{Na}_2\text{S}_2\text{O}_4$ at pH 11.
- $3.0 \cdot 10^{-3} \text{ M}$ and $1.0 \cdot 10^{-2} \text{ M}$ hydroquinone (Merck); homogeneous solutions.
- $1.0 \cdot 10^{-3} \text{ M}$ FeCl_2 / $1.0 \cdot 10^{-4} \text{ M}$ FeCl_3 (Alfa Aesar); Fe(II) dissolved / suspension of Fe(III) and Fe(II) hydroxide precipitates at $\text{pH} > 4$ and $\text{pH} > 8$, respectively.
- $1.0 \cdot 10^{-3} \text{ M}$ $\text{Na}_2\text{S}_2\text{O}_4$ (Merck); homogeneous solutions.
- 1 mg Fe powder (Merck, grain size $10\mu\text{m}$); suspensions in 15 ml 0.1 M NaCl/NaOH .
- $1.6 \cdot 10^{-3} \text{ M}$ 2-hydroxy-1,4-naphthoquinone (Lawsone); homogeneous solutions (oxid. form / red. form = 1:3); oxidized form from Sigma; partly reduced with $\text{Na}_2\text{S}_2\text{O}_4$ at pH 11.
- $1.0 \cdot 10^{-3} \text{ M}$ SnCl_2 ; Sn(II) dissolved / suspension of Sn(II) hydroxide at pH 5 – 11.

The pH values were adjusted by adding HCl (Merck) and carbonate-free NaOH (Baker). In the samples with neutral pH, pH buffers (0.01 M MES (Sigma) for samples at pH 5 – 7, and 0.01 M PIPES (Sigma) for those at pH 7 – 9) were used. The values of $\text{pH} = -\log a_{\text{H}^+}$ (activity scale) were measured using a combination glass electrode (type ROSS,

Orion) calibrated against standard buffers (pH 1 – 10, Merck). All samples were prepared with ultrapure deionized water and purged with Ar before use. The samples were prepared in polyethylene vials and stored at $22 \pm 2^\circ\text{C}$ in an Ar glove box under inert gas atmosphere.

The redox potentials were measured with a combined Pt and Ag/AgCl reference electrode (Metrohm). The measured redox potentials were converted to E_h versus the standard hydrogen electrode by the correction for the potential of the Ag/AgCl reference electrode (+208 mV for 3 M KCl junction electrolyte). The apparent electron activity ($p_e = -\log a_{e^-}$) was calculated from $E_h = -(RT/F) \ln a_{e^-}$ according to the relation: $p_e = 16.9 E_h$ (V) at 25°C .

After given periods up to 6 months, pH and redox potential values were measured and the supernatants of the solutions were filtrated through 10 kD (2-3 nm) ultrafiltration membranes (Pall Life Sciences). To assess the potential presence of colloidal Tc(IV) species, the samples were also measure without any phase separation for comparison. The Tc concentrations were determined by Liquid Scintillation Counting (TriCarb 2500 Tr/AB instrument, Canberra-Packard) with a detection limit of $\sim 10^{-8}$ M. The Tc oxidation state of the soluble species was investigated by a solvent extraction technique, where TcO_4^- was extracted into chloroform using tetrakisphosphorylchloride (TPPC) (Aldrich). The supernatant of the sample solution was filtrated through 10 kD membranes and contacted to chloroform containing 1 mM TPPC. After vigorous mixing and subsequent separation of the aqueous and organic phases by centrifugation, the Tc concentrations in both phases were determined using LSC.

Results and discussion

1. Redox behavior of Tc(VII)/Tc(IV) in the individual reducing system

1.1 AQDS / AH₂QDS redox buffer solutions

The Tc concentrations after the filtration with 10 kD membranes were investigated over a wide pH range as a function of time. The results are shown in Fig. 1. In 3 mM AQDS / AH₂QDS (1:3) at pH 2.1, 5.0 and 8.1, the initial Tc concentration (10^{-5} M) decreased rather rapidly to $10^{-7} - 10^{-8}$ M, which is near the detection limit of LSC, the stable state being achieved within 20 days after Tc(VII) was added to the solutions. In contrast, at pH 10.5, considerably slower reduction was observed and stable state conditions not obtained within the investigated time (94 days). Under alkaline condition at pH > 11, the Tc concentration was constant at initial TcO_4^- concentration level, indicating no reduction of Tc(VII) occurred within the investigated time.

At pH 2.1, the Tc concentration obtained without filtration showed similar values like after filtration with 10 kD membrane, suggesting no significant contribution from colloidal species to the total Tc concentration. On the other hand, at pH 8.1 and 10.5, the Tc concentrations without filtration were about $10^{-5.5}$ M after 94 days and 10^{-6} M after 178 days, indicating the possible existence of colloidal species under given condition.

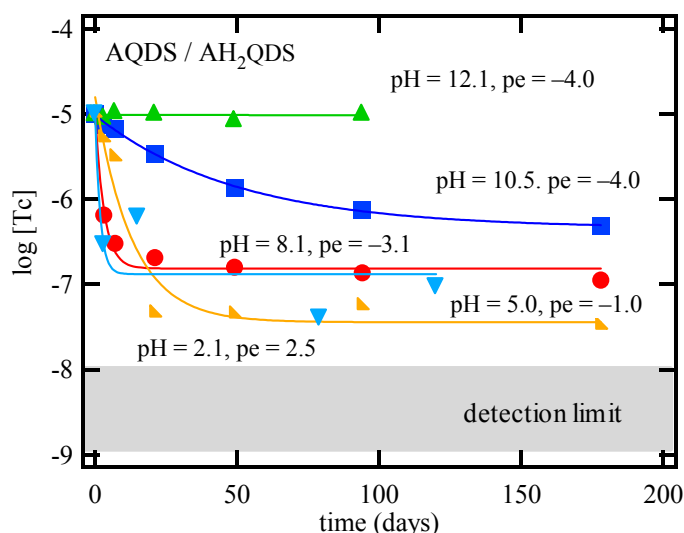


Figure 1: Tc concentrations (10 kD filtration) in 3 mM AQDS / AH₂QDS (1:3) solutions as a function of time.

1.2 Hydroquinone solutions

In 3 mM hydroquinone solutions, Tc concentration was constant at initial TcO_4^- concentration level up to 49 days in the entire pH range (2.2 – 12.3). In the oxidation state analysis for the samples at pH 3.9, 8.5, and 12.3, more than 85% of total Tc in solutions was extracted to the organic phase, indicating dominant Tc(VII) species. No significant decrease in Tc concentration was observed in more concentrated 10 mM hydroquinone solutions.

1.3 Lawsone (oxidized form / reduced form) redox buffer solutions

In 1.6 mM Lawsone solutions (oxidized form / reduced form = 1:3), the Tc concentration decreased from the initial Tc(VII) concentration level over the entire investigated pH range 2 – 12. In the alkaline pH region, extremely slow reduction kinetics was observed and the equilibrium state not reached over 85 days.

1.4 Fe(II) / Fe(III) redox buffers and suspensions of Fe(II) / Fe(III) precipitates

At pH = 2.1 and pe = 11.3, no change in the Tc concentration was observed up to 49 days. On the other hand, at pH 6.0 (pe = -0.2) and pH 8.4 (pe = -0.2), the Fe(II) / Fe(III) precipitates were observed before adding Tc(VII) stock solution and the Tc concentrations decreased to almost detection limit (10^{-8} M) within three days after Tc(VII) was added. The reduction of Tc(VII) with Fe(II) / Fe(III) redox buffers and suspensions of the precipitates has been reported in several studies. Cui et al. (1996) observed that the TcO_4^- concentration at pH < 7.5 was constant at initial concentration level within a few days in the presence of about 10^{-5} M aqueous Fe(II), while Tc(VII) was reduced at pH 6.0 in this study. As Ben Said et al. (1998) showed that the reduction kinetics was dependent on Fe(II) concentration, Fe(II)/Fe(III) ratio, and initial Tc(VII) concentration, the difference between Cui et al.(1996), Ben Said et al. (1998), and our results probably arise from the different experimental conditions such as Fe(II) concentration. Unfortunately, the redox potentials in the study of Ben Said et al (1998)

were not reported. Zachara et al. (2007) also investigated the reduction of Tc(VII) in Fe(II) systems in near neutral pH range and the redox behavior was supported by measured redox potentials. The observed rapid reduction at pH > 6.8 generally agrees with the results in this study, although the reported E_h values were higher than those in this study.

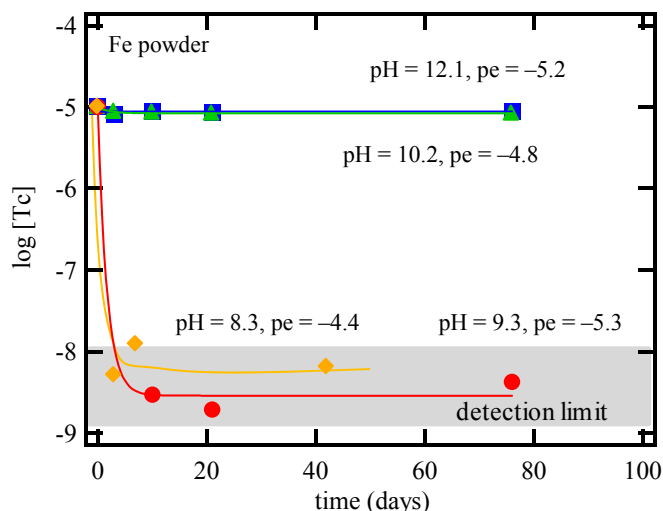


Figure 2: Tc concentrations (10 kD filtration) in 1 mg / 15 ml Fe powder suspensions as a function of time.

1.5 Suspensions of Fe powder

In the samples containing corroding iron powder (1 mg / 15 ml) in the pH range 6 – 10, the Tc concentration rapidly decreased to the detection limit (10^{-8} M) within three days. In contrast, no reduction was observed in all samples at pH > 10 as shown in Fig. 2.

1.6 Sodium dithionite solutions

In 1 mM $\text{Na}_2\text{S}_2\text{O}_4$ solution in the pH range 6.9 – 10.9, the Tc concentrations in the solutions decreased significantly and stable state conditions (10^{-7} – 10^{-8} M) were achieved within a few weeks, indicating the reduction of Tc(VII) to the Tc(IV) solid. Similarly to the literature where $\text{Na}_2\text{S}_2\text{O}_4$ were used to reduce Tc(VII) to prepare Tc(IV) solid phase ($\text{TcO}(\text{OH})_2 \cdot x\text{H}_2\text{O}$) (Hess et al. (2004)), a black-colored Tc(IV) solid phase was immediately precipitated, however, an aging time of a few weeks was needed to reach equilibrium state. On the other hand, at pH > 11, the Tc concentrations after a few weeks less decreased compared to those below pH 11 (Fig. 3). In the oxidation state analysis using liquid extraction, less than 10 % of total Tc species in the solutions at pH 10.9, 12.1, and 13.0 were extracted to the organic phase as Tc(VII) species. It was considered that the dominant Tc species at pH > 11 was reduced Tc(IV) species such as anionic $\text{TcO}(\text{OH})_3^-$ as proposed by Eriksen et al (1992). It should be noted that at pH 6.9, the ratio of Tc(VII) in the solution was more than 30 %, as under neutral pH conditions $\text{Na}_2\text{S}_2\text{O}_4$, which was supposed to maintain reducing conditions, is not stable over prolonged periods of a few months under these conditions.

The Tc concentrations obtained without filtration after 49 days were about $10^{-5.5}$ M and independent of pH in the pH range 7 – 12.5, suggesting the possible existence of the colloidal species, similarly to the results in the AQDS / AH₂QDS system. However, the concentrations without phase separation decreased to about 10^{-7} M after 94 days, pointing to thermodynamic instability of the colloidal Tc(IV) species under the given conditions.

1.7 Sn(II) solutions and suspensions of Sn(II) hydroxide precipitates

Sn(II) chloride has been widely used to reduce Tc(VII) and rather fast reduction to the Tc(IV) species has been observed over the entire pH range (Maset et al. (2006), Warwick et al. (2007)). In the present study, the white Sn(II) hydroxide precipitated was observed in the range of pH 5 – 11 before adding Tc(VII). At higher pH the precipitates disappeared and anionic Sn(II) hydrolysis species ($\text{Sn}(\text{OH})_3^-$) considered dominant (House and Kersall (1984)).

The Tc concentration decreased rapidly over the pH range 2 – 11 and stable state conditions achieved within several days. At pH > 11, the Tc concentration less decreased compared to those at lower pH similar to the Na₂S₂O₄ system. The results of the oxidation state analysis by solvent extraction under these pH conditions also indicated negligible contribution of remaining Tc(VII), suggesting the formation of anionic Tc(IV) hydrolysis species in the Sn(II) system as well.

2. General interpretations of the redox behavior of Tc(VII)/Tc(IV) couple and kinetic effects of the reduction

The results discussed above are summarized in the E_h-pH diagram shown in Fig. 5. Samples in which no reduction was observed are plotted as filled symbols. Samples in

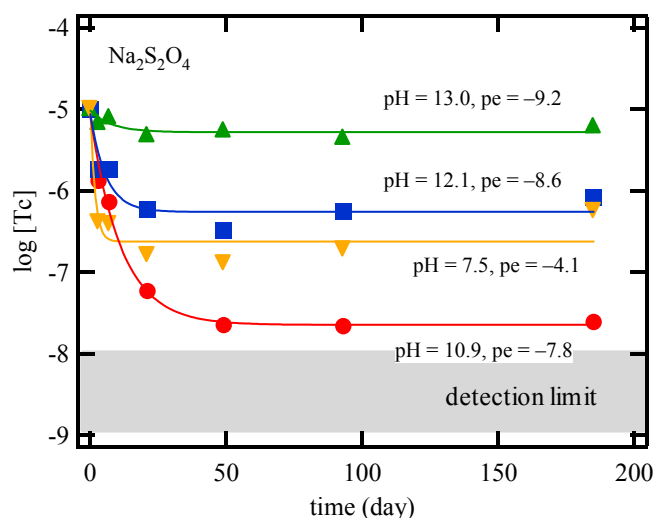


Figure 3: Tc concentrations (10 kD filtration) in 1 mM Na₂S₂O₄ solutions as a function of time.

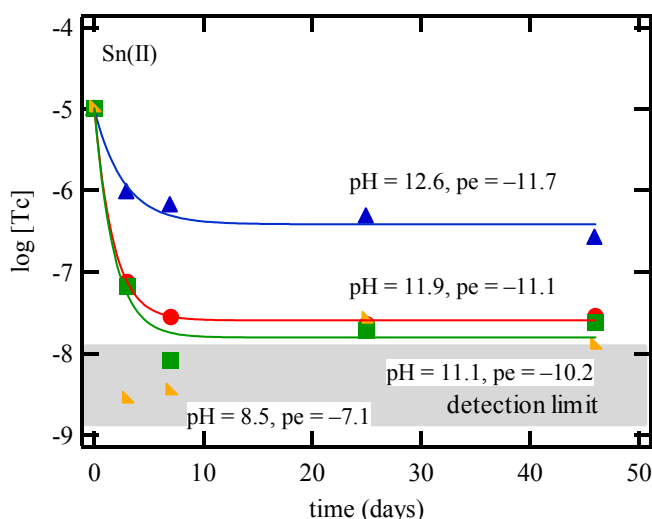
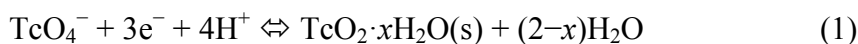


Figure 4: Tc concentrations (10 kD filtration) in 1 mM Sn(II) solutions and suspensions as a function of time.

which the initial Tc(VII) was reduced are plotted as open symbols even if Tc(VII) was not completely reduced. The bold broken line in the figure represents a borderline for the reduction of Tc(VII) under the given conditions. The reduction of Tc(VII) to Tc(IV) occurred in both homogeneous solutions and heterogeneous suspensions with redox potentials below this borderline and in the systems with redox potentials above the borderline Tc(VII) was not reduced.

The reaction rate for the reduction of Tc(VII) generally showed a significant dependence on pe. The reduction rate decreased when pe increased from strongly negative values to near the borderline. The extremely slow reduction was observed in Lawsone system which was close to the borderline, while fast reduction was observed in Sn(II) which showed far lower pe values than the borderline. However, in Fe powder suspension system under neutral pH conditions, fast reduction of Tc(VII) was observed, although the measured pe values were similar to those in Lawsone system, possibly pointing to a specific surface mediated effect of the iron solid. It should also be noted that in Fe powder system, no reduction was observed at pH = 10.2 and pe = -4.8 up to 49 days, on the other hand, Tc(VII) was slowly reduced at pH = 10.5 and pe = -4.0 in the AQDS / AH₂QDS solution. For a more precise determination of the borderline and for assessing the intrinsic properties of mineral surfaces, further investigations will be required.

In the investigated systems, the equilibrium line for the reduction of Tc(VII) (50 % Tc(VII), 50 % Tc(IV)) can be described and calculated from the thermodynamic constant (shown as dotted line in Fig. 5):



with $\log K^\circ = 37.8 \pm 0.6$ from the data selected by the NEA-TDB (Rard et al. (1999)). For 0.1 M NaCl/NaOH solution, the equilibrium constant (K) at $I = 0.1$ for Eq.(1) was calculated to be $\log K = 38.3$ using the SIT method and ion interaction coefficients of $\varepsilon(\text{H}^+, \text{Cl}^-) = 0.12$ and $\varepsilon(\text{ClO}_4^-, \text{Na}^+) = 0.01$ (Guillaumont et al. (2005)), which is

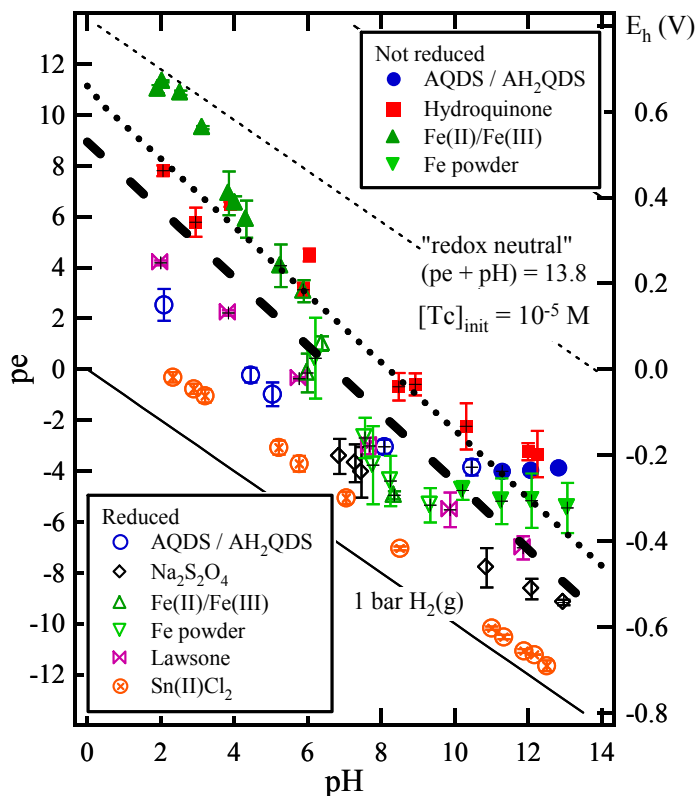
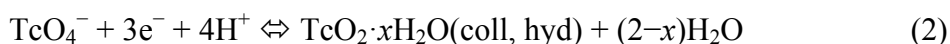


Figure 5: Experimental studies on the reduction of Tc(VII) in 0.1 M NaCl/NaOH ($[\text{TcO}_4^-]_{\text{init}} = 10^{-5} \text{ M}$). In the systems shown as open symbols Tc(VII) is reduced to Tc(IV), in the systems shown as filled symbols Tc(VII) is not reduced within the time of investigation.

analogue for ε (TcO_4^- , Na^+). Under the condition of $[\text{Tc}]_{\text{init}} = 10^{-5} \text{ M}$, i.e., $\log [\text{TcO}_4^-] = \log ([[\text{Tc}]_{\text{init}} / 2]) = -5.30$, the calculated borderline was $\text{pe} = -1.3 \cdot \text{pH} + 11.0$. However, the experimental results in Fig. 5 suggested that the borderline for the reduction of Tc(VII) (bold broken line) was about 2 pe-units lower than the calculated line (dotted line). This may suggest that the reduction of small amounts of the total Tc ($[\text{TcO}_4^-] = 10^{-5} \text{ M}$) by reducing chemicals under rather slow reduction kinetics leads to a different solid phase (or at least different particle size distribution!) compared to the solid phases assumed for the thermodynamic calculation. The value of $\log K^\circ$ for Tc(IV) solid phase selected by Rard et al. (1999) was calculated from the standard redox potential (E°) of Eq. (1), which was determined from the investigation of redox potential measurement data of $\text{TcO}_4^- / \text{TcO}_2 \cdot x\text{H}_2\text{O}(\text{s})$ couple (Meyer et al. (1991), Cobble et al. (1953)). In these literatures, the solid phases were prepared by electrochemical reduction of macroscopic amounts of TcO_4^- . Under the condition of lower initial Tc concentration in this study, Tc(VII) may be precipitated not as $\text{TcO}_2 \cdot x\text{H}_2\text{O}(\text{s})$ but rather small colloidal particles, $\text{TcO}_2 \cdot x\text{H}_2\text{O}(\text{coll, hyd})$. This explanation would be similar to the Np(V) reduction processes and the role of colloidal Np(IV) phases described recently by Neck et al. (2009). In this study on the reduction of Np(V) to Np(IV), the experimental borderline was also observed to be lower than the calculated equilibrium line from the thermodynamic constant of $\text{NpO}_2(\text{am, hyd})$ and $\text{NpO}_2(\text{coll, hyd})$ considered as small solid phase particles was proposed. The formation of $\text{TcO}_2 \cdot x\text{H}_2\text{O}(\text{coll, hyd})$ is given by the following equation.



The lowest pe values at each pH among the data of “not reduced” samples and the highest pe values at each pH among the data of “reduced” samples were used to calculate the experimental borderline and the equilibrium constant ($K_{\text{coll, hyd}}$) according Eq.(2). By assuming three electron reduction, the experimental borderline was determined to be $\text{pe} = -1.3 \cdot \text{pH} + 8.9$ by the least-square analysis and $K_{\text{coll, hyd}}$ at $I = 0.1$ was calculated to be $\log K_{\text{coll, hyd}} = 31.6 \pm 1.0$. As discussed above, in the systems with redox potentials near the borderline, the rate of reduction was extremely slow and some inconsistencies still remain. For the confirmation of the proposed $\text{TcO}_2 \cdot x\text{H}_2\text{O}(\text{coll, hyd})$ species, further investigation including solid phase analysis is ongoing.

Summary and Conclusions

The redox behaviour of Tc(VII)/Tc(IV) couple was investigated in various homogeneous and heterogeneous reducing systems and systematized according to their pH- E_h conditions. It was shown that the redox behaviour is depending on the pe values of the system and that there was a borderline for the reduction of Tc(VII) independent of the reducing chemicals or the presence of Fe solid phases. The reduction occurred in both homogeneous solutions and heterogeneous suspensions with redox potentials below this borderline. In the systems with redox potentials above the borderline, Tc(VII) was not reduced. The experimental borderline was about 100 mV lower than the equilibrium line calculated from the standard potential of $\text{TcO}_4^- / \text{TcO}_2(\text{s})$, which was electrochemically prepared from macroscopic amounts of TcO_4^- . The difference may suggest that analog solid phases with significantly smaller particle size control the

redox processes investigated in this study. The kinetics of the Tc(VII) reduction was generally correlated to the pH-E_h condition, however further investigation is needed in the system containing Fe solid phases.

Acknowledgement

The research leading to these results has received funding from the European Union's European Atomic Energy Community's (Euratom) Seventh Framework Programme FP7/2007-2011 under grant agreement n° 212287 (RECOSY project). This work was partially supported by the German BMWi under the project of VESPA. The authors want to thank Vivien Reuscher for experimental support.

References:

- Ben Said, K., Fattahi, M., Musikas, C., Delorme-Hiver, A., Abbe, J. (1998). A Novel Approach to the Oxidation Potential of the Tc(VII)/Tc(IV) Couple in Hydrochloric Acid Medium through the Reduction of TcO_4^- by Fe^{2+} Ion. *Radiochim. Acta.* 83, 195-203.
- Cobble J., Smith W., Boyd. G. (1953). Thermodynamic Properties of Technetium and Rhenium Compounds. II. Heats of Formation of Technetium Heptoxide and Pertechnic Acid, Potentials of the Technetium(IV) – Technetium(VII) Couple, and a Potential Diagram of Technetium. *J. Am. Chem. Soc.* 75, 5777-5787.
- Cui. D., Eriksen, T. (1996). Reduction of Pertechnetate by Ferrous Iron in Solution: Influence of Sorbed and Precipitated Fe(II). *Environ. Sci. Technol.* 30, 2259-2262.
- Eriksen, T., Ndalamba, P., Bruno, J., Caceci, M. (1992). The solubility of $\text{TcO}_2 \cdot n\text{H}_2\text{O}$ in Neutral to Alkaline Solutions under Constant p_{CO_2} . *Radiochim. Acta*, 58/59, 67-70.
- Guillaumont, R., Fanghänel, Th., Fuger, J., Grenthe, I., Neck, V., Palmer, D., Rand, M. (2003) *Update on the Chemical Thermodynamics of Uranium, Neptunium, Plutonium, Americium and Technetium*, In: *Chemical Thermodynamics* (Eds.: F. J. Mompean et al.) Vol. 5. Elsevier, North-Holland, Amsterdam.
- Hess, N., Xia, Y., Rai, D., Conradson, S. (2004). Thermodynamic Model for the Solubility of $\text{TcO}_2 \cdot x\text{H}_2\text{O(am)}$ in the Aqueous Tc(IV)- Na^+ - Cl^- - H^+ - OH^- - H_2O System. *J. Solution Chem.* 33, 199-226.
- House, C. I., Kersall, G. H. (1984). Potential-pH diagrams for the Sn/ H_2O -Cl system, *Electrochimica Acta.* 29, 1459-1464.
- Maset, E., Sidhu, S., Fisher, A., Heydon, A., Worsfold, P., Cartwright, A., Keith-Roach, M. (2006). Effect of Organic Co-Contaminants on Technetium and Rhenium Speciation and Solubility under Reducing Conditions. *Environ. Sci. Technol.*, 40, 5472-5477.
- Meyer, R., Arnold, W. (1991). The Electrode Potential of the Tc(IV)-Tc(VII) Couple. *Radiochim. Acta* 55, 19-22.
- Neck V., Altmaier M., Fellhauer, D., Runke, J., Fanghänel, Th. (2009). Quantification of the redox potential for the reduction of Np(V) in non-complexing aqueous solutions at pH 5 – 10. Collaborative Project “Redox Phenomena Controlling Systems” 1st Annual Workshop Proceedings, 65-73.

Rard, J., Rand, M., Anderegg, G., Wanner, H. (1999). *Chemical Thermodynamics of Technetium*, In: *Chemical Thermodynamics* (Eds.: Sandino M.C.A. and Östhols E.) Vol. 3. Elsevier. North-Holland. Amsterdam.

Warwick, P., Aldridge, S., Evans, N., Vines, S. (2007). The solubility of technetium(IV) at high pH. *Radiochim. Acta.* 95, 709-716.

Zachara, J., Heald, S., Jeon, B., Kukkadapu, R., Liu, C., McKinley, J., Dohnalkova, A., Moore, D. (2007). Reduction of pertechnetate [Tc(VII)] by aqueous Fe(II) and the nature of solid phase redox products. *Geochim. Cosmochim. Acta.* 71, 2137-2157.

STUDY OF THE DIFFUSIVE BEHAVIOUR OF SELENITE AND SELENATE THROUGH THE CALLOVO-OXFORDIAN CLAYSTONES (FRANCE): EFFECT OF THE INITIAL SELENITE CONCENTRATION

Sébastien Savoye^{*,1}, Benjamin Frasca^{1,2}, Agnès Fayette¹, Bernard Grenut¹, Jean Radwan¹

¹ CEA, DEN/DANS/DPC/SECR/Laboratoire de Mesures et Modélisation de la Migration des

Radionucléides, F-91191 Gif-sur-Yvette, France

² UMR “IDES” CNRS–Université de Paris-Sud, F-91405 Orsay, France

* Corresponding author: sebastien.savoye@cea.fr

Abstract

⁷⁹Se might be one of the key mobile fission products for nuclear waste disposal hosted in deep argillaceous formations due to its longevity and its anionic character. An in-depth understanding of the transport properties of selenium is therefore essential. However, because of its high sensitivity to redox condition, the mobility of such an element is highly related to its speciation forms. Under in-situ reducing conditions, the selenium migration would be restricted by the low solubility of selenide, but more mobile oxidizing forms, as the oxyanions selenite and selenate are expected to be released from both reprocessing and spent fuel wastes.

The objective of this study was to investigate the diffusive behaviour of selenium, injecting under its two more oxidized forms (+IV & +VI), like assumed in the source term, through indurated clay rock samples originating from the Callovo-Oxfordian formation (COx) and lying in physico-chemical conditions as close as possible to those prevailing in-situ, by means of the use of a N₂/CO₂ glove-box. Two initial selenite concentrations (10⁻³ and 10⁻⁶ mol L⁻¹) were studied for assessing the role of this parameter on the kinetics of the selenite-reduction. For this purpose, two through-diffusion experiments were performed with a regular monitoring of the solutions (⁷⁵Se activity, Se redox state, chemistry). Lastly, after dismantling the cells, the ⁷⁵Se rock profiles in the solid were acquired by means of an abrasive peeling method.

Despite the reducing conditions prevailing in the experiments, Se (+VI) diffused more or less like ³⁶Cl⁻, with a very low retardation ($R_D < 0.5 \text{ mL.g}^{-1}$) and with no change of its redox state for the 240 days of the experiments. On other hand, Se (+IV) exhibited a much stronger affinity towards the COx samples, in inverse ratio to its initial concentration, R_D values ranging from about 10 mL.g⁻¹ for [Se (+IV)]_{ini}=10⁻³ mol L⁻¹ to about 100 mL.g⁻¹ for [Se (+IV)]_{ini}=10⁻⁶ mol L⁻¹. Lastly, the diffusion experiment carried out at the lowest Se(+IV) concentration, showed in its high-concentration reservoir,

after about 20 days of diffusion, a clear drop of its ^{75}Se activity, related to suspected precipitations of selenite in more reduced forms. Nevertheless, such a phenomenon did not strongly alter the diffusive selenium profile acquired into the solid.

Introduction

^{79}Se might be one of the key mobile fission products for nuclear waste disposal hosted in deep argillaceous formations due to its longevity and its anionic character (Altmann, 2009; De Cannière et al., 2010). The correct understanding of selenium migration behaviour through the clay barrier is therefore essential to underpin its transport parameters selected for the performance assessment calculations of a deep repository for spent fuel and high-level waste. However, up to now, there remains unclear under which predominant stable mobile species selenium would be capable of migrating from the nuclear wastes through these clayey media. Indeed, on one hand, ^{79}Se is generally assumed to be released from both reprocessing or spent fuel wastes in an oxidized state (+VI or +IV), while thermodynamic calculations deduce that Se should be in lower oxidation states, Se(0, -II) under conditions prevailing in the geological barrier system such as the Callovo-Oxfordian formation (Altmann, 2009). On other hand, selenium is a redox-sensitive element, its reduction rate of which can be hindered because it involves the transfer of multiple electrons along with multiple oxygen atoms between its various oxidation states (VI, IV, 0, -I, -II) (De Cannière et al., 2010). The reduction rate strongly varies with the oxidation number of the central atom in an oxyanion, and the higher the oxidation number, the slower the reaction (Shriver et al., 1990). As a consequence, Se(+VI) can be very reluctant to the reduction process and can subsist in metastable conditions, far from the thermodynamical equilibrium for undetermined periods of time. Conversely, selenite is more easily reduced. According to Bruggeman et al. (2005), the decrease in Se(+IV) concentration as a function of time seems proportional to the initial concentration of dissolved selenite and to the amount of solid FeS_2 present in the system. These authors observed that the Se (+IV) reduction rate slowed down when clay minerals and dissolved Boom Clay organic matter (OM) were present in the system. It was interpreted as a competition mechanism because SeO_3^{2-} also remained associated with illite by an inner-sphere complex or with OM by an iron bridge.

While several studies focused on the sorption behaviour of selenium on clay formations, especially the Boom clay, and their components (pyrite, calcite, clay minerals) by means of batch methods (Bruggeman et al., 2005, Liu et al., 2008, De Cannière et al., 2010), only few studies investigated the selenium diffusive behaviour. The former studies show that selenate is not solubility limited and selenite could precipitate as CaSeO_3 in cement environment only. Moreover, while selenate is not or weakly sorbed under Boom clay conditions, selenite is the most reactive selenium species, capable of being sorbed on pyrite and illite edges. Lastly, among the more reduced selenium species (0, -I, -II), only selenide could be considered as a mobile element, even though its solubility limit is very low, especially in presence of iron (from $3 \times 10^{-8} \text{ mol L}^{-1}$ to $4.5 \times 10^{-10} \text{ mol L}^{-1}$). To our knowledge, diffusive data regarding selenate in hard clay rocks are only available for the Boom clay formation (De Cannière et al., 2010). In this case, the diffusive parameters for selenate are very close to those of sulfate. Descostes et al. (2008) deduced from through-diffusion experiments performed on clayey samples from the Callovo-Oxfordian formation, values for diffusive parameters of selenite that were one order of magnitude lower than those obtained for ^{36}Cl . The authors

hypothesized that the chemical speciation of Se changed during the diffusion tests. Nevertheless, no monitoring of the Se speciation had been undertaken to verify such an assumption.

This non-exhaustive overview underlines the tricky task aiming at predicting the fate of the selenium diffusing through such argillaceous media. The objective of this study was to investigate the diffusive behaviour of selenium, injecting under its two more oxidized forms (+IV & +VI), like assumed in the source term, through indurated clay rock samples originating from the Callovo-Oxfordian formation and lying in physico-chemical conditions as close as possible to those prevailing in-situ, by means of the use of a N₂/CO₂ glove-box. Two initial selenite concentrations (10^{-3} and 10^{-6} mol L⁻¹) were tested for assessing the role of this parameter in the kinetics of the selenite-reduction, as already mentioned by Bruggeman et al. (2005). For this purpose, two through-diffusion experiments were performed with a regular monitoring of the solutions (⁷⁵Se activity, Se redox state, chemistry). Lastly, after dismantling the cells, the ⁷⁵Se rock profiles in the solid were acquired by means of the abrasive peeling method initially developed by Van Loon and Eikenberg (2005).

Materials and Methods

Sample Origin and Sample Preparation

The rock core used for the measurements was collected from the borehole OHZ1202 (X= 823252 m; Y=1091659.37m; Z=-115.54 m NGF), argon-drilled upwards in the Meuse/Haute Marne Underground Laboratory, located in the eastern portion of the Paris basin. The sedimentary host formation (152-160 Ma) is a ~130-m-thick clay-rich Callovo- Oxfordian formation and with a burial depth of ~420-550 m below ground level (bgl). According to Gaucher et al. (2004), the level from which the core originates (EST30471 core 480.7-481.7 m bgl) corresponds to silty and calcareous argillites, containing 35-65% of clay minerals (with 27-38% of mixed layer Illite/smectite), 15-28% of carbonates, 21-31% of quartz, and accessory minerals. Two samples were sliced into a N₂ glove box, from the EST30471 claystone core using a diamond wire saw (no lubricating fluid was used) into 1-cm-thick pieces and then cut as a disk.

Analytical procedure for estimating the fraction of ⁷⁵Se(+IV) and of ⁷⁵Se(+VI)

The principle for deriving the selenium speciation was based on an ion chromatography separation stage followed by a gamma counting of the fraction of Se(+IV) and that of Se(+VI). The high-performance anion exchange chromatography system was a Metrohm 761 Compact IC (Metrohm, Switzerland) with a 50 µL Peek injection loop and a 500 µL sample syringe. The separation of Se(+IV) and Se(+VI) was performed on an 4 x 250 mm A-Sup5 column (Metrohm, Switzerland) using an elution of 3.5 mmol L⁻¹ NaHCO₃/ Na₂CO₃ at a flow of 0.6 cm³ min⁻¹. Elution of the analytes was monitored in the conductivity mode.

In order to determine the times during which ⁷⁵Se(+VI) and ⁷⁵Se(+IV) fractions had to be collected, aqueous standards of stable Se(+VI) and Se(+IV) at a concentration of 10^{-3} mol L⁻¹ were eluted and monitored by conductivity, as shown in Figure 1.

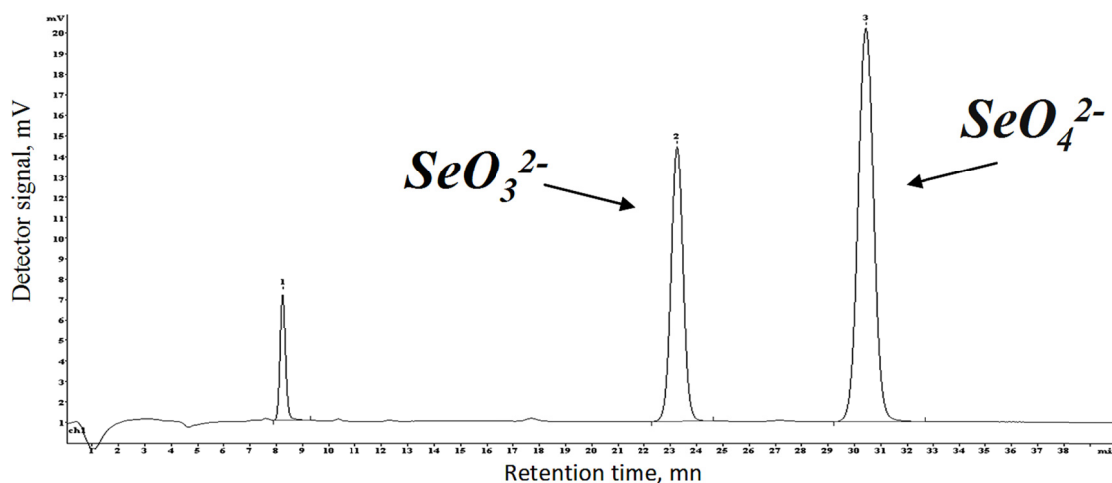


Figure 1: Chromatograms of selected calibration standards measured by HPAEC in the conductivity mode Through-diffusion design

Figure 2 schematically represents the diffusion cells used in this study. The through-diffusion cells comprise two reservoirs in polypropylene (up and downstream: 175 and 130 mL, respectively), a polypropylene sample holder, two PEEK holed plates, the whole being pasted with glue and screwed together. It is noteworthy that the classical stainless steel filterplates were replaced by chemically-inert PEEK plates. Each part of the diffusion cell was previously cleaned successively with HNO_3 , water, isopropanol and ethanol and dried. All the preparation of the diffusion cells were made in an anoxic glove box.

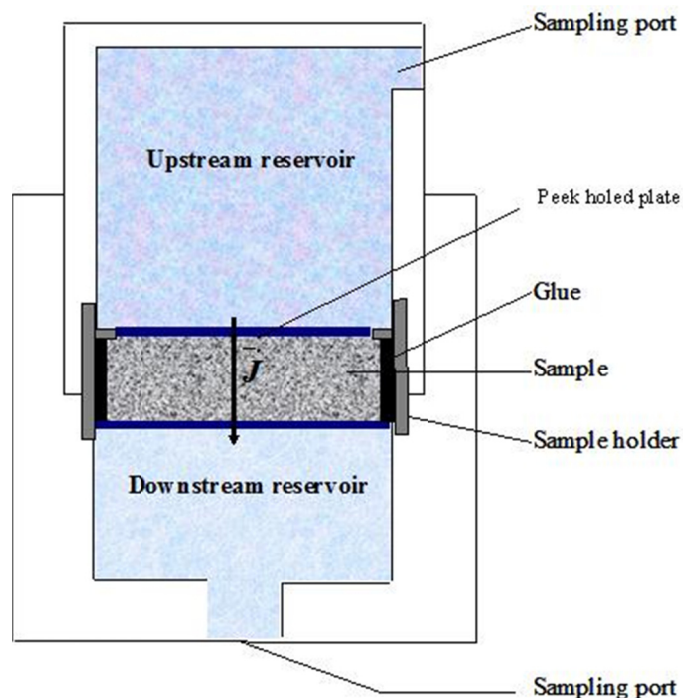


Figure 2: Experimental set-up for through diffusion experiment

Afterwards, all experiments were carried out in an oxygen-depleted (~2 ppm O₂) glove box with a 99.6% N₂/0.4% CO₂ gas mixture and operated at ambient temperature (21 ± 1 °C). The CO₂ content was used to simulate the in-situ Callovo-Oxfordian claystone CO₂ partial pressure (Vinsot et al., 2007), which controls the carbonate concentration and solution pH. That allows the chemistry of the solutions to be close to the equilibrium state with respect to the carbonate minerals (Beaucaire et al., 2008). Rock disks in the diffusion cells were equilibrated over at least 4 weeks, with the synthetic solutions of composition given by Table 1. This time was found to be sufficient to reach chemical equilibrium (Descostes et al., 2008).

Table 1: Composition of synthetic water used in this study

[Cl ⁻] (mmol L ⁻¹)	[SO ₄ ²⁻] (mmol L ⁻¹)	ΣCO ₂ (mmol L ⁻¹)	[Na ⁺] (mmol L ⁻¹)	[K ⁺] (mmol L ⁻¹)	[Ca ²⁺] (mmol L ⁻¹)	[Mg ²⁺] (mmol L ⁻¹)
41.00	15.6	2.57	51.9	1.04	6.44	4.48

Through-diffusion stage

Subsequently, the solution was replaced by a fresh one. First of all, the solution in the upstream reservoir was spiked with HTO, a water tracer and ³⁶Cl. Their activities were set at 4.6 and 5.2 GBq m⁻³ (resp.). Both compartments were periodically sampled, the solution volume being renewed in each compartment either by the radiolabelled solution or by the synthetic water. The monitoring of the ³⁶Cl flux through the rock sample allows the determination of the diffusion-accessible porosity of a non-reactive anionic tracer (ε_a). After completion of the first through-diffusion stage, an out-diffusion procedure was applied to the two cells. Thus, the solutions in both reservoirs were replaced by synthetic solution without tracer, for making HTO and ³⁶Cl diffuse out of the rock samples. At selected time intervals, the activity in the solutions was measured just before replacing them by fresh ones. This procedure was repeated until the activity measurement led to values close to the background activity values. Then, a second through-diffusion stage was performed by introducing into the upstream reservoir, both stable dissolved selenite (Na₂SeO₃, Fluka) either at a concentration of 10⁻³ mol L⁻¹ or at 10⁻⁶ mol L⁻¹ and the ⁷⁵Se-labelled source (Eckert & Ziegler, Germany) at an activity of 5 GBq m⁻³. As already mentioned by De Cannière et al. (2010), most of the ⁷⁵Se(+IV) sources supplied by the manufacturers were accompanied by Se(+VI), because of the water radiolysis of the ⁷⁵Se stock solution. Therefore, using the ionic chromatography method as described above, we determined that 5.3% of the ⁷⁵Se stock was under selenate form, enabling us to perform a double spike with on one hand, stable and radioactive Se(+IV) and, on other hand, only radioactive Se(+VI).

For the diffusion experiments, careful attention was paid to keep a nearly low concentration in the downstream reservoir (not higher than 3% of the upstream reservoir concentration, renewed if higher). Conversely, the upstream reservoir concentration was allowed to decrease in order to evidence for the selenium, any possible sorption phenomenon in this compartment, especially for the Se(+IV) species.

In addition to the regular sampling used for monitoring the ⁷⁵Se activity evolution (i.e. 0.1 mL and 3 mL in the upstream and the downstream reservoirs, resp.), larger amounts of solutions (2 mL) were withdrawn four times throughout the selenium diffusion stage

in order to monitor any changes of the selenium speciation with the help of the ionic chromatography separation and of the physico-chemical parameters (Eh, pH, chemistry of the solutions).

Acquisition of the ⁷⁵Se rock profiles in solid

After 240 days of selenium diffusion, the cells were dismantled by removing the sample holders from these cells. The sample holders were roughly dried overnight in the dried atmosphere of the glove box, and afterwards in an oven at 70°C, out of the glove box, for 3 days. Then, the abrasive peeling technique developed by Van Loon and Eikenberg (2005) for Opalinus Clay, was applied to the two rock samples, previously extracted from the sample holder and the glue. This technique enables the abrasion of a sample layer, thickness of which can vary from 10µm to 250 µm depending of the abrasion duration and the type of the grit grinding paper used (from P220 to P80). The choice of the thickness is directly related to the distance to the disk surface previously in contact with the upstream reservoir solution. That means that the closer to the disk surface the layer, the higher the specific ⁷⁵Se activity and the smaller the thickness. The ⁷⁵Se activity in the abraded layers was measured by χ -spectroscopy.

Data analysis

The analysis of the results was based on Fick's second law for one-dimensional reactive transport:

$$\frac{\partial C}{\partial t} = D_a \frac{\partial^2 C}{\partial x^2} = \frac{D_e}{\alpha} \frac{\partial^2 C}{\partial x^2} = \frac{D_e}{\varepsilon_a + \rho R_D} \frac{\partial^2 C}{\partial x^2} \quad (1)$$

Where C is the concentration or activity per volume unit (mol m^{-3} or Bq m^{-3}); t , the time (s); D_a , the apparent diffusion coefficient ($\text{m}^2 \text{s}^{-1}$); D_e , the effective diffusion coefficient ($\text{m}^2 \text{s}^{-1}$); α , the rock capacity factor; ε_a , the diffusion-accessible porosity; ρ , the bulk dry density (kg m^{-3}); and R_D , the distribution ratio ($\text{m}^3 \text{kg}^{-1}$).

According to van Brakel and Heertjes (1974), D_e can be written as follows:

$$D_e = D_p \varepsilon_a = \frac{\delta}{\tau^2} D_0 \varepsilon_a = \frac{D_0}{G} \varepsilon_a \quad (2)$$

Where D_0 is the free-solution (aqueous) diffusion coefficient ($\text{m}^2 \text{s}^{-1}$), δ represents the constrictivity factor (-), and τ is the tortuosity factor. G is the geometrical factor. Tortuosity and constrictivity are purely geometric factors, which, compared with a specific cross-section in free water, lengthen the diffusion pathway and reduce the diffusion cross-section, respectively (van Brakel and Heertjes, 1974).

In a first order approach, PEEK holed plates were considered for modelling like stainless steel filterplates. The boundary and initial conditions of the through diffusion problem are given by:

$$C(x, t) = 0, \quad t = 0 \quad (3)$$

$$C(x, t) = C_0, \quad x = 0, t = 0 \quad (4)$$

$$C(x, t) = 0, \quad x = L+2l, t > 0 \quad (5)$$

Where L and l are, respectively, the sample and plate thicknesses (m). C_0 is the concentration of the tracer in the upstream reservoir (Bq.m^{-3}). For a non reactive tracer ($R_D = 0$), α is equal to ε_a .

Fully analytical solutions for through-diffusion, reservoir-depletion and ^{75}Se -rock profile studies are obtained in the Laplace space, which are subsequently numerically inverted to provide the solution in time (Moridis, 1998). It is noteworthy that the analytical solution used for the interpretation of ^{75}Se -reservoir-depletion and ^{75}Se -rock profile data is that used for in-diffusion study (Moridis, 1998, Van Loon and Eikenberg, 2005). The analysis of the results was performed by a least-square fitting of the model to the results of either the incoming flux in the downstream reservoir, the ^{75}Se reservoir-depletion or the ^{75}Se -rock profile, using analytical solutions of Eq. (1) (Put, 1991; Melkior, 1999) taking into account the presence of two look-like filterplates (thickness: 1.95 mm; filterplate geometry factor $D_0/D_e = 8.19$, Descostes et al., 2008; porosity: 37%).

Analyses

Analyses of principal anions and cations (Na, K, Mg, Ca, Cl, SO_4) were performed by ion exchange chromatography with an accuracy of about 5%. Anions and cations were analysed by Ion Chromatography. The analytical uncertainties were 5%. Alkalinity was determined by spectrophotometry with an accuracy of 5%. The Eh was corrected *versus* the standard hydrogen electrode (SHE).

Activities were counted either by α - β liquid scintillation (Packard TRICARB 2500, USA) or by χ counter (Packard 1480 WIZARD, USA) in the case of ^{75}Se . The counting efficiency for each tracer was measured using synthetic water with known amounts of radioactivities. Background measurements were performed in a similar way using synthetic water without radiotracers. ^{75}Se solution data were corrected for radioactive decay with respect to the tracer injection time, while ^{75}Se rock profile data were corrected with respect to the dismantling time.

Results and Discussion

Evolution of physico-chemical parameters

The first results obtained on the chemical composition of the solutions showed that no change was observed for the first 80 days of the Se-diffusion experiments, the discrepancies being comprised in the analytical error. The analysis of the remaining samples is still on progress.

pH values varied from 7.35 ~ 7.40 in the beginning, to 7.8 ~ 7.9 just before the dismantling. Such an evolution towards a slightly more alkaline pH is still unanswered. The measurement of the Eh, at the beginning of the experiments, led to quite high

values (from 200 to 280 mV/SHE), also observed in the upstream reservoirs just before dismantling (Eh/cell 1= 250 mV/SHE & Eh/cell 2= 170 mV/SHE). Such high values were already observed by Bruggeman et al. (2005) in batch experiments carried out with FeS₂ in synthetic Boom clay water for studying Se(+IV) interaction. These authors attributed this discrepancy to the fact that, due to O₂ traces in the glove box (2-3 ppm), like in our case, the Eh electrode (which is stored in a 3 M KCl solution in the glove box) suffers from a memory effect, whereby the “real” Eh value is not reached in standard measurement times (10-15 min), the HS⁻/SO₄²⁻ redox couple not possessing enough buffer capacity to accurately sustain low Eh values. Conversely, lower values were measured in the downstream reservoirs at the end of the experiments, with Eh values equal to – 145 mV/SHE and – 70 mV/SHE in cell 1 and cell 2 (resp.).

Through-diffusion and rock profile data

The cell 1 with the highest initial Se(+IV) content ($10^{-3} \text{ mol L}^{-1}$)

Figure 3 shows the evolution of the ⁷⁵Se activity in the upstream reservoir as a function of time. A clear activity decrease was observed for the 240 days of the experiment. The results of the fractionation indicated that the activity values originating from the active Se(+VI) remained quite constant throughout the duration of the experiment, while the evolution of the total measured activity can clearly be related to the decrease of the ⁷⁵Se(+IV) activity values (Figure 3).

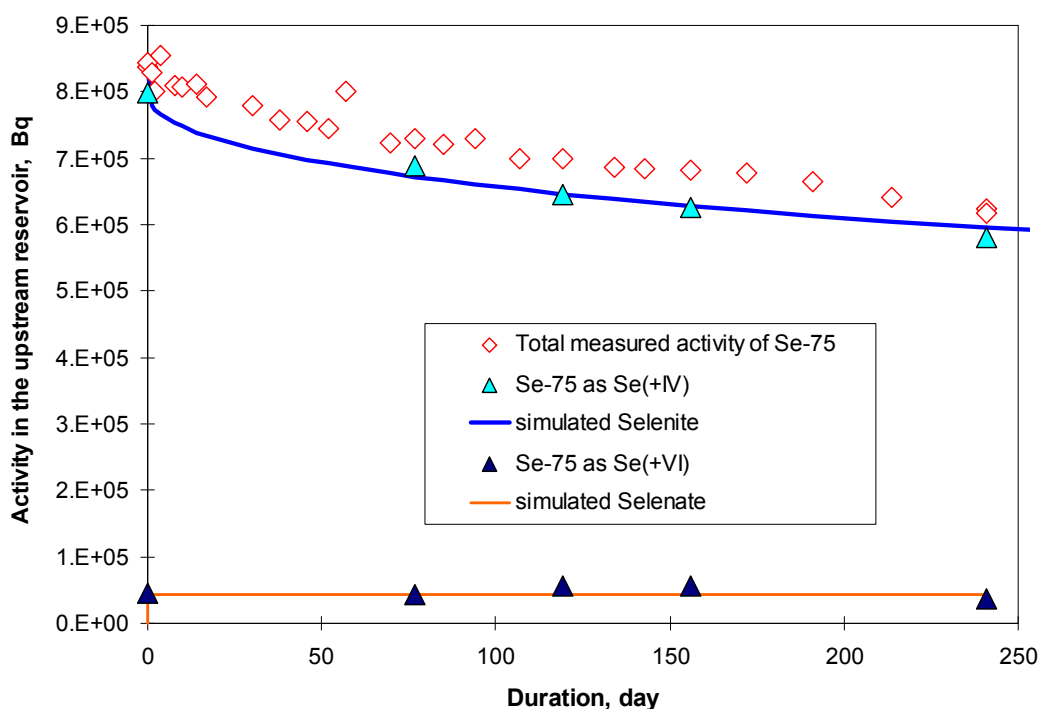


Figure 3: Evolution of the ⁷⁵Se activity in the upstream reservoir spiked with Se(+IV)= $10^{-3} \text{ mol L}^{-1}$ as a function of time. The curves have been calculated using the corresponding analytical solution using the parameters from Table 2. Closed symbols denote the results of the fractionation. Open symbols denote the activity of total Se determined from the total radioactivity in the samples.

The normalised incoming fluxes measured in the downstream reservoir for ^{36}Cl and ^{75}Se were reported in Figure 4. Owing to the too low activities measured in this reservoir, which prevented us from applying the fractionation method, only indirect approach was used for estimating the redox state of the selenium having diffused through the rock sample. In fact, some answers can be brought by the fits of the experimental data – Se(+IV) and Se(+VI)- obtained both from the downstream and upstream reservoirs but also from the rock profile (see above) and using the parameters from the Table 2. Indeed, on one hand, fitting the downstream reservoir data, by assuming Se(+IV) as the sole activity contributor can only be achieved, using very low values for the diffusive parameters ($D = 1.1 \cdot 10^{-13} \text{ m}^2 \text{ s}^{-1}$ & $\alpha = 0.01$), such as those selected by Descostes et al. (2008) (see Table 2) and leads to a simulated curve in the upstream reservoir, displaying no decrease and thus, clearly not consistent with the corresponding $^{75}\text{Se}(+IV)$ data. Moreover, taking the parameters used for the fit of the Se(+IV) data determined in the upstream reservoir leads to calculate a very delayed breakthrough curve, clearly not in agreement with the experimental data, as it can be seen in Figure 4. On other hand, assuming Se(+VI) as the sole activity contributor to the downstream reservoir allows us to fit well both upstream and downstream data and by means of diffusive parameter values sounding quite consistent (Table 2). Indeed, these values are quite close to those obtained by Descostes et al. (2008) for sulphate on sample originating from the same location (Table 2) and De Cannière et al. (2010) indicated that Se(+VI) displayed a diffusive behaviour similar to sulphate from diffusive studies on Boom Clay.

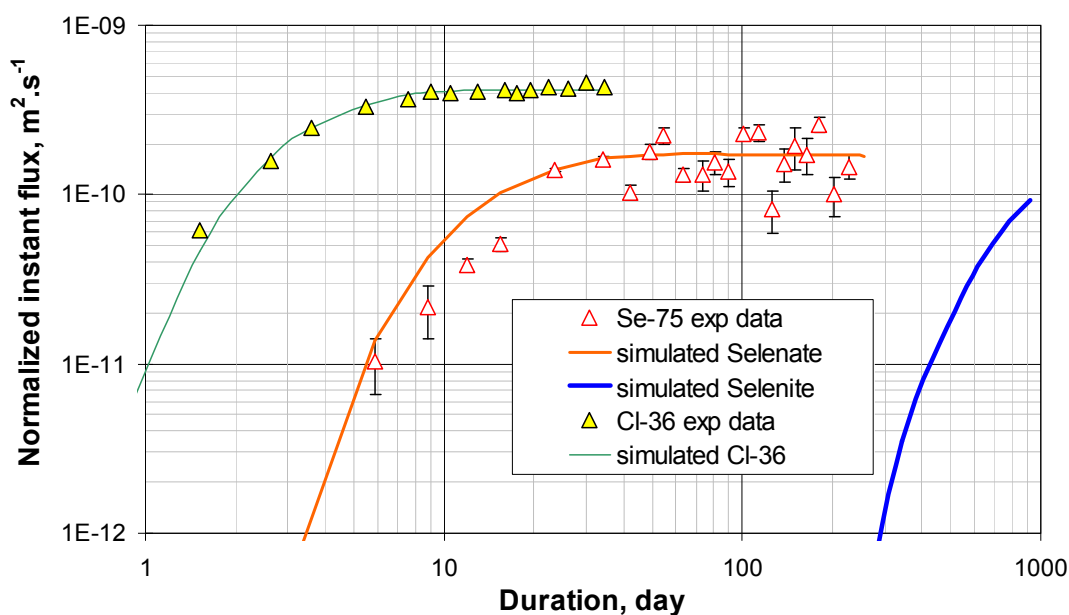


Figure 4: Normalized instantaneous fluxes of the cell with $\text{Se}(+IV) = 10^{-3} \text{ mol L}^{-1}$ for ^{36}Cl and ^{75}Se . The solid curves for the fluxes were calculated using the analytical solutions with the parameters specified in Table 2. Normalized flux is the ratio of instantaneous flux in $\text{Bq m}^{-2} \text{ s}^{-1}$ over the concentration in the upstream reservoir in $\text{Bq} \cdot \text{m}^{-3}$.

Table 2: Values of rock capacity factor (α), effective diffusion coefficient (De) and distribution ratio (R_D) for the diffusion of HTO, $^{36}\text{Cl}^-$, $^{35}\text{SO}_4^{2-}$, $^{75}\text{Se}(+\text{IV})$ and $^{75}\text{Se}(+\text{VI})$. Data from Descostes et al. (2008) were obtained on core from borehole EST205. n-d: not determined.

		HTO	$^{36}\text{Cl}^-$	$^{75}\text{Se}(+\text{IV})$	$^{75}\text{Se}(+\text{VI})$	$^{35}\text{SO}_4^{2-}$
Cell 1	$\alpha[-]$	0.19	0.07	24.5	0.13	n-d
Se(+IV)=10^{-3} M	$De \times 10^{-12}$	31.0	4.8	4.0	2.0	n-d
EST30471	$[\text{m}^2 \text{ s}^{-1}]$					
480.70–481.70	Rd	0	0	10.4	0.025	n-d
	$[\text{mL g}^{-1}]$					
Cell 2	$\alpha[-]$	0.20	0.08	300 to 640	0.09	n-d
Se(+IV)=10^{-6} M	$De \times 10^{-12}$	27.0	3.7	2 to 4	1.2	n-d
EST30471	$[\text{m}^2 \text{ s}^{-1}]$					
480.70–481.70	Rd	0	0	100 to 300	0.005	n-d
	$[\text{mL g}^{-1}]$					
Descostes et al. (2008)	$\alpha[-]$	0.195±0.045	0.065	0.009	n-d	0.31
	$De \times 10^{-12}$	22±7	4.6	0.15	n-d	1.9
EST05641	$[\text{m}^2 \text{ s}^{-1}]$					
476.97–477.37	Rd	0	0	0	n-d	0.1
	$[\text{mL g}^{-1}]$					

Finally, our experiment permits to shed light on the singular data previously obtained by Descostes et al. (2008) with Se(+IV). In fact, the $^{75}\text{Se}(+\text{IV})$ labelled source they used could be suspected to contain a sufficient amount of $^{75}\text{Se}(+\text{VI})$ for diffusing through the sample instead of the more sorbing $^{75}\text{Se}(+\text{IV})$, as described in our study, and thus, for making Descostes et al. (2008) give wrong estimates for the diffusive parameters.

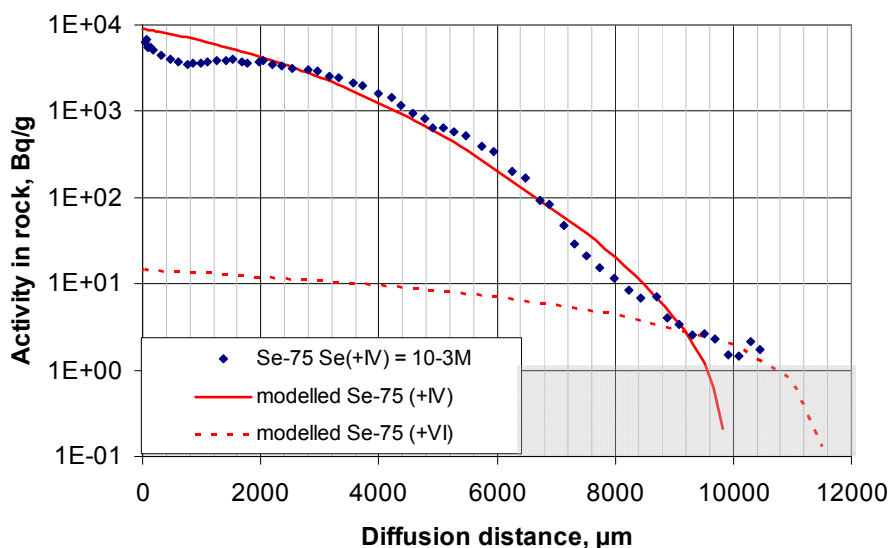


Figure 5: Concentration profile of ^{75}Se for the cell 1 with $\text{Se}(+\text{IV})=10^{-3} \text{ mol L}^{-1}$. Symbols represent experimental data. The curves are the best fits with the parameters summarised in Table 2. ^{75}Se activities in the sample beyond a diffusion distance of 10000 μm were below the detection limit. The shaded area denotes concentration ranges around or well below the detection limit.

Figure 5 shows the concentration of ^{75}Se (Bq g^{-1}) as a function of the diffusion distance. The diffusion profile data of the solid sample were fitted using only diffusive parameter values for Se(+IV) (Table 2), the contribution to the activity coming from Se(+VI) being negligible, except maybe in the last centimetre. It is noteworthy that some scattering of the experimental data can be observed in the Figure 5. Two types of explanation can be proposed: (i) our assumption about a unique value of R_D , whatever the Se(+IV) concentrations, for modelling the sorption of Se(+IV) is quite too strong and (ii) some mineralogical heterogeneities occur inside the rock sample so that some minerals exhibit more affinity towards selenium than others.

The cell 2 with the lowest initial Se(+IV) content ($10^{-6} \text{ mol.L}^{-1}$)

Figure 6 shows the evolution of the ^{75}Se activity in the upstream reservoir as a function of time. A regular decrease is observed for the first 20 days until a rapid drop, and a sort of plateau is reached from the 70th day. The fractionation technique indicates that $^{75}\text{Se(+IV)}$ would be mainly responsible for such an evolution. As already mentioned by Bruggeman et al. (2005), Se(+IV) was capable of being undertaken to some reduction phenomena, leading to the precipitation of the more reduced Se forms, and likely kinetics-controlled, as more than 20 days were necessary to reach such a decrease. However, an attempt to roughly fit the first Se(+IV) data (before 20 days) was carried out using parameters given in Table 2.

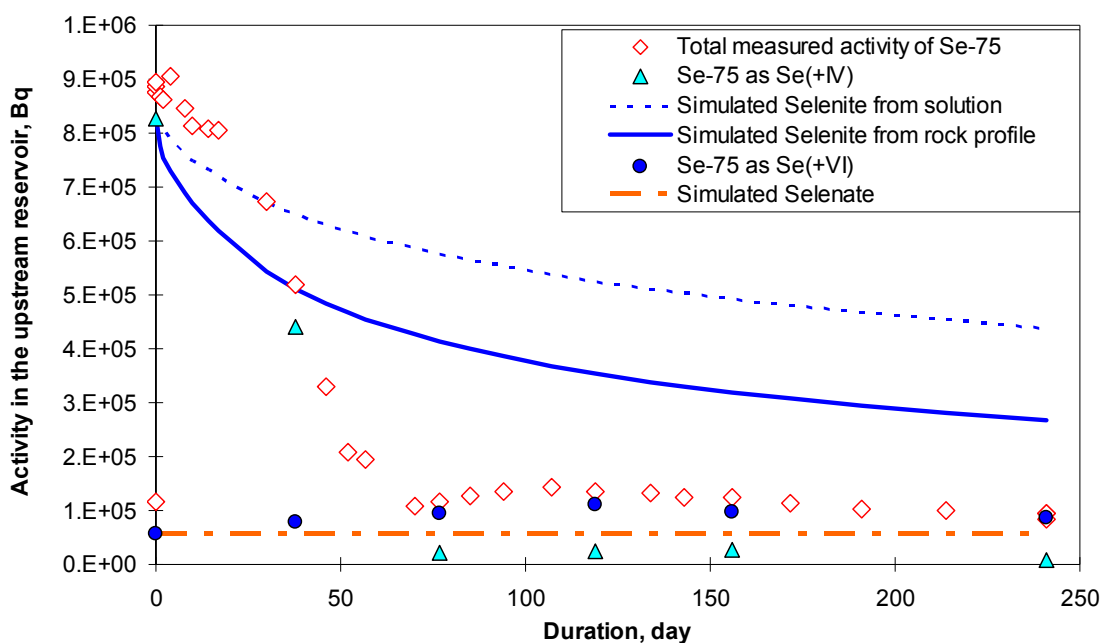


Figure 6: Evolution of the ^{75}Se activity in the upstream reservoir spiked with $\text{Se(+IV)} = 10^{-6} \text{ mol L}^{-1}$ as a function of time. The curves have been calculated using the corresponding analytical solution using the parameters from Table 2. Closed symbols denote the results of the fractionation. Open symbols denote the activity of total Se determined from the total radioactivity in the samples.

The normalised incoming fluxes measured in the downstream reservoir for ^{36}Cl and ^{75}Se were reported in Figure 7. Even though the experimental ^{75}Se data were more scattered than those for the cell 1, they were fitted with diffusive parameter values very close to those used for the cell 1, assuming that only $^{75}\text{Se}(+\text{VI})$ was involved, as for the cell1 (Table 2).

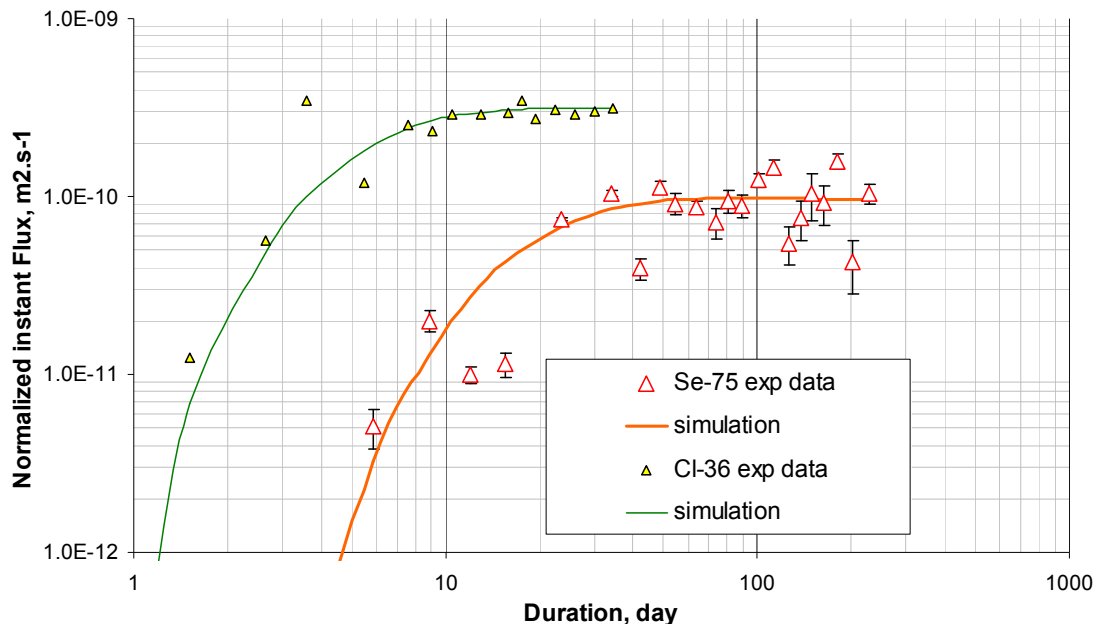


Figure 7: Normalized instantaneous fluxes of the cell 2 with $\text{Se}(+\text{IV})=10^{-6} \text{ mol L}^{-1}$ for ^{36}Cl and ^{75}Se . The solid curves for the fluxes were calculated using the analytical solutions with the parameters specified in Table 2. Normalized flux is the ratio of instantaneous flux in $\text{Bq m}^{-2} \text{ s}^{-1}$ over the concentration in the upstream reservoir in $\text{Bq} \cdot \text{m}^{-3}$.

Figure 8 shows the concentration of ^{75}Se (Bq g^{-1}) as a function of the diffusion distance. Three areas can be distinguished in the solid: one in the very first 100 μm with very high measured activities, the second, from 100 μm to about 4000 μm , showing a regular and rapid decrease and the last one, from 4000 μm to the 11600 μm , with a smoother activity decrease. Given the fact that some chemical instability had likely disturbed the diffusion stage in the upstream reservoir, experimental data acquired in the solid were only roughly fitted. However, on one hand, the last part of the profile looks like quite consistent with the corresponding modelled $^{75}\text{Se}(+\text{VI})$, and on other hand, the second part can be roughly fitted using parameters given in Table 2 for $\text{Se}(+\text{IV})$.

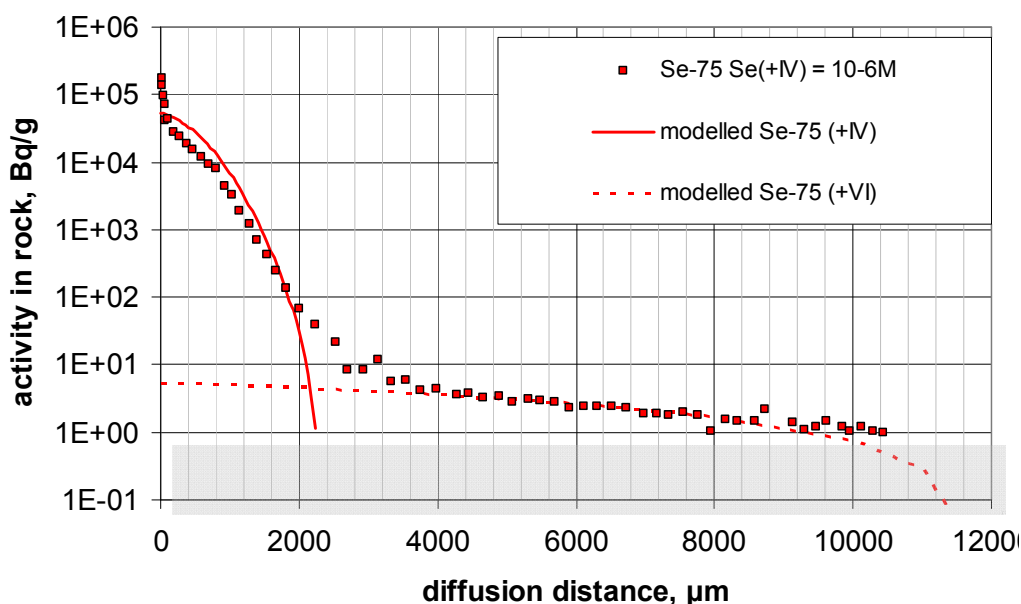


Figure 8: Concentration profile of ^{75}Se for the cell 2 with $\text{Se}(+\text{IV})=10^{-6} \text{ mol L}^{-1}$. Symbols represent experimental data. The curves are the fits with the parameters summarised in Table 2. ^{75}Se activities in the sample beyond a diffusion distance of 10000 μm were below the detection limit. The shaded area denotes concentration ranges around or well below the detection limit.

Summary and Conclusions

The diffusive behaviour of selenium, injecting under its two more oxidised forms (+IV and +VI), was investigated through rock samples originating from the Callovo-Oxfordian (Cox) formation (France) and lying in physico-chemical conditions as close as possible to those prevailing in-situ, by means of the use of a N_2/CO_2 glove-box. Two initial $\text{Se}(+\text{IV})$ concentrations (10^{-3} and $10^{-6} \text{ mol L}^{-1}$) were tested. For this purpose, two through-diffusion experiments were performed with a regular monitoring of the solutions (^{75}Se activity, Se redox state, chemistry). Lastly, after dismantling the cells, the ^{75}Se rock profiles in the solid were acquired by means of an abrasive peeling method.

Despite the reducing conditions prevailing in the experiments, Se (+VI) diffused almost like ^{36}Cl ($\text{De}(\text{Se}+\text{VI})/\text{De}^{36}\text{Cl} \approx 2$), with a very low retardation ($R_D < 0.5 \text{ mL g}^{-1}$) and assuming no change of its redox state for the 240 days of the experiments. On other hand, Se (+IV) exhibited a much stronger affinity towards the COx, in inverse ratio to its initial concentration, R_D values ranging from about 10 mL g^{-1} for $[\text{Se}(+\text{IV})]_{\text{ini}}=10^{-3} \text{ mol L}^{-1}$ to about $200 \pm 100 \text{ mL g}^{-1}$ for $[\text{Se}(+\text{IV})]_{\text{ini}}=10^{-6} \text{ mol L}^{-1}$. It is noteworthy that the experiment carried out with the lowest $\text{Se}(+\text{IV})$ concentration, showed in its high-concentration reservoir, after about 20 days of diffusion, a clear drop of its ^{75}Se activity, related to suspected precipitations of selenite in likely more reduced forms.

In perspective, in addition to classical batch experiments, synchrotron-based spectroscopic methods are also planned to investigate the redox state of the selenium having diffusing through COx samples and to identify the particular minerals onto which selenium is capable of being sorbed.

Acknowledgement

The research leading to these results has received funding from the European Union's European Atomic Energy Community's (Euratom) Seventh Framework Programme FP7/2007-2011 under grant agreement n° 212287 (RECOSY project). The authors also thank Andra for providing the core used in this study.

References

- Altmann S. (2009). 'Geo'chemical research: A key building block for nuclear waste disposal safety cases. J. Contam. Hydrol. 102, 174-179.
- Beaucaire C., Michelot J.-L., Savoye S., Cabrera J. (2008) Groundwater characterisation and modelling of water-rock interaction in an argillaceous formation (Tournemire, France). Appl. Geochem. 23, 2182–2197.
- Bruggeman C., Maes A., Vancluysen J., Vandemussele P. (2005) Selenite reduction in Boom clay: Effect of FeS₂, clay minerals and dissolved organic matter. Environ. Pollut. 137, 209–221.
- De Cannière P., Maes A., Williams S., Bruggeman C., Beauwens T., Maes N., and Cowper M. (2010) Behaviour of selenium in Boom Clay. Work performed under contract: SCK•CEN ref:CO 90 01 1467.01 1467 RP.W&D.037 – NIROND ref: CCHO2004/00/00 DS251-A44/2.1.
- Descostes M., Blin V., Bazer-Bachi F., Meier P., Grenut B., Radwan J., Schlegel M. L., Buschaert S., Coelho D., Tevissen E. (2008). Diffusion of anionic species in Callovo-Oxfordian argillites and Oxfordian limestones (Meuse/Haute-Marne, France). Appl. Geochem. 23, 655-677.
- Gaucher E., Robelin C., Matray J.-M., Negrel G., Gros Y., Heitz J.-F., Vinsot A., Rebours H., Cassagnanere A., Bouchet A. (2004). ANDRA underground research laboratory: interpretation of the mineralogical and geochemical data acquired in the Callovian-Oxfordian formation by investigative drilling. Phys. Chem. Earth 29, 55-77.
- Liu X., Fattahi M., Montavon G., and Grambow B. (2008). Selenide retention onto pyrite under reducing conditions. Radiochimica Acta 96 (8), 473–479.
- Melkior T. (1999) Etude méthodologique de la diffusion de cations interagissant dans des argiles. Ph.D. thesis, Ecole Centrale de Paris.
- Moridis G. J. (1998) A set of semi-analytical solutions for parameter estimation in diffusion cell experiments. Report LBNL-41857, Lawrence Berkeley National Laboratory, Berkeley, California.
- Put M.J. (1991). An improved mathematical-model for the interpretation of the flow-through type diffusion test with influence of filterplates. Radioact. Waste Manage. Environ. Restoration 16, 69–81.
- Shriver D.F., Atkins P.W., Langford C.H. (1990). Inorganic chemistry. 706 pp. Oxford University Press. Oxford, Melbourne, Tokyo.

Van Brakel J. and Heertjes P. M. (1974). Analysis of diffusion in macroporous media in terms of a porosity, a tortuosity and a constrictivity factor. *Int. J. Heat Mass Transfer* 17, 1093–1103.

Van Loon L.R., Eikenberg J. (2005). A high-resolution abrasive method for determining diffusion profiles of sorbing radionuclides in dense argillaceous rocks. *Appl. Rad. Isot.* 63, 11–21.

Vinsot A., Mettler, S., Wechner, S. (2007). In situ characterization of the Callovo-Oxfordian pore water composition. *Phys. Chem. Earth* 33, 75-86.

INFLUENCE OF THE REDOX STATE ON THE NEPTUNIUM SORPTION BY CEMENTITIOUS MATERIALS

Jan Tits^{1*}, Xavier Gaona², Andy Laube¹, Erich Wieland¹

¹ Laboratory for Waste Management, Paul Scherrer Institute, Villigen-PSI, (CH)

² Institut für Nukleare Entsorgung, Karlsruhe Institute of Technology (DE)

*Corresponding author: jan.tits@psi.ch

Abstract

The uptake of neptunium in different oxidation states (+IV, +V and +VI) on calcium silicate hydrate (C–S–H) phases, a major component of hardened cement paste, was investigated in the pH range $10 \leq \text{pH} \leq 13.3$. Dithionite, at a concentration of $5 \cdot 10^{-3}$ M, was applied as a reducing agent to stabilize Np(IV) whereas $5 \cdot 10^{-3}$ M hypochlorite was applied to stabilize Np(VI) in the C–S–H suspensions. In parallel, sorption experiments with Th(IV) and U(VI), two actinides often regarded as chemical analogues for the other tetravalent and hexavalent actinides, were carried out.

Sorption values were found to be very high for all actinides (An(IV): $R_d = (5 \pm 3) \cdot 10^5 \text{ L kg}^{-1}$, An(V): $3 \cdot 10^5 \text{ L kg}^{-1} < R_d < 3 \cdot 10^6 \text{ L kg}^{-1}$, An(VI): $6 \cdot 10^2 \text{ L kg}^{-1} < R_d < 10^6 \text{ L kg}^{-1}$). The oxidation state analogy appears to be valid for the sorption on cementitious materials in the case of the tetravalent actinides, while this is not strictly true in the case of the hexavalent actinides.

Several observations suggest that the uptake of the actinides is controlled by an incorporation process in the C–S–H interlayer rather than by surface complexation.

Introduction

In most current concepts for repositories for intermediate level radioactive waste (ILW), cementitious materials are planned to be used for the solidification of the waste materials, as backfill and as construction materials. Calcium silicate hydrates (C–S–H phases) are major constituents of hardened cement paste (HCP). They may control the release of radionuclides from the cementitious near-field of an ILW repository due to their high immobilization potential for many metal cations and their long term stability during cement degradation.

The uptake of redox-sensitive actinides such as neptunium, by cementitious materials under hyperalkaline conditions is poorly known (e.g. Wieland and Van Loon, 2002), and even their aqueous speciation is still a matter of debate (Gaona et al., 2011d). Neptunium is commonly believed to exist in oxidation states +IV and +V in a cementitious environment under reducing, respectively oxidizing conditions. However, the possible formation of anionic Np(VI) species ($\text{NpO}_2(\text{OH})_3^-$ and $\text{NpO}_2(\text{OH})_4^{2-}$) under

oxidizing hyperalkaline conditions, in analogy to U(VI), may significantly limit the stability field of Np(V) in favour of Np(VI) species. Whereas experimental data concerning the sorption of Np(V) by cementitious materials are scarce, sorption data concerning Np(IV) and Np(VI) are non-existing in the literature.

Aqueous complexation constants of actinide cations are known to increase proportional to the electrostatic interaction energy between the metal cation and the surface ligand due to their “hard-acid” character favouring electrostatic interaction with hard bases such as oxygen (Fanghänel and Neck, 2002). The electrostatic interaction energy may be expressed by Z_{eff}/d (Z_{eff} is the effective charge of the metal cation; d is the distance between the metal and the ligand). Sorption reactions on surfaces mainly involve coordination with surface hydroxyl groups. Therefore, it may be anticipated that in the case of a surface complexation process, in analogy to solution chemistry, sorption distribution ratios (R_d values) show a roughly similar correlation with Z_{eff}/d , which is expected to increase in the series Np(V) ($Z_{\text{eff}}=2.2$, $d=0.25\text{nm}$) < Np(VI) ($Z_{\text{eff}}=3.0$, $d=0.242\text{nm}$) < Np(IV) ($Z_{\text{eff}}=4.0$, $d=0.24\text{nm}$) (Choppin, 1984; Neck and Kim, 2000).

The present study was carried out to determine robust sorption data for Np(IV), Np(V) and Np(VI) on C–S–H phases under hyperalkaline conditions with the aim of assessing the above sorption sequence on C–S–H phases. The redox state of Np in the sorption tests was fixed by the addition of Na-dithionite as a reducing agent (Np(IV)) or Na-hypochlorite as an oxidizing agent (Np(VI)). No redox buffer was used for the experiments with Np(V). The discussion of the experimental data aims at elucidating whether or not the observed sorption behaviour can be explained by an adsorption process.

Materials and methods

2.1. General

Sample preparations, as well as batch sorption tests, were performed in glove boxes under a N_2 atmosphere ($p\text{O}_2$, $p\text{CO}_2 < 2$ ppm). Solutions were prepared using deionized, decarbonated water (Milli-Q water) generated by a Milli-Q Gradient A10 System (Millipore, Bedford, USA). Prior to use, all containers employed for the wet chemistry experiments were washed, left overnight in a solution of 0.1 M HCl, and thoroughly rinsed with Milli-Q water.

2.2. Materials

C–S–H phases consist of short silica chains (dimers to pentamers) connected to CaO sheets. In the interlayers between the Ca-silicate sheets, varying amounts of Ca atoms may be located. The $\text{CaO}:\text{SiO}_2$ (C:S) mol ratios can vary between 0.67 and 1.8 (Chen et al., 2004; Richardson, 2008). At low C:S ratios, the interlayer positions are filled with H_2O molecules. With increasing C:S ratios, the bridging Si tetrahedra are progressively replaced by Ca ions (see Figure 1)

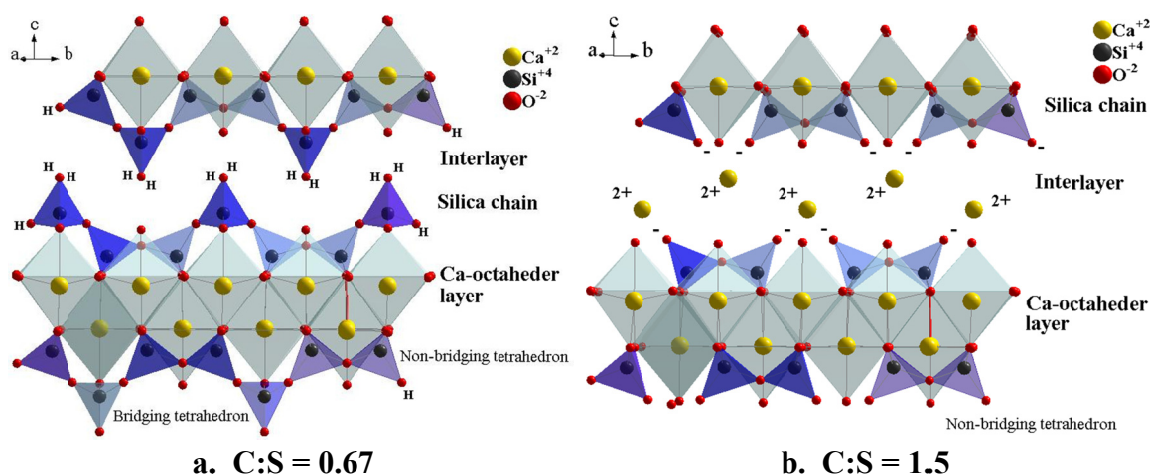


Figure 1: Schematized structural representation of C–S–H phases after RICHARDSON (2008) : a. low C:S ratio; b. high C:S ratio.

C–S–H phases with varying CaO:SiO₂ (C:S) ratios ($0.65 < C:S < 1.65$) were synthesised in MilliQ water and in an Artificial Cement pore Water (ACW) following a procedure described elsewhere (Tits et al., 2006). In brief, AEROSIL 300 (SiO₂) (Degussa-Huls AG, Baar Switzerland) was mixed with CaO in polyethylene bottles to give target C : S ratios between 0.6 and 1.82. To this, ACW or Milli-Q water was added to achieve suspensions (250 ml) having a S : L ratio of $5 \cdot 10^{-3}$ kg L⁻¹.

The composition of ACW was based on an estimate of the pore water composition in a hardened cement paste before any degradation of the material had occurred. The ACW contained 0.18M KOH and 0.114M NaOH and had a pH of 13.3. The Ca and Si concentrations in the pore water were fixed by the solubility of the respective C–S–H phase.

After ageing for 2 weeks, the pH of each suspension was measured with a Metrohm 780 pH/ion meter and a Metrohm unitrode pH electrode calibrated with buffers at pH = 7.0 and 13.0. 200 mL of each suspension was centrifuged for 15 minutes at 14'000g(max) on a Beckman L7-35 ultracentrifuge (Beckman, Instruments Inc., Fullerton, USA) and the supernatant was used to dilute the remaining C–S–H suspension to a S:L ratio of $2.5 \cdot 10^{-4}$ kg L⁻¹. An aliquot of each supernatant solution was used for the determination of the concentrations of Ca, Si Na and K using an Applied Research Laboratory ARL 3410D inductively-coupled plasma optical emission spectrometer (ICP-OES). Knowledge of the initial amount of CaO and SiO₂ added to the suspensions, and of the equilibrium Ca and Si concentrations allowed the real C:S ratio of the C–S–H phases to be calculated. Tits et al. (2006) showed that, using the procedure described above, C–S–H suspensions with target C:S ratios above 1.25 in ACW, always contained significant amounts portlandite as impurities. Therefore, in ACW, only C:S ratios below 1.25 were selected for the sorption experiments.

²³⁹Np tracer solutions were obtained by using a procedure described earlier by Sill (Sill, 1966). The separation of this short-lived actinide isotope from its parent ²⁴³Am (Eckert & Ziegler Isotope Products, USA) was achieved by extraction into long-chain amines (tri-iso-octylamine in xylene) followed by back-extraction with Milli-Q water. ²²⁸Th and ²³³U radionuclide solutions were purchased from Eckert & Ziegler Isotope Products, USA.

2.3. Batch sorption experiments

The uptake of the actinides by the cementitious materials was studied by determining the partitioning between solid and liquid phase. Uptake was expressed in terms of a distribution ratio, R_d ($L\ kg^{-1}$), which is the ratio of the amount of radionuclide sorbed ($mol\ kg^{-1}$) and the radionuclide concentration in solution (M). The R_d value was obtained from activity measurements in suspensions and in supernatant solutions using the following equation:

$$R_d = \frac{(A_{susp} - A_{eq}) \cdot V}{A_{eq} \cdot m} \quad (L\ kg^{-1}) \quad (1)$$

A_{susp} is the activity measured in suspension ($Bq\ L^{-1}$), A_{eq} is the activity measured in the supernatant solution ($Bq\ L^{-1}$), V is the sample volume (L) and m is the mass of C–S–H phase in suspension (kg).

C–S–H suspensions with S:L ratios of $2.5 \cdot 10^{-4}\ kg\ L^{-1}$ were prepared in 40 mL centrifuge tubes. To these suspensions, aliquots of radionuclide solutions (^{239}Np , ^{228}Th , ^{233}U) were added. The final radionuclide concentrations were $1.5 \cdot 10^{-10}\ M$, $8.5 \cdot 10^{-9}\ M$ and $1.3 \cdot 10^{-7}\ M$ for ^{239}Np , ^{228}Th and ^{233}U , respectively. The oxidation state of Np in the suspensions was adjusted by the addition of either $5 \cdot 10^{-3}\ M$ Na-dithionite (Np(IV)) or $5 \cdot 10^{-3}\ M$ Na hypochlorite (Np(VI)). In the experiments with Np(V) no redox-controlling agent was used. UV-Vis spectra of samples containing high Np concentrations confirmed that $5 \cdot 10^{-3}\ M$ Na-dithionite and $5 \cdot 10^{-3}\ M$ Na-hypochlorite were able to keep Np in the tetravalent and hexavalent state, respectively (Gaona et al., 2011b; Gaona et al., 2011d). Thus it may be safely assumed that these reducing and oxidising agents are capable of controlling the redox state of the much lower ^{239}Np concentrations in the present experiments. In addition, EXAFS analysis of Np sorbed on C–S–H phases in the presence of the above-mentioned reducing and oxidizing agents confirmed that the +IV, +V and +VI oxidation states were preserved (Gaona et al., 2011a).

The centrifuge tubes filled with the actinide-containing C–S–H and HCP suspensions were shaken end-over-end for three days. After equilibration, 5 mL aliquots of the suspensions were withdrawn and stored for further analysis. Phase separation of the remaining suspensions was carried out by centrifugation (1h at 90'000g (max)). After centrifugation, duplicate 5 mL samples were withdrawn from the supernatant solutions. ^{239}Np , ^{228}Th and ^{233}U activities in the suspensions and in the supernatant were determined together with standards and blanks by liquid scintillation counting (LSC) using a Tri-carbTM 2750A (Perkin Elmer, USA) liquid scintillation analyzer equipped with an alpha-beta discrimination option. Prior to LSC analysis, all 5 mL samples were mixed with 15 mL scintillator liquid (Ultima-Gold AB, Perkin Elmer, USA, in the case of the alpha emitting isotopes and Ultima-Gold XR in the case of ^{239}Np). The ^{228}Th samples were stored for 1 month prior to LSC analysis to allow secular equilibrium between this radioisotope and its daughters to be re-established. The amount of actinide sorbed was obtained by subtracting the activities determined in the suspension and in the supernatant solution from each other, and used along with the activity in solution for calculating the R_d value.

2.4. Experimental uncertainties and the maximum measurable sorption value

R_d values are deduced from activity measurements of the C–S–H suspension and the supernatant solution. The sorption of tetravalent and hexavalent actinides is usually very strong. When the sorption is strong, the activity in the supernatant solution is low and may reach levels close to the detection limit of LSC. This results in large uncertainties. Therefore, a maximum measurable sorption value ($R_{d,max}$) was estimated for the present experiments based upon an acceptable relative uncertainty on the measured activities in the supernatant of 10% at maximum, a total ^{239}Np activity in each experiment of $7 \cdot 10^3$ Bq/mL and a background activity of 0.12 Bq/mL. The procedure for the determination of the $R_{d,max}$ was described in detail elsewhere (Tits et al., 2002). For the present sorption studies with ^{239}Np and C–S–H phases, a value for the $R_{d,max}$ of $5 \cdot 10^8 \text{ L kg}^{-1}$ was obtained.

2.5. Speciation calculations

Thermodynamic speciation calculations were performed using the speciation code “Medusa” (Puigdomenech, 1983) and the PSI thermodynamic database (Hummel et al., 2002).

Results and discussion

3.1 Solution composition

The composition of the solutions in equilibrium with C–S–H phases with different C:S ratios reveal opposite trends in the Ca and Si concentrations: the Ca solubility of the C–S–H phases increases whereas the Si concentration decreases with increasing C:S ratio (Figure 2).

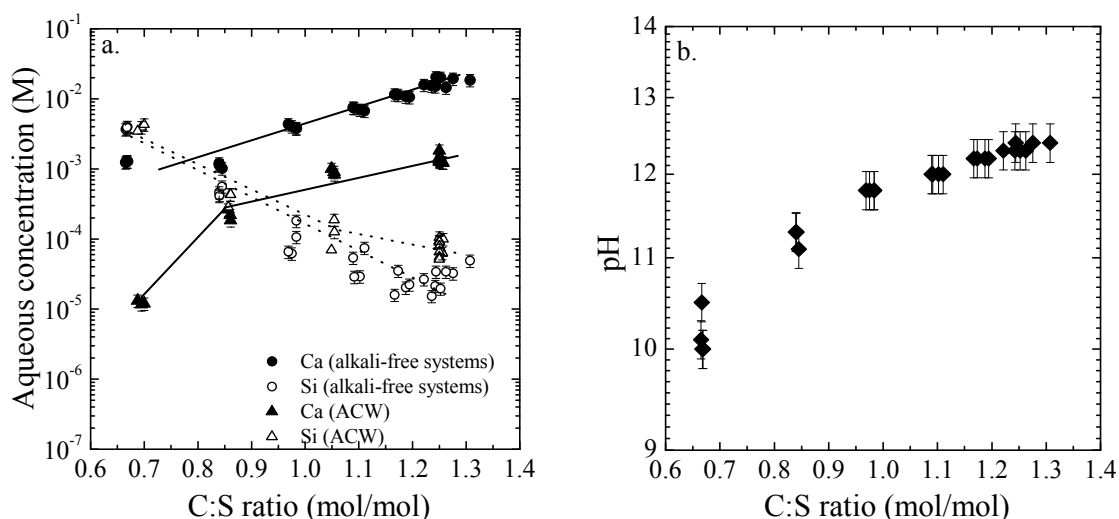


Figure 2: Composition of aqueous solutions in equilibrium with C–S–H phases in alkali-free suspensions and in ACW suspensions: a. Ca and Si concentration. b. pH in alkali-free systems

The pH of the C–S–H suspensions in the absence of alkalis correlates with the C:S ratio of the C–S–H phases and varies between 10.1 and 12.5 (Figure 2b). The Ca solubility of the different C–S–H phases synthesised in ACW at pH 13.3 is approximately a factor 10 lower than the Ca solubility of C–S–H phases with the same C:S ratio in alkali-free systems due to the common ion effect of the hydroxyl groups (Rothstein et al., 2002). In contrast, the Si solubility was found to be similar in both systems.

3.2. Sorption experiments

Sorption tests with Th(IV) on C–S–H phases in the absence and in the presence of Na-dithionite showed that the presence of this reducing agent has no influence on the sorption of tetravalent actinides under alkaline conditions up to a concentration of at least 10^{-2} M (Rojo et al. 2011. In preparation). In a similar way, preliminary test experiments indicate that the presence of $5 \cdot 10^{-3}$ M Na-hypochlorite probably does not have a significant influence on the U(VI) sorption after 3 days equilibration time, but further evidence is still needed. Consequently it is expected that neither Na-dithionite nor Na-hypochlorite will have an influence on the sorption behaviour of Np(IV) and Np(VI) respectively.

Preliminary sorption tests with Np, Th and U showed that the sorption process on C–S–H phases and on hardened cement paste is fast irrespective of the oxidation states, and that sorption equilibrium is always reached within less than three days (data not shown). In Figure 3, R_d values obtained for Np(IV), Np(V), Np(VI), Th(IV) and U(VI) under alkali-free conditions and in ACW are plotted against the C:S ratio. The large scatter in some of the datasets (e.g. Np(IV) and Np(V)) are attributed to incomplete phase separation. Due to strong sorption of the radionuclides onto colloidal materials, incomplete phase separation may result in a large increase in supernatant activity and thus in a significant decrease of R_d values.

The sorption data indicate a very high affinity of Np(IV), Th(IV), Np(V) and U(VI) for C–S–H phases, whereas the affinity of Np(VI) appears to be significantly lower. In spite of this high affinity, the measured R_d values were always well below the $R_{d,max}$ determined for the present sorption experiments with ^{239}Np .

The sorption data in the presence of ACW at a constant pH of 13.3 show that R_d values for Np(IV), Th(IV) and Np(V) are independent of the C:S ratio and therefore of the Ca and Si concentrations (see Figure 2a). Furthermore, a comparison of R_d values for sorption on C–S–H phases with the same C:S ratio under alkali-free conditions and in ACW suggests that the influence of the pH is quite small in the case of Np(IV) and Th(IV). In the case of Np(V), however, significantly higher R_d values were observed in ACW. The R_d values for Np(VI) and U(VI) clearly decreased with increasing C:S ratios in alkali-free systems but they increased in ACW.

3.3 Sorption of tetravalent actinides

The sorption of metal cations is known to be influenced by their aqueous speciation. Surface complexation models often assume that at any pH the predominant aqueous species are involved in the surface complex formation (e.g., Bradbury and Baeyens., 2005; Bradbury and Baeyens, 2009). Thus, with progressing hydrolysis of the metal cation in solution, surface complexation will involve more hydrolysed species. A

constant aqueous speciation with one dominating hydrolysed species, in the pH range under investigation would thus imply that one single hydrolyse species is sorbing. In the case of Np(IV) and Th(IV), thermodynamic speciation calculations indicate that the tetra hydroxo complex is the only species present in solution in the pH range between pH 7 and pH 14. Thus, the constant R_d values observed for Ac(IV) sorption on C–S–H phases in alkali-free systems are in agreement with the constant aqueous speciation in the pH range studied thus supporting the assumption that An(IV) sorption could be controlled by a surface complexation process.

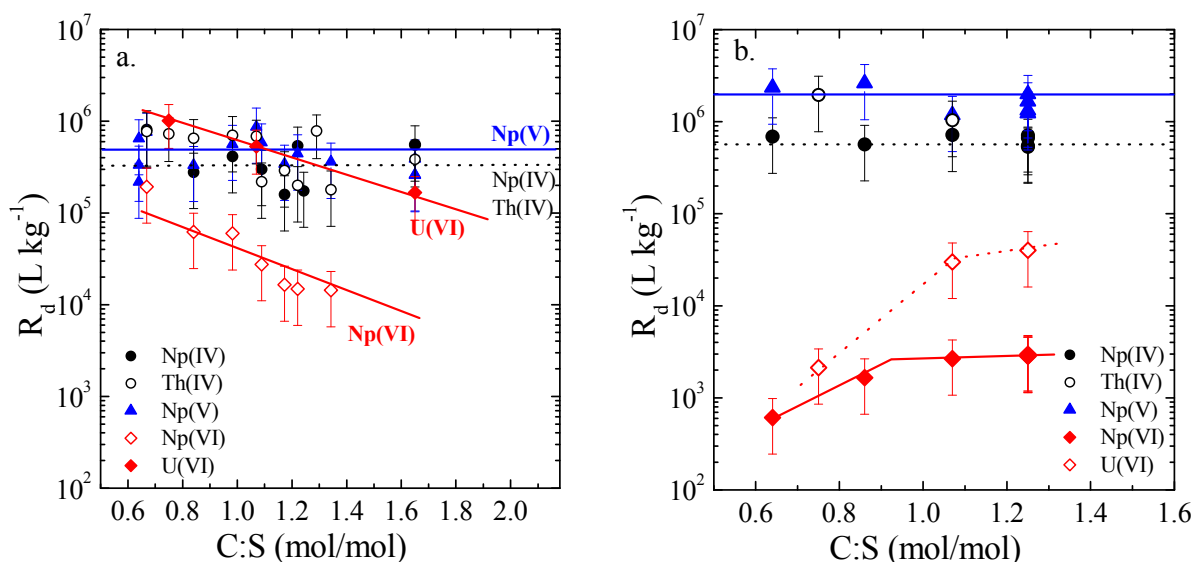


Figure 3: Sorption of Np(IV), Np(V), Np(VI), Th(IV) and U(VI) on C–S–H phases. Effect of the C:S ratio. a) in alkali-free systems. b) in ACW. Lines are added to guide the eye.

EXAFS investigations of Np(IV) sorbed onto C–S–H phases with different C:S ratios and at different pH revealed the presence of 3 to 5 Si atoms at a distance of 3.6 Å from the sorbed

Np atoms (Gaona et al., 2011b). In the case of the formation of a surface complex, the number of Si atoms around the sorbed Np(IV) is expected to be limited to two at maximum (e.g. Sylwester et al., 2000). Only the interlayer can provide a structural environment with three to five Si atoms coordinating to the central U atom. Thus, the higher coordination number for Si is a strong indication that Np(IV) is incorporated in the C–S–H structure, very likely in the interlayer. At higher C:S ratios (> ~1.0) such an incorporation process should take place in combination with the release of interlayer Ca or Na/K (Figure 1b). At low C:S ratios, the negative charge on the silandiol groups of the bridging tetrahedra in the Si tetrahedral chains is compensated by protons and Np(IV) incorporation in the interlayer would result in a release of protons. Hence, the effect of Ca or Na/K on the Np(IV)/Th(IV) sorption is difficult to observe in an experiment where only the C:S ratio is varied due to the action of two exchange reactions, one with protons at low C:S ratio and one with Ca or Na/K at high C:S ratio.

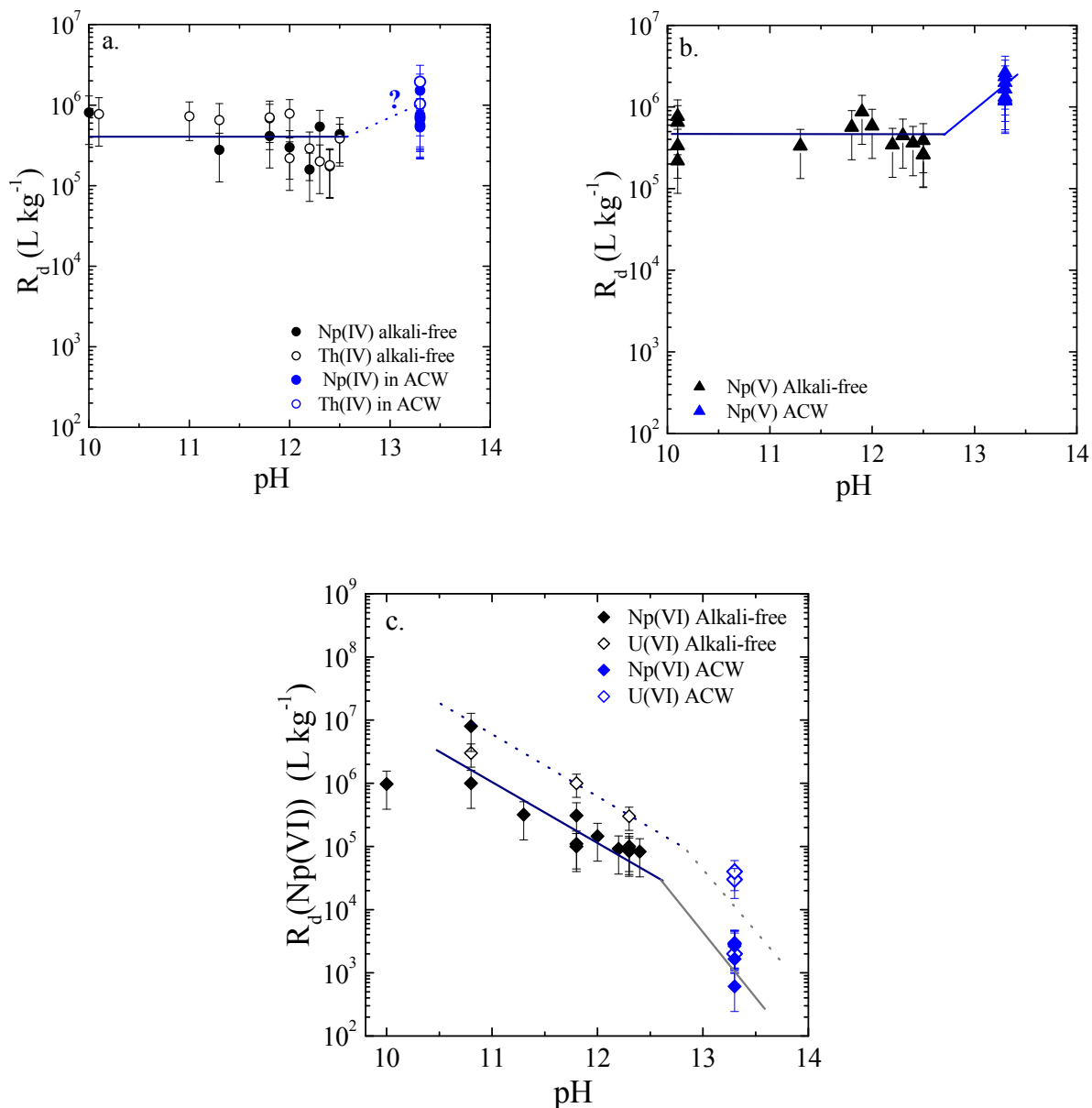


Figure 4: Sorption of a) Np(IV), and Th(IV), b) Np(V) and c) Np(VI) and U(VI) as function of pH. Lines are included to guide the eye.

3.4. Sorption of pentavalent neptunium

The aqueous speciation of Np(V) varies significantly with increasing pH in the range between 10 and 14. Speciation calculations show that at a pH = 10, NpO_2^+ is the dominating species. With increasing pH, NpO_2^+ is progressively hydrolysed to the mono-hydroxy species, NpO_2OH , between pH ~10 and ~11.8, while the negatively charged di-hydroxy species, $\text{NpO}_2(\text{OH})_2^-$, forms above pH ~12.3. Previous investigations of the sorption of cations onto different types of solids at high pH show that the formation of anionic hydroxy species in solution often coincides with a decrease of the R_d values due to a lower affinity of the anionic species for the surface sorption sites (e.g. Barnett et al., 2002; Yamaguchi et al., 2004). The measured R_d values for

Np(V) on C–S–H phases appear to be independent of pH up to a value of 12.5 (Figure 4b), suggesting that, under the assumption of surface complexation, cationic (NpO_2^+), neutral (NpO_2OH) and the negatively charged ($\text{NpO}_2(\text{OH})_2^-$) species have similar affinities for C–S–H. Changes in pH from 12.5 in alkali-free systems to 13.3 in ACW, however, causes an increase of the measured R_d values which is in contradiction with the lower sorption of anionic hydroxyl species observed in the literature. This contradiction suggests that the uptake of Np(V) by C–S–H phases is not controlled by a surface complexation process. The increase in R_d value between pH 12.5 in alkali-free systems (higher aqueous Ca concentrations) and pH 13.3 in ACW (lower aqueous Ca concentrations) might be an indication for an incorporation process in the C–S–H interlayer accompanied by the release of Ca.

3.5. Sorption of hexavalent actinides

The sorption of Np(VI) was found to be a factor 5 to 10 lower compared to the sorption of U(VI) (Figure 4c). Figure 4c further shows the significant reduction of the Np(VI) and U(VI) sorption with increasing pH in contrast to the sorption behaviour of the tetravalent actinides and Np(V). Applying the surface complexation approach and assuming the existence of $\text{NpO}_2(\text{OH})_3^-$ and $\text{NpO}_2(\text{OH})_4^{2-}$ in analogy to the U(VI) speciation under alkaline conditions, this decrease suggests that the sorption constants of the subsequent sorbing hydrolysed species decrease with progressing hydrolysis in solution.

The sorption data in ACW further show that the U(VI) and Np(VI) uptake increases with increasing Ca concentration (increasing C:S ratio) at constant pH (Figure 3b), suggesting simultaneous binding of An(VI) and Ca on the C–S–H phases. Furthermore spectroscopic investigations carried out on C–S–H phases with different U(VI) loadings provide strong evidence for U(VI) incorporation in the C–S–H interlayer (Harfouche et al., 2006; Tits et al., 2011).

Based on the high recrystallisation rates of C–S–H phases (Mandaliev et al., 2009) and information from EXAFS and luminescence spectroscopy investigations, Gaona et al. (2011c) concluded that U(VI) is immobilised by C–S–H phases through a solid solution formation process whereby U(VI) is incorporated in the C–S–H interlayer. The uptake of U(VI) by C–S–H phases with C:S ratios varying between 0.67 and 1.65 was modelled by extending the CSH3T solid solution model developed recently by Kulik (2010) for “pure” C–S–H solubility with three U(VI) end-members. In general terms, the model developed here can be qualitatively described by the mass-balances shown in Table 1. Reactions proposed in the table account for the predominant species of Ca, Si, U(VI)_{aq} , C–S–H end members and C–S–H-U(VI) end-members, and therefore aim at providing a closer overview of the net H^+ , Ca, Si and U(VI) balance taking place in the uptake process.

Table 1 points out the complexity of the system C–S–H-U(VI), and the high degree of coupling among the different parameters participating in the uptake process. Some general trends, though, can be qualitatively highlighted:

Table 1: Reactions of U(VI) uptake by C–S–H phases expected to dominate in the pH range 10 to 12.5 according to the CSH3T-U solid solution model described in (Gaona et al., 2011c).

Conditions	Uptake reaction
low C:S, pH ~ 10	$(\text{CaO})_2(\text{SiO}_2)_3(\text{H}_2\text{O})_5 + \text{UO}_2(\text{OH})_3^- + 0.5\text{H}^+ =$ $(\text{CaO})_2(\text{UO}_3)_1(\text{SiO}_2)_{2.5}(\text{H}_2\text{O})_5 + 0.5\text{SiO}(\text{OH})_3^- + \text{H}_2\text{O}$
C:S ~ 1, pH ~ 12	$(\text{CaO})_{2.5}(\text{SiO}_2)_{2.5}(\text{H}_2\text{O})_5 + 1.5\text{UO}_2(\text{OH})_3^- + 2\text{H}^+ =$ $(\text{CaO})_2(\text{UO}_3)_{1.5}(\text{SiO}_2)_2(\text{H}_2\text{O})_5 + 0.5\text{SiO}(\text{OH})_3^- + 0.5\text{Ca}^{2+} + 2.5\text{H}_2\text{O}$
high C:S, pH ~ 12.5	$(\text{CaO})_3(\text{SiO}_2)_2(\text{H}_2\text{O})_5 + 1.5\text{UO}_2(\text{OH})_4^{2-} + 3\text{H}^+ =$ $(\text{CaO})_3(\text{UO}_3)_{1.5}(\text{SiO}_2)_2(\text{H}_2\text{O})_{5.5} + 4\text{H}_2\text{O}$

The three uptake reactions described in Table 1 involve H^+ as reagents. Hence, the increase of pH should be accompanied by a decrease in the U(VI) taken up by C–S–H.

The content of Ca in C–S–H and C–S–H-U(VI) end-members increases when changing the C:S ratio from low to high values. Taking only this parameter into consideration, sorption is expected to enhance at high C:S ratios. In non-alkali conditions, sorption decreases with increasing pH (increasing C:S ratio) very likely due to the coupling of [Ca] with pH and [Si], which also influence the uptake of U(VI).

For sorption experiments in ACW at increasing C:S ratio, pH is fixed and the effect of Ca can be assessed independently. Here, as predicted by the stoichiometry of the C–S–H and C–S–H-U(VI) end-members, uptake increases with increasing [Ca] (and therefore with increasing C:S).

Based on the chemical analogy between U(VI) and Np(VI) and the comparable sorption behaviour it may be expected that Np(VI) is incorporated in C–S–H phases in a similar way as U(VI).

Due to the similar linear trans-dioxo structures of NpO_2^+ and NpO_2^{2+} , both redox states are expected to have similar coordination environments in the C–S–H structure. Nevertheless, very different trends were observed when comparing Np(V) / Np(VI) uptake at different pH values (Figure 4b, c). The underlying reasons for this different sorption behaviour are still unclear.

Summary and conclusions

The sorption data determined in this study clearly demonstrate that the uptake of tetravalent, pentavalent and hexavalent actinides on C–S–H phases is very strong resulting in R_d values larger than 10^5 L kg^{-1} under alkali-free conditions in the pH range 10 to 12.5.

The sorption behaviour of the tetravalent actinides (Np(IV) and Th(IV)) and the hexavalent actinides (Np(VI) and U(VI)) were found to be very similar, although the absolute R_d values for Np(VI) are lower by a factor 5 to 10 when compared to the U(VI) data. Thus, the oxidation state analogy seems to be valid only in the case of the tetravalent actinides while the analogy is not strictly valid in the case of the hexavalent actinides.

R_d values were found to decrease with increasing concentrations of anionic hydroxyl species formed in solution in the case of An(VI). The uptake of Np(V) by C–S–H phases is an exception: the very high R_d values measured for this pentavalent actinide remained constant in the pH range between 10 and 12.5.

The observed tendencies for the sorption of the tetravalent, pentavalent and hexavalent actinides from the batch sorption experiments along with spectroscopic information suggest that all these actinides are incorporated in the C–S–H interlayer independent of their oxidation state. Such an incorporation process could explain why the correlation between sorption and electrostatic interaction energy, expressed in terms of the Z_{eff}/d ratio, is not valid for uptake processes by C–S–H phases.

Acknowledgements

The research leading to these results has received funding from the European Union's European Atomic Energy Community's (Euratom) Seventh Framework Programme FP7/2007-2011 under grant agreement n° 212287 (RECOSY project). Partial financial support was provided by the National Cooperative for the Disposal of Radioactive waste (Nagra), Switzerland.

References

- Barnett, M.O., Jardine, P.M., Brooks, S.C., (2002). U(VI) Adsorption to Heterogeneous subsurface media: application of a surface complexation model. Environ. Sci. Technol. 36, 937-942.
- Bradbury, M. H. and B., B., (2005). Modelling the sorption of Mn(II), Co(II), Ni(II), Zn(II), Cd(II), Eu(III), Am(III), Sn(IV), Th(IV), Np(V) and U(VI) on montmorillonite: Linear free energy relationships and estimates of surface binding constants for some selected heavy metals and actinides. Geochim. Cosmochim. Acta, 69, 875-892.
- Bradbury, M. H. and Baeyens, B., (2009). Sorption modelling on illite. Part II: Actinide sorption and linear free energy relationships. Geochim. Cosmochim. Acta 73, 1004-1013.
- Chen, J. J., Thomas, J. J., Taylor, H. F. W., and Jennings, H. M., (2004). Solubility and Structure of Calcium Silicate Hydrates. Cem. Concr. Res., 34, 1499-1519.
- Choppin, G. R., (1984). Complexation of pentavalent and hexavalent actinides by fluoride. Radiochim. Acta, 37, 143-146.
- Fanghänel, T. and Neck, V., (2002). Aquatic Chemistry and Solubility Phenomena of Actinide oxides / hydroxides. Pure Appl. Chem., 74, 1895-1907.
- Gaona, X., Dähn, R., Tits, J., Scheinost, A., and Wieland, E., (2011a). Redox chemistry of neptunium in cementitious systems: EXAFS investigations under anoxic to oxidizing conditions. Radiochim. acta, In preparation.
- Gaona, X., Dähn, R., Tits, J., Scheinost, A., and Wieland, E., (2011b). Uptake of Np(IV) by C–S–H phases and cement: an EXAFS study. Environ. Sci. Technol., In preparation.

- Gaona, X., Kulik, D., Macé, N., and Wieland, E., (2011c). Aqueous solid-solution thermodynamic model of U(VI) uptake in C–S–H phases. *Appl. Geochem.*, Submitted.
- Gaona, X., Tits, J., Dardenne, K., Wieland, E., and Altmaier, M., (2011d). XAFS investigations of Np(V/VI) redox speciation in hyperalkaline TMA-OH solutions. In: M. Altmaier, B. K., L.Duro, M. Grivé, V. Montoya (Ed.), 3rd Annual Workshop proceedings of the collaborative project "Redox Phenomena controlling systems" (7th EC FP CP RECOSY), Balaruc-les-Bains, France.
- Harfouche, M., Wieland, E., Dähn, R., Fujita, T., Tits, J., Kunz, D., and Tsukamoto, M., (2006). EXAFS study of U(VI) uptake by calcium silicate hydrates. *J. Colloid Interface Sci.*, 303, 195-204.
- Hummel, W., Berner, U. R., Curti, E., Pearson Jr, F. J., and Thoenen, T., (2002). Nagra-PSI chemical thermodynamic database, version 01/01. Universal Publishers / Upubl.com, New York.
- Kulik, D., (2010). Improving the structural consistency of C–S–H solid asolution thermodynamic models. *Cem. Concr. Res.*, In press.
- Mandaliev, P., Wieland, E., Dähn, R., Tits, J., Churakov, S.V., Zaharko, O. (2009). Mechanisms of Nd(III) uptake by 11Å tobermorite and xonotlite. *Appl. Geochem.*, 25, 763-777.
- Neck, V. and Kim, J. I., (2000). An electrostatic approach for the prediction of actinide complexation constants with inorganic ligands - application to carbonate complexes. *Radiochim. acta.* 88, 815-822.
- Puigdomenech, I., (1983). INPUT-SED-PREDOM : "Computer programs drawing equilibrium diagrams",. Royal Institute of Technology, Stockholm, Sweden.
- Richardson, I. G., (2008). The calcium silicate hydrates. *Cem. Concr. Res.*, 38, 137-158.
- H. Rojo, J. Tits, X. Gaona, M. García-Gutiérrez, T. Missana, E. Wieland. (2011). Experimental investigation of Np(IV) complexation with gluconic acid under alkaline conditions. *Radiochim. acta*, In preparation.
- Rothstein, D., Thomas, J.J., Christensen, B.J., Jennings, H.M., (2002). Solubility behavior of Ca-, S-, Al-, and Si-bearing solid phases in Portland cement pore solutions as a function of hydration time. *Cem. Concr. Res.* 32, 1663-1671.
- Sill, C. W., (1966). Preparation of Neptunium-239 tracer. *Anal. chem.* 38, 802-804.
- Sylwester, E. R., Hudson, E. A., and Allen, P. G., (2000). The structure of uranium(VI) sorption complexes on silica, alumina, and montmorillonite. *Geochim. Cosmochim. Acta*, 64, 2431-2438.
- Tits, J., Bradbury, M. H., Eckert, P., and Schaible, A., (2002). The Uptake of Eu and Th by Calcite under high pH Cement Pore Water Conditions. PSI report Nr. 02-03, Paul Scherrer Institut, Villigen, Switzerland and Nagra Technical Report NTB 02-08, Nagra, Wettingen, Switzerland.
- Tits, J., Wieland, E., Müller, C. J., Landesman, C., and Bradbury, M. H., (2006). Strontium binding by calcium silicate hydrates. *J. Colloid Interface Sci.*, 300, 78-87.
- Tits, J., Geipel, G., Macé, N., Eilzer, M., and Wieland, E., (2011). Determination of uranium(VI) sorbed species in calcium silicate hydrate phases. A laser-induced

luminescence spectroscopy and batch sorption study. J. Colloid Interface Sci., In press (doi:10.1016/j.jcis.2011.03.046.)

Wieland, E. and van Loon, L. R., (2002). Cementitious Near-Field Sorption Data base for performance Assessment of an ILW Repository in Opalinus Clay. PSI Report. Nr. 03-06, Paul Scherrer Institute, Villigen-PSI, Switzerland and Nagra Technical Report NTB 02-20, Nagra, Wettingen, Switzerland.

Yamaguchi, T., Nakayama, S., and Yoshida, T., (2004). Interactions between anionic complex species of actinides and negatively charged mineral surfaces. Radiochim. Acta, 92, 677-682.

ACTINIDE PARTITION IN HUMIC COLLOIDAL TERNARY SYSTEMS: EXPERIMENTS AND PRELIMINARY MODELLING

R. Kay¹, L. Abrahamsen¹[†], A. Stockdale¹, K. Smith¹, N.D. Bryan^{1*}, P. Warwick², N. Evans²

¹ Centre for Radiochemistry Research, School of Chemistry, University of Manchester (U.K.)

² Department of Chemistry, University of Loughborough (U.K.)

* Corresponding author: nick.bryan@manchester.ac.uk

Abstract

The partition of radionuclides between solid and solution phase has been studied in humic/quartz sand ternary systems. Data have been recorded under ambient (air) and inert (O₂ and CO₂ free) atmospheres. For Eu(III) and Th(IV), the systems show simple behaviour, with sorption decreasing (and mobility increasing) in the presence of humic, whilst for uranyl, the behaviour is more complex, with the humic enhancing sorption and reducing mobility. There is also evidence that the sorbed humic has an enhanced affinity for the uranyl, which is probably due to fractionation of the humic. Data have also been obtained for the U(IV) ion. A simple mathematical model has been developed to predict the behaviour of both metal ion and humic acid. The model performs well in predicting the partition of the humic and that of the metal ions in the systems that show simpler ternary behaviour.

Introduction

Over the last 20 years there has been a significant improvement in the understanding of the interactions of humic substances with radionuclides, and models have been developed to describe them. More recently, studies have expanded from the study of more simple (metal ion-humic) binary systems to ternary systems, where natural organic matter, metal ion and mineral phase are all present together. For predicting the movement of radionuclides through the sub-surface, it is essential that this ternary system behaviour be predicted. Unfortunately, these systems are prone to complex behaviour, not least because significant size and chemical fractionation accompanies sorption of humics to mineral surfaces. There are a number of issues that are specific to radionuclides and the requirements of Radiological Performance Assessment (RPA), which is the process by which the containment and impact of a proposed radioactive waste repository are assessed. These extend beyond the problems associated with handling radioactive materials. The actinide elements can show significant redox effects and be prone to hydrolysis. For example, plutonium can exist in a variety of oxidation states: III; IV; V; and VI, and (depending upon the pH and Eh) these multiple oxidation

states can co-exist. Further, their chemistry can make data very difficult to obtain. In particular, the actinide IV oxidation state is hard to study, because these ions are generally sparingly soluble, very prone to hydrolysis and sorption to vessel walls.

Previous work has shown that kinetic effects can be crucial in controlling radionuclide behaviour (Bryan et al 2007). The effects of humics form a very small part of RPA calculations, which are complex and computationally intensive. Therefore, there is a need for very simple mathematical models to describe processes. The aim of this project is to study the partition of radionuclides in humic ternary systems and develop models (suitable for inclusion in RPA calculations) to predict the solid/solution partition. The ultimate objective is to provide a simple model that can predict the behaviour of redox sensitive elements, particularly Pu, and the effect of E_h changes on partition. This paper describes experimental work and initial modelling to simulate single oxidation state systems.

Methods

Commercially available humic acid from the Aldrich Chemical Company (Germany) was used in the experiments. Natural quartz sand (Aldrich) was also used without pre-treatment. All reagents used in the experiments were of analytical grade. Fresh Millipore de-ionized water (18 M Ω) was used in the preparation of all solutions.

Batch experiments were performed at room temperature. Some of these experiments took place under an ambient atmosphere ($p\text{CO}_2 = 10^{-3.5}$ atm and presence of atmospheric O_2), whilst others were performed under ‘inert atmosphere’ conditions. These latter experiments took place in a Perspex glovebox that was flushed with O_2 free N_2 to exclude oxygen. E_h measurements in the box confirmed the absence of O_2 . Also, the N_2 gas was passed through 2 Dreschel bottles with sintered frits containing concentrated NaOH solutions to remove traces of CO_2 . The gas was then passed through a further Dreschel bottle to remove any aerosols of NaOH solution before it entered the glove box.

The solid to solution ratio in all experiments reported here was 500 g·L⁻¹. Known small amounts of metal nitrate (Th(IV), U(VI) and Eu(III)) solution were added to electrolyte solutions (total volume 100 ml) containing humic concentrations in the range 0 – 200 ppm in polypropylene containers. The solutions were adjusted to the required pH by adding appropriate quantities of NaOH or HCl. In all experiments, the ionic strength was maintained using NaClO_4 , added as a small volume of a concentrated stock solution. It was assumed that the contributions of mineral and humic counter-ions to the ionic strength were negligible. The actinide and humic were allowed to equilibrate for 24 hours before known masses of mineral phase were added to the system, and the pH readjusted. The containers were placed in an automatic shaker. At regular intervals, they were removed from the shaker, and the solution phase separated from the solid by double centrifugation (3500 rpm, 5 minutes, twice). 0.5 ml of the supernatant were removed so that the solution metal concentration could be measured. As soon as the sample had been removed from the polypropylene container, the mineral phase was resuspended and the system returned to the shaker. This sampling procedure was repeated over a period of several weeks. For some systems, once (apparent) equilibrium was reached, the supernatant was separated from the mineral phase and replaced with a

fresh electrolyte containing the same concentration of humic. The distribution of metal between solid and solution was then monitored as before with time.

A set of experiments studied the quartz sand/U(IV) system. These experiments used UCl₄ that was prepared from UO₃ by refluxing in hexa-chloropropene for 7 hr at 158 °C. All of these experiments took place in the glovebox, because of the instability of U(IV) in air. In a further set of experiments, the uptake of the humic acid was determined: the procedure was exactly as above, but without any Eu, U or Th present. Uranium and thorium concentrations were measured by Liquid Scintillation Counting (Quantulus) or Inductively Coupled Plasma Mass Spectrometry (ICP-MS). For the Eu experiments, ¹⁵²Eu radio-tracer was added to the systems, so that the solution concentration could be determined by γ-ray spectrometry. Humic acid concentrations were measured using UV-visible spectroscopy (400 nm). In all cases, sorbed amounts were calculated by difference from the known total amounts.

The results of the experiments have been compared with the predictions of a simple ternary system model. In this model, The interaction of metal, M, with the humic (HA) is described using two components, with initial uptake to an exchangeable fraction, M_{exch}, which is assumed to be instantaneous,

$$M_{(soln)} + HA_{exch} \leftrightarrow M_{exch},$$

$$K_{exch} = \frac{[M_{exch}]}{[M_{(soln)}].[HA_{exch}]}$$

where HA_{exch} is the humic exchangeable binding site, and K_{exch} an equilibrium constant for the process. Subsequent transfer to and from the non-exchangeable fraction, M_{non-exch}, is a first-order kinetic (slow) process.

$$M_{exch} \xrightleftharpoons[k_b]{k_f} M_{non-exch},$$

$$\frac{d[M_{non-exch}]}{dt} = k_f[M_{exch}] - k_b[M_{non-exch}]$$

where k_f and k_b are the forward and backward rate constants, respectively. The interaction of metal with the quartz surface is described with a single reaction,

$$M_{(soln)} + S_M \xrightleftharpoons[k_{MSb}]{k_{MSf}} M_S,$$

$$\frac{d[M_S]}{dt} = k_{MSf}[M_{(soln)}].[S_M] - k_{MSb}[M_S]$$

where S_M is a metal binding site on the quartz sand surface, M_S is M sorbed to the surface and k_{MSf} and k_{MSb} are the forward and backward rate constants, respectively. The humic uptake data (discussed later, Figure 1) show evidence of heterogeneity, i.e., either more than one type of HA molecule or surface binding site, or of course, both. The modelling work described here assumes that the surface is the source of the heterogeneity (a companion approach has also been applied that contains HA

heterogeneity, but that is not described here). The model assumes a single type of humic species in solution and two surface sites:

$$\begin{aligned} \text{HA}_{\text{free}} + \text{S}_{\text{HA1}} &\xrightleftharpoons{\quad} \text{HA}_{\text{S1}}, \\ \frac{d[\text{HA}_{\text{S1}}]}{dt} &= k_{\text{HAS1f}}[\text{HA}_{\text{free}}] \cdot [\text{S}_{\text{HA1}}] - k_{\text{HAS1b}}[\text{HA}_{\text{S1}}] \\ \text{HA}_{\text{free}} + \text{S}_{\text{HA2}} &\xrightleftharpoons{\quad} \text{HA}_{\text{S2}}, \\ \frac{d[\text{HA}_{\text{S2}}]}{dt} &= k_{\text{HAS2f}}[\text{HA}_{\text{free}}] \cdot [\text{S}_{\text{HA2}}] - k_{\text{HAS2b}}[\text{HA}_{\text{S2}}] \end{aligned}$$

where: S_{HA1} and S_{HA2} are surface binding sites, type 1 and 2, respectively; HA_{S1} and HA_{S2} are humic bound to surface sites, type 1 and 2, respectively; and k_{HAS1f} , k_{HAS1b} , k_{HAS2f} and k_{HAS2b} are rate constants. Note, $M_{(\text{soln})}$ is the total solution concentration of the metal ion, i.e., the constants involving $M_{(\text{soln})}$ are conditional (k_{MSf} , K_{exch}).

The majority of previous humic ternary system modelling for actinides has been for iron oxides. Therefore, we can compare the model reported here with approaches for these systems. For the interaction of metal ion with the mineral surface, our approach is effectively a kinetic single site Langmuir approach. For iron oxides, a single site approach has been shown to work for Th(IV) (Murphy et al 1999), although 2 sites have been required for uranyl (Waite et al 1994). Previously, sorption of humic to iron oxides has been modelled by treating the humic as a number of discrete heterogeneous ligands (upto 6 fractions have been used) with either equilibrium (Murphy et al 1999) or kinetic (van de Weerd et al 1999) reactions. Our approach is a simplified version of the approach of Van de Weerd et al (1999) using one humic fraction, but two surface sites. There are numerous models of metal ion/humic interactions, but most are too complex for inclusion in RPA calculations (Bryan et al, 2007). Therefore, we have used the 2 fraction (exchangeable and non-exchangeable) model of Bryan et al (2007) that has been shown to simulate the effects of humics during transport. The model includes ternary complexes, mineral surface-humic-radionuclide, i.e., radionuclide bound to humic bound to the mineral. It is assumed that the interaction between metal ion and humic is the same whether the humic molecule is free in solution or bound to the mineral. Murphy et al (1999) have modelled uranyl and thorium behaviour in iron oxide ternary systems and made the same assumption. Their model uses one binding constant for thorium, like our approach, but two for uranyl.

The best fit parameters for the humic sorption data were: $k_{\text{HAS1f}} = 1.4 \times 10^{-6} \text{ ppm}^{-1} \text{ s}^{-1}$; $k_{\text{HAS1b}} = 2.0 \times 10^{-5} \text{ s}^{-1}$; $k_{\text{HAS2f}} = 2.0 \times 10^{-8} \text{ ppm}^{-1} \text{ s}^{-1}$ and $k_{\text{HAS2b}} = 6.0 \times 10^{-7} \text{ s}^{-1}$. Table 1 contains the parameters for the Eu(III) and Th(IV) ternary model fits. All fits were obtained by a process of manual trial and error.

Table 1: Model parameters for the Eu(III) and Th(IV) ternary systems

	$[\text{S}_T] \cdot k_{\text{MSf}}$	k_{MSb}	k_f	k_b	$[\text{HA}_{\text{exch},T}] \cdot K_{\text{exch}}$
Eu(III)	$1.0 \times 10^{-3} \text{ s}^{-1}$	$1.43 \times 10^{-5} \text{ s}^{-1}$	$1.1 \times 10^{-8} \text{ s}^{-1}$	$1.0 \times 10^{-7} \text{ s}^{-1}$	0.99
Th(IV)	$1.0 \times 10^{-5} \text{ s}^{-1}$	$5.0 \times 10^{-6} \text{ s}^{-1}$	$1.1 \times 10^{-8} \text{ s}^{-1}$	$1.0 \times 10^{-7} \text{ s}^{-1}$	0.09

Results and Discussion

Examples of the experimental data that have been produced thus far are shown in the figures. Because of space restrictions it is not possible to show all of the data. Figure 1 shows the uptake of HA onto the sand surface. There are two components to the reaction, an initial, fast component that is relatively fast (sorption complete within 1 day), followed by a second that is slower (sorption takes place over several weeks).

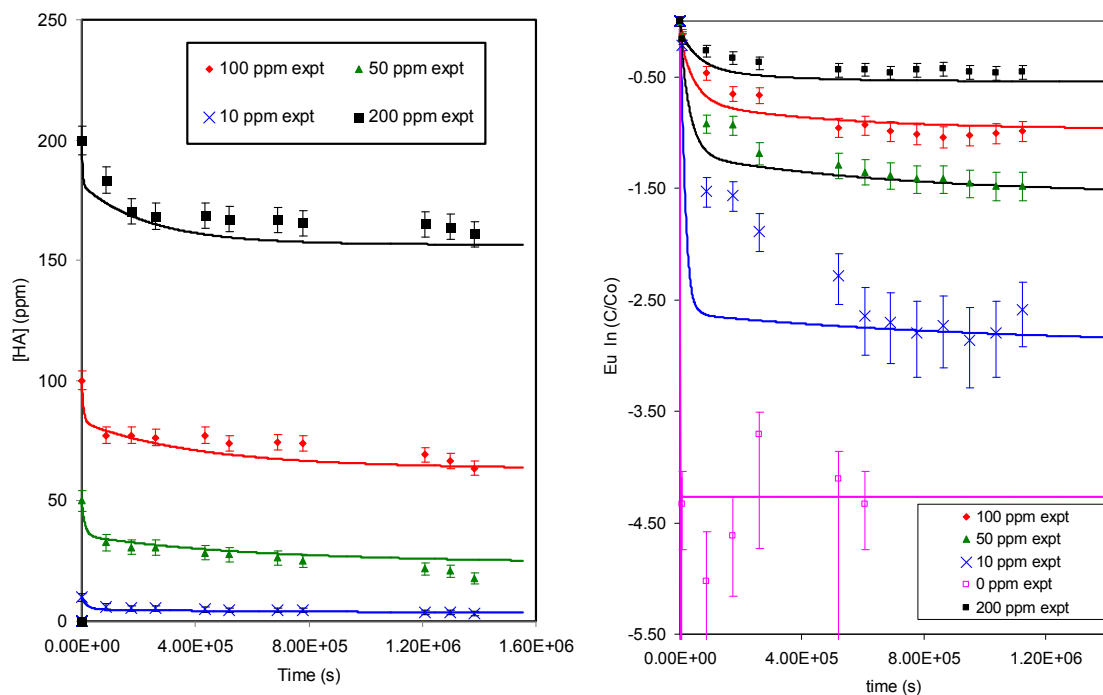


Figure 1 (left): results for binary humic acid/quartz sand system, $I = 0.1$, $pH = 6$, total $[HA] = 10, 50, 100, 200$ ppm: experimental data (points) and model fits (lines). **Figure 2 (right):** results for Eu sorption in ternary humic acid/quartz sand system, $[M_T] = 7.91 \times 10^{-10}$ M, $I = 0.1$, $pH = 6$, in air, as a function of humic acid concentration: experimental data (points) and model fits (lines).

The HA solutions contain a mix of heterogeneous species, all of which are different. Despite this, the simple model with only 2 components produces an adequate fit to the data. It is not perfect of course, but given the gross complexity of the system, the fit is acceptable, particularly remembering the need for mathematical simplicity in RPA speciation models.

Figure 2 shows the uptake of Eu(III) onto the mineral in the presence of HA. The data are plotted as the **natural log** of C/C_0 , where C is the concentration in solution at any point, and C_0 is the concentration of metal in solution before exposure to the mineral surface. Note, all metal data are presented as the **natural log** of C/C_0 . The aim of this work is to develop a model of the actinide ternary system. Eu has been studied first, because it is an f-element, but its chemistry is simpler than many actinide ions (also it is an analogue of Am(III)). The Eu shows fairly simple, 'classical' ternary system behaviour. As the concentration of the humic increases, the amount of Eu sorbed to the

mineral surface decreases. Hence, in this system, the main effect of the humic is to act a competing solution phase ligand, which holds it in solution. The model performs reasonably well: although there are problems with the 10 ppm system over the first week, it can predict the rest of the behaviour reasonably well. Given the complexity of the system, the quality of the fit is encouraging. Figure 3 shows the results of the equivalent experiment for the Th(IV) ‘in air’ system.

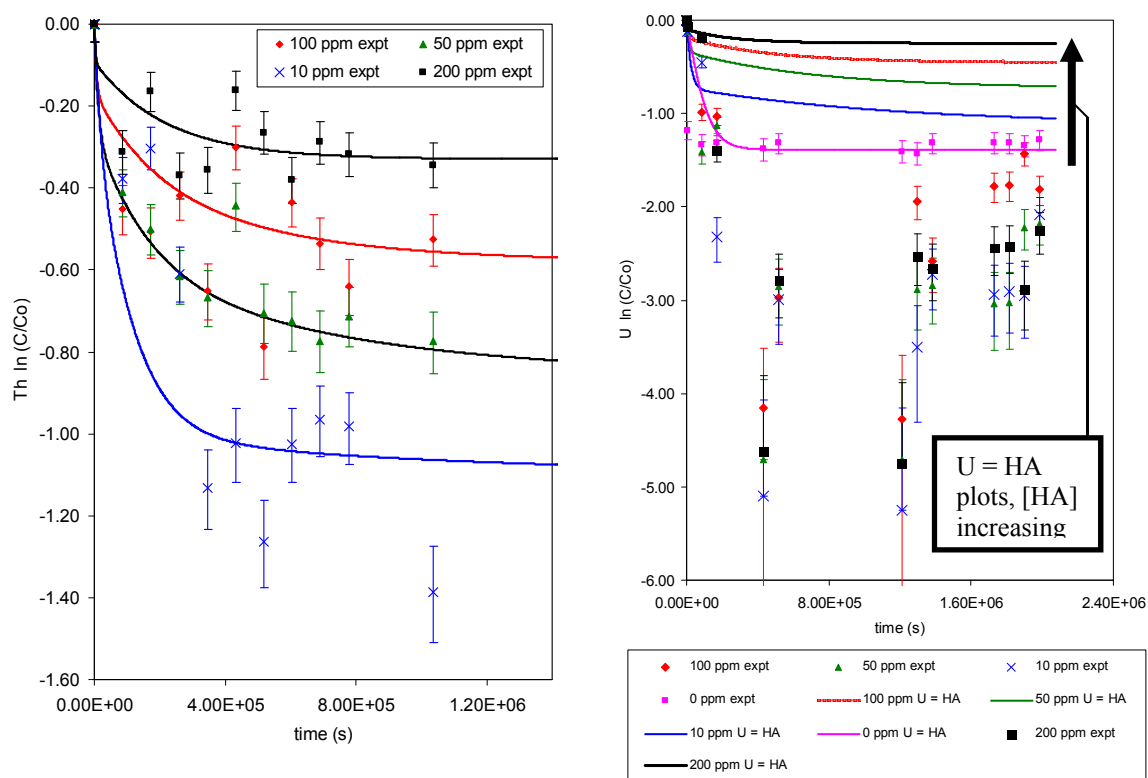


Figure 3 (left): results for Th sorption in ternary humic acid/quartz sand system, $[M_T] = 188 \text{ Bq l}^{-1}$, $I = 0.1$, $\text{pH} = 6$, in air, as a function of humic acid concentration: experimental data (points) and model fits (lines). **Figure 4 (right):** results for UO_2^{2+} sorption in ternary humic acid/quartz sand system, $[M_T] = 100 \text{ Bq l}^{-1}$, $I = 0.1$, $\text{pH} = 6$, in air, as a function of humic acid concentration: experimental data (points) and the behaviour of the U if it followed the humic (lines)

Qualitatively, the behaviours in Figures 2 and 3 are similar in that the Th(IV) is showing simple ternary system behaviour (solution phase Th concentration increasing with [HA]). As for the system in Figure 2, the model is able to simulate the behaviour, although the goodness of fit is harder to judge, because there is much more scatter in the experimental data (due to the greater difficulty in measuring Th). There are quantitative differences: the sorption to the surface is somewhat slower and weaker, as is the apparent binding strength of the metal ion for the humic. At first sight, this might seem surprising, given that we would expect stronger binding by the Th^{4+} ion. However, this is due to the competition with the OH^- and CO_3^{2-} ions (Figures 2 and 3 show data recorded in the presence of air), which both form very strong complexes with Th^{4+} .

Figure 4 shows the results of the analogous experiment for the uranyl system. In this case, the effect of the humic is very different: the presence of the humic actually increases the sorption of uranyl. This can happen in systems where the interaction of the metal ion with the mineral surface is weak compared to that with the humic. In that case, ternary surface complex formation is particularly favourable for the metal and the presence of humic enhances sorption. The situation is more complex than that.

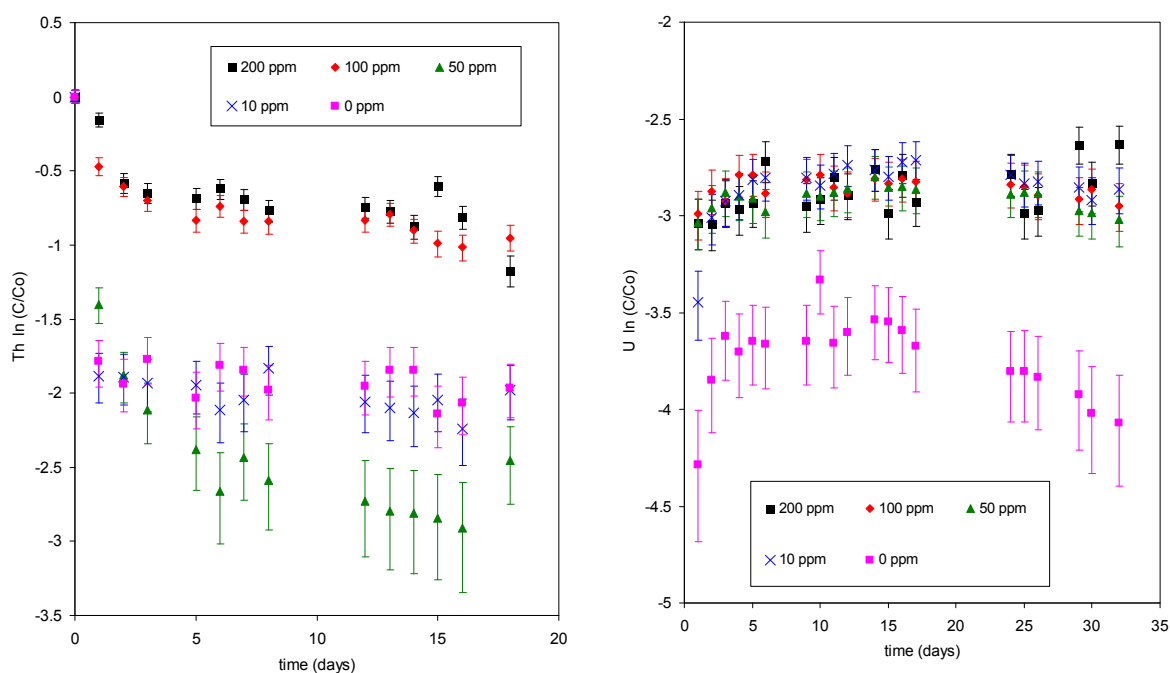


Figure 5(left): results for Th sorption in ternary humic acid/quartz sand system, $[M_T] = 188 \text{ Bq l}^{-1}$, $I = 0.1$, $pH = 6$, in inert atmosphere, as a function of humic acid concentration. **Figure 6 (right):** results for U(IV) sorption in ternary humic acid/quartz sand system, $[M_T] = 50 \text{ Bq l}^{-1}$, $I = 0.1$, $pH = 6$, in inert atmosphere, as a function of humic acid concentration.

In a system where the humic binding strength dominates, if the humic behaves like a simple homogeneous ligand, then the metal ion should ‘follow’ the humic: that is the solid/solution partition of the metal should approach that of the humic. The lines in Figure 4 show the behaviour of the humic (calculated using the model) in this system.

The fact that the solution concentration is depressed in the presence of humic shows that ternary complexes are significant, whilst the difference between the humic partition and that of the uranyl shows that the humic on the surface has different interaction to that in solution (i.e., K_{exch} is different for the sorbed and solution phase material). This is probably due to chemical and/or size fractionation of the humic during sorption, which has been observed previously (Pitois et al 2008).

Note: the data in the subsequent figures have not yet been modelled. Figure 5 shows the sorption of Th(IV) in the absence of air. In this project, it has been essential to develop inert atmosphere techniques, because some actinide ions are oxidized in the presence of air. However, the data show that excluding air can significantly affect the results, even for redox insensitive ions, such as Th^{4+} . The main difference between the Th data in Figures 3 and 5 is that the sorption is stronger in the absence of air, almost certainly due

to the absence of the CO_3^{2-} competing ligand in the Figure 5 system. In the absence of air, the behaviour of the system is intermediate between the simple behaviour of Eu and the more complex sorption of uranyl (high [HA] reduces sorption, but lower [HA] enhances sorption).

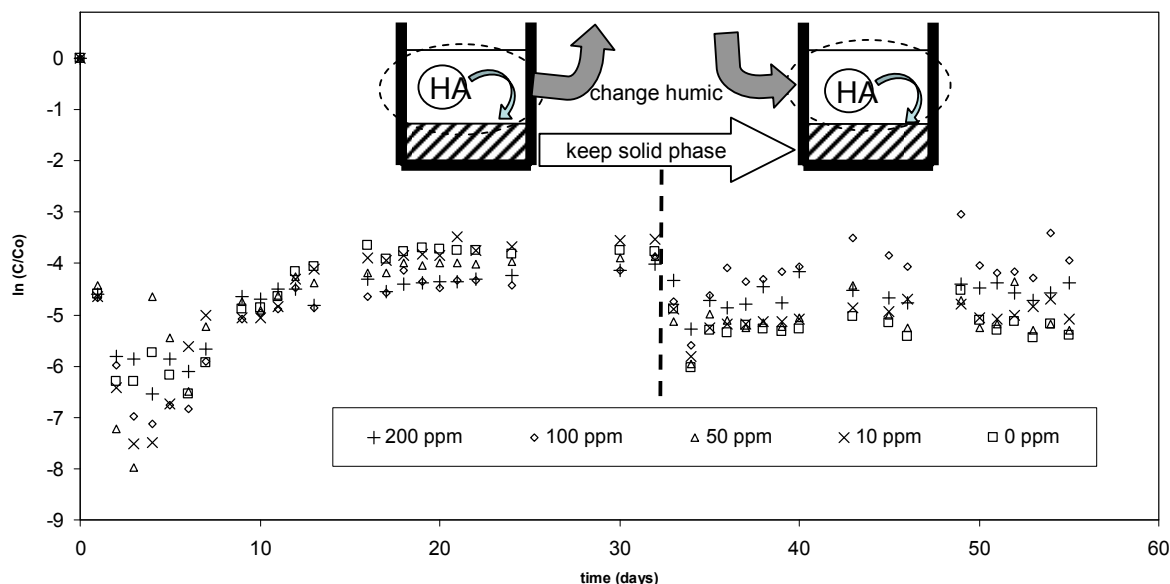


Figure 7: results for U(IV) sorption in ternary humic acid/quartz sand system, $[M_T] = 100 \text{ Bq l}^{-1}$, $I = 0.1$, $\text{pH} = 6$, in inert atmosphere, as a function of humic acid concentration. After 32 days, the supernatant was removed and replaced with fresh HA solution.

The ultimate aim of this project is to provide data for the little studied Pu systems, and particularly for the Pu(IV) ion. In preparation for that, experiments with U(IV) (a Pu(IV) analogue) have been performed. Figure 6 shows a simple uptake experiment for the U(IV) system. In this experiment, the presence of humic does increase the concentration of uranium in solution, but the dependence on humic concentration is complex. Figure 7 shows the result of an experiment where the solution phase was exchanged part way through the experiment. Experiments such as this provide useful information, because at a contaminated site there would be a constant supply of fresh humic, and the experiment simulates that process. They also show how long it takes for the reestablishment of equilibrium after the system has been disturbed and will provide a rigorous test of the model.

Conclusions

Ternary system data have been recorded for a number of metal ions. Eu^{3+} and Th^{4+} show simple ternary system behaviour in that the main role of the humic is to act as a competitor, pulling the metal ion into the solution and so increasing mobility. Conversely, in the uranyl system the behaviour is much more complex, and the humic actually decreases the solution concentration and hence mobility.

Simple ternary system models have been developed that are able to simulate the behaviour of the humic itself very well, as well as the metal sorption in the Eu and Th (in air) systems. However, the data in Figure 4 cannot be simulated with the current approach, which assumes that the interactions of solution phase and sorbed humic with the metal ion are the same. Previous work has shown that uranyl behaviour in iron oxide/humic ternary systems is much more affected by the presence of carbonate than that of Th(IV) (Murphy et al, 1999). Our results suggest this is also the case for sand/humic ternary systems. Murphy et al (1999) also found that it was necessary to include ternary complexes (mineral-humic-radionuclide) to simulate sorption in the presence of humic. Although the surface studied here is different, ternary complexes are essential to explain our results too.

Outlook

The next steps in this project are:

1. Extend the experimental data to the most difficult, but important Pu(IV) system;
2. Attempt to model the data that have not yet been modelled;
3. Adapt the model, so that it can cope with the more complex ternary systems, such as the uranyl data in Figure 4.
4. Apply a model with two humic fractions and one humic surface binding site to the actinide sorption data.

Acknowledgement

The authors would like to thank the United Kingdom EPSRC and NERC for funding this work as part of the DIAMOND and BIGRAD consortia.

References

- Bryan, N.D., Jones, D.L.M., Keepax, R.E., Farrelly, D.H., Abrahamsen, L.G., Warwick, P., Evans, N. (2007). The Role of Humic Non-Exchangeable Binding in the Promotion of Metal Ion Transport in the Environment, *J. Environ. Monit.*, 9, 329-347.
- Murphy, R.J., Lenhart, J.J., Honeyman, B.D. (1999). The sorption of thorium (IV) and uranium (VI) to hematite in the presence of natural organic matter, *Colloids and Surfaces A: Physicochemical and Engineering Aspects*, 157, 47–62.
- Pitois, A., Abrahamsen, L.G., Ivanov, P.I., Bryan, N.D. (2008). Humic acid sorption onto a quartz sand surface: A kinetic study and insight into fractionation, *Journal Of Colloid And Interface Science*, 325, 93 – 100.
- Waite, T.D., Davis, J.A., Payne, T.E., Waychunas, G.A., Xu, N. (1994). Uranium(VI) Adsorption To Ferrihydrite - Application Of A Surface Complexation Model, *Geochimica Cosmochimica Acta*, 58, 5465.
- Van de Weerd, H., Riemsdijk, W.H.V., Leijnse, A. (1999). Modeling the dynamic adsorption desorption of a NOM mixture: Effects of physical and chemical heterogeneity. *Environmental Science and Technology*, 33, 1675 - 1681.

BEHAVIOUR OF Tc (VII) IN AQUEOUS SOLUTIONS IN THE PRESENCE OF IRON OXIDES AND MICROORGANISMS

¹R.Druteikienė, ¹B.Lukšienė, ²D.Pečiulytė, ¹K.Mažeika, ¹A.Gudelis, ¹D.Baltrūnas

¹ Center for Physical Sciences and Technology, Vilnius, Lithuania

² Institute of Botany of Nature Research Center, Vilnius, Lithuania

* Corresponding author: dalis@ar.fi.lt

Abstract

This study investigates the redox behaviour of Tc(VII) in a heterogeneous system containing well-defined amounts of hematite and magnetite with emphasis on transformation of oxidation state through microbial-mediated processes under oxic conditions. A set of experiments was performed to determine the factors (pH, incubation time) that influenced TcO_4^- reduction, and sorption onto iron oxides, and to explore the effect of microbial activity on the variation of solubility of technetium. Gradual sorption of technetium, added as TcO_4^- , in aquatic solution onto $\text{FeO/Fe}_3\text{O}_4$ mineral under aerobic conditions was observed. Under alkaline and acidic conditions no pronounced effect of sorption of technetium onto hematite (Fe_2O_3) was determined. Mineral hematite at neutral or slightly alkaline pH under aerobic conditions is attributed to minerals which do not sorb Tc (VII). Sorption of Tc (VII) onto hematite is achieved because of the presence of specific microorganisms.

Introduction

Technetium-99 is relevant in geochemical systems of both intermediate and high-level nuclear waste repositories, it is present in aquifers, marine environment and rivers (Burke et al., 2006; Frederickson et al., 2004; Keith-Roach et al., 2003; Standring et al., 2002). ^{99}Tc (half-life 2.1×10^5 years) is originated with a 6% yield from the fission of ^{235}U (Maset et al., 2006). Technetium is a redox active radionuclide and its migration behaviour primarily depends on its oxidation state, either +IV or +VII. Under oxic conditions technetium forms the highly soluble TcO_4^- ion, which is weakly sorbed onto mineral surfaces. However, the reducing conditions of geochemical surroundings can bring about an alteration of technetium oxidation state. In anoxic surroundings the pertechnetate anion TcO_4^- is reduced to the lower valence form of Tc(IV) which because of hydrolysis forms the insoluble solid phase and sorbs to mineral phases or organic fractions of the environment (Maes et al., 2004; Burke et al., 2005). The chemical and redox behaviour of technetium in different systems has been investigated in numerous studies, for example in natural sediments containing sediment-associated Fe(III) and Mn(III/IV) oxide and metal-reducing bacteria (Frederickson et al., 2004),

organic co-contaminants (Maset et al., 2006), or dissolved iron and iron minerals (Peretyazhko et al., 2008). Reduction of TcO_4^- under iron- and nitrate-reducing conditions as well as sulfide-reducing conditions has been observed (Wharton, 2000; Istok, 2004; Burke, 2005). The dissimilatory reduction of Tc(VII) by microorganisms in neutral, acidic and alkaline environments is extensively studied (Lloyd et al., 1997; 1999; 2000; Wildung, 2000; Lyalikova et al., 1996). The biotransformation of redox sensitive radionuclides is complex and achieved by the direct enzymatic interaction at the metal/microorganism interface or by abiotic reaction with microbial reduction products (Mohapatra et al., 2010; Law et al., 2010).

In summary, the potential either of migration or retention of Tc at contaminated sites and also from the waste repository depends on the Tc geochemical behaviour determined by its chemical speciation. The geochemical and physical characteristics of the environment (mineralogy, pH, complexing agents, redox conditions) and microbial activity play an important role in technetium behaviour in various environmental systems.

The goal of the present study is to investigate the redox behaviour of Tc(VII) in the heterogeneous system containing well-defined amounts of hematite and magnetite with emphasis on transformation of oxidation state through microbial mediated processes under oxic conditions. A set of experiments was performed to determine the factors (pH, incubation time) that influenced TcO_4^- reduction, and sorption onto iron oxides, and to explore the effect of microbial activity on the variation of solubility of technetium.

Experimental

Materials and methods

Microorganisms

Microorganisms, bacteria and fungi, were isolated from groundwater of two different boreholes and from soil of known physical-chemical properties. They were tested under different conditions and only some strains were screened according to their peculiarities: ability to reduce nitrate, H_2S formation, organic acid production and resistance to different pH values. Microorganisms *Streptomyces* sp., *Aspergillus niger*, *Bacillus mycoides*, *Penicillium* sp., *Rhodococcus* sp., *Spicaria* sp. and bacterium No.1 were isolated from groundwater and identified. Microorganisms *Arthrobacter globiformis*, *Cellulomonas cellulans*, *Fusarium oxysporum* were isolated from waterlogged soil.

Measurements

The composition of two powdered iron oxides was verified using Mössbauer spectroscopy. One of them showed properties characteristic of hematite (Fe_2O_3). The Mössbauer spectra of another powdered mineral consisted of two sextets and two singlets that correspond to the mixture of magnetite with wustite ($\text{Fe}_3\text{O}_4/\text{FeO}$). The relative area of $\text{Fe}_3\text{O}_4/\text{FeO}=61\%/39\%$ and calculations have approximately shown the ratio Fe (II)/Fe (III) to be 50%/50%.

Technetium-99 was measured by the liquid scintillation counting (LSC) method. An ultra low-level LSC counter Quantulus-1220 was used. For Tc-99 activity measurement, 4 ml of the original sample was mixed with 16 ml of the liquid scintillation cocktail OptiPhase HiSafe 3. For counting window optimization, the quenching curve construction and the efficiency calibration the reference standard solution of technetium-99 (overall uncertainty 1.4%) in the form of ammonium pertechnetate in 0.1 M ammonium hydroxide supplied by the National Physical Laboratory (UK) was used. The beta-particles emitted by Tc-99 were counted in the window [100-650] channels, while the counting efficiency for slightly quenched samples was around 90%. The quenching correction was applied for each sample using the external standard techniques.

The pH_i measurements were performed using a WTW pH-meter pH 315i with combined pH electrodes calibrated against standard buffers (pH4, pH7, HANNA) with a measurement error of ± 0.01 pH unit.

Procedure

For the tests (sorption studies) under ambient conditions, mineral suspensions in the 1:25 (solid:solution) ratio in deionized water were prepared. Ammonium pertechnetate with initial Tc(VII) concentrations of $[Tc(VII)] = 3.5 \times 10^{-6} M$ was added, and the pH in determined stages were measured. Investigations of the time-dependent Tc(VII) behaviour in the presence of both hematite (Fe_2O_3) and wustite/magnetite (FeO/Fe_3O_4) were performed. All sorption experiments were carried out within 48 – 360 hours.

For the tests of ability of microorganisms to participate in the Fe (III)/Tc(VII) reduction process, the suspensions of both iron oxides and each type of microorganisms in the estimated amount of 0.08 M NaCl solution were prepared and ammonium pertechnetate with the initial Tc(VII) concentrations of $[Tc(VII)] = 1.8 \times 10^{-6} M$ or $[Tc(VII)] = 8.8 \times 10^{-7} M$ was added.

All experiments were conducted in triplicate.

Batch experiments

The tests of TcO_4^- reduction and sorption onto iron oxides were performed under ambient conditions. The iron oxide (Fe_2O_3 and Fe_3O_4/FeO) powder suspensions were prepared by adding 2 g of iron oxide powder into 100 ml flasks containing 50 ml of deionized water. The suspensions were well shaken and 400 μL of technetium ($3.5 \times 10^{-6} M$), prepared from stock solution, was added. The pH value was monitored, and the suspensions were thoroughly stirred, corked up, and allowed to stand at room temperature. At the fixed intervals 4-ml of samples were taken from the solution and filtered through 0.45 μm filters before ^{99}Tc measurement. The tests continued until the residual Tc concentration in the aqueous phase became $< 1\%$ of the initial concentration.

For investigation of the microbial-mediated processes the microorganism cells were separated from growing media by centrifugation, washed thoroughly with deionized water and 0.08 M NaCl, and then they were resuspended in 0.08 M NaCl solution. The $1.8 \times 10^{-6} M$ Tc(VII) solution was prepared using ^{99}Tc stock solution. 0.1g of the iron oxide powder was resuspended in 5-10ml of 0.08 M NaCl solution, pH of solution was adjusted to the value 7 either with HCl or with NH_4OH , and suspensions of each type of

microorganisms (1.0-1.7 g of biomass) were added. The suspensions of hematite and microorganisms were pre-conditioned at 30 °C without shaking for 3 days prior to the addition of Tc(VII). Then technetium was added and the flasks were kept at room temperature (~24°C) for 48, 72 and 168 hours. Prior to Tc analysis, the solution was filtered through 0.45µm filters to remove bacteria cells.

Results

Gradual sorption of technetium, added as Tc(VII)O_4^- , in aquatic solution onto $\text{FeO/Fe}_3\text{O}_4$ mineral under aerobic conditions was observed. Preliminary results of the combined effect of microorganisms and iron-bearing minerals on Tc (VII) sorption peculiarities using batch-type experiments have been obtained.

Adsorption of Tc(VII) on wustite/magnetite ($\text{Fe}_3\text{O}_4/\text{FeO}$) as a function of contact time is shown in Fig.1. The results showed that under alkaline conditions (pH 8-9) after a short exposure period (48 hours) more than 75% of TcO_4^- was associated with $\text{FeO/Fe}_3\text{O}_4$ particles and removed from solution. During the period of 360 hours < 1% of Tc(VII) remained in solution. It can be seen that adsorption of technetium on wustite/magnetite in alkaline solution is sufficiently rapid and 360 hours are enough to remove it from solution.

Under these circumstances no pronounced effect of sorption of technetium onto hematite (Fe_2O_3) was determined. Within the first 48 hours 99% of TcO_4^- remained in solution. After 144 hours of exposure negligible decreasing to 97% of Tc(VII) concentration in solution was obtained. The amount of Tc(VII) in solution remained almost unaltered during all 360 hours of exposure.

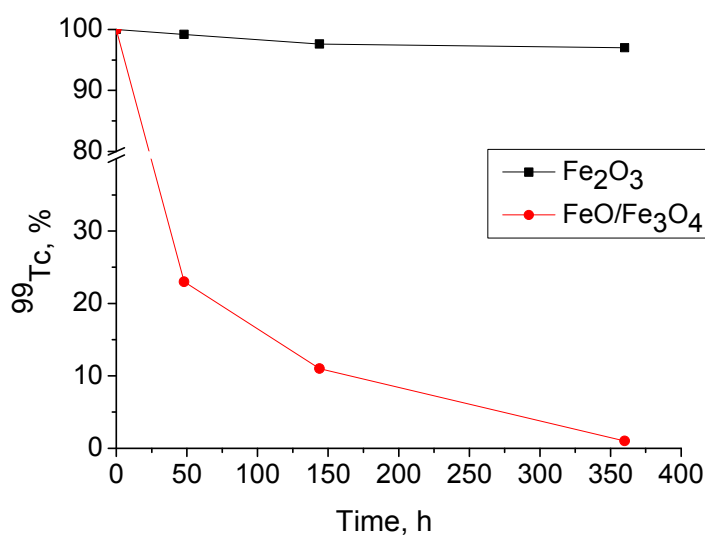


Figure 1. Sorption of Tc(VII) onto iron oxides as a function of contact time

Ferrous iron (Fe(II)) can be a strong reductant of Tc(VII) when in the sorbed or mineral state (Peretyazhko et al, 2008). Furthermore, the reactivity of Fe(II) toward Tc(VII)O_4^- is pH dependent and related to the chemical forms of iron – Fe-bearing minerals, mineral surface complexes, etc. In non-complexing aqueous solution, under reducing conditions TcO_4^- undergoes stage-by-stage one-, two- or three-electron reductions

leading to the formation of different aqueous species of technetium (TcO^{2+} , $\text{TcO}(\text{OH})^+$, $\text{TcO}_{2(\text{s})}$, TcO_4^-) (Heller-Grossman, 1981; Warwick, 2007). A recent study showed that the presence of biogenic Fe(II) in aqueous solution (pH 8-9) can affect the reduction of Tc(VII) to Tc(IV). The results of batch experiment suggest that the removal of Tc from solution may be controlled by reduction of Tc(VII) to Tc(IV) by Fe(II), whether it is associated with minerals. It can be seen that adsorption of technetium on FeO/Fe₃O₄ is rapid, which indicates that chemical adsorption rather than physical adsorption contributes to Tc(IV) adsorption on wustite/magnetite. According to our previous determination (unpublished data) the pH_{pzc} of wustite/magnetite is ~ 7 , which indicates that the surface charge is negative below pH 7. Whereas, as mentioned above, in non-complexing aqueous solution under reducing conditions aqueous species of technetium are positively charged (Heller-Grossman, 1981), they are easily adsorbed on the negatively charged surface of minerals.

Mössbauer spectra (Figure 2) indicate the presence of hematite (Fe₂O₃) in the first sample and wustite and magnetite in the second sample. For wustite, Fe(II) and Fe(III) components of Mössbauer spectra in the ratio 18:82 are detected in agreement with wustite formula Fe_{1-x}O. Two subspectra which are attributed to tetrahedral and octahedral sublattices are characteristic of magnetite. The ratio of area of magnetite subspectra is 45:55, tetrahedral sublattice of magnetite is occupied by Fe(III) ions, while octahedral sublattice is occupied by Fe(II)+Fe(III) ions. Thus, Fe(II) may be found either in magnetite or wustite. After treatment small changes in composition are detected only for the second sample (FeO/Fe₃O₄).

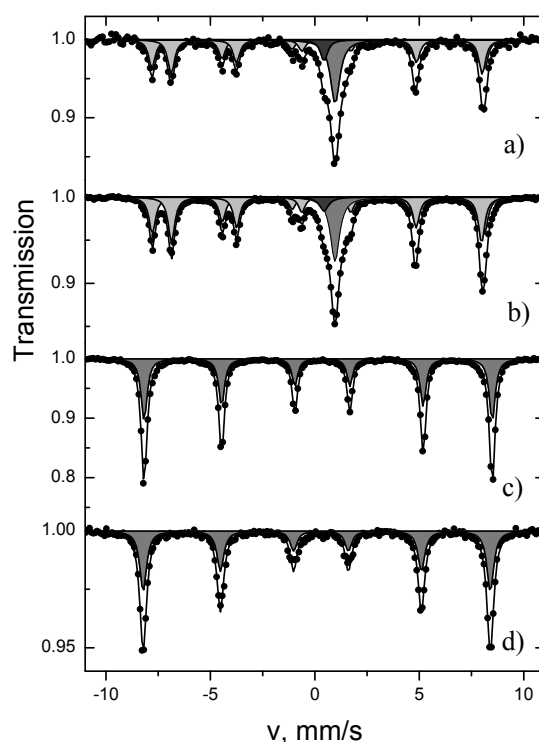


Figure 2. Mössbauer spectra of wustite/magnetite (a, b) and hematite samples (c, d) before (a, c) and after treatment (b, d)

The investigation of technetium reduction and sorption onto hematite (Fe_2O_3) under the acidic (pH 3-5) and neutral (pH 6-7) conditions (Fig. 3) suggested that pH of solution had a very slight influence on the technetium sorption. The experiment with the hematite suspension at pH 6.3 revealed no reduction of Tc either during 48 or 456 hours, the major amount ($\sim 98\%$) of Tc remained as truly soluble Tc(VII). Inconsiderable effect of the Tc(VII) reduction was obtained in solution at pH 2.7 and 4.5 within 48 hours.

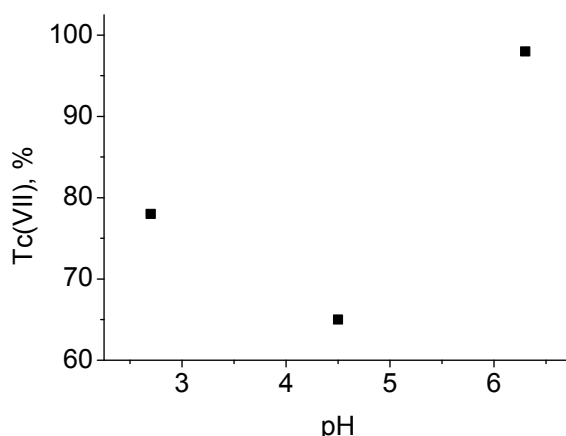


Figure 3 The amount of Tc(VII) remained in solution after 48 hours of exposure

The amount of Tc(VII) in solution at pH 2.7 and 4.5 remained 78% and 65%, respectively. Thereafter, the Tc(VII) concentration in solution remained constant for further 456 hours.

The fate of pertechnetate during bioreduction was investigated in the presence of Fe(III) associated with hematite and microorganisms isolated from groundwater and water-logged soil. The tests under ambient conditions were performed. The duration of the experiments was from 72 to 144 hours. The pH of experimental systems was increased from the initial value 6.5 to the value 7-9 after adding microorganisms. The percentage of residual Tc(VII) in solution after 144 hours of exposure is presented in Table 1.

Table 1. The percentage of residual Tc(VII) in solution

Microorganism		Tc in solution, %
Soil	<i>Arthrobacter globiformis</i>	78
	<i>Cellulomonas cellulans</i>	98
	<i>Fusarium oxysporum</i>	15
Groundwater	<i>Aspergillus niger</i>	82
	Bacterium No1	49
	<i>Bacillus mycoides</i>	46
	<i>Streptomyces</i> sp.	29
	<i>Penicillium</i> sp.	24
	<i>Rhodococcus</i> sp.	18
	<i>Spicaria</i> sp.	98

Results of the combined effect of microorganisms and iron-bearing minerals on Tc (VII) sorption peculiarities using batch-type experiments have shown that bacteria *Cellulomonas cellulans* isolated from water-logged soil practically did not have any influence on Tc (VII) sorption onto hematite under aerobic conditions. After exposure of Tc(VII) for 144 hours in the presence of such microorganisms 98% of Tc remained in solution. The amount of Tc(VII) remaining in the experimental system exhibited a tenuous ability of studied microorganisms to influence the sorption of technetium onto hematite. Micromicete *Fusarium oxysporum* of the same substrate altered sorption to approximately 85% compared to that in the system without microorganisms.

Differences in Tc (VII) sorption processes onto hematite due to microbial activity of microorganisms isolated from the groundwater borehole were observed as well. The presence of microorganisms *Penicillium* sp., *Rhodococcus* sp and *Streptomyces* sp. in the tested system induced Tc (VII) sorption onto hematite up to 71-82%. After interaction of Tc with microorganisms *Penicillium* sp., *Rhodococcus* sp and *Streptomyces* sp. 24, 18 and 29% of Tc, respectively, remained in solution. The effect of microbial activity of *Bacillus mycoides*, *Aspergillus niger* on Tc (VII) sorption onto hematite was less, 54% and 18%, respectively. Micromicete *Spicaria* sp. practically had no influence on the sorption of Tc onto hematite, approximately 98% of Tc remained in solution. Thus, we can state that mineral hematite at neutral or slightly alkaline pH under aerobic conditions is attributed to minerals which do not sorb Tc (VII). Sorption of Tc (VII) onto hematite is achieved because of the presence of specific microorganisms.

We believe that the mechanism of Tc accumulation in the biosystem is reduction of the Tc(VII) brought about by microbial activity, followed by sorption of reduced species on mineral surface. Our previous studies of the interaction of aerobic fungi and bacteria with Pu (IV) (Druteikienė et al, 2010) have shown a weak ability of bacterium *Bacillus mycoides* to accumulate Pu (IV) and its possibilities to alter Pu oxidation state and enhance its environmental mobility. Therefore, we are making the assumption that tested microorganisms could bring about the reduction of Fe and Tc. However, the process of uptake of Tc by the cells of microorganisms can take place. Additional experiments in studying abilities of soil microorganisms to participate in technetium mobility processes by accumulating them are underway.

Conclusions

From the results of the study of the redox behaviour of Tc(VII) in the heterogeneous system with Fe-bearing minerals in the presence of microorganisms under oxic conditions, the following conclusions can be drawn:

1. Fe(II) associated with wustite/magnetite is reactive toward Tc(VII). The presence of biogenic Fe(II) in non-complexing aqueous solution (pH 8-9) under oxic conditions can affect the reduction of Tc(VII) to Tc(IV). The chemical adsorption of aqueous species of reduced Tc on wustite/magnetite particles is likely to be dominating.
2. Fe(III) associated with hematite did not affect the reduction of Tc(VII) to Tc(IV) under alkaline conditions. The low pH (2.7-4.5) enhances Tc(VII) adsorption on hematite, which suggests that the process is dependent on pH.

3. We suggest that sorption of Tc (VII) onto hematite is achieved because of the presence of specific microorganisms. With considerations in mind, whether the presence of microorganisms affects the reduction of Tc(VII) to Tc(IV) or the uptake of technetium in the biomass took place here, investigations will be undertaken.

Acknowledgements

The research leading to these results has received funding from the European Atomic Energy Community' Seventh Framework Programme (FP7/2007-2011) under grant agreement n° FP7-212287 and from the Agency for Science, Innovation and Technology in Lithuania under grant agreement n° 31V-6

References

- Burke I.T., Boothman C., Lloyd J.R., Livens F.R., Charnok J.M., Mcbeth J.M., Mortimer R.J.G., and Morris K. (2006). Reoxidation behaviour of technetium, iron, and sulfur in estuarine sediments. *Environ. Sci. Technol.* 40, 3529-3635
- Burke I.T., Mortimer R.J.G., Boothman C., Lloyd J.R., Livens F.R., Morris K. (2005) Effects on progressive anoxia on the solubility of technetium in sediments. *Environ. Sci. Technol.*, 39, 4109-4119.
- Druteikienė R., Lukšienė B., Pečiulytė D., Baltrūnas D., (2010) Interaction of biomass of aerobic bacteria and fungi with Pu(IV) at low pH, *J Radioanal Nucl Chem*, 286, 387–391
- Frederickson J.K., Zachara J.M., Kennedy D.W., Kukadapu R.K., McKinley J.P., Heald S.M., Liu C., Plymale A.E. (2004). Reduction of TcO_4^- by sediment associated Fe(II). *Geochim. Cosmochim. Acta*, 68, 3171-3187
- Heller-Grossman L., Abrashkin S., Shafferman A., Davis M., Taube R., (1981) Tc-99m generators. Physico-chemical factors in the radiolytic reduction of pertechnetate, *App.Rad.Iso*, 32, 501-506.
- Istok, J.D., Senko J.M., Krumholz L.R., Watson D., Bogle M.A., Peacock A., Chang Y.J., (2004) In situ bioreduction of technetium and uranium in nitrate-contaminated aquifer. *Environ. Sci. Technol.*, 38, 468-475.
- Keith-Roach M.J., Morris K., Dahlgaard H. (2003) An investigation into technetium binnding in sediments. *Mar.Chem.* 81, 149-162
- Law G.T.W., Geissler A., Lloyd J.R., Livens F.R., Boothman C., Begg J.D.C., Denecke M.A., Rothe J., Dardenne K., Burke I.T., Charnock J.M., Morris K., (2010) Geomicrobial redoxs cycling of the transuranic element neptunium. *Environ. Sci. Technol.* 44, 8924-8929.
- Lloyd J.R., Cole J.A., Macaskie L.E., (1997) Reduction and removal of heptavalent technetium from solution by *Escherichia coli*. *J. of Bacteriology*, 179, 2014-2021.
- Lloyd J.R., Ridley J., Khizhnyak T., Lyalikova N.N., Macaskie L.E., (1999) Reduction of technetium by *Desulfovibrio desulfuricans*: biocatalyst charakterization and use in a flowthrough bioreactors. *Appl. Environ. Microbiol.* 65, 2691-2696.

- Lloyd J.R., Sole V.A., Van Praagh C.V.G., Lovely D.R., (2000) Direct and Fe(II) – mediated reduction of technetium by the Fe(III)- reducing bacteria. Appl. Environ. Microbiol., 66, 3743-3749.
- Lyalikova N.N., Khizhnyak T., (1996) Reduction of heptavalent technetium by acidophilic bacteria of the genus *Thiobactillus*. Microbiologia, 65, 468-473.
- Maset E.R., Sidhu S.H., Fisher A., Heydon A., Worsfold P.J., Cartwright A.J., and Keith-Roach M.J., (2006) Effect of organic co-contaminants on technetium and rhenium speciation and solubility under reducing conditions. Environ. Sci. Technol. 40 5472-5477.
- Maes A., Geraedts K., Bruggeman C., Vanchuysen J., Rossberg A., Henning C., (2004) Evidence for the interaction of technetium colloids with humic substances by X-ray absorption spectroscopy. Environ. Sci. Technol., 38, 2044-2051.
- Mohapatra B.R., Dinardo O., Gould W.D., Koren D.W., (2010) Biochemical and genomic facets on the dissimilatory reduction of radionuclides by microorganisms – A review, Minerals Engineering, 23, 591-599.
- Peretyazhko T., Zachara J.M., Heald S.M., Jeon B.-H., Kukadapu R.K., Liu C., Moore D., Resch C.T., (2008) Heterogeneous reduction of Tc(VII) by Fe(II) at the solid-water interface. Geochim. Cosmochim. Acta, 72, 1521-1539.
- Standring W.J.F., Oughton D.H., Salbu B., (2002) Potential remobilization of ¹³⁷Cs, ⁶⁰Co, ⁹⁹Tc, and ⁹⁰Sr from contaminated Mayak sediments in river and estuary environments. Environ. Sci. Technol. 36, 2330-2337.
- Warwick P., Aldridge S., Evans N., Vines S., (2007) The solubility of technetium (IV) at high pH, Radiochim. Acta, 95, 709-716.
- Wharton M.J., Atkins B., Charnock J.M., Livens F.R., Patrick R.A.D., Collison D., (2000) An X-ray absorption spectroscopy study of the co-precipitation of Tc and Re with mackinawite (FeS). Appl. Geochem. 15, 347-354.
- Wildung R.E., Gorgy Y.A., Krupka K.M., Hess N.J., Li S.W., Plymale A.E., McKinley J.P., Frederickson J.K., (2000) Effect of electron donor and solution chemistry on products of dissimilatory reduction of technetium by *Shewanella putrefaciens*. Appl. Environ. Microbiol., 66, 2451-2460.

THE RESPONSE IN REDOX FROM ADDITIONS OF HYDROGEN AND OXYGEN TO NATURAL DEEP GROUNDWATER/ROCK SYSTEMS WITH ACTIVE MICROORGANISMS

Karsten Pedersen*, Johanna Arlinger, Lotta Hallbeck, Sara Lydmark, Jessica Johansson and Anna Pääjärvi.

¹ Microbial Analytics Sweden AB, Mölnlycke Fabriker 9, SE-435 35 Mölnlycke, (SE)

* Corresponding author: kap@micans.se

Abstract

Biological life systems are non-equilibrium systems and in most cases, they will never reach equilibrium. The overall influences of microbial activity on the E_h are complex and dependent on availability of sources of energy and carbon, either inorganic or organic compounds, and the nature of these. In this work, pressure resistant Pt electrodes and Ag/AgCl reference electrodes were constructed and installed into pressurized (2 MPa) circulation systems. Investigations of the relations between E_h and microorganisms growing with different electron donors (lactate or hydrogen) and electron acceptors (nitrate or sulphate) were performed. The influence of pulses of oxygen on the redox stability under different growth conditions was analysed. It became clear that microbial activity was very important for how the E_h developed in the studied systems. Microbial lactate and hydrogen oxidation, sulphide production and oxygen reduction occurred and the effect from introduction of oxygen on E_h was mitigated by microbial activity. The presence and activity of microorganisms consequently have a great influence on E_h in natural water systems.

Introduction

Biological life systems are non-equilibrium systems and in most cases, they will never reach equilibrium (Madigan et al. 2008). The maintenance of non-equilibrium conditions is, consequently, a pre-requisite for life processes to progress. The overall influences of microbial activity on the E_h are, therefore, complex and dependent on availability of sources of energy and carbon, either inorganic or organic compounds, and the nature of these. For instance, microorganisms are known to produce or consume gases, of which particularly hydrogen may influence the E_h of a system. The types and activities of microorganisms that will prevail in any system depend strongly on environmental parameters such as temperature, salinity, pH, and the presence or absence of gaseous oxygen. While some microorganisms, such as methanogens, can use hydrogen and carbon dioxide as energy and carbon sources, respectively, others require organic material, such as the low molecular compounds acetate and lactate, or polymeric substances such as cellulose as their combined source of carbon and energy.

A huge range of microorganisms of various species and genera are adapted to all possible environmental niches within the limits of life, including extreme habitats such as deep oil deposits (Jones et al. 2008) and hot springs (Stetter 1996). Microorganisms have been found at all temperatures between -20°C and 120°C , at all pH levels from 1 to approximately 12.5, and in saturated salt solutions (30% salt). As a group, they can extract energy from light, from inorganic gases such as methane and hydrogen, and from inorganic reduced elements such as sulphide, ferrous iron, and ammonium – to mention just a few. Similarly, microorganisms have been demonstrated to be able to degrade the absolute majority of naturally occurring organic compounds. About the only factor limiting active microbial life is the absence of liquid water; fungi and mould do well in humid air, but bacteria must be immersed in water to be active. However, many bacteria have developed mechanisms to survive periods of desiccation.

Safety analysis of future repositories for radioactive wastes requires understanding about the influence of microorganisms in general. The study of subsurface life poses a methodological challenge, due to the high groundwater pressure at typical repository depths. The installation of redox electrodes into high pressure systems can be difficult. Microelectrodes have been in use for decades in the study of redox gradients in sediments (Kühl and Revsbech 2001). The very small surface areas of such electrodes make them well adapted for high pressure applications. In this work, we constructed pressure resistant Pt and Ag/AgCl reference electrodes and installed them into pressurized (2 MPa) circulation systems. Investigations of the relations between E_h and microorganism growing with different electron donors (lactate or hydrogen) and electron acceptors (nitrate or sulphate) were performed. The influence of pulses of oxygen on the redox stability under different growth conditions was analysed.

Experimental

Circulation flow cell systems with natural microbial populations and groundwater from borehole KJ0052F01 at -447 m depth in the Äspö Hard Rock Laboratory (HRL) were used. A detailed description of the circulation systems and the diversity and numbers of microorganisms in the studied groundwater can be found as original work published in scientific journals (Nielsen et al. 2006; Hallbeck and Pedersen 2008). Each circulation system had four flow cells supplied with heat sterilized (160°C for 5 hours), crushed rock from the drill core of the KJ0052F01 borehole. The rock was crushed and the 2-4 mm fraction was used to fill up each flow cell with 110 g of crushed rock; total amount of crushed rock in each circulating system then became 440 g. Groundwater was circulated from KJ0052F01 over the crushed rock material at a flow rate of 40 ml min^{-1} , a pressure of 2.07 MPa and a temperature of about 18°C . Circulation was withheld for 3 months in an open mode from the borehole section through the system and back to the borehole section. The half life of groundwater in the circulation systems was determined to be approximately 10 h. Consequently, there was a continuous supply of groundwater constituents, including microbes, dissolved gases, and organic carbon to the developing biofilms on the crushed rock surfaces. The basic requirements for the attachment and development of microbial biofilms on rock in the flow cells were thus fulfilled. Pressure resistant platinum micro-electrodes (0.5 mm tip) from Unisense A/S were installed in the circulating system loops. As reference, pressure resistant microelectrodes, also from Unisense A/S, with Ag/AgCl in a gel-stabilized electrolyte

were used. See www.unisense.com for details. The electrodes were calibrated against redox standards (Reagecon, Fisher Scientific, Göteborg) at +124 mV, +358 mV and +650 mV. At 44 different times during the 110 days the hydrogen experiment lasted, E_h was analysed in sampled, depressurized groundwater with a HACH HQ 40d portable meter equipped with an ORP Redox electrode (HACH Lange Stockholm Sweden) and the results were compared with the readings from the Unisense electrodes.

Influence of oxygen on E_h in nitrate systems added with and without lactate

Two circulation systems were closed with 5 L of groundwater in each system after 3 months establishment of microbial populations. Both systems were subsequently added with nitrate (20.8 mM) and one added with lactate (11 mM). Each system was installed with 3 redox electrode pairs and was cultivated with these additions for 30 days. Thereafter, ~0.1 mM oxygen was introduced in both systems and the response in E_h was followed for about 10 days.

Influence of oxygen on E_h in systems added with hydrogen

Three circulation systems were closed with 5 L of groundwater in each system after 3 months establishment of microbial populations. They were subsequently added with three different concentrations of hydrogen, 0.1, 1.0 and 10 mM. Each system was installed with 2 redox electrode pairs and was cultivated with these additions for 64 days and the decrease in hydrogen and increase in microbial sulphide production was analysed. After build-up of sulphide in the three systems, the effect from five pulses of oxygen (~0.5 mM per pulse) on the E_h was followed in intervals between 6 and 14 days. The diversity of SRB and other microorganisms in the circulation systems has been described elsewhere (Jägevall et al., 2011).

Results

Influence of oxygen on E_h in nitrate systems added with and without lactate

The nitrate-lactate system electrodes registered an average E_h of about -20 mV while the nitrate system registered an average of +5 mV before the oxygen pulse was introduced (Figure 1A). Immediately after the oxygen pulse there were increases of E_h in the nitrate-lactate and nitrate systems to +160 mV and +220 mV, respectively. The E_h in nitrate-lactate system was lowered to about +20 mV in less than 24 hours stabilizing at 0 mV after 3 days, while the E_h of the nitrate system showed a much more sluggish response and eventually stabilized at about +40 mV after 4 days. It became obvious that the E_h of the nitrate-lactate system was much less sensitive to the oxygen pulse than was the nitrate system. The numbers of attached and unattached bacteria were analysed and the amount of bacteria in the nitrate system was about half of the amount in the nitrate-lactate system.

Influence of oxygen on E_h in systems added with hydrogen

The investigations of the influence of hydrogen on microbial sulphate reducing activity, analysed as sulphide production, showed that the produced amount of sulphide was

dependent on the added amount of hydrogen and production increased with increasing start hydrogen concentration (Figure 1B). The hydrogen concentrations decreased over time in the systems with a rate of about 0.1 mM day^{-1} (Figure 1C). Initially, there were some technical problems with the E_h measurements, but they were solved and unbroken data series were obtained from around day 40 until end of the experiments after 110 days (Figure 1D-F). Additions of 0.1, 1.0 and 10 mM hydrogen day 1 initially lowered the E_h to approximately -200 mV , -400 mV , and -600 mV , respectively (Figure 1D-F).

After build-up of sulphide in the three systems, the effect from five pulses of oxygen ($\sim 0.5 \text{ mM}$ per pulse) on the E_h was followed. The E_h of all three systems were intermittently influenced by the oxygen pulses, but they generally recovered almost the same E_h they had before the pulse after a couple of days. The 10 mM hydrogen system showed a more rapid and distinct recovery followed by the 1 and 0.1 mM hydrogen systems. It was also found that the 10 mM hydrogen system had a much lower E_h than the other two systems. The two pairs of redox electrodes per circulation system reproduced E_h readings excellently with small discrepancies, except for the pairs in the 0.1 mM hydrogen system where the response to oxygen was 150 mV larger for one of the electrode pairs compared to its companion electrode pair. In addition to E_h and sulphide, several other parameters were analysed as well. They were: pH, sulphate, acetate, dissolved organic carbon, total number of microorganisms, and the content of other dissolved gases, helium, oxygen, nitrogen, carbon monoxide, carbon dioxide and methane. Detailed interpretation and analysis of the data is presently ongoing and will be published during 2011.

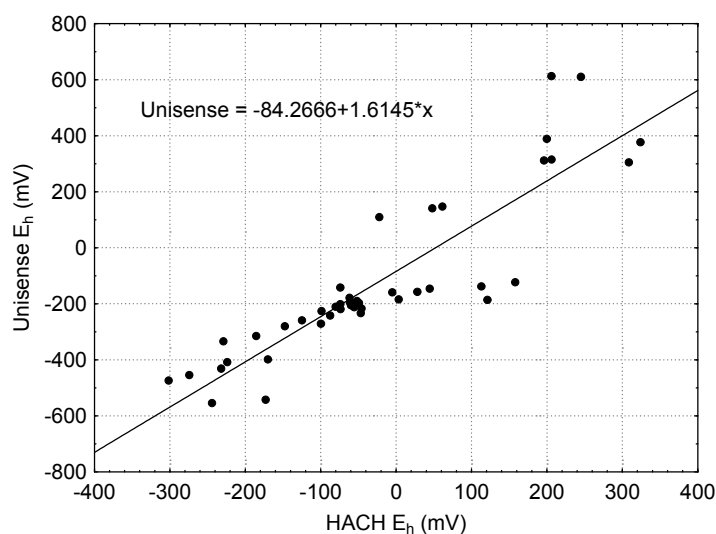


Figure 2: Comparisons of Eh readings from the in line Unisense pressure resistant electrodes with readings obtained with a HACH HQ40d portable field instrument.

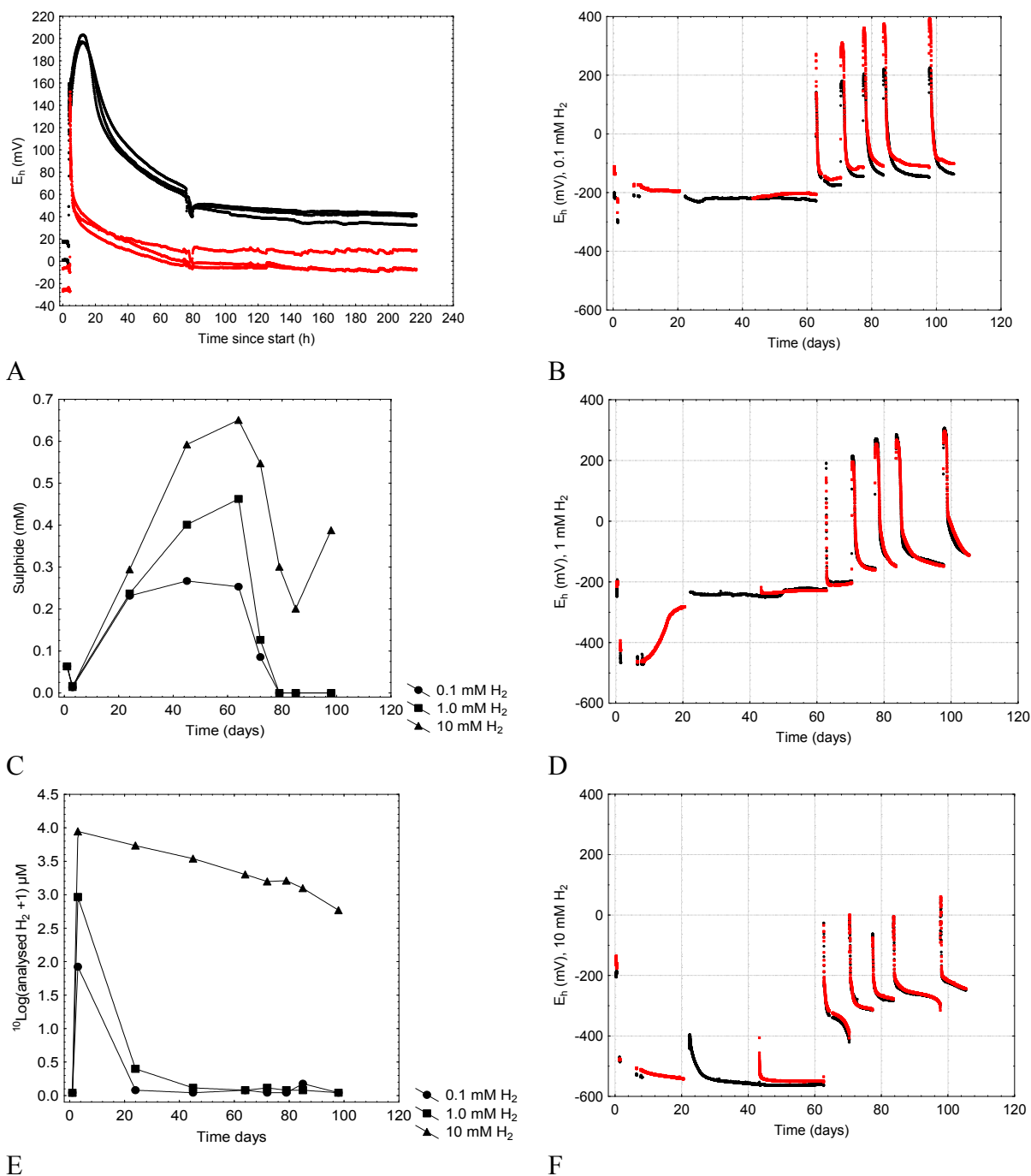


Figure 1: A. E_h analysed with three parallel electrode pairs after addition of 0.1 mM oxygen in a circulation system added with 20.8 mM nitrate (black) and a system added with 20.8 mM nitrate and 11 mM lactate (red). B. The produced amounts of sulphide in three circulation systems added with different concentrations of hydrogen at day 1. C. The analysed concentration of hydrogen in three circulation systems added with different concentrations of hydrogen at day 1. D. The response in E_h from addition of 0.1 mM hydrogen at day 1 and five repeated additions on 0.5 mM oxygen. E. The response in E_h from addition of 1 mM hydrogen at day 1 and five repeated additions on 0.5 mM oxygen. F. The response in E_h from addition of 10 mM hydrogen at day 1 and five repeated additions on 0.5 mM oxygen. Two parallel electrodes were used in D-F (black and red).

Discussion

Performance of the redox electrode system

The redox electrodes showed very good agreement with the calibration standards of +124 mV, +358 mV and +650 mV, but were difficult to calibrate at the low E_h values and under the high pressure encountered. The approach to control readings at very negative E_h values was to utilize the experiment with hydrogen that showed E_h values below -400 mV at hydrogen concentrations > 1 mM which is consistent with the E_0' at pH 7.0 for the redox couple $2H^+/H_2$ (-0.42 mV) (Madigan et al. 2008). The electrodes consequently showed good and linear response between +650 mV down to at least -420 mV. The configuration with three electrodes in the lactate experiment and two electrodes in the hydrogen experiment showed that the electrodes generally reproduced well. In the work described here, it is the change in E_h values as a function of treatments with oxygen that was in focus, rather than absolute E_h values. Analysis of E_h in depressurized groundwater with the HACH field meter did not reproduce E_h analysed with the in line Unisense electrodes (Figure 2). This sampling degasses the water and hydrogen, and to some extent hydrogen sulphide (pH dependent) will disappear from the sample and the E_h reading will be higher than in the pressurized circulation systems that kept these gases in solution.

Influence of oxygen on E_h in nitrate microbial systems added with and without lactate

The first experiment studied the effect of nitrate reducing bacteria (NRB) on E_h with and without addition of a carbon source. There was a clear difference in response in E_h for the nitrate circulation system compared to the nitrate-lactate circulation system. The only treatment difference was the addition of lactate to the system that returned more rapidly to an E_h value similar to the value observed before the oxygen pulse. Microorganisms respire oxygen with lactate, which will reduce oxygen to water and E_h will decrease again. Without an organic carbon source in the nitrate system, the decrease in E_h was much slower. This result demonstrates the relation between of microbial activity and a decreasing E_h . When there is energy and carbon available for microbial activity in deep groundwater, the microorganisms will cause a decrease E_h , as observed previously in sediment systems (Madigan et al. 2008). A complicating attenuation factor was that viruses which attack bacteria were present in both systems. These viruses controlled the number of living cells that can exist in a population and the bacterial numbers were 0.83×10^6 and 1.6×10^6 cells mL^{-1} in the nitrate and the nitrate-lactate system, respectively. The numbers of viruses were 4-5 times higher in both systems (data not shown), which attests that a population controlling effect from viruses was present, because the only way for viruses to propagate is via the attack and destruction of host cells (Madigan et al. 2008). Similar effects have been demonstrated for SRB previously (Eydalet al. 2009). The effect from lactate on the E_h was consequently mitigated by viruses because more bacteria would obviously have respired more oxygen per time.

Influence of oxygen on E_h in microbial systems added with hydrogen

Addition of nitrate to an anaerobic water system suppresses activity of sulphate reducing bacteria (SRB), and this fact is utilised to hinder microbial sulphide souring of sub-seafloor oil wells. The addition of nitrate in the experiment discussed above totally suppressed the production of sulphide (data not shown), although there were about 5 mM sulphate in the groundwater. The hydrogen addition experiment without nitrate but with a natural concentration of about 5 mM sulphate developed in a very different way. There, SRB in all three systems produced significant concentrations of sulphide (Figure 1 A). Increasing the hydrogen gas concentration (background in groundwater was about 0.1 μ M hydrogen) stimulated the microbial sulphide producing activity. This system then became more complicated to interpret, compared to the nitrate added system. In the nitrate system, oxygen was the main component influencing E_h . In the hydrogen system, sulphide, hydrogen and oxygen all did have an influence on the E_h . At day 1 when hydrogen was added, it became clear that hydrogen had a strong influence on E_h , at concentrations above 1 mM. Hydrogen was consumed by SRB as explained elsewhere (Pedersen et al. 2009). This hydrogen removing activity of SRB consequently should raise the E_h but because the product of hydrogen oxidation is mainly sulphide, the SRB lower the E_h towards about -200 mV at the same time due to the increase in sulphide concentration and the resulting E_h may not change more than marginally. This becomes quite clear from the results, where hydrogen decreases (Figure 1C) at the same time as sulphide increases (Figure 1B) and the E_h remains about constant.

The stable E_h situation changed dramatically when pulses of oxygen were introduced. Oxygen reacts readily with sulphide which then acts as a kind of microbially built up buffer for the E_h stability. Sulphide was rapidly consumed by the oxygen pulses in the two systems where hydrogen was consumed and the recovery of the system to oxygen free conditions took several days (Figure 1 D-E). This was probably because aerobic microorganisms respire the oxygen while degrading available organic carbon in the circulating systems (dissolved organic carbon was about 1.5 mM), which takes some time. However, the 10 mM hydrogen system had plentiful of hydrogen throughout the experiment (Figure 1 C) and there, SRB production of sulphide continued and the sulphide concentration never reached nil (Figure 1 A). Therefore, this 10 mM hydrogen system very rapidly returned to the low E_h it had before the oxygen pulses. This difference was because the microbial oxygen respiration is a metabolic process that takes time to establish from an anaerobic population, while oxygen reacts almost instantaneously with sulphide.

Conclusions

Although a more complex interpretation was required for this experiment, it became clear that microbial activity was very important for how the E_h developed. It is very difficult to make sterile controls in the studied circulation systems without totally upsetting the E_h conditions; set-up of a proper sterile control was not possible. However, without bacteria, sulphide production and oxygen reduction would not have occurred and the introduction of oxygen would probably have raised the E_h as observed (Figure 1D-F), but in difference to a microbial system, the recovery of the E_h at values observed before the oxygen pulses would not have occurred or had been very sluggish.

Acknowledgement

This work was performed under the European Atomic Energy Community Seventh Framework Program under grant agreement 212287, Collaborative Project Recosy with co-funding from the Swedish Nuclear Fuel and Waste Management Co.

References

- Eydal, H.S.C., Jägevall, S., Hermansson, M. and Pedersen, K. (2009). Bacteriophage lytic to *Desulfovibrio aespoeensis* isolated from deep groundwater, *The ISME Journal*, 3, 1139-1147.
- Hallbeck, L. and Pedersen, K. (2008). Characterization of microbial processes in deep aquifers of the Fennoscandian Shield, *Applied Geochemistry*, 23, 1796-1819.
- Jones, D.M., Head, I.M., Gray, N.D., Adams, J.J., Rowan, A.K., Aitken, C.M., Bennett, B., Huang, H., Brown, A., Bowler, B.F.J., Oldenburg, T., Erdmann, M. and Larter, S.R. (2008). Crude-oil biodegradation via methanogenesis in subsurface petroleum reservoirs, *Nature*, 451, no. 775, 176-180.
- Jägevall S., Rabe L. and Pedersen K. (2011) Abundance and diversity of biofilms in natural and artificial aquifers of the Äspö Hard Rock Laboratory, Sweden. *Microbial Ecology* 61, 410-422.
- Kühl, M. and Revsbech, N. (2001). Biogeochemical microsensors for boundary layer studies, in: Boubreau, B.P. and Jørgensen, B.B. (eds) *The Benthic boundary layer*, 180-210. Oxford University Press, New York
- Madigan, M.T., Martinko, J.M., Dunlap, P.V. and Clark, D.P. (2008). *Brock Biology of Microorganisms*, 12th edition, 1-1168. Benjamin Cummings, London UK
- Nielsen, M.E., Pedersen, K., Fisk, M. and Istok, J. (2006). Microbial nitrate respiration of lactate at in situ conditions in groundwater from a granitic aquifer situated 450 m underground, *Geobiology*, 4, 43-52.
- Pedersen, K., Arlinger, J., Eriksson, S., Rabe, L. and Hallbeck, L. (2009). The effect from microorganisms on the redox state of laboratory and natural systems, 1st Annual Workshop Proceedings 7TH EC FP - Recosy CP Barcelona 10th – 12th February 2009,
- Stetter, K.O. (1996). Hyperthermophilic procaryotes, *FEMS Microbiology Reviews*, 18, 145-148.

SORPTION AND REDOX BEHAVIOUR OF RADIONUCLIDES IN NATURAL CLAY ROCKS

N. L. Banik^{*}, C.M. Marquardt, D. Schild, J. Rothe, T. Schäfer

Karlsruhe Institute of Technology (KIT), Institute for Nuclear Waste Disposal (INE),
D-76344 Eggenstein-Leopoldshafen, Karlsruhe, Germany

* Corresponding author: nidhu.banik@kit.edu

Abstract

The sorption and redox speciation of Np, Pu and Tc have been performed on crushed OPA and COx clay rocks with artificial pore water. The batch experiments are performed at pH 7.6 for OPA and pH 7.2 for COx under argon atmosphere (<1 ppm O₂) under 1% CO₂ conditions at room temperature. Four different solid to liquid ratio, S/L (10, 20, 50, 200) at constant ionic strength (0.1 M NaCl), and with contact times between 1 week and 1 year have been studied. The initial concentration of Np(V), Pu(V) and Tc(VII) in solution varied between 3.0×10^{-4} and 1.0×10^{-8} M.

We observed that the sorption of the radionuclides (RN) increases with increasing clay amounts (S/L ratio) and with increasing contact time. More than 80 % of Np and Pu are sorbed on the clay whereas only 35 % of Tc is bound on OPA and COx with S/L ratios 10-20 after 4 months contact time. The K_d values for batch experiments of OPA and COx are calculated to be 6.33; 5.53 mL/g for Pu, 5.50; 5.35 mL/g for Np, 0.053; 0.036 mL/g for Tc with 10 S/L ratio after 4 months contact time. The calculated K_d values show good agreement with literature data. Np(V), Pu(V), and Tc(VII) redox speciation in OPA and COx suspensions at high RN concentrations are investigated by x-ray absorption fine structure (XAFS), UV-Vis absorption, x-ray photoelectron spectroscopy (XPS). XAFS and XPS studies show that Np is sorbed on both solid phases in the form of Np(V), Pu is sorbed as Pu(IV), and Tc as Tc(VII) after 1 week contact time. Hence, the sorbed amount of the anionic pertechnetate ion is significant lower than for Np and Pu. In the supernatant solution Np(V), Pu(IV) and Tc(VII) is characterized after 1 week contact time by the extraction method and UV-Vis spectroscopy. At lower concentration, redox speciation of radionuclide is only done by liquid-liquid extraction. As a second speciation method at very low concentrations capillary electrophoresis coupled to ICP-MS was introduced and tested on the Np samples. It could be shown, that Np(V) is detected in solution at concentrations of 10^{-9} M.

Introduction

In order to perform the long-term safety assessments of high-level nuclear waste repositories in clay formation, a detailed knowledge of redox behaviour, solubility, complexation, sorption, and diffusion of actinides (An) and fission products (FP) in natural clay rocks are essential. Opalinus Clay (OPA, Mont-Terri, Switzerland) (Bradbury 2003) and the Callovo-Oxfordian argillite (COx, Bure, France) (Latrille 2006) are considered as potential host rocks for deep geological disposal of radioactive waste due to their good swelling behaviour, low permeability, and high surface area. Numerous studies have been performed clearly demonstrating that transport in these argillaceous rocks is controlled by molecular diffusion. However, only few studies have been performed on the sorption and redox behaviour of neptunium (Np), plutonium (Pu), and technetium (Tc) in natural clay rocks like OPA and COx. A few batch and diffusion experiments of Np(V) on OPA [Wu 2009], Pu(IV) on COx (Latrille 2006) has been performed. Furthermore, Wu et al. studied Np sorption in OPA clay rocks with a low solid to liquid ratio (S/L) and performed only short kinetic experiments.

The aim of this study is to characterize the retention of Np, Pu, and Tc on the two selected clay rocks OPA and COx taking into consideration the redox processes. Since the distribution coefficients (K_d) for the sorption of radionuclides on the host rock of a nuclear waste repository are important parameters for diffusion and transport modelling. The K_d values for the sorption of RN on OPA/COx are determined directly by batch experiments on crushed material. The objective at the end of the project is to compare this K_d value with the value derived from the in-diffusion experiments.

The redox speciation of Np(V), Pu(V), and Tc(VII) in OPA and COx suspensions are investigated by x-ray absorption fine structure (EXAFS), UV-Vis absorption, and liquid-liquid extraction. The redox speciation on the solid clay was performed by EXAFS and x-ray photoelectron spectroscopy (XPS). Because of the strong sorption of some radionuclides, the concentrations in solutions are very low and reach the detection limit of radiometric measurements combined with the extraction methods. As a speciation method at such low concentrations and below, capillary electrophoresis (CE) coupled to ICP-MS was introduced and tested on the neptunium samples.

Materials & Methods

Chemicals

All chemicals are of p.a. quality or better and are obtained from Merck (Darmstadt, Germany) or Riedel de Haen (Seelze, Germany). All of the experiments are conducted using de-ionized, “MilliQ” water ($\rho = 18 \text{ M}\Omega \cdot \text{m}$). ^{242}Pu , ^{237}Np , and ^{99}Tc are used from laboratory stock solutions. The activity of ^{242}Pu , ^{237}Np , and ^{99}Tc is measured by liquid scintillation counting (LSC) using the scintillation cocktail Ultima Gold XR (Packard) and LSC Tricab (Hewlett Packard).

Measurements of pH and Eh

The pH is measured with a combined orion type glass electrode (Orion with a combined electrode). The redox potentials of suspension solution are measured with a Pt combination electrode with Ag/AgCl reference system (Metrohm) and converted into

Eh vs. standard hydrogen electrode (SHE) by correction for the potential of the Ag/AgCl reference electrode at 3M KCl and 22° C.

Radionuclides

For all sorption experiments, stock solutions of plutonium and neptunium in the pentavalent oxidation state and technetium in the heptavalent oxidation state are used. The pentavalent oxidation state of Pu(V) and Np(V) were obtained by potentiostatic electrolysis and its purity was verified by UV-Vis spectroscopy (Cohen 1961). The RN concentration is determined by liquid scintillation counting (LSC).

Opalinus Clay (OPA)

For the batch type sorption studies Opalinus Clay mineral (OPA) is crushed, sieved (< 500 µm) and freeze dried under atmospheric conditions. The anaerobic OPA crushed powder is prepared in under Ar atmosphere (inert glove box) from the OPA bore core BHE-24-2 (Mont Terri) (Wu 2009, Van Loon 2005). OPA from Mont Terri consists mainly (> 65%) of different sheet silicates (kaolinite, illite, illite/smectite mixed layers, and chlorite) but also >10% quartz and calcite. In addition to these main fractions, OPA contains ~4% Fe(II) minerals like pyrite and siderite as well as traces of albite, feldspars, and organic carbon. The N₂-BET surface area was determined to be 39.0 m²/g and the cation exchange capacity determined by the COHEX method is 12.93 ± 0.04 meq/100g.

Callovo Oxfordian Clay (COx)

The Callovo Oxfordian argillites come from boreholes (EST 25691) located on the site of the underground laboratory operated by Andra at Bure (Meuse/Haute Marne, France). A complete description of the core sample drilling and conditioning procedures is available elsewhere (Gaucher 2004). The sample is grounded and sieved at <500 µm in the absence of oxygen, under Ar atmosphere, in order to prevent any oxidation of redox sensitive materials such as, for example, pyrite, organic matter, adsorbed Fe(II) and iodide. The N₂-BET surface area was determined to be 36.7 m²/g and the cation exchange capacity determined by the COHEX method is 12.02 ± 0.10 meq/100g.

Batch experiments

All sorption experiments are conducted according to batch procedures described below at initial radionuclides concentrations in the range of 3.0×10⁻⁴ - 1.0×10⁻⁸ M. The batch experiments are carried out in Zinsser vials (20 mL, material: HDPE) over a period up to about 1 year at room temperature. The solid to liquid ratio (S/L) of 10, 20, 50, 200 of clay rocks are chosen for the experiments, preconditioned with pore water in 0.1 M NaCl by shaking continuously the suspension for 10-15 days to achieve equilibrium pH of 7.2 for COx and 7.6 for OPA. After mixing Pu(V), Np(V), and Tc(VII) solutions with the preconditioned clay rocks suspension, the pH values were readjusted by adding 0.1 M HCl or 0.1 M NaOH. For characterisation of the suspension the solid and liquid phases were separated by ultrafiltration using 10 kD filters (5000 rpm for 1 h). The supernatants were analysed in order to determine the content of free RN in the liquid

phase by liquid scintillation counting (LSC). The sorbed amount of Np, Pu, Tc (dried clay rocks, solid phase) was also measured for some samples by XAFS and XPS. For all sorption experiments, about 10 % adsorption of RN on the Zinsser vials walls depending on S/L ratio of the clay rocks and radionuclide has been taken into consideration for evaluating the K_d values.

UV-Vis absorption spectroscopy (UV-Vis)

The oxidation states of Np(V), Pu(V), Tc(VII) in the stock and sample solutions are confirmed by UV-Vis spectroscopy with a high-resolution UV-Vis/NIR spectrometer Cary 5 (Varian). The samples are measured in 1 cm inert-gas quartz cuvettes (Hellma) with tight screw tops, or in polystyrene semi-micro cuvettes (Brandt). UV-Vis/NIR spectra are taken from 800 nm to 1200 nm for Np, 400 nm to 900 nm for Pu, and 200 nm to 600 nm for Tc.

X-ray photoelectron spectroscopy (XPS)

Clay suspensions and wet pastes were prepared for XPS analysis by drying small portions on an indium foil in an anoxic glove box. The samples were moved into the XP spectrometer (PHI model 5600ci) without air contact by means of a vacuum transfer vessel. Monochromatic Al K_{α} x-rays were used for excitation in conjunction with an electron flood gun for sample surface neutralization. Atomic concentrations were calculated from the areas of elemental lines of survey spectra. Narrow scans of elemental lines were recorded for determination of chemical shifts and spectral features.

X-ray absorption fine structure spectroscopy (XAFS)

For the XAFS measurements, filtrate solutions and suspension with clay were filled into 400 μ L capped PE vials and mounted in a special air tight sample holder, which is connected to an Ar supply line at the experimental station to keep the samples under oxygen-free conditions during XAFS measurements. The measurements were performed at the INE beam line using a new inert gas sample cell design (Brendebach 2009) for redox sensitive radionuclides. The spectra were calibrated against the first derivative X-ray absorption near edge structure (XANES) spectrum of a Zr foil, defining the energy of the first inflection point as $E(\text{Zr } 1s) = 17998.0 \text{ eV}$. All Pu L3, Np L3, Tc K XAFS spectra are measured in standard fluorescence yield detection mode.

Capillary electrophoresis coupled with ICP-MS (CE-ICP-MS)

A commercial Beckman Coulter P/ACE MDQ capillary electrophoresis system (Fullerton, U.S.A.) was coupled to an inductively coupled plasma sector field mass spectrometer (Element XR, Thermo Fisher Scientific, Bremen, Germany). Conventional fused silica capillaries (Beckman Coulter, Fullerton, U.S.A.) with an internal diameter of 50 μ m and lengths of 74 cm were used for the separations. A commercial parallel path micro-nebulizer (Mira Mist CE, Burgener, Canada) with a borosilicate spray chamber (Mini glass chamber, Burgener, Canada) interfaces both apparatuses. To generate an aerosol a makeup liquid (2 % HNO_3 , 10 % ethanol, 1 ppb Rh as internal standard) was introduced by a syringe pump at a nominal flow rate of 8 $\mu\text{L min}^{-1}$. For the measurement, separated supernatant solutions from clay suspension

were taken in 1 mL glass vials under inert atmosphere. However the fast injection of the sample into the CE has been performed under air atmosphere. Therefore, the effect of air cannot be excluded from the experiments. Separations were performed at -20 kV and at a constant pressure of 0.8 psi (to avoid clogging) and they were completed within 15-18 min.

Liquid-liquid extraction

The oxidation state of Np, Pu, Tc at low concentration after the separation by centrifugation using 10 KD ultrafilter under anaerobic conditions and supernatant solution was analyzed by liquid-liquid extraction using 1-phenyl-3-methyl-4-benzoylpyrazolone-5 (PMBP) [Nitsche 1994] and 2-thenoyltrifluoroacetone (TTA) (Merck, Germany) as extracting agents. A 0.6 mL portion of the supernatant filtrate solution was taken together with 0.2 mL 2 M HCl and 0.8 mL 0.025 M PMBP (in Xylene) and 0.5 M TTA (in Toluene) solutions and then vigorously shaken for 10 min. The phases were separated by centrifugation for 10 min (5000 rpm) and aliquots of each phase were taken for radiometric analysis.

Results and discussions

Sorption of radionuclides on clay rocks

The fraction of RN sorbed and the distribution coefficient were calculated by using the following equations:

$$Sorption = 1 - \frac{[RN]_{eq}}{[RN]_0} \times 100 \quad (\%) \quad (1)$$

$$K_d = \frac{x}{m} \times \frac{1}{[RN]_{eq}} \quad (\text{mL/g}) \quad (2),$$

where $[RN]_{eq}$ and $[RN]_0$ (mol/L) are the equilibrium and initial concentrations of radionuclides in solution, respectively; x (mol) is the amount of sorbate; m (g) is the mass of sorbent.

The sorption of Pu, Np, Tc onto clay rocks (COx, OPA) has been investigated as a function of solid to liquid ratio. The sorption experiments are performed with different contact times (1 week to 7 months). As can be seen from Figure 1 for Np(V), there is a linear dependency between the K_d values and the liquid to surface area ratio (S/L range from 20-200 g/L) under these conditions showing the effect of available sorption sites. The highest sorption is about 80% at 200 g/L. The same trends was observed for Pu(V) and Tc(VII). Table 1 and 2 show the K_d values and the percentage of RN sorbed on COx or OPA in pore water.

Table 1: K_d values and percentage sorption of RN on COx (pH 7.2) in pore water at 3×10^{-7} M after 4 months contact time

Solid to liquid ratio, [g/L]	K_d [mL/g] & sorption [%] of Np	K_d [mL/g] & sorption [%] of Pu	K_d [mL/g] & sorption [%] of Tc
10	5.4/76	5.5/71	0.04/19
20	0.9/81	3.2/88	0.02/20
50	0.3/84	0.8/89	0.02/28
200	0.1/87	0.3/93	0.01/53

Table 2: K_d values and percentage sorption of RN on OPA (pH 7.6) in Pore water at 3×10^{-7} M after 4 months contact time

Solid to liquid ratio, [g/L]	K_d [mL/g] & sorption [%] of Np	K_d [mL/g] & sorption [%] of Pu	K_d [mL/g] & sorption [%] of Tc
10	5.5/83	6.3/84	0.05/28
20	1.0/81	3.0/86	0.03/28
50	0.7/86	1.3/88	0.01/36
200	0.1/88	0.3/89	0.01/65

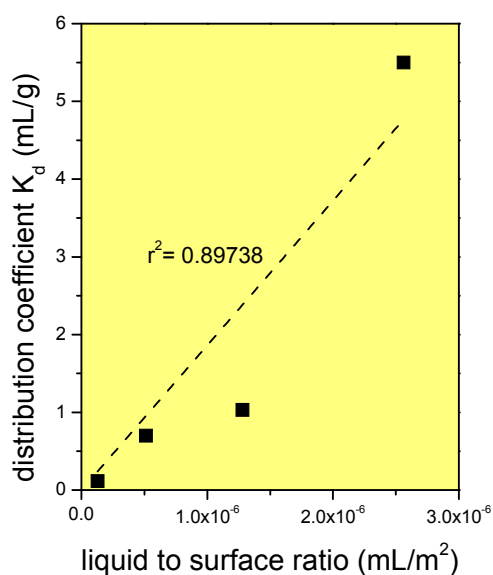


Figure 1: Distribution coefficient (K_d) for the sorption of Np on OPA (Mont Terri) in pore water as a function of liquid to surface area ratio, pore water, $[Np(V)] = 3E-07$ M, contact time= 4 months.

Speciation of radionuclides in clay solution

UV-Vis spectroscopy of Np(V)

One of the key questions is in what redox state each radionuclide occurs during the sorption process. For that the solution of each sample was measured by UV-Vis absorption spectroscopy.

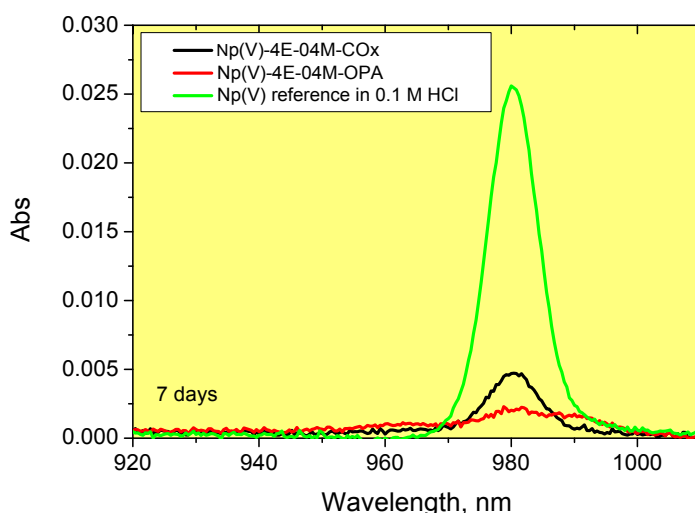


Figure 2: Absorption spectra of Np in supernatant solution after ultrafiltration from suspension solution of clay rocks, contact time = 1 week, S/L = 50, NaCl = 0.1 M.

In the following sections we only focus on the neptunium, because it shows a characteristic absorption band for the aquo NpO_2^+ ion at 981 nm. Figure 2 represents the UV-Vis spectra of the Np(V) reference solution and the supernatant solution of Np in OPA and COx clay minerals. Due to the similarity of spectral features for both the Np samples and the Np(V)reference spectra, we conclude that the neptunium remaining in solution occurs in the pentavalent oxidation state. The amount of Np in solution calculated from the absorption coefficient is similar to the result from the radiometric measurement within the range of uncertainties.

Eh Measurements

The sorption of Pu, Np, and Tc increases with time supposing that they are slowly reduced to the tetravalent oxidation state. This can be confirmed by a steadily decrease of the Eh to values between -100 mV (Pu), + 50 mV (Np), and -80 mV (Tc) after 4 months without reaching a constant value. Looking in detail on the Np redox speciation diagram under the Eh/pH conditions for (OPA) pore water shows that the reduction to tetravalent Np is thermodynamically feasible.

CE-ICP-MS

Due to the limitation of the absorption spectroscopy and the radiometric measurement we have performed Np speciation by CE-ICP-MS. The first test should show how significant the impact of air on the Np(IV) is by using our commercial injection system.

For that we injected a reference solution of 100% Np(IV) at concentration of 3×10^{-7} M in 0.01 M HClO_4 into the capillary and made a separation at a potential of 20 kV in an acetic acid buffer system. Figure 3 shows, that the Np(IV) was partly oxidized to Np(V), but that it should be possible to qualitatively detect Np(IV). Several mixtures of Np(V) and Np(IV) with different ratios are tested, to ensure the reliability of this separation and the migration time for our system.

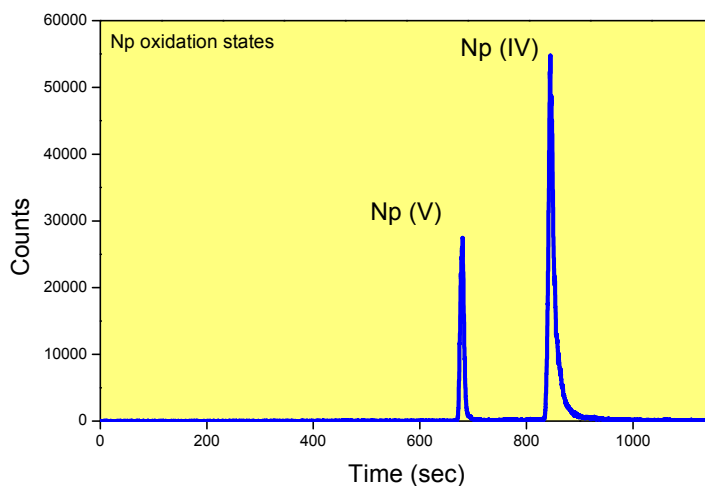


Figure 3: Electropherogram of an Np(IV) reference solution characterized by CE-ICP-MS, $[\text{Np}] = 3 \times 10^{-7}$ M, 0.01 M HClO_4 , separation in 1 M AcOH buffer system, at a potential of 20 kV.

For the speciation of Np in clay solutions, filtrate (10 kD) supernatant solution was taken in small vials under Ar atmosphere and then injected under air into the CE. Figure 4 demonstrates that only Np(V) was found in supernatant solution with a concentration of about 2×10^{-8} M and this confirms the spectroscopic result at higher concentrations.

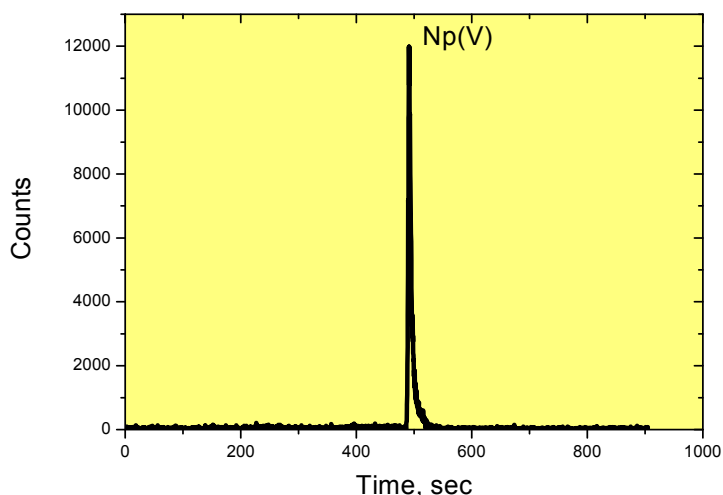


Figure 4: Electropherogram of Np in filtrate COx clay rock, $[\text{Np}] = 2 \times 10^{-8}$ M, 0.1 M NaCl, S/L = 20, 7 months contact time, separation with 1 M AcOH buffer system at 30 kV.

Speciation of radionuclides on clay solid phases

XANES

The results of the XANES of Np, Pu and Tc are shown in Table 3. In all samples the Np was detected as Np(V) (NpO_2^+ , ‘neptunyl’) with the characteristic XANES features (low white line intensity, multiple scattering shoulder ~ 10 eV above white line). Note that the energy positions of Np(IV) and Np(V) almost coincide. This anomaly is explained for actinyl cations by charge transfer from the double-bond axial oxygen anions to the metal cation. The XANES spectrum of Np(V)ref, Np-OPA, Np-COx are shown in Figure 5.

Table 3: Energy positions of the XANES first inflection point and white line maximum positions for reference species and sorption samples. All values are given in eV (estimated calibration error $\Delta E \pm 0.5$ -1 eV).

Sample description	first inflection point	white line maximum
Np(IV)ref, solution	17609.6	17614.7
Np(V)ref, solution	17609.0	17614.0
Np(V)-OPA, solid	17608.4	17613.0
Np(V)-COx, solid	17607.7	17612.5
Pu(IV)ref, solution	18062.4	18067.6
Pu(V)ref, solution	18059.8	18064.3
Pu(V)-OPA, solid	18062.1	18067.9
Pu(V)-COx, solid	18063.0	18067.8
Tc(VII)ref, solution	21053.1	-
Tc(IV)ref, solid	21055.6	-
Tc(VII)-OPA, solid	21052.6	-
Tc(VII)-COx, solid	21052.8	-

As expected, the white line maxima of the XANES of Pu in the OPA and COx samples are clearly located at the white line position of the Pu(IV) at 18067.8 eV. Hence, Pu(V) is reduced to Pu(IV) for all sorption samples. The XANES spectra exhibit no multiple scattering resonance (as expected for Pu(V) and Pu(VI) ‘plutonyl’ moieties) and a strong white line intensity - the energy positions are in accordance with the Pu(IV) aquo ion.

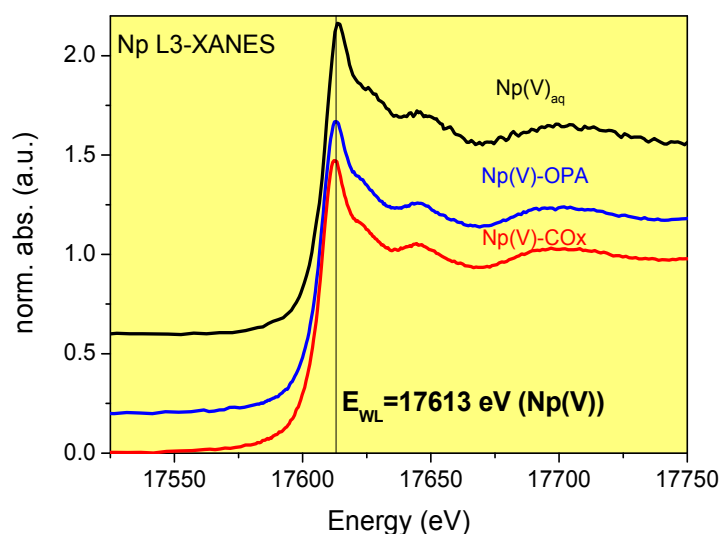


Figure 5: *Np L3-XANES spectra of Np speciation in clay rocks (OPA, COx), $[Np] = 3E-04$ M, 0.1 M NaCl, S/L = 50, kinetic = 1 week, sample= filtrate suspension.*

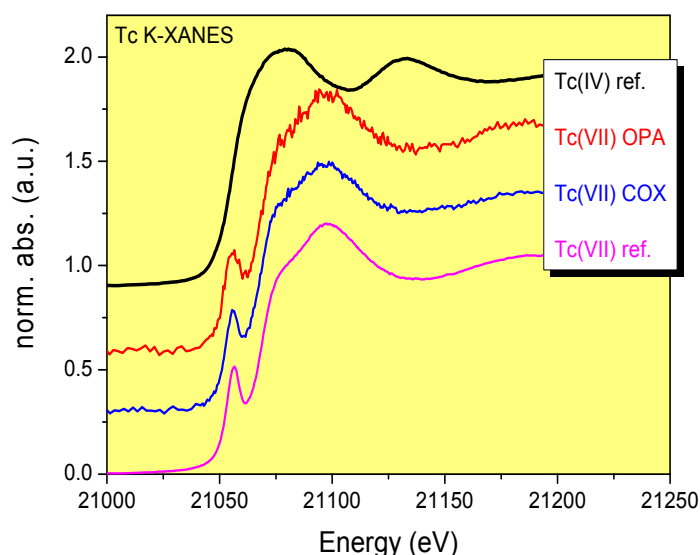


Figure 6: *Tc K-XANES spectra of Tc speciation in clay rocks (OPA, COx), $[Tc] = 3E-04$ M, 0.1 M NaCl, S/L = 50, kinetic = 1 week, sample= filtrate suspension.*

The Tc K-edge x-ray absorption spectroscopy was measured at the INE-KIT Beamline in a first time. As a reference sample, $Tc(VII)_{aq}$ and $Tc(IV)_{solid}$ are prepared and measured. The Tc-clay samples have been measured as a solid. The XANES spectrum of $Tc(IV)_{ref}$, $Tc(VII)_{ref}$, Tc-OPA, Tc-COx are shown in Figure 6. The Tc K-XANES of the $Tc(VII)O_4^-$ ‘pertechnetate’ moiety, where Tc is surrounded by 4 oxygen atoms in tetrahedral conformation, exhibits a strong pre-edge resonance, reflecting a $Tc\ 1s \rightarrow 5p/4d$ transition allowed due to p-d mixing in the final state. $Tc(IV)$ is generally octahedrally coordinated (inversion symmetry), where this transition is forbidden.

Hence, the XANES spectra of the clay samples clearly point to the preservation of Tc(VII) upon sorption and no reduction has occurred after one week contact time.

XPS

To investigate the redox state of sorbed radionuclides on the clay particles, surface sensitive XPS (x-ray photoelectron spectroscopy) is applied. Besides photoelectron spectroscopy of the radionuclides, analyses of the chemical states of iron and sulphur of the clay suspension indicate which of these elements may be available for reduction of the radionuclides to a less soluble state. Actinides (Pu, Np) and technetium are doped into the clay suspensions at low concentrations, thus only the actinide 4f and Tc 3d main lines are detected with low intensity. Fortunately, no complete spectral superpositions with elemental lines from the constituents of the clays are present. Only Pu 4f_{5/2} is superposed by the intense Ca 2s elemental line, while Pu 4f_{7/2} is not superposed. Np 4f_{7/2}, 4f_{5/2}, and Tc 3d_{5/2}, 3d_{3/2} elemental lines can thoroughly be detected if present. However, Tc was not detected at the clay surfaces after a contact time of 7 days in suspension.

The Pu 4f_{7/2} elemental line at Pu-OPA samples has a binding energy of 426.0 eV typical for the tetravalent state (Figure 8). In addition, a satellite at about 6.5 eV higher binding energy is detected indicating Pu(IV)oxide, presumably due to Pu eigencolloids.

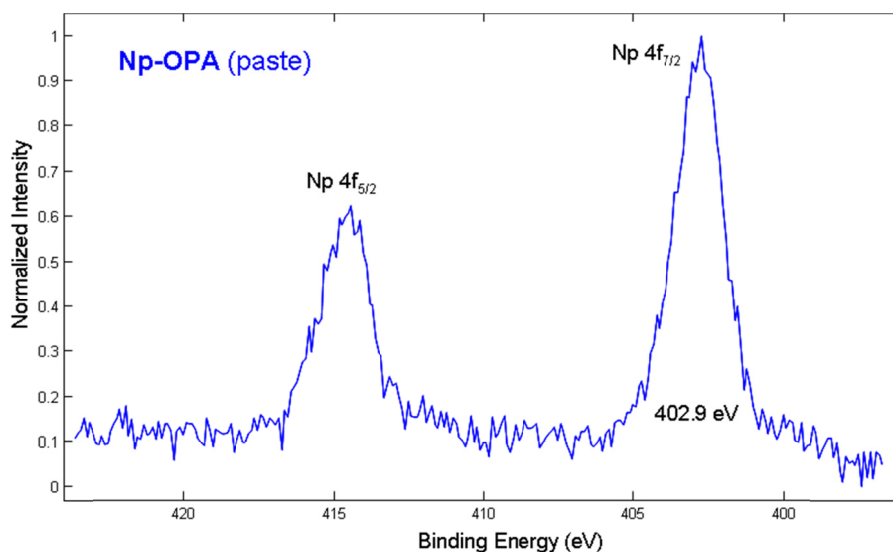


Figure 7: Np 4f spectrum, Al K α mono x-ray excitation, charges referenced C1s (CH): 284.8 eV. Wet Paste: Opalinus clay, Np(V) 4×10^{-4} M, 7 days contact time.

In case of Np-OPA, the Np 4f_{7/2} elemental line has a binding energy of 402.9 eV (Figure 7). However, Np(V) and Np(IV) have similar binding energies of the 4f elemental lines and conclusions concerning the valence state of Np are solely derived from the positions of 4f satellites if present. A satellite at about 6.5 eV higher binding energy is not detected indicating absence of Np(IV)oxide or Np(IV) eigencolloids. However, a distinction between sorbed Np(V) and ideal Np(IV) sorption of single, non-interacting Np atoms cannot be performed.

The S 2p spectra indicate solely the presence of sulfate and no sulfur in a reduced state like sulfide.

The Fe 2p_{3/2} spectra has two components assigned to Fe(III) and Fe(II). No satellite typical for the Fe³⁺ ion was observed. No clear conclusions could be drawn about the bonding of the iron. The spectra are similar to reference spectra of Fe₃O₄ and iron silicates (iron bound in the clays).

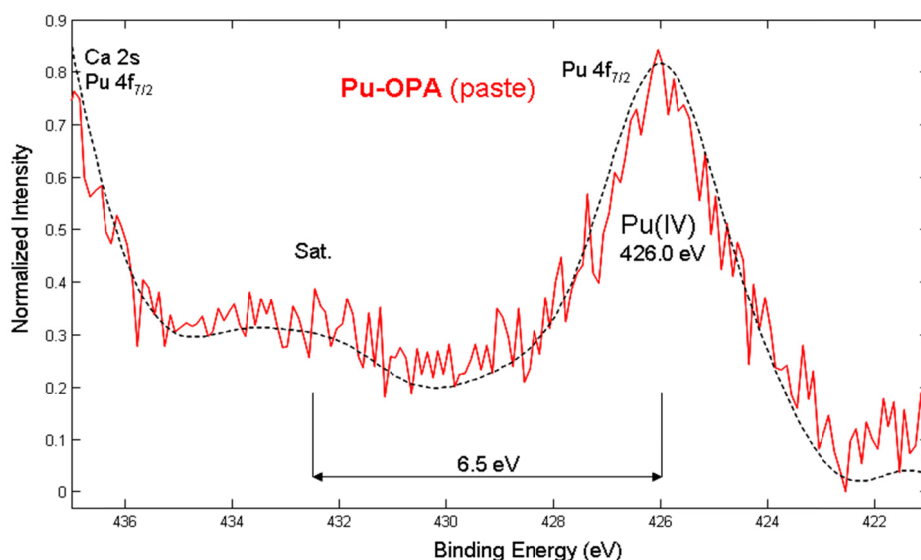


Figure 8: Pu 4f spectrum, Al K α mono x-ray excitation, charges referenced Cls (CH): 284.8 eV. Wet Paste: Opalinus clay + Pu(V) 3×10^{-4} M, 7d contact time.

The relative portion of Fe(II) in the COx sample is less than in the OPA clay. The absolute Fe concentrations within OPA and COx clays are comparable. A change of the Fe 2p spectra upon redox reaction Np and Pu is not detected which is explained by the low actinide concentration.

COx and OPA clays both contain Fe(II) which may be available for redox reaction with added radionuclides while sulphur is oxidized to sulfate and thus is not involved in redox reactions.

Summary and Conclusions

The Np and Pu showed significant sorption on the clay after 1 week, whereas the sorption of Tc is much weaker. Redox speciation by spectroscopic methods exhibits that initial Pu(V) was reduced to Pu(IV), whereas Np(V) and Tc(VII) remains in their initial oxidation states. The sorption of both elements increases with time supposing that they are slowly reduced to the tetravalent oxidation state. This can also be confirmed by a steadily decrease of the Eh to values between -100 and + 50 mV after 4 months without reaching a constant value. More than 80 % of Np and Pu are sorbed on the both clays whereas only 35 % of Tc is bound on OPA and COx with S/L ratios 10-20 after 4 months contact time. Which oxidation state of the radionuclides occurs on the clay after the longer contact times will be characterized by spectroscopic methods (EXAFS, XPS, and TEM) in the next time.

Acknowledgement

This work was supported by the EURATOM 7th Framework Program Collaborative Project “Redox Phenomena Controlling Systems” (CP ReCosy). We thank Mr. D. Fellhauer and Dr. T. Kobyashi for their help with the preparation and electrolysis of the Pu(V) and Tc(VII) stock solution.

References

- Bradbury, M.H.; Baeyens, B.A. (2003). Comparison of Apparent Diffusion Coefficients Measured in Compacted Kunigel V1 Bentonite with Those Calculated from Batch Sorption Measurements and De (HTO) Data: A Case Study for Cs(I), Ni(II), Sm(III), Am(III), Zr(IV) and Np(V). PSI Bericht Nr. 03-02: Villigen, Switzerland.
- Brendebach, B.; Banik, N. L.; Marquardt, C. M.; Rothe, J.; Denecke, M. A.; Geckeis, H. (2009). Radiochim. Acta, 12, 701-708.
- Cohen, D. (1961). Electrochemical studies of plutonium ions in perchloric acid solutions, Journal of Inorganic Nuclear Chemistry, 18, 207.
- Gaucher, E.; Robelin, C.; Matray, J.M.; Negrel, G., Gros, Y., Heitz, J.F., Vinsot, A., Rebours, H., Cassabagnere, A., Bouchet, A., (2004). ANDRA underground research laboratory: Interpretation of the mineralogical and geochemical data acquired in the Callovian– Oxfordian Formation by investigative drilling. Physics and Chemistry of the Earth 29/1, 55 77 (special issue: Water Geochemistry and Hydrogeology).
- Kaszuba, J. P.; Runde, W. H. (1999). The aqueous geochemistry of neptunium: Dynamic control of soluble concentrations with applications to nuclear waste disposal. Environ. Sci. Technol., 33, 4427–4433.
- Krause M. O., Haire R. G., Keski-Rahkonen O. and Peterson J. R. (1988). Photoelectron spectrometry of the actinides from Ac to Es. J. Electron Spectrosc. Relat. Phenom. 47, 215–226.
- Latrille, C.; Herbette, J. Ly and M. (2006). Retention of Sn(IV) and Pu(IV) onto four argillites from the Callovo–Oxfordian level at Bure (France) from eight equilibrated sedimentary waters, Radiochim. Acta, 94, 421–427.
- Nitsche, H., Roberts, K., Xi, R., Prussin, T., Becraft, K., Mahamid, I. A., Silber, H. B., Carpenter, S. A., Gatti, R. C. (1994). Long term plutonium solubility and speciation studies in a synthetic brine. Radiochim. Acta, 66, 3-7.
- Van Loon, L. R.; Baeyens, B.; Bradbury, M. H. (2005). Diffusion and retention of sodium and strontium in Opalinus clay: Comparison of sorption data from diffusion and batch sorption measurements, and geochemical calculations. Appl. Geochem., 20, 2351–2363.
- Wu, T.; Amayri, S.; Drebert, J.; Van Loon, L. R.; Reich, T. (2009). Neptunium(V) sorption and diffusion in Opalinus clay. Environ. Sci. Technol. 43, 6567–6571

QUANTIFICATION OF PYRRHOTITE O₂ CONSUMPTION BY USING PYRITE OXIDATION KINETIC DATA

Domènech, C.¹, Duro, L.^{1*}, Grivé, M.¹, Arcos, D.¹, Rojo, I.², Clarens, F.², de Pablo, J.²

¹Amphos 21 Consulting, S.L. (SP)

²FundacióCTM, Centre Tecnològic (SP)

* Corresponding author: lara.duro@amphos21.com

Abstract

Experiments on the dissolution kinetics of natural pyrrhotite (FeS_{1-x}) and pyrite (FeS₂) under imposed redox conditions have been carried out at 25°C and 1 bar to evaluate the oxygen uptake capacity of both minerals. Measured data indicate that in both cases, Fe^(II) released from kinetic dissolution of Fe-bearing sulphides is kinetically oxidized to Fe^(III), precipitating as Fe^(III)-oxyhydroxides. While the pH of the system is controlled by the extent of sulphide minerals oxidation, the Eh is controlled by the redox pair Fe²⁺/Fe(III)-oxyhydroxides. Pyrrhotite dissolution is faster than that of pyrite but generates less acidity. Consequently, the achieved redox value is more reducing. Experimental data show that oxidation rates of both minerals (in mol·g⁻¹·s⁻¹) are equivalent under the studied conditions. This fact gives a new opportunity to quantify the reductive buffering capacity of pyrrhotite, for which no kinetic rate law has been still established.

Introduction

The maintenance of reducing conditions in and in the vicinity of a hypothetical repository for high level nuclear waste is one of the main issues of concern in any safety assessment exercise. Uranium and other redox sensitive actinides mobility is importantly decreased under reducing conditions. The same happens with selenium and other components of the nuclear wastes. The study of processes contributing to the maintenance of the systems under reducing redox potentials has received special attention and has generated a lot of publications both in the open scientific literature as well as in specifically focused national programmes.

It is well accepted that in most deep groundwaters the redox state is governed by electron transfer between Fe^(II) and Fe^(III) species and/or by sulphate/sulphide reactions. The occurrence of Fe^(II) in nature is dominated by minerals such as Fe^(II) sulphides, pyrite and pyrrhotite being the most common natural Fe-bearing minerals (Belzile et al. 2004).

Due to the difficulty to obtain stable redox potentials from field data, Scott and Morgan (1990) proposed the use of intensive magnitudes to define the redox state of geological systems. They used the concepts of OXidising and ReDucing Capacities (OXC and RDC) defined similarly to magnitudes such as acidity or alkalinity in the case of acid/base systems. The major contribution to the ReDucing Capacity of a system will be given by those species able to react with oxidants and therefore buffer an increase in oxidant concentration.

Despite the intensive magnitudes presented above can give us an idea of the maximum redox buffering capacity of a system, it is also important to consider the rates at which the redox buffer reacts. Iron sulphides are solid phases whose oxidative dissolution is kinetically controlled. The oxidation of sulphide to sulphate implies the transfer of 8 electrons, so that kinetics is possibly going to play a role in the system. In fact, the scientific literature is full with references indicating that the oxidation of sulphide to sulphate is not reversible unless it is catalyzed by the presence of biotic activity.

Pyrrhotite dissolution rates reported in literature are in the range $10^{-10} \sim 10^{-8} \text{ mol m}^{-2} \text{ s}^{-1}$ (Janzen et al. 2000, Wang 2008). However, although there are several studies assessing the mechanism of pyrrhotite oxidation (Belize et al. 2004; Wang 2008), the dependence of the rate on oxygen concentration or pH has not been provided. The lack of reaction rates for pyrrhotite oxidation forces the modeller to use other well-established kinetic rates for Fe-bearing sulphide minerals, being that of pyrite (modified or not) the most widely used. However, the uncertainty concerning the use of this approach is not known.

In this work we present the study of the rate at which common iron sulphide minerals, such as pyrite and pyrrhotite, consume oxygen and are, therefore, able to buffer oxidant intrusions under environmental conditions common to be found in natural groundwaters. To this aim, new kinetic experimental data has been interpreted and quantitatively modelled.

The assessment of the redox buffering capacity, or the ReDucing Capacity of systems containing this type of minerals and their implications for redox front migration will be part of the final investigations within this project.

Description of experimental procedure

Pyrrhotite and pyrite

The pyrrhotite and pyrite used in the experiments were natural samples from the skarn sulfide deposit of Gualba (NE Spain) and from Arnedo (N Spain), respectively. The solids were crushed and sieved to a 100-150 μm particle size.

Experimental setup

Kinetics experiments to evaluate the oxygen uptake capacity of pyrrhotite or pyrite have been performed at two initial dissolved oxygen concentrations, 70 and 20%, at 25 ± 0.2 °C.

The experiments were carried out in a batch reactor as shown in Figure 1. A volume of 350 cm³ of NaClO₄ 10⁻² mol dm⁻³ was placed in the reactor and was saturated with O₂(g) depending on the initial dissolved oxygen concentration desired (70% or 20% respectively). Between 0.5 and 3 g of pyrrhotite or pyrite were added (except in the case of the blank), and the free gas phase was eliminated. Stirring was provided by orbital shaker at 90 rpm in order to keep the solution as homogenous as possible while minimising the risk of solid grinding.

Continuous monitoring of pH, Eh (Pt and Au electrodes) and dissolved oxygen (DO) were carried out with combined-glass electrodes and with an optical sensor. Calibration of pH and Au and Pt Eh electrodes (Crison, models 5221, 5262 & 5269 respectively) was performed against commercial standard buffers before and after each experiment. Additionally, Eh electrodes were mechanically cleaned before each experiment. DO concentrations were measured with an optical sensor (Ocean Optics, FoxyOR125GT & red eye) calibrated at two points: 0 % in 20 % Na₂SO₃ or N₂(g) and 20.9% in open air.

During the experiments aqueous samples were taken periodically and immediately filtered through 0.45 µm pore size filters for analysis. Concentrations of iron Fe^(II) and Fe(total) were determined by the ferrozine method (Gibbs (1976)) by means of UV-Vis spectrophotometry (Shimadzu, 1600). Anion concentrations (sulphate, thiosulphate, chloride...) were determined by ionic chromatography with ion suppression (Dionex, ICS2100). Scanning electron microscopy (SEM) (Zeiss, Ultraplus) was used to characterize the solids.

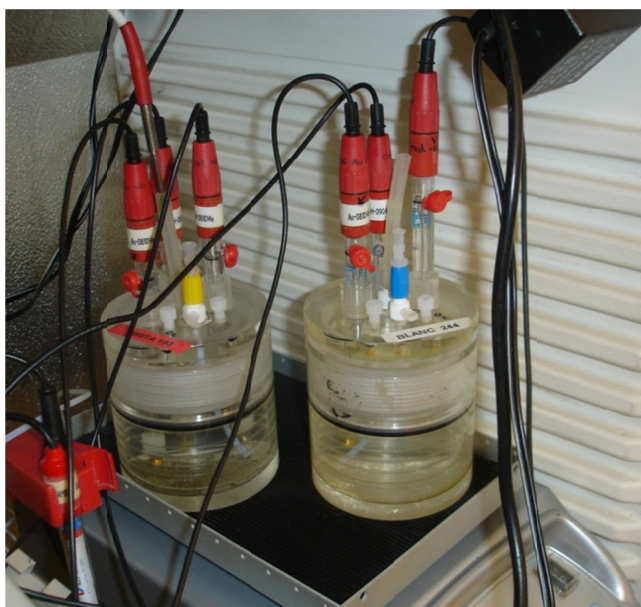


Figure 1: Volume variable batch reactors used for the kinetic experiments.

Discussion

Figures 1 and 2 show the evolution over time of the pH and the Eh (measured with both Pt and Au electrodes) values measured in the pyrite and pyrrhotite kinetic experiments.

These figures also show the temporal evolution of O₂, SO₄²⁻, S₂O₃²⁻, Fe^(II) and Fe_{total} aqueous concentration in both experiments.

In both cases, [O₂] decreases and SO₄²⁻, S₂O₃²⁻, Fe^(II) and Fe_{total} aqueous concentrations increase with time. In the case of pyrrhotite, faster processes are observed. According to the information found in the literature (Nicholson, 1994, Belzile et al. 2004; Murphy and Strongin, 2009) the presence of ordered vacancies within the Fe lattice in the non-stoichiometric pyrrhotite crystal structure (Fe_{1-x}S, x from 0.125 to 0), may be the reason accounting for the faster oxidation rate of pyrrhotite when compared with pyrite.

As seen in r.1 and r.2 oxidation of both pyrite and pyrrhotite generates protons and hence, cause a decrease in pH. However, due to the different crystal structure of both minerals, pyrrhotite oxidation generates less acidity than pyrite oxidation (Nicholson, 1994).

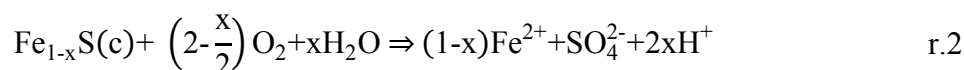
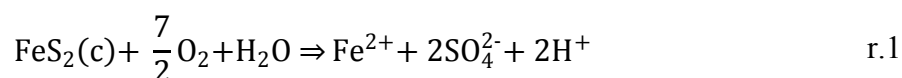
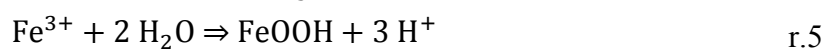
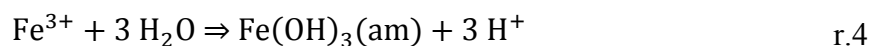


Figure 3 compares the redox potential measured in both experiments with that calculated by assuming a redox control of Fe²⁺-Fe(OH)₃(am) and Fe²⁺/goethite at the measured pH.

In the case of pyrite, the Eh calculated by assuming a Fe²⁺-Fe(OH)₃(am) equilibrium satisfactorily agree with the measured values. In the pyrrhotite case, this equilibrium also seems to control the Eh of the solution at the initial stage after the O₂ injection, while a transition to the redox pair Fe²⁺/goethite seems to occur at longer reaction times.

These results are consistent to both experimental observations and information gathered from literature. From the experiments, the precipitation of Fe-oxyhydroxides onto the pyrrhotite surface can be observed. Fe-oxyhydroxides are the most common oxidation products of pyrite and pyrrhotite under near neutral and alkaline pH (Feng and Van Deventer 2002, Belzile et al. 2004, Wang 2008, Murphy and Strongin 2009).

Results shown in Figure 3 indicate that although pyrite or pyrrhotite dissolution processes are kinetically driven and control the pH of the solution, the redox potential is controlled by the redox pair Fe²⁺/Fe(III)-oxyhydroxides. Fe²⁺ generated in r.1 and r.2 is oxidized to Fe³⁺ (r.3) which under the favourable conditions of neutral to alkaline pHs leads to the precipitation of amorphous Fe-oxyhydroxides which, in turn, may evolve to more crystalline phases (r.4, r.5).



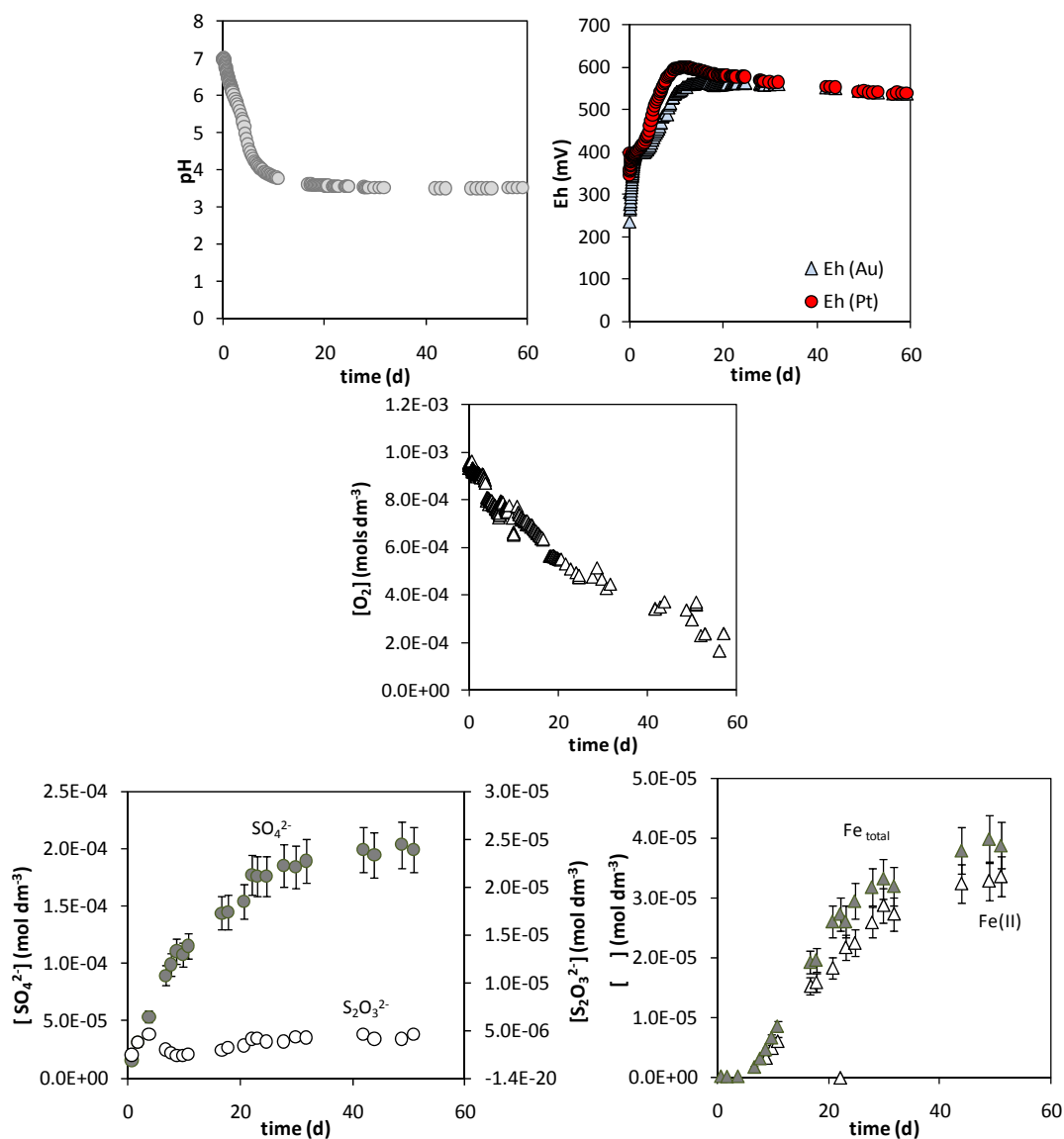


Figure 1: Temporal evolution of pH, Eh and O_2 , SO_4^{2-} , $S_2O_3^{2-}$, $Fe^{(II)}$ and Fe_{total} aqueous concentration obtained in the pyrite kinetic dissolution experiment.

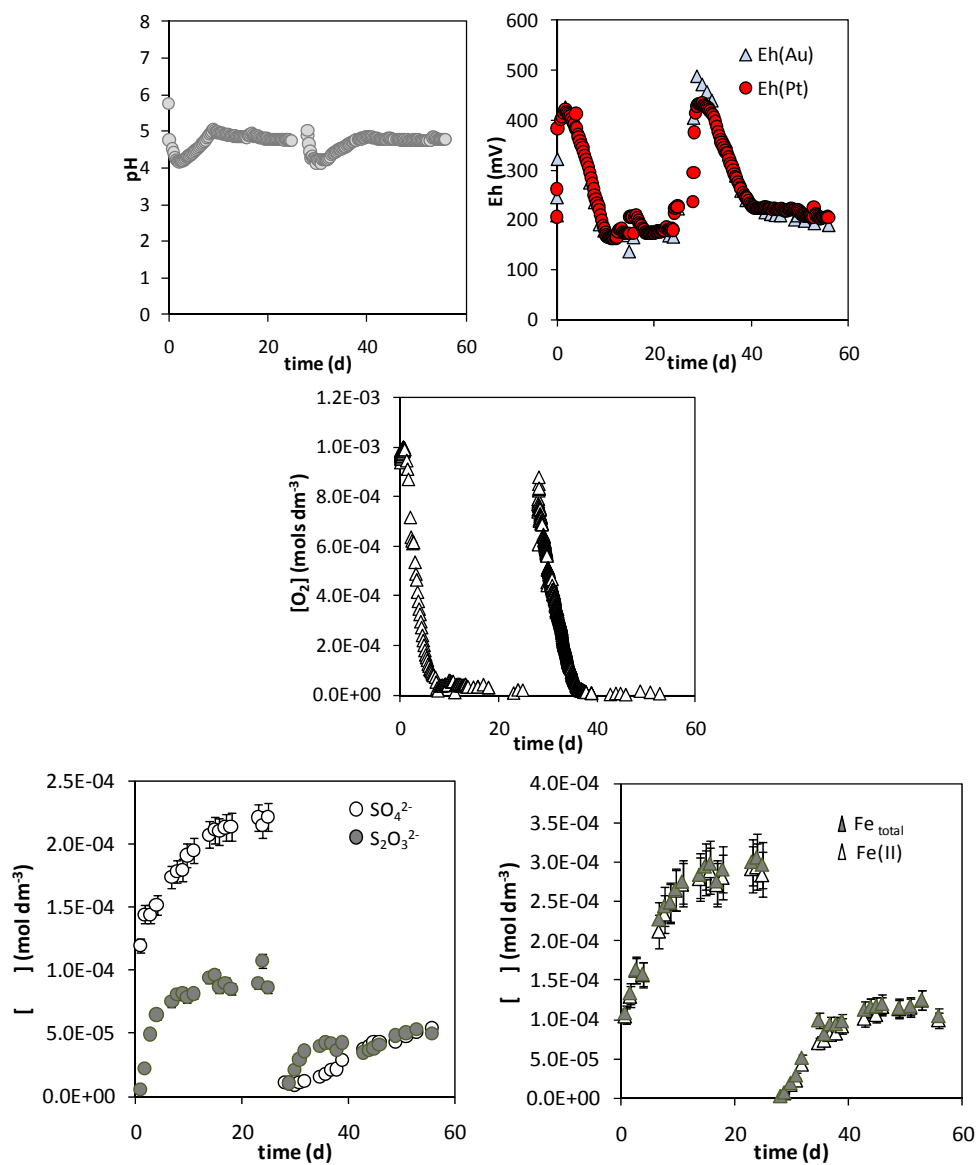


Figure 2: Temporal evolution of pH, Eh and O_2 , SO_4^{2-} , $S_2O_3^{2-}$, $Fe^{(II)}$ and Fe_{total} aqueous concentration obtained in the pyrrhotite kinetic dissolution experiment.

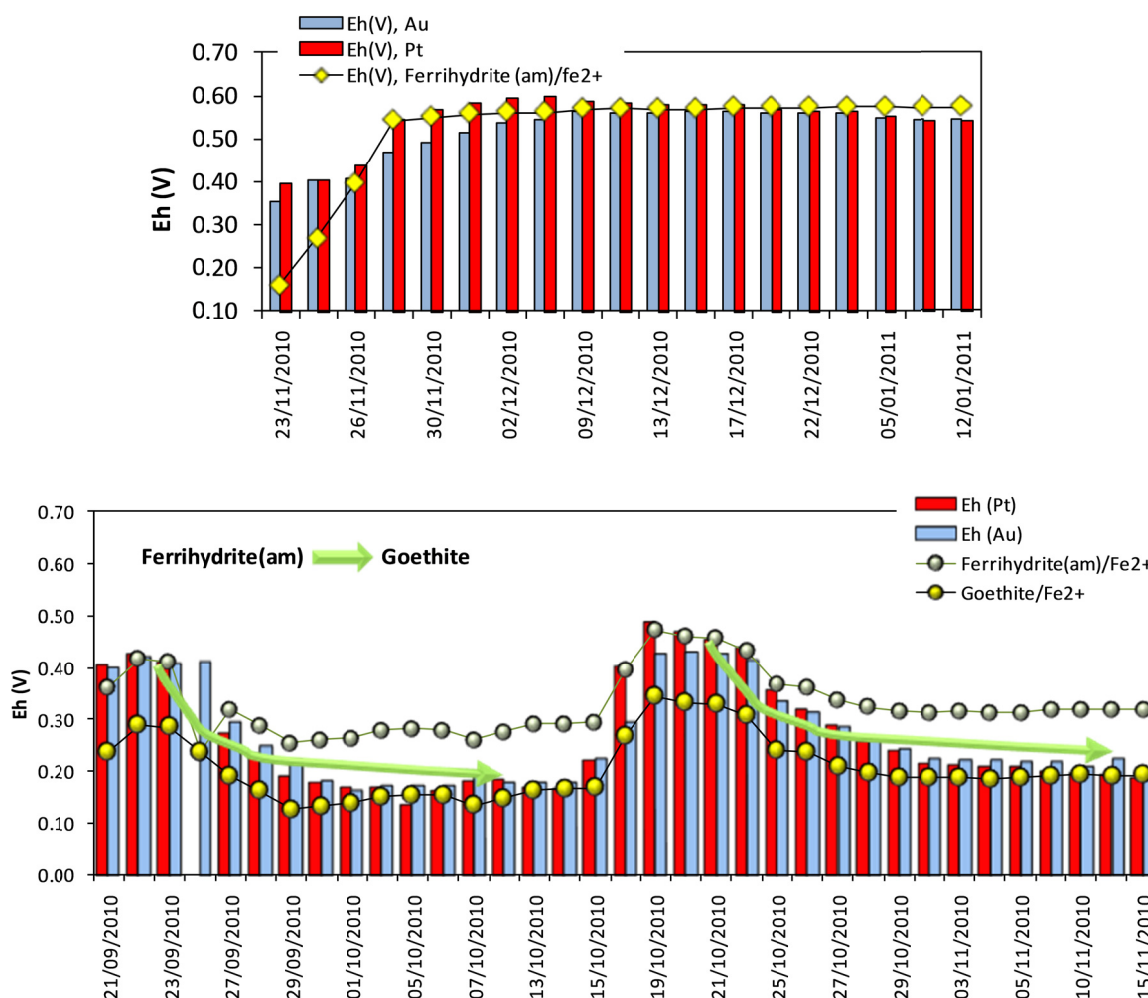


Figure 3: Comparison of the measured Eh values (in V, bars) with the calculated Eh values assuming a redox control by Ferrihydrite (am)/Fe²⁺ and goethite/Fe²⁺ equilibrium at the sample pH. Top: pyrite experiment. Bottom: pyrrhotite experiment.

Oxidation of Fe^(II) to Fe^(III) (r.3) is kinetically controlled. Singer and Stumm (1970) proposed a reaction rate of second order with respect OH⁻ for this reaction, according to which, for pH above pH 4, the abiotic oxidation rate of Fe(II) is high enough to compete with the biotic oxidation rate. For pH below 4, the abiotic oxidation rate is not significant and Fe²⁺ can only be oxidized to Fe³⁺ biotically.

Figure 4 shows that the redox potential determined in the pyrite experiments is in agreement with the oxidation to ferrihydrite, while in the case of using pyrrhotite the control exerted by goethite prevails with time.

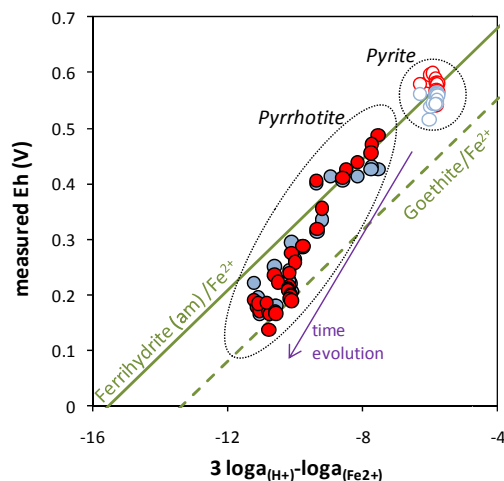


Figure 4: Measured Eh values (blue: Au electrode; red: Pt electrode) vs $3 \log a_{(H^+)} - \log a_{(Fe^{2+})}$ obtained in the pyrite and pyrrhotite kinetic experiments. Lines show the Eh values corresponding to the equilibrium $Fe(OH)_3(am)/Fe^{2+}$ and goethite/ Fe^{2+} .

The evolution of pH and Eh in the different systems is shown in Fig. 5.

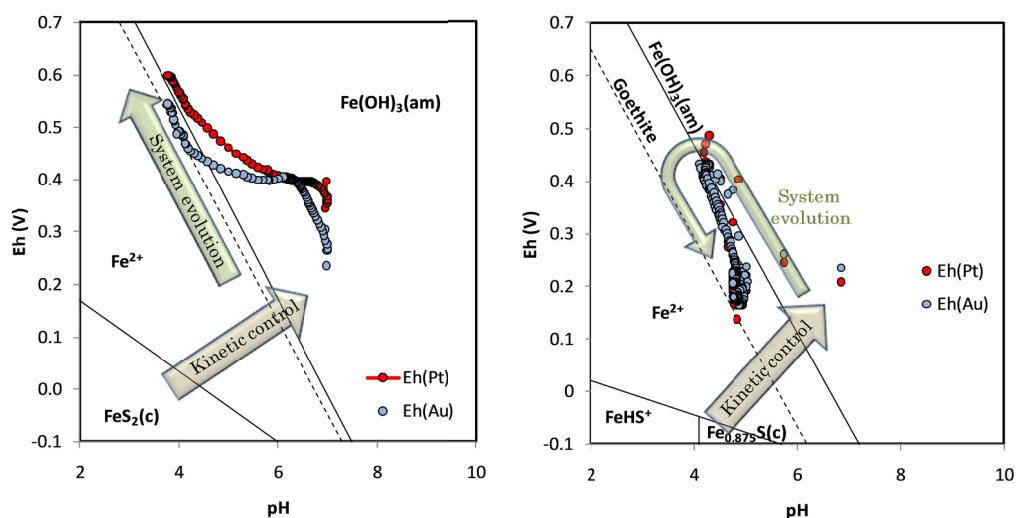


Figure 5: Evolution of Eh and pH values measured in the pyrite (left) and pyrrhotite (right) kinetic experiments plotted in a Eh-pH predominance diagrams of Fe-S system ($[Fe]_{total} \sim [SO_4^{2-}] \sim 10^{-4}$ M, $T=25^\circ C$). Arrows indicate the direction of the system evolution.

We have tested the above derived observations, by reproducing the experimental values with the code PHREEQC (Parkhurst and Appelo, 1999) and ThermoChimie data base (Duro, 2010). In the case of pyrite kinetic experiment we have assumed that pyrite is dissolving kinetically according to the rate of Williamson and Rimstidt (1994) and that Fe^{2+} generated oxidises kinetically to Fe^{3+} according to the kinetic law of Singer and Stumm (1970). Ferrihydrite is left to precipitate in equilibrium. Initial O_2 aqueous concentration corresponds to that in equilibrium with 70% $O_2(g)$ in the gas phase. The reactive area of pyrite has been set to $0.06 \text{ m}^2 \text{ g}^{-1}$. As can be seen in Figure 6, the numerical model satisfactorily explains the experimental data.

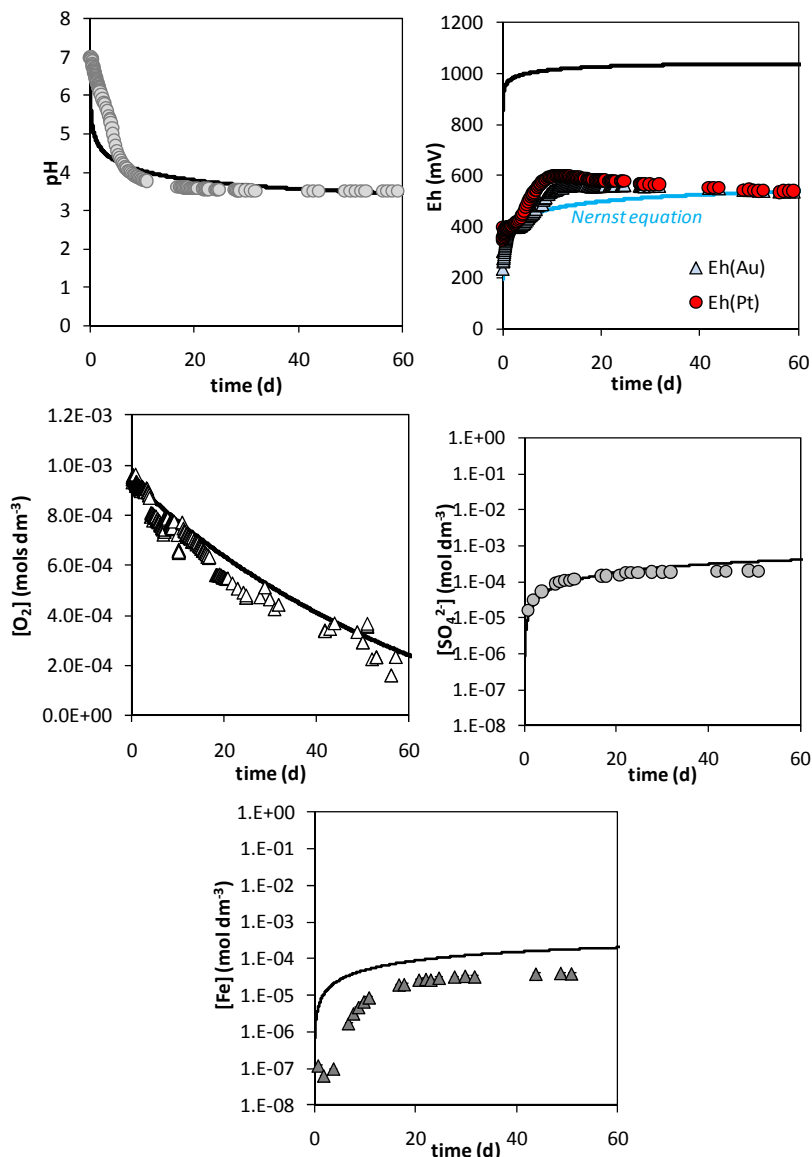


Figure 6: Temporal evolution of pH, Eh and O_2 , SO_4^{2-} , $S_2O_3^{2-}$, Fe(II) and Fe_{total} aqueous concentration obtained in the pyrite kinetic dissolution experiment (dots) compared to the curves obtained in the model (black solid lines). Eh blue line has been calculated using eq.1 with $Eh^0 = 0.919$ V.

In this paper we have seen that processes occurring in both experiments are similar and that the observed differences are a consequence of the extent of mineral oxidation. Figure 7 compares the O_2 consumption rates (in $mol \cdot g^{-1} \cdot s^{-1}$) we have calculated from O_2 concentration data measured in each experiment. In the case of pyrrhotite only data for the first cycle has been used. As can be seen, once the transient state has finished, the consumption rate in $mol \ O_2 \ g^{-1} \cdot m^{-2}$ of pyrrhotite and pyrite is equivalent. This observation opens a new door to estimate the effects that pyrrhotite oxidation can have on the final pH and Eh of a host rock of a HLNWR. Results shown in this paper have revealed that processes occurring in the oxidation of pyrite and pyrrhotite can be quantified by the same oxidation rates in terms of $mol \ O_2 \ g^{-1} \ m^{-2}$ at mid-term.

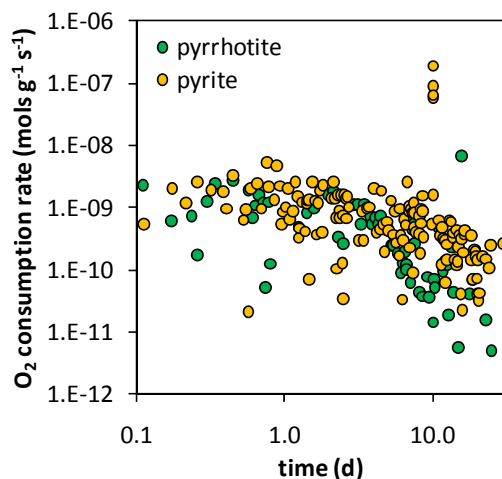


Figure 7: O_2 consumption rate (in $\text{mols g}^{-1} \text{s}^{-1}$) calculated from pyrite and pyrrhotite kinetic experiments.

Summary and Conclusions

In this paper we present the results of the kinetic dissolution of pyrite and pyrrhotite in a 0.01M NaClO_4 solution and an initial concentration of $O_2(\text{g})$ of 70%. Results indicate that pyrrhotite dissolves faster but generates less acidity than pyrite. In both cases, the final Eh is controlled by the redox pair $\text{Fe}^{2+}/\text{Fe(III)}$ oxyhydroxides. Differences in redox potentials can be explained by the different pH. O_2 consumption rates calculated from pyrite and pyrrhotite experiments are equivalent indicating that knowledge gathered from pyrite oxidation process can be applied to evaluate the reduction capacity of pyrrhotite. Next steps within this project will be focused on studying how to achieve the incorporation of these kinetic data in the calculations in reactive transport codes, in order to account for the consumption of oxidants in geological media.

Acknowledgements

The European Atomic Energy Community Seventh Framework Programme [FP7/2007-2013] under grant agreement n° 212287, Collaborative Project ReCosy is thanked for financial support.

References

- Belzile, N., Chen, Y.W., Cai, M.F., Li, Y. (2004) A review on pyrrhotite oxidation. *Journal of geochemical exploration* 84, 65-76.
- Feng, D., van Deventer, J.S.J. (2002) Leaching behaviour of sulphides in ammoniacal thiosulphate systems. *Hydrometallurgy* 63, 189–200.
- Gibbs C. (1976). Characterization and application of ferrozine iron reagent as ferrous iron indicator. *Anal. Chem.* 48, 1197-1200.
- Grenthe, I., Stumm, W., Laaksoharju, M., Nilsson, A.C., Wikberg, P. (1992) Redox potentials and redox reactions in deep groundwater systems. *Chemical Geology*, 98, 131-150.

Janzen, M.P., Nicholson, R.V., Scharer, J.M. (2000) Pyrrhotite reaction kinetics: Reaction rates for oxidation by oxygen, ferric iron, and for nonoxidative dissolution. *Geochimica et Cosmochimica Acta*, 64 (9) 1511–1522.

Murphy, R.; Strongin, D.R. (2009) Surface reactivity of pyrite and related sulfides. *Surface Science Reports* 64, 1-45.

Nicholson, R.V. (1994) Iron-sulfide oxidation mechanisms: laboratory studies. In J.L. Jambor, D.W. Blowes (eds). *Short course handbook on environmental geochemistry of sulfide mine wastes* 22, Mineralogical Association of Canada, 163-183.

Parkhurst, D.L.; Appelo, C.A.J. (1999) User's guide to PHREEQC ((v 2.17.5))-A computer program for speciation, batch-reaction, one-dimensional transport and inverse geochemical calculations. Washington D.C., USGS, Water resources investigations report 99-4259, 326p.

Scott, M.J., Morgan, J.J. (1990) Energetic and conservative properties of redox systems. In (eds) American Chemical Society, 368-378.

Singer, P.C. and Stumm, W. (1970) Acidic mine drainage: the rate determining step. *Science* 167, 1121-1123.

Wang, H. (2008) A review on process-related characteristics of pyrrhotite. *Mineral Processing and Extractive Metallurgy Reviews*, 29, 1 -41.

Williamson, M.A., Rimstidt, J.D. (1994) The kinetics and electrochemical rate-determining step of aqueous pyrite oxidation. *Geochimica et Cosmochimica Acta* 58 (4), 5443-5454.

ELECTROCHEMICAL INVESTIGATIONS ON DOPED AND UNDOPED UO₂ SPENT FUEL MODEL SURFACES

T. Petersmann¹, A. Seibert¹, D.H. Wegen¹, T. Gouder^{1*}, S. Stumpf¹, Th. Fanghänel¹

¹ European Commission, JRC, Institute for Transuranium Elements, Herrmann-von-Helmholtz-Platz 1, 76344 Eggenstein-Leopoldshafen (D)

* Corresponding author: thomas.gouder@ec.europa.eu

Abstract

Electrochemistry studies were carried out on UO₂ and Pd-doped UO₂ films, prepared by sputter deposition. The UO₂/Pd films are used as models to study the influence of ϵ -particles on the surface corrosion of spent nuclear fuel (SNF). The films provide a less complex system than real SNF samples, allowing for mechanistic investigations. Surface composition and chemical state are checked by X-ray Photoelectron Spectroscopy (XPS). The redox behaviour was investigated by open circuit potential measurements (OCP). Previous measurements under oxidative conditions were extended to a more reductive environment (Ar, Ar/H₂). Aim of the studies is to clarify the mechanism of SNF matrix stabilization by H₂ in aqueous solution. Special emphasis was put on the reaction of the system when switching from oxidative to reductive conditions or vice-versa.

Introduction

Spent nuclear fuel (SNF) consists of 95% UO₂. The remaining 5% is a mixture of radionuclides and fission products, which are heterogeneously distributed throughout the fuel matrix in different phases e.g.: gases (Xe, Kr, I), oxides (U, Pu, Np, ...) and metallic precipitates, the so called ϵ -particles (Pd, Mo, Rh, Ru, ...) (Kleykamp 1985; Bruno 2006).

For long-term storage in a nuclear waste repository oxidation and dissolution of SNF matrix represents an important source term for the mobilization of radionuclides (Johnson 1988; Shoesmith 2000; Buck 2004; Johnson 2005)

The solubility of UO₂ in water (Neck 2001) is low under reductive conditions providing high stability of the spent fuel matrix. Nevertheless radiolysis at the SNF surface in contact with water, after groundwater intrusion into corroded container, produces oxidants like $\cdot\text{OH}$, $\cdot\text{HO}_2$ and H₂O₂. These can oxidize the fuel surface leading to generation of U(VI) species, which then dissolve more easily to the aqueous phase due to the higher solubility of the hexavalent uranium and complexation by ligands present in the groundwater (Sunder 1997; Christensen 2000; Rondinella 2000; King 2004;

Poinssot 2005).

On the other hand reducing species, such as hydrogen, are also produced during water radiolysis (Spinks 1964) and mainly by the corrosion of the steel containment. Spent fuel leaching experiments in the presence of H₂ have shown a very strong influence of hydrogen on the radionuclide leaching and fuel corrosion rates, which could be decreased by four orders of magnitude in the presence of hydrogen [Roellin 2001].

The precise mechanism of the effect of H₂ is unclear up to now. SIMFUEL studies show that Pd plays a significant role in the corrosion inhibition by H₂ for SNF (Cui 2004; Nilsson 2008b; Nilsson 2008a; Trummer 2008; Trummer 2009) but there might be also an effect of the UO₂ surface itself (Heynen 1977; Spahiu 2004; Carbol 2009).

It is reasonable that the first reaction step is a dissociative adsorption of the H₂ on the fuel surface. For Pd such dissociative adsorption is well known (Mitsui 2003). A (similar) dissociative adsorption may take place on defect sites of the UO₂ surface itself. The activated hydrogen can react in several ways:

1. Galvanic coupling of the H₂ / H⁺ reaction at the Pd surface to the UO₂ surface (introducing electrons into the UO₂ matrix). This shifts the observed (mixed) potential (OCP) to lower values, even below the potential for surface oxidation of UO₂ (~ 0.15 V vs. SHE) (Broczkowski 2005).
2. Radiolytically produced oxidants are reduced in heterogeneous surface reactions, taking place between adsorbed H_{atom} and the adsorbed oxidants (Trummer 2008; Trummer 2009)
3. The reduction of U(V)/(VI) surface sites by activated H_{atom} that has diffused from the adsorption site to the reaction site (King 2004). This mechanism has been observed in gas adsorption experiments (Stumpf 2010), but it is not clear yet if it is also active at a solid-solution interface, instead the solid-gas interface

The corrosion processes consists in a series of different electrochemical reactions occurring on the surface of the corroding material. The potential at which the anodic and cathodic reaction currents are of equal magnitude (therewith producing a net current of 0) is named corrosion potential for homogeneous material. For heterogeneous materials the measured (steady-state) potential is a mixed potential depending on all the anodic and cathodic reactions. In literature the corrosion behaviour of UO₂ surfaces as function of the surface redox conditions is often described by means of this open circuit potential, OCP. Shoesmith et al. developed the Mixed-Potential Model which is most reliable under oxidizing conditions (Shoesmith 1998). The same model can also predict the dissolution rate under reducing conditions, because the dissolution rate should be related to the potential also in this case.

In a first set of experiments, the reactivity of SNF model surfaces (UO₂/Pd_x thin films) was investigated in electrochemical experiments under oxic conditions. The corrosion of UO₂ in (aerated) aqueous solution is decreased (lower anodic currents / less dissolution observed in cyclic voltammetry) when Pd is incorporated into the oxide surface. The formation of secondary phases on the UO₂ surface (built up in subsequent cathodic scans) disabled this inhibiting effect of Pd.

In the present work the electrochemical studies are extended to a more reductive environment (Ar, Ar/H₂) to clarify the mechanism of SNF matrix stabilization especially by H₂ in aqueous solution. Emphasis is put on the reaction of the system when switching from an oxidative environment to a reductive or vice-versa.

Experimental

Thin films of UO₂Pd were prepared by in situ sputter co-deposition from U (99.9% purity) and Pd (99.9% purity) targets at an O₂ (99.99% purity) partial pressure of $1.2 \cdot 10^{-6}$ mbar and Argon (99.9999% purity) was used as sputter gas at $4 \cdot 10^{-3}$ mbar. The Argon plasma was generated electrons (50-100eV) emitted from a hot W cathode and ionizing the Ar atoms. The films were deposited on piezoelectric quartz crystals coated with gold electrodes, used for the electrochemical investigations. Films were heated to ~200°C during deposition to allow ϵ - particles formation (Cui 2004; Stumpf 2009). The film composition was determined by photoelectron spectroscopy (XPS). In our investigation we focused on Pd dopings ~5 %, which is high enough to allow for analysis by XPS, although the ϵ -particle concentration in spent fuel is lower (1% total, 0.17% Pd and 0.3% Mo (Bruno 2006)).

Open circuit potential measurements (OCP) were carried out with an electrochemical quartz microbalance system (Model 430) from CH Instruments. The electrochemistry cell was placed in a closed box with gas inlet and electrolyte storage (Figure 1). This set-up allows providing oxidative (air), anoxic (Ar) and reducing conditions (Ar/H₂) during the experiments.

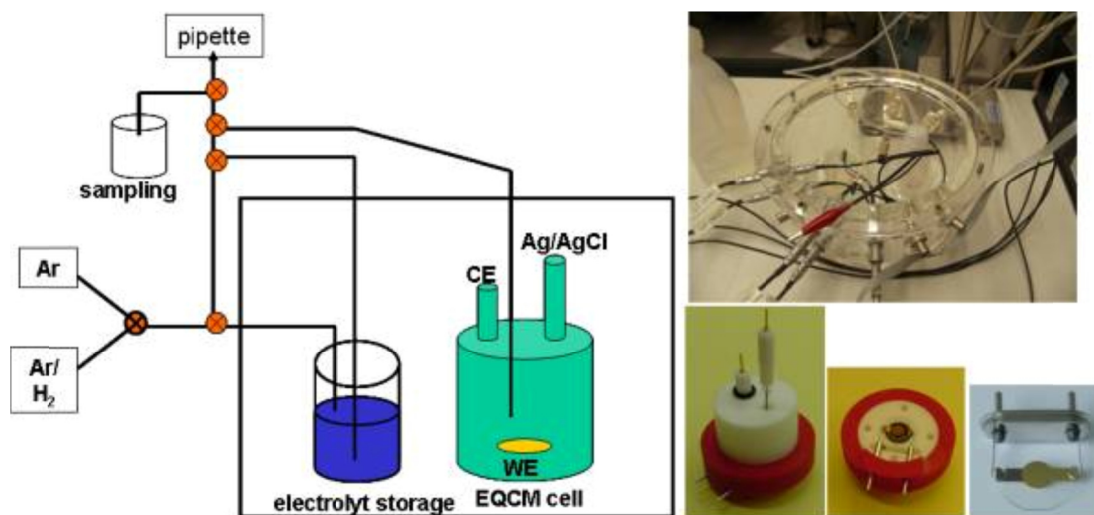


Figure 1: Electrochemical set-up used for measurements under controlled conditions.

For all experiments the films were prepared freshly and analysed by XPS under UHV. 0.01M NaCl was used as electrolyte and purged with the reaction gas (Ar, Ar/H₂) for 30 min before the experiment. The closed box was purged with the gas for the complete time of the experiment with a pressure of about 0.3 mbar. Experiments were carried out at room temperature. An Ag/AgCl (3M KCl) reference electrode was used and data

were corrected to standard hydrogen electrode (SHE) afterwards.

Before each OCP measurement the electrodes were conditioned by cathodic polarisation at -0.995 V (vs. SHE) for 400 sec.

Results and Discussion

Oxidizing and anoxic conditions

The influence of Pd doping on the OCP of UO_2 under air was investigated by using the freshly prepared films as working electrode.

Figure 2 summarises the measurements for thin film electrodes (UO_2 , and UO_2/Pd with different Pd content) and a Pd metal electrode. For a pure UO_2 film the OCP reaches a steady state after 6 hours at about 250 mV (vs SHE) which is similar to results found for SIMFUEL (without ϵ -particles) under oxygen. Selected literature data are shown together with our own results in *Table 1*. The potential is clearly higher than the potential for the onset of surface oxidation (Shoesmith 2000; Santos 2004) and therewith UO_2 corrosion can be expected.

With increasing palladium amount the open circuit potential increases, shifting closer to the value of a pure Pd metal electrode. Even the 2% doped film shows an increase of the potential (~ 0.05 V vs. SHE) which is thought to be due to the noble metal doping.

For the literature data (SIMFUEL with and without ϵ -particle doping under O_2) no significant change of the OCP is observable.

The measured potential is always a combination of single potentials therefore the mixed potentials of UO_2/Pd are placed between pure UO_2 and pure Pd electrodes.

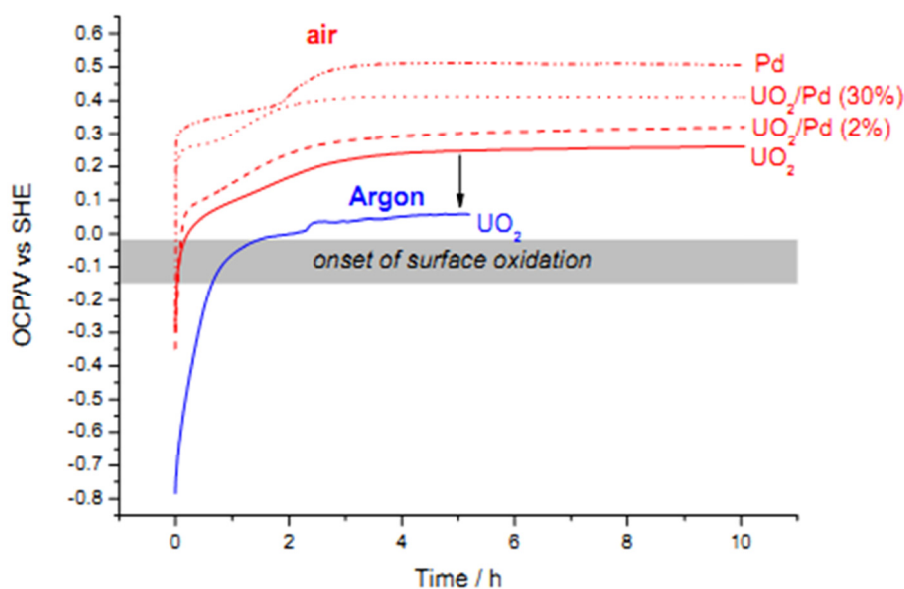


Figure 2: OCP measurements on thin film electrodes (UO_2 , UO_2/Pd) and a Pd-film electrode under air (resp. argon).

OCP measurements under argon atmosphere give lower potentials (see also Table 1) than found for the oxic system. This is in accordance with literature where for

SIMFUEL with and without ε -particles values ~ 0 mV are observed, for UO_2 pellets even values down to -0.166 mV.

Reducing conditions

Experiments under reducing conditions were carried out under Ar/H_2 (5% H_2); results are summarised in Figure 3. For the pure UO_2 film a potential of around 0 mV (vs SHE) is measured which is 250 mV lower compared to the one obtained under air. The absolute value is similar to measurements under Argon. This indicates a decrease of the corrosion potential due to very low concentrations of oxidants. A much stronger response to the presence of H_2 is shown by the UO_2/Pd electrodes. Here the potential after 4 h is still below the threshold for surface oxidation of UO_2 . These findings correspond to the trend reported in literature (the given absolute values are higher). Although the steady state was not reached during the experiment the clear effect of H_2 in presence of Pd could be demonstrated. The different behavior observed for electrodes with and without Pd doping shows that this element plays an important role in suppressing the oxidation of UO_2 .

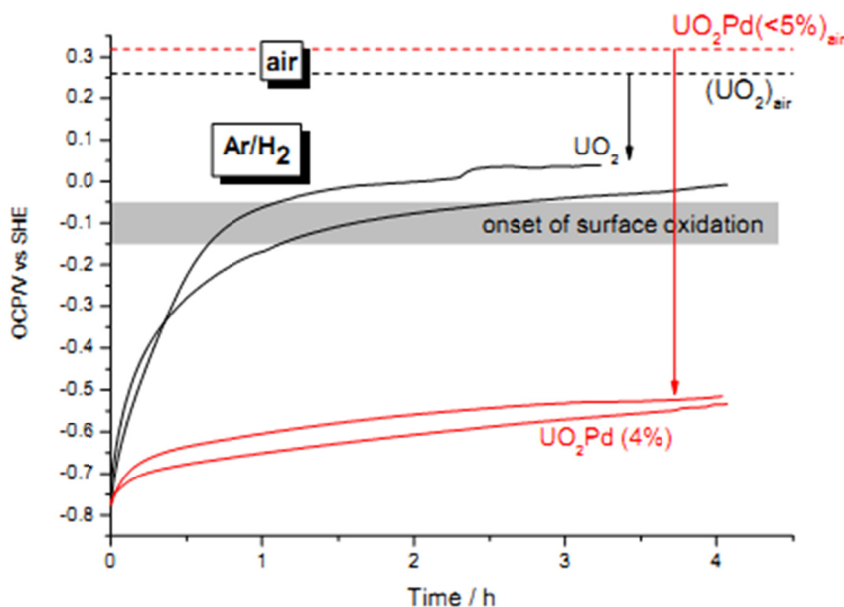


Figure 3: Influence of Pd doping on the OCP under Ar/H_2 atmosphere; black curves: undoped UO_2 films, red curves UO_2 doped with 4 % Pd. Dotted lines indicate corresponding OCP values under air (compare Figure 2).

One possible explanation is that H_2 is activated on Pd, which is acting as galvanically coupled anode within the UO_2 matrix and is leading to a decrease of the corrosion potential and inhibition of UO_2 oxidation. But also reduction of dissolved oxidants or the surface itself by surface hydrogen is possible, as described in the introduction.

The reversibility of the redox reactions was checked by experiments under changing redox conditions.

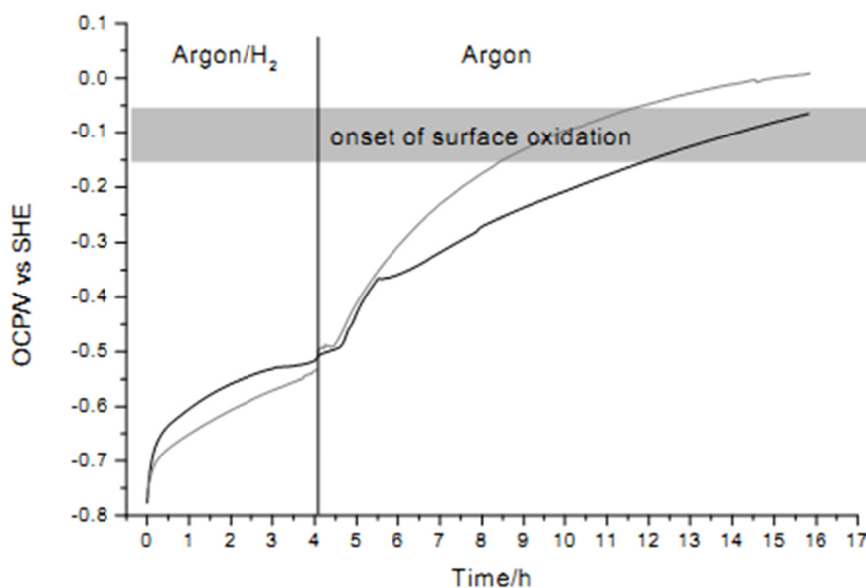


Figure 4: OCP of UO_2 films doped with 5% Pd; changing experimental conditions from Ar/H_2 to Ar .

The OCP of UO_2Pd (5% Pd) was measured first under Ar/H_2 , then the atmosphere was switched to pure Ar and vice versa. *Figure 4* shows that after half an hour the system reacts strongly to the changed conditions. The OCP increases from around -500 mV (vs SHE) to 0 mV (SHE) after 12 h.

The initial delay may be explained by the time needed to remove the remaining H_2 from solution and the dissociated H from surface.

Figure 5 shows the results of the reverse experiment: starting under anoxic (Ar) and switching to reducing conditions (Ar/H_2). Under Argon the OCP reaches a steady state at about 0 mV after ~ 1 h. After switching to Ar/H_2 the potential immediately decreases. At the end of the experiment (after nearly 5 h) the potential has dropped to -177 mV. But it does not reach a value as low as in the experiments started directly under Ar/H_2 (Fig. 3).

This might be due to the fact that after 1 hour of Ar purging, during which the surface was at a potential ~ 0 mV, the surface composition has changed due to oxidation and afterwards Ar/H_2 treatment cannot drop the potential during scan time. This could be due to a kinetic effect, that 4-5 h is not enough to obtain a steady state in this reverse scenario.

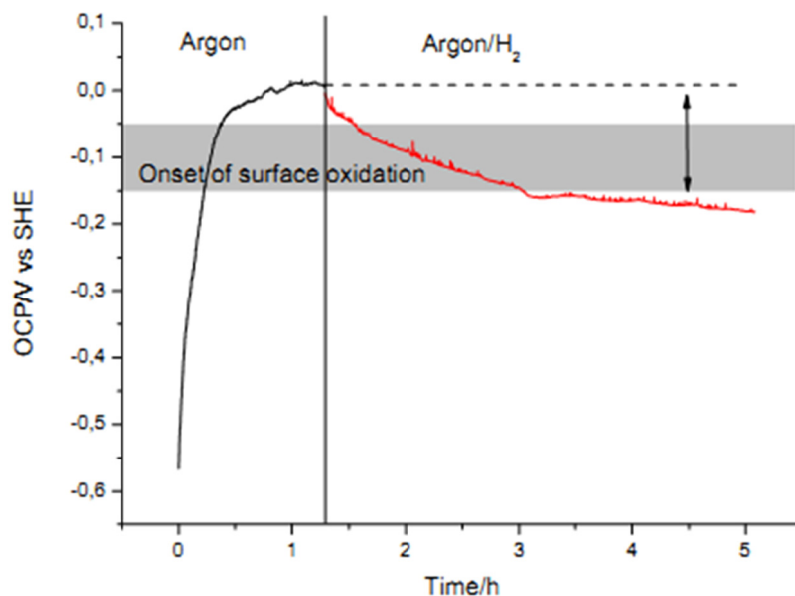


Figure 5: OCP of UO_2Pd film (4% Pd); changing from anoxic to reducing conditions.

Table 1: Summary of the measured OCP (bold) and selected reference data from ^aSIMFUEL experiments with (w) and without (wo) ϵ -particles (Broczkowski 2007), ^bSKB UO_2 pellets (Kim, 1999), ^cCANDU UO_2 pellets (Shoesmith, 1989) and ^dthin film (Miserque, 2001).

Material	Properties	Purging gas	OCP/V vs. SHE
Pd	100%Pd	air	0.505
UO_2Pd	30% Pd	air	0.408
UO_2Pd	2% Pd	air	0.319
UO_2	100% UO_2	air	0.260
UO_2^d	100% UO_2	air	0.189
CANDU ^c	UO_2 pellets (unirradiated)	O_2	0.344
SIMFUELwo ^a	3.0 at. % burn up	O_2	0.250
SIMFUELw ^a	3.0 at. % burn up (with ϵ -particles)	O_2	0.254
UO_2	100% UO_2	Ar	0.061
SKB1 ^b	UO_2 pellets (unirradiated)	Ar	-0.126
SKB2 ^b	UO_2 pellets (unirradiated)	Ar	-0.166
SIMFUELwo ^a	3.0 at. % burn up	Ar	0.064
UO_2Pd	5% Pd	Ar	0.019
SIMFUELw ^a	3.0 at. % burn up (with ϵ -particles)	Ar	0.014
UO_2	100% UO_2	Ar/H_2	0.041
SKB3 ^b	UO_2 pellets (unirradiated)	H_2	-0.216
SKB4 ^b	UO_2 pellets (unirradiated)	H_2	-0.186
SIMFUELwo ^a	3.0 at. % burn up	H_2	0.064
UO_2Pd	4% Pd	Ar/H_2	-0.519
SIMFUELw ^a	3.0 at. % burn up	H_2	-0.106

Conclusions

The influence of oxic (air), anoxic (Ar) and reducing (Ar/H₂) conditions on the corrosion of UO₂ has been studied by OCP measurements on UO₂/Pd thin films.

Under oxic conditions open circuit potentials above the threshold of UO₂ oxidation were obtained. With increasing amount of Pd in the UO₂ matrix the OCPs shifted from 0.260 V (UO₂) to 0.408 V (UO₂/Pd 30 %) and up to 0.505 V for the pure Pd-system. These values are similar to literature data.

Under Ar/H₂ conditions the potential of both UO₂ and UO₂Pd films decreased. For UO₂ this is just due to the absence of oxidants and the reached potentials are equal to those under pure Ar. The presence of Pd led to a decrease of the OCP below the threshold for surface oxidation of UO₂ and therefore fuel corrosion should be inhibited.

Switching between anoxic and reducing conditions showed that the UO₂/Pd system reacts to the presence and absence of H₂. It is not clear up to now if the reaction is completely reversible. When switching from Ar to Ar/H₂ the surface potential dropped significantly. But it was not possible to reach the low OCP value of a surface only exposed to Ar/H₂ without pre-oxidation, at least on the time scale of the measurement. .

Outlook

The studies in anoxic / reductive environment (Ar, Ar/H₂) will be accomplished by other electrochemical methods to clarify the mechanism of SNF matrix stabilization especially by H₂ in aqueous solution. In addition to the described open circuit potential measurements, cyclic voltammetry measurements and current-time measurements at a given potential are planned. We plan to use an in-situ electrochemistry cell directly mounted on the surface science instrument, where thin film preparation and analysis are accomplished under ultra- high vacuum conditions. This setup allows carrying out thin film preparation, electrochemical measurements and surface analysis by XPS without exposing the samples to the laboratory atmosphere. Surface oxidation by air can thus be avoided.

In a next step similar experiments will be carried out on UO₂/Mo films. Although Mo is less efficient than Pd for hydrogen activation, it is the main component of the ϵ -phase. It buffers the oxidation of UO₂ (Kleykamp 1985; Kleykamp 1985a). Therefore it will also have an influence on the overall corrosion process.

References

- Broczkowski, M. E., Noell, J. J. and Shoesmith, D. W. (2005). "The inhibiting effects of hydrogen on the corrosion of uranium dioxide under nuclear waste disposal conditions." *Journal of Nuclear Materials* 346: 16-23.
- Broczkowski, M. E., Noell, J. J. and Shoesmith, D. W. (2007). "The influence of dissolved hydrogen on the surface composition of doped uranium dioxide under aqueous corrosion conditions." *Journal of Electroanalytical Chemistry* 602: 8-16.
- Bruno, J. and Ewing, R. C. (2006). "Spent Nuclear Fuel." *Elements* 2: 343 - 349.

- Buck, E. C., Hanson, B. D. and McNamara, B. K. (2004). The geochemical behaviour of Tc, Np and Pu in spent nuclear fuel in an oxidizing environment. Energy, waste and the environment : a geochemical perspective. R. Gieré, P. Stille,(eds.), The Geological Society of London Special Publication. 236: 65-88.
- Carbol, P., Fors, P., Van Winckel, S. and Spahiu, K. (2009). "Corrosion of irradiated MOX fuel in presence of dissolved H₂." Journal of Nuclear Materials 392: 45-54.
- Christensen, S. and Sunder, S. (2000). "Current state of knowledge of water radiolysis effects on spent nuclear fuel corrosion." Nuclear Technology 131: 102-123.
- Cui, D., Low, J., Sjöstedt, C. J. and Spahiu, K. (2004). "On Mo-Ru-Tc-Pd-Rh-Te alloy particles extracted from spent fuel and their leaching behavior under Ar and H₂ atmospheres." Radiochimica Acta 92: 551-555.
- Heynen, H. W. G., Berkel, C. G. M. M. C.-v. and van der Baan, H. S. (1977). "Kinetics of the reduction of uranium oxide catalysts." Journal of Catalysis 48: 386-394.
- Johnson, L., Ferry, C., Poinssot, C. and Lovera, P. (2005). "Spent fuel radionuclide source- term model for assessing spent fuel performance in geological disposal. Part I: Assessment of the instant release fraction." Journal of Nuclear Materials 346: 56-65.
- Johnson L. H. and Shoesmith, D. W. (1988). Spent Fuel. Radioactive waste forms for the future. W. Lutze,(eds.): 635-698.
- King, F., Quinn, M. J. and Miller, N. H. (1999). "The effect of hydrogen and gamma radiation on the oxidation of UO₂ in 0.1 mol NaCl solution." SKB Svensk Kärnbränslehantering AB: TR-99-27
- King, F. and Shoesmith, D. W. (2004). "Electrochemical studies of the effect off H₂ on UO₂ dissolution." SKB Svensk Kärnbränslehantering AB: TR-04-20
- Kleykamp, H. (1985). "The chemical state of the fission products in oxide fuels." Journal of Nuclear Materials 131: 221-246.
- Kleykamp, H., Paschoal, J. O., Pejša, R. and Thümmel, F. (1985). "Composition and structure of fission product precipitates in irradiated oxide fuels: Correlation with phase studies in the Mo-Ru-Rh-Pd and BaO-UO₂-ZrO₂-MoO₂ Systems." Journal of Nuclear Materials 130: 426-433.
- Miserque, F., Gouder, T., Wegen, D. H. and Bottomley, P. D. W. (2001). "Use of UO₂ films for electrochemical studies." Journal of Nuclear Materials 298: 280-290.
- Mitsui, T., Rose, M. K., Fomin, E., Ogletree, D. F. and Salmeron, M. (2003). "Dissociative hydrogen adsorption on palladium requires aggregates of three or more vacancies." Nature 42:705-707.
- Neck, V. and Kim, J. I. (2001). "Solubility and hydrolysis of tetravalent actinides." Radiochimica Acta 89: 1.
- Nilsson, S. and Jonsson, M. (2008a). "On the catalytic effect of Pd(s) on the reduction of UO₂²⁺ with H₂ in aqueous solution." Journal of Nuclear Materials 374: 290-292.
- Nilsson, S. and Jonsson, M. (2008b). "On the catalytic effects of UO₂(s) and Pd(s) on the reaction between H₂O₂ and H₂ in aqueous solution." Journal of Nuclear Materials 372: 160-163.

Poinssot, C., Ferry, C., Lovera, P., Jegou, C. and Gras, J.-M. (2005). "Spent fuel radionuclide source term model for assessing spent fuel performance in geological disposal. Part II: Matrix alteration model and global performance." *Journal of Nuclear Materials* 346: 66-77.

Röllin, S., Spahiu, K. and Eklund, U. B. (2001). "Determination of dissolution rates of spent fuel in carbonate solutions under different redox conditions with a flow-through experiment." *Journal of Nuclear Materials* 297: 231-243.

Rondinella, V. V., Matzke, H. and Wiss, T. (2000). "Leaching behaviour of UO₂ containing alpha-emitting actinides." *Radiochimica Acta* 88: 527-531.

Santos, B. G., Nesbitt, H. W., Noel, J. J. and Shoesmith, D. W. (2004). "X-ray photoelectron spectroscopy study of anodically oxidized SIMFUEL surfaces." *Electrochimica Acta* 49: 1863-1873.

Shoesmith, D. W. (2000). "Fuel corrosion processes under waste disposal conditions." *Journal of Nuclear Materials* 282: 1-31.

Shoesmith, D. W., Sunder, S., Bailey, M. G. and Wallace, G. J. (1989). "The Corrosion of Nuclear Fuel (UO₂) in Oxygenated Solutions." *Corrosion Science* 29: 1115-1128.

Shoesmith, D. W., Sunder, S. and Tait, J. C. (1998). "Validation of an electrochemical model for the oxidative dissolution of used CANDU fuel." *Journal of Nuclear Materials* 257: 89-98.

Spahiu, K., Devoy, J., Cui, D. and Lundström, M. (2004). "The reduction of U(VI) by near field hydrogen in the presence of UO₂." *Radiochimica Acta* 92: 597.

Spinks, J. W. T. and Woods, R. J. (1964). *An introduction to radiation chemistry*, John Wiley and Sons Inc.

Stumpf, S., Seibert, A., Gouder, T., Huber, F., Petersmann, T., Denecke, M. A. and Fanghänel, T. (2010). "UO₂ Fuel Corrosion – Reactions at a UO₂-Palladium spent fuel model surface" in 2nd Annual Workshop Proceedings 7th EC FP - Recosy CP, Larnaca (Cyprus). KIT Scientific Report KIT-SR 7557: 161-170

Stumpf, S., Seibert, A., Gouder, T., Huber, F., Wiss, T. and Römer, J. (2009). "Development of fuel-model interfaces: Investigations by XPS, TEM, SEM and AFM." *Journal of Nuclear Materials* 385: 208-211.

Sunder, S., Shoesmith, D. W. and Miller, N. H. (1997). "Oxidation and dissolution of nuclear fuel (UO₂) by the products of the alpha radiolysis of water." *Journal of Nuclear Materials* 244:66-74.

Trummer, M., Nilsson, S. and Jonsson, M. (2008). "On the effects of fission product noble metal inclusions on the kinetics of radiation induced dissolution of spent nuclear fuel." *Journal of Nuclear Materials* 378: 55-59.

Trummer, M., Roth, O. and Jonsson, M. (2009). "H₂ inhibition of radiation induced dissolution of spent nuclear fuel." *Journal of Nuclear Materials* 383: 226-230.

REDOX REACTIVITY OF DOPED UO_2 – EFFECTS ON THE REACTIVITY TOWARDS H_2O_2

Reijo Pehrman^{1,2}, Martin Trummer², Claudio Lousada², Mats Jonsson^{2*}

¹ University of Helsinki (FIN)

² Royal Institute of Technology (SWE)

* Corresponding author: matsj@kth.se

Abstract

The reactivity of doped UO_2 such as SIMFUEL, Y_2O_3 doped UO_2 and $\text{Y}_2\text{O}_3/\text{Pd}$ doped UO_2 towards H_2O_2 has been shown to be fairly similar to that of pure UO_2 . However, the oxidative dissolution yield, i.e. the ratio between the amount of dissolved uranium and the amount of consumed H_2O_2 is significantly lower for doped UO_2 . The rationale for the observed differences in dissolution yield is a difference in the ratio between the rates of the two possible reactions between H_2O_2 and the doped UO_2 . In this work we have studied the effect of doping on the two possible reactions, electron transfer and catalytic decomposition. The catalytic decomposition was studied by monitoring the hydroxyl radical production (the primary product) as a function of time. The redox reactivity of the doped pellets was studied by using MnO_4^- and IrCl_6^{2-} as model oxidants, only capable of electron transfer reaction with the pellets. In addition, the activation energies for oxidation of UO_2 and SIMFUEL by MnO_4^- were determined experimentally. The experiments show that the rate of catalytic decomposition of H_2O_2 varies by 30 % between the fastest and the slowest material. This is a negligible difference. The redox reactivity study shows that doping of UO_2 influences the redox reactivity of the pellet. This is further illustrated by the observed activation energy difference for oxidation of UO_2 and SIMFUEL by MnO_4^- . The redox reactivity study also shows that the sensitivity to dopants increases with decreasing reduction potential of the oxidant. These findings imply that the relative impact of radiolytic oxidants in oxidative dissolution of spent nuclear fuel must be reassessed taking the actual fuel composition into account.

Introduction

UO_2 has been used as a model for spent nuclear fuel in numerous experimental studies. Rates and rate constants for oxidation as well as dissolution of the oxidized UO_2 matrix of spent nuclear are derived from experiments on pure UO_2 powder or pellets (*Roth and Jonsson (2008)*). On the basis of these results the relative impact of radiolytic oxidants have been assessed and also employed in simulations of spent nuclear fuel dissolution under deep repository conditions (*Ekeröth et al. (2006)*). One important conclusion from these studies is that H_2O_2 is the major oxidant responsible for radiation induced

oxidative dissolution of spent nuclear fuel under deep repository conditions. H_2O_2 can react with UO_2 by catalytic decomposition and by oxidizing U(IV) to U(VI). Recent experiments have shown that the oxidative dissolution yield, i.e. the amount of dissolved uranium per consumed H_2O_2 varies dramatically between different UO_2 -based materials (Trummer et al. (2010), Nilsson and Jonsson (2011)). It has not been clear whether this variation can be attributed to changes in redox reactivity or in the catalytic ability of the material. Since spent nuclear fuel can be regarded as highly doped UO_2 , the effects of the presence of dopants in the UO_2 matrix should be regarded as key-knowledge in the field of spent nuclear fuel dissolution. To elucidate this we have studied the reactivity of a number of oxidants towards doped UO_2 materials. In parallel we have studied the catalytic formation of hydroxyl radicals (upon reaction with H_2O_2) on the doped UO_2 materials.

Experimental

Instrumentation

γ -Irradiation was performed using a MDS Nordion 1000 Elite Cs-137 γ -source with a dose rate of $0.15 \text{ Gy} \cdot \text{s}^{-1}$, this value was determined by Fricke dosimetry. The reactions were performed under inert atmosphere with a constant flux of N_2 gas (AGA Gas AB) with a flow rate of $0.21 \text{ L} \cdot \text{min}^{-1}$ that was also used for the purpose of stirring the solutions. The temperature was kept constant throughout the experiments by using a Huber CC1 or a Lauda E100 thermostat, calibrated against a Thermo 1 Thermometer coupled to a submersible K-type (NiCrNi) temperature probe, with a precision of $\pm 0.1 \text{ K}$. UV/Vis spectra were collected using a WPA Lightwave S2000 or a WPA Biowave II UV/Vis Spectrophotometer. The U analysis was performed with an ICP-OES (Thermo Scientific iCAP 6000 series) at 367.0 nm and 385.9 nm. The values from both wavelengths were averaged.

Reagents and experiments

All the solutions used in this study were prepared using water from a Millipore Milli-Q system.

In this work, UO_2 powder (ABB), a uranium dioxide pellet (ABB) and a SIMFUEL pellet (AECL) were used. Furthermore, four in-house UO_2 pellets were manufactured from UO_2 powder. The pellets were doped with 0.3 wt% Y_2O_3 , with 0.3 wt % Y_2O_3 and 0.1 wt % Pd, or with 0.1 wt % Pd. All the pellets were placed in a 10 mM NaHCO_3 (Merck, p.a.) solution for a period of 14 hours. The specific surface area of the UO_2 powder was obtained from the BET isotherm (30% N_2 , 70% He) on a Micrometrics Flowsorb II 2300 instrument. The obtained surface area was $5.4 \pm 0.2 \text{ m}^2 \cdot \text{g}^{-1}$. The average particle size of the powder is $16 \mu\text{m}$, with a size distribution of $99.9\% < 100 \mu\text{m}$. The total impurities present in the UO_2 powder have a concentration of $48 \mu\text{g/gU}$. The geometrical surface areas of the pellets were 352 mm^2 for the Westinghouse pellet, 471 mm^2 for the SIMFUEL pellet and 372 mm^2 for the doped UO_2 pellets. The weights of the pellets were 5.3 g for the Westinghouse pellet, 7.9 g for the SIMFUEL pellet and 3.5 g for the UO_2 doped pellets.

Catalytic decomposition of H₂O₂ on UO₂ powder and pellets

A mechanistic study of the decomposition of H₂O₂ on the surface of the pellets and on the UO₂ powder was carried out where the production of hydroxyl radicals was measured. This was done by measuring the produced formaldehyde from the reaction between tris(hydroxymethyl)aminomethane (tris buffer) (BDH Chemicals 99%) and the hydroxyl radicals. This method has been described earlier. In this study, the reaction between the pellets or UO₂ powder and H₂O₂ was performed at 293.15 K, at the midpoint of the buffering range of the tris buffer. The reaction mixture consisted of one of the above mentioned pellets or 0.1 g of UO₂ powder, in 5 mM in H₂O₂ (Sigma-Aldrich, 30% standard solution, p.a.) aqueous solution (50 mL). These solutions also contained 10mM NaHCO₃ and 20 or 80 mM tris buffer at a pH of 7.5. The pH was adjusted with HCl (VWR BDH Prolabo, 30 %). In the case of the UO₂ powder experiments, the samples were filtered through a Gamma Medical 0.45µm–25mm Cellulose Acetate syringe filter before measuring. For all materials studied, a sample volume of 1.5 ml was used for the determination of formaldehyde. The formaldehyde produced was then quantified spectrophotometrically at 368 nm. This method is based on the reaction of formaldehyde with acetoacetanilide AAA (Alfa Aesar > 98%) in the presence of ammonium acetate (Lancaster 98%) to form a dihydropyridine derivative which has the maximum absorption wavelength at 368 nm. A calibration curve plotting the absorbance of the dihydropyridine derivative as a function of formaldehyde concentration was obtained at 368 nm, giving a linear correlation between the absorbance and the concentration, in the range from 3.0 µM to 0.5 mM in formaldehyde.

Redox reactions of MnO₄⁻ and IrCl₆²⁻ with UO₂ pellets

For the study of the redox reactions of the pellets with one-electron oxidants, we followed the evolution in the concentrations of these oxidants as a function of reaction time. The one-electron oxidants used in this work were MnO₄⁻ and IrCl₆²⁻. The concentrations of these species were measured directly with UV/visible spectroscopy. The absorbance of MnO₄⁻ was measured at λ=525 nm and the one of IrCl₆²⁻ at λ=488 nm. After the measurements, the solutions were poured back into the reaction vessel. The reaction media for the reactions of the pellets with MnO₄⁻ consisted of 10 mL aqueous solution with 0.6 mM MnO₄⁻ and 10 mM NaHCO₃. For the reactions with IrCl₆²⁻, the reaction media contained 0.3 mM IrCl₆²⁻ and 10 mM NaHCO₃. The reactions were performed under inert atmosphere with a constant flow of N₂.

Reactivity of H₂O₂ towards doped UO₂

Rate of H₂O₂ consumption

The rate of H₂O₂ consumption has been measured in a number of previous studies (Roth and Jonsson (2008), Trummer et al. (2010), Nilsson and Jonsson (2011)). The rate constant for UO₂ oxidation by H₂O₂ was obtained in experiments on UO₂ powder suspensions. This rate constant can be used to make fairly reasonable predictions of the rate of oxidation for UO₂ pellets as well as for doped UO₂ pellets. Hence, the overall rate of H₂O₂ consumption on UO₂ surfaces is relatively insensitive to the presence of

dopants. However, noble metal particles have been shown to catalyze oxidation to some extent (Trummer et al. (2009)).

Hydroxyl radical formation

Hydroxyl radicals formed as a primary product in metal oxide catalyzed decomposition of H_2O_2 can be detected using a modified version of the Hantzsch method (Lousada and Jonsson (2010)). In short, tris-buffer is added to the system. Upon reaction with hydroxyl radicals (or other hydrogen abstracting radicals), formaldehyde is produced. The formaldehyde concentration is the used to monitor the accumulated hydroxyl radical production in the system.

The consumption of H_2O_2 and the production of OH on UO_2 powder are illustrated in figure 1.

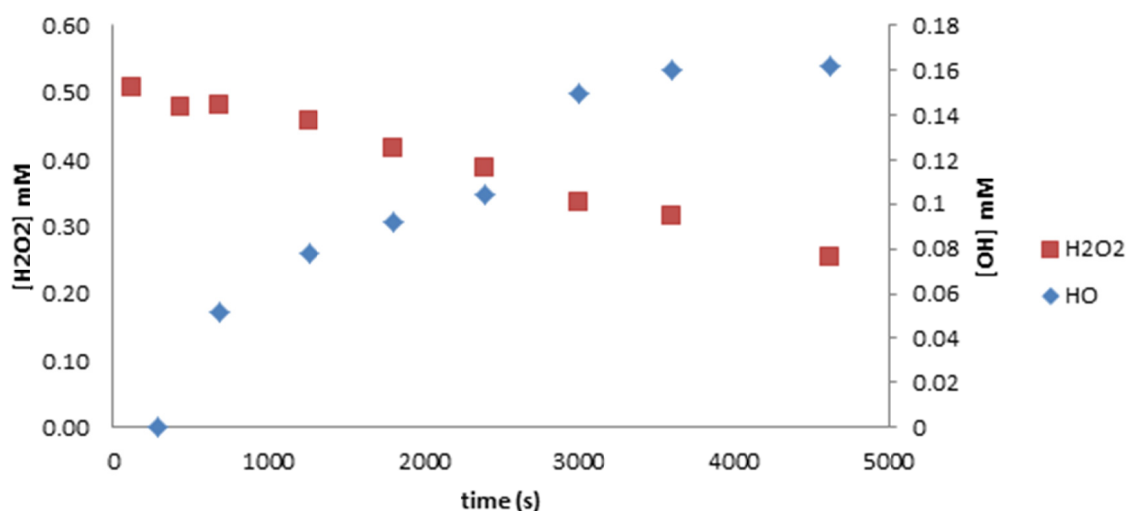


Figure 1: Hydrogen peroxide concentration and accumulated hydroxyl radical concentration as a function of reaction time in UO_2 powder suspension.

It can clearly be seen that the consumption of H_2O_2 is accompanied by production of OH. For UO_2 powder, the dissolution yield, expressed as the ratio between dissolved U(VI) and consumed H_2O_2 , has been determined to 80 % (Jonsson et al. (2004)). The present experiments on hydroxyl radical production confirms this as the hydroxyl radical production corresponds to ca 20 % of the H_2O_2 consumption.

OH production for doped pellets normalized to the surface area of the Westinghouse pellet is presented in figure 2. As can be seen, the rate of hydroxyl radical production varies by less than 30 % for UO_2 , SIMFUEL, Y_2O_3 doped UO_2 , Pd-doped UO_2 and Y_2O_3 /Pd-doped UO_2 .

Uranium dissolution data from the same experiments are presented in figure 3. Also in this case the concentrations are normalized to the surface area of the Westinghouse pellet.

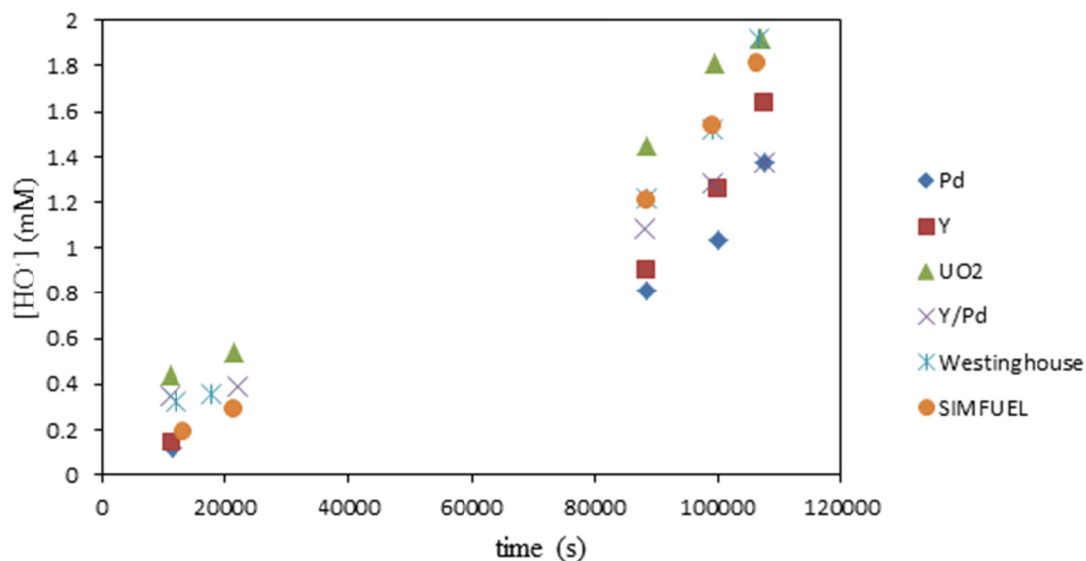


Figure 2: Accumulated hydroxyl radical concentration as a function of reaction time in pellet experiments (results normalized to the surface area of the Westinghouse pellet).

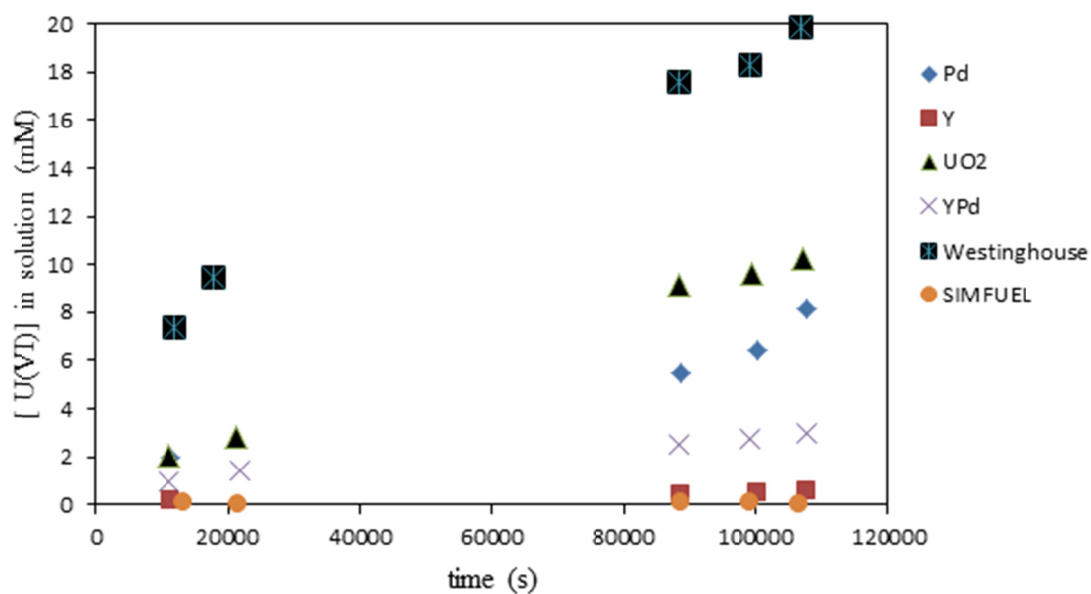


Figure 3: Uranium concentration as a function of reaction time in pellet experiments.

As can be seen, the uranium dissolution displays a much larger variation. Dissolution yields for the different materials used in this study are presented in table 1

Clearly, the variation in dissolution yield cannot be directly attributed to differences in the catalytic ability of the doped UO_2 pellets.

Table 1: Dissolution yields

Material	Dissolution yield (%)
UO ₂ powder	80
UO ₂ pellet (Westinghouse)	14
SIMFUEL pellet	0.2
UO ₂ pellet (In house)	6
UO ₂ /Y ₂ O ₃ pellet (In house)	2.5
UO ₂ /Y ₂ O ₃ /Pd pellet (In house)	0.9
UO ₂ /Pd pellet (In house)	11.5

Redox reactivity of doped UO₂

Reactivity of different oxidants

If differences in the ability to catalyze decomposition of H₂O₂ cannot explain the observed differences in dissolution yield, the rationale must be differences in the redox reactivity of the doped materials. In order to elucidate this possibility we performed experiments using pure oxidants that cannot undergo catalytic decomposition. In addition to H₂O₂, which has already been studied quite extensively, we used IrCl₆²⁻ and MnO₄⁻ to monitor the redox reactivity of the doped UO₂ materials. In figures 4 and 5 the reactivity of the different pellets towards these oxidants can be seen.

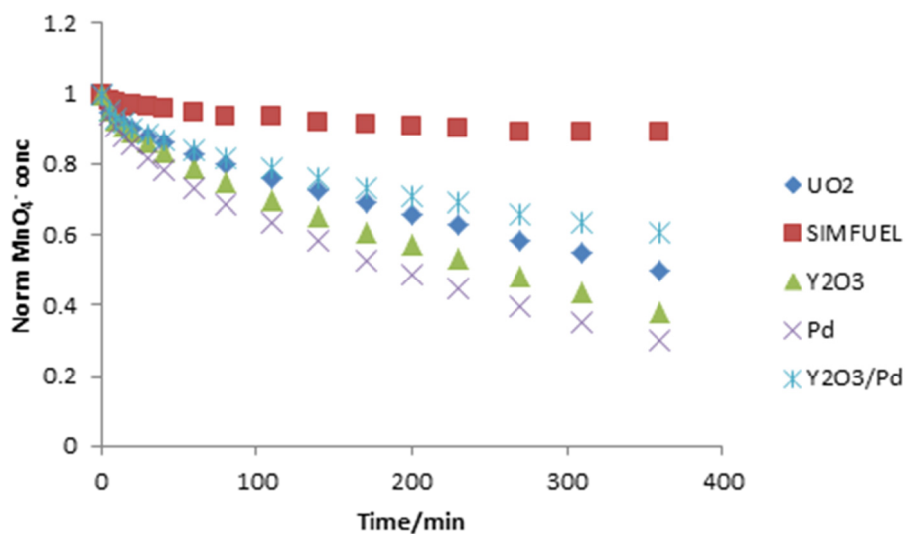


Figure 4: Normalized MnO₄⁻ concentration as a function of reaction time in pellet experiments.

What can clearly be seen here is that the redox reactivity of the doped materials differs significantly for the weaker oxidant (MnO₄⁻) while the reaction with the stronger oxidant (IrCl₆²⁻) is much faster and the difference between the doped materials is also less pronounced. Furthermore, experiments (kinetics as a function of temperature) show that the activation energy for oxidation of UO₂ by MnO₄⁻ is lower than the activation energy for oxidation of SIMFUEL by MnO₄⁻. The measured activation energies are 7.4

and 12.9 kJ mol⁻¹, respectively. This shows that the redox reactivity is significantly influenced by doping. The Arrhenius plots are given in Figure 6.

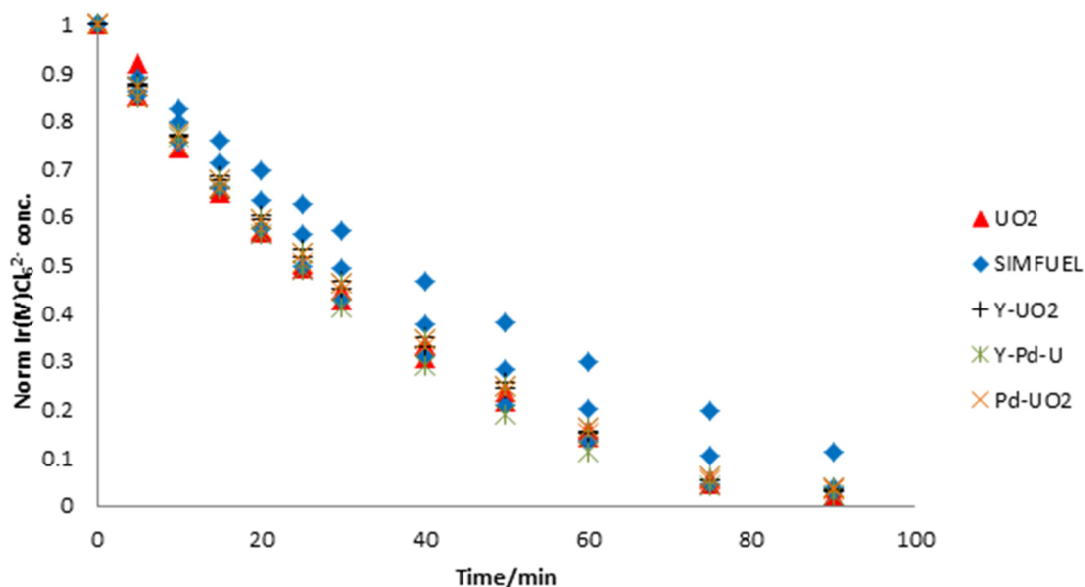


Figure 5: Normalized IrCl_6^{2-} concentration as a function of reaction time in pellet experiments.

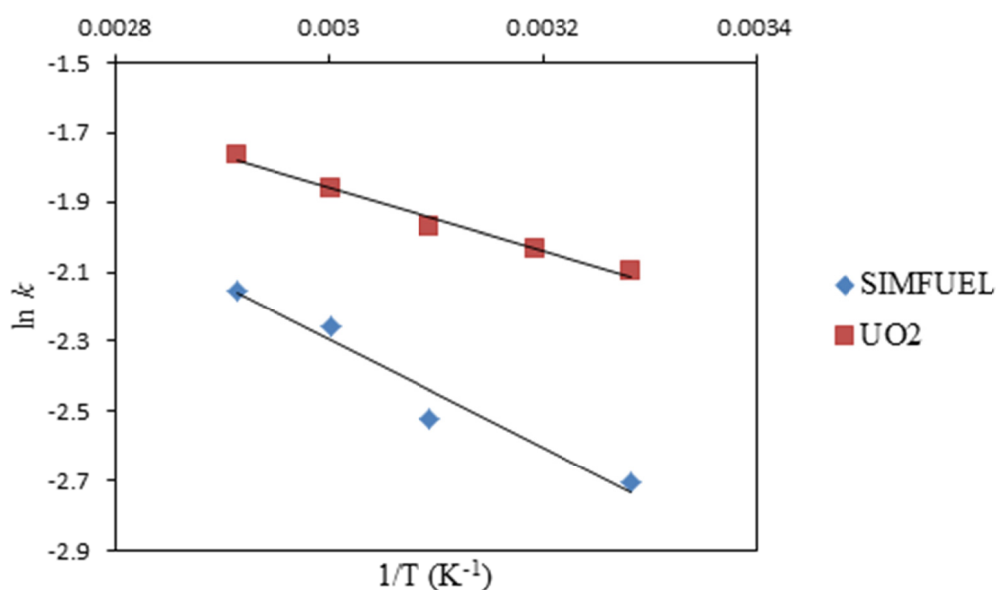


Figure 6: Arrhenius plots for oxidation of SIMFUEL and UO_2 by MnO_4^- .

Extrapolation to other oxidants

In table 2, the rate constants (determined from the initial rates) for pellet oxidation by H_2O_2 , MnO_4^- and IrCl_6^{2-} are summarized. It should be stressed that the rate constants for oxidation by H_2O_2 are determined from the overall rate constants for consumption of H_2O_2 and the measured dissolution yields.

Table 2: Rate constants for oxidation of pellets

Pellet	$k(\text{H}_2\text{O}_2)/\text{min}^{-1}$	$k(\text{MnO}_4^-)/\text{min}^{-1}$	$k(\text{IrCl}_6^{2-})/\text{min}^{-1}$
UO ₂ (Westinghouse)	1.5×10^{-4}	3.3×10^{-3}	2.0×10^{-2}
SIMFUEL	1.4×10^{-6}	6.0×10^{-4}	1.7×10^{-2}
UO ₂	4.3×10^{-5}	6.2×10^{-3}	2.0×10^{-2}
UO ₂ /Y ₂ O ₃	1.3×10^{-5}	5.3×10^{-3}	2.1×10^{-2}
UO ₂ /Y ₂ O ₃ /Pd	4.3×10^{-6}	4.6×10^{-3}	2.3×10^{-2}
UO ₂ /Pd	6.6×10^{-5}	7.8×10^{-3}	2.2×10^{-2}

As can be seen, the rate constant for oxidation increases with increasing reduction potential of the oxidants for all the pellets included in the study. It is also clear (as indicated above) that the difference in reactivity between the different pellets decreases with increasing oxidizing power of the oxidant. To illustrate this, we have plotted the logarithm of the ratio between the rate constants for oxidation of SIMFUEL and UO₂ (Westinghouse) against the reduction potential of the oxidant in figure 7.

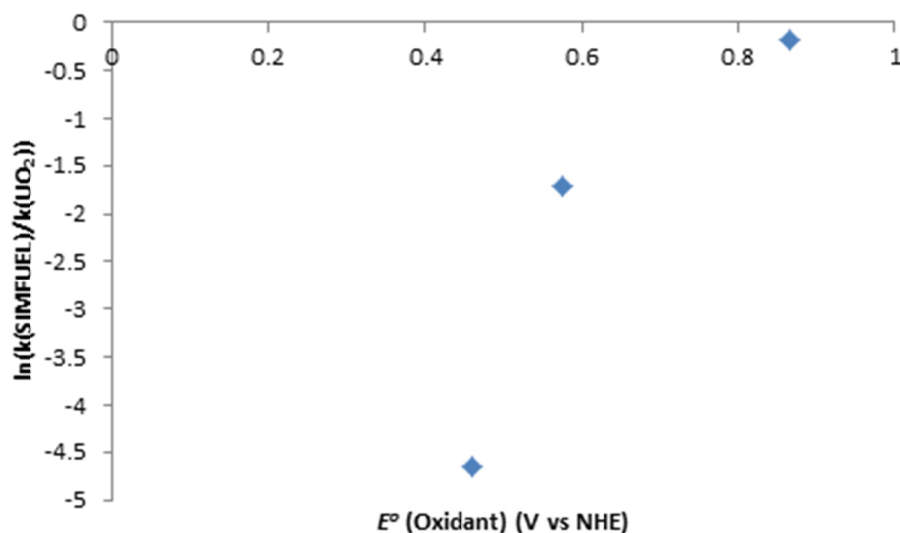


Figure 7: Logarithm of the ratio between the rate constants for oxidation of SIMFUEL and UO₂ (Westinghouse) plotted against the reduction potential of the oxidant for H₂O₂, MnO₄⁻ and IrCl₆²⁻.

Plotting the logarithm of the ratio between the rate constants is identical to plotting the difference in activation energy. From the trend displayed in figure 7 we can conclude that the reactivity of O₂ towards SIMFUEL and UO₂ will differ by at least four orders of magnitude. For oxidants stronger than IrCl₆²⁻ (i.e. OH and CO₃⁻) for which the activation barrier will be very low, the rate constants are expected to be similar for UO₂ and SIMFUEL (diffusion controlled).

A similar trend is observed for the Y₂O₃ and Y₂O₃/Pd doped UO₂ pellets. Hence, doping of UO₂ will change the relative impact of the radiolysis products. The impact of radicals will increase while the impact of molecular oxidants will decrease. In general, the weaker the oxidant, the more the relative impact will decrease. These findings are

important to keep in mind when applying data from pure UO_2 -systems on spent nuclear fuel dissolution.

Summary and Conclusions

In this work we have investigated the reasons behind the previously observed difference in dissolution yield between different doped UO_2 materials upon reaction with H_2O_2 in HCO_3^- containing aqueous solution. The experimental results show that, while the dissolution yield varies by more than one order of magnitude, hydroxyl radical production due to catalytic decomposition of H_2O_2 varies by 30 %. Experiments using pure oxidants show that the redox reactivity between the pellets varies significantly. This is further confirmed by the difference in activation energy for oxidation of SIMFUEL and UO_2 (Westinghouse).

Acknowledgement

The Swedish Nuclear Fuel and Waste Management Company (SKB) is gratefully acknowledged for financial support. Part of this work was funded by EURATOM's 7th Framework Programme (Redox Phenomena Controlling Systems, Grant No. FP7-212287).

References

- Ekeröth E., Roth O., Jonsson M. (2006), The relative impact of radiolysis products in radiation induced oxidative dissolution of UO_2 . J. Nucl. Mater. 355, 38-46
- Jonsson M., Ekeröth E., Roth O. (2004), Dissolution of UO_2 by one- and two-electron oxidants. Mat. Res. Soc. Symp. Proc. 807, 77-82
- Lousada C. M., Jonsson M. (2010), Kinetics, Mechanism and Activation Energy of H_2O_2 Decomposition on the Surface of ZrO_2 . J. Phys Chem. C. 114, 11202-11208
- Nilsson S., Jonsson M. (2011), H_2O_2 and radiation induced dissolution of UO_2 and SIMFUEL pellets, J. Nucl. Mater. 410, 89-93.
- Roth O., Jonsson M. (2008), Oxidation of $\text{UO}_2(\text{s})$ in aqueous solution. Cent. Eur. J. Chem. 6, 1-14
- Trummer M., Roth O., Jonsson M. (2009), H_2 Inhibition of Radiation Induced Dissolution of Spent Nuclear Fuel. J. Nucl. Mater. 383, 226-230
- Trummer M., Dahlgren B., Jonsson M. (2010). The effect of Y_2O_3 on the dynamics of oxidative dissolution of UO_2 . J. Nucl. Mater. 407, 195-199.

REDOX-CONTROLLING PROCESSES FOR MULTIVALENT METALS AND ACTINIDES IN THE WIPP

Donald Reed*, Marian Borkowski, Juliet Swanson, Michael Richmann, Hnin Khaing, Jean Francois Lucchini, and David Ams

Earth and Environmental Sciences Division, Carlsbad Operations,
Los Alamos National Laboratory, USA

*Corresponding author: dreed@lanl.gov

Abstract

The subsurface chemistry of multivalent actinide contaminants is highly dependent on their oxidation state distribution and associated redox conditions. These redox conditions are established by coupled direct and indirect subsurface processes such as microbial activity, geochemical reactions with the host rock, and the chemical effects of other co-contaminants present. The ability to predict actinide migration, especially over the very long times that are typically of concern, is directly linked to the ability to establish the nature, stability, and mobility of dissolved species formed within the bounds of the prevailing redox conditions. The measurement of system-specific redox conditions (E_h) can be problematic under the most ideal groundwater conditions but is especially problematic in high ionic strength systems such as brines with $I > 5$ M.

The redox chemistry and key assumptions pertaining to the key multivalent metals and actinides present in the WIPP underground, which is expected to be a strongly reducing high ionic-strength brine system, is presented. Long-term actinide solubility studies and redox kinetics of lower-valent iron show varied degrees of correlation between Pu(III)/Pu(IV) and Fe(II)/Fe(III) concentration ratios with E_h measurements. Linkages between the observed microbial activity and redox chemistry of neptunium were also observed. Overall, these system-specific results are discussed and interpreted in the context of their broader application to understanding the redox chemistry and migration behavior of multivalent metals and actinides in high ionic-strength brine systems and salt-based repositories.

Introduction

The fate and potential mobility of multivalent transuranic actinides in the subsurface is receiving increased attention as the DOE considers remedial alternatives for many of their legacy nuclear waste sites and associated groundwater contamination. The oxidation state distribution of multivalent elements is frequently linked to the redox

conditions in groundwater (see Table 1). Plutonium is often the subsurface contaminant of concern in groundwater at contaminated DOE sites and remains a key contributor to potential actinide release from permanent geologic repositories. Americium and neptunium may also be key contributors for some repository conditions. The experience in the field is that the biogeochemistry of these transuranics is favorable towards their subsurface immobilization under a wide range of conditions.

The migration potential for transuranics in groundwater is highly dependent on its oxidation-state distribution and associated extent of aggregation. Under anoxic conditions in nutrient-rich groundwater where organic co-contaminants may coexist, the oxidation state distribution is primarily defined by the combined effects of reduced iron, organic chelating agents, and microbial activity. Understanding these processes, and their synergisms, is critical to establishing the subsurface fate of transuranics, including plutonium, and explaining their apparent immobility.

Table 1. *Prevalent Oxidation States of Multivalent Actinides in Groundwater*

Redox Environment	U	Np	Pu	Am
Oxic	VI	V, VI?	V, VI? IV	III, V?
Suboxic	VI IV	IV	IV III	III
Anoxic	IV	IV	IV III	III

The issue of redox, and in particular the measurement of a meaningful E_h in groundwaters has been controversial for a number of years (Lindberg and Runnells, 1984; Kehew et.al, 2000). Redox disequilibria, rather than equilibrium is the norm and the meaning of E_h measurements to predicting the oxidation state of multivalent actinides, which are often present in much lower concentrations than other redox active metals (e.g., Fe(II/III) and Mn(II/IV)), is even less clear. The interpretation of E_h measurements from high ionic strength media such as brines is even more problematic since high ionic strength can significantly affect the response of the electrode (Capdevila and Vitorge, 1990; Wiesner et.al, 2006; Degueldre et.al, 1999; Christensen et.al, 2000). A better approach may be to link the behavior of known redox couples with the actinide oxidation state distribution, as was done in low ionic-strength systems (Masue-Slowey et.al, 2011; Holm and Curtiss, 1989; Christensen et.al, 2000), to more reliably predict the actinide redox chemistry.

Herein we report on recent progress towards understanding the key factors that influence the oxidation state distribution, fate, and potential transport of actinides in high ionic-strength brine systems present in the Waste Isolation Pilot Plant (WIPP) transuranic repository. This research, although not directly performed as part of the Recosy project, reflects many of the scientific interests on redox controlling systems that influence all subsurface actinide chemistry. Our research (Reed et.al, 2006, Reed et.al, 2007, Reed et.al. 2011; Lucchini et.al, 2007; Borkowski et.al, 2009) is centered on the speciation of key actinides under WIPP-specific conditions. The goals of this

research are to improve the robustness and quantify conservatisms in the geochemical conceptual models for the WIPP site. As a component of this research, the key linkages that help predict oxidation state distributions in high ionic strength systems are being investigated. This is an important consideration for the ongoing recertification of the WIPP, which is the only United States transuranic nuclear waste repository, as well as other nuclear repository options being considered in a salt geology.

Redox Environment and Actinide Oxidation-State Distribution in the WIPP

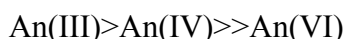
The WIPP transuranic repository remains a cornerstone of the U.S. Department of Energy's (DOE) nuclear waste management effort. Waste disposal operations began at the WIPP on March 26, 1999 however the WIPP is required to be recertified every five years for its disposal operations. The WIPP received its second recertification in November 2010 and the geochemical conceptual model for the site provides a starting point for redox discussions that were tested in a peer and regulatory review process.

The expected redox environment in the WIPP, based on the current conceptual model, is that strongly reducing conditions will prevail early in repository history leading to a lower-valent actinide oxidation state distribution (Reed et al., 2011). Early after repository closure (within a few hundred years) self-sealing of the salt will occur that will geologically isolate the repository. Very shortly thereafter the excess iron and microbial activity is predicted to consume all the oxygen initially present leading to an anoxic environment. The expected scenario is that the repository will remain anoxic and “dry” throughout repository history unless low probability human intrusions lead to brine inundation. At the point of brine inundation, should this occur, the reactivity of the remaining zero-valent iron and activity of facultative and anaerobic halotolerant and halophilic micro-organisms will maintain a strongly reducing environment that promotes and stabilizes lower-valent actinides in solution. Although some localized oxidizing conditions may exist, e.g. due to radiolysis, these are quickly overwhelmed by the excess of reduced iron present and do not significantly contribute to the overall chemistry of the repository. The predominantly lower-valent actinides have low solubility and a high tendency towards sorption which leads to a low probability of migration and subsequent release from the WIPP.

For the low-probability inundated brine scenarios, some release through migration of dissolved actinides is possible. The potential dose-to-man contribution of the actinides, where both activity and solubility are considered, leads to the following overall ranking of the actinides with respect to release from the WIPP:



Uranium, based on current assumptions, has the highest potential for release by mass. The relative importance of oxidation states, also from a dose-to-man perspective, is:



Both plutonium and americium speciate as An(III) species, with plutonium as the main contributor to An(IV) release. The An(V) oxidation state is largely ignored since Np,

which is the only actinide that speciates significantly as in the An(V) oxidation state, has a very low inventory in the WIPP and does not contribute significantly to the predicted release of actinides.

The oxidation state distribution that is used in WIPP performance assessment (PA) is shown in table 2. These distributions are designed to be conservative with respect to potential for actinide release and are based on expert judgment that reflects the expected redox conditions in the WIPP. In this context, they are not calculated values nor are they based directly on measurements made in the laboratory. In the calculated releases, an oxidized (50% of the PA vectors) and reduced (50% of the PA vectors) bounding condition, are used. In the reduced bounding condition, the multivalent actinides are in their lower oxidation state. This is U(IV), Pu(III), and Np(IV). In the oxidizing bounding state, the multivalent actinides are in their higher oxidation state. This is U(VI), Pu(IV) and Np(V). In all cases, thorium is only present as Th(IV); americium and curium are only present as Am(III) and Cm(III).

The calculated oxidation-state-specific actinide solubility, for the past certification and recertification of the WIPP are tabulated in Table 3. These base solubilities are coupled with assumptions about colloid enhancement to generate an oxidation-state-specific dissolved concentration that is used in the assessment of actinide release from the WIPP.

Table 2. Actinide Oxidation State Distribution Assumed in the WIPP Performance Assessment Model (Reed et al, 2011)

Actinide	Oxidation State				Speciation Data used in Model Predictions
	III	IV	V	VI	
Thorium		100%			Thorium
Uranium		50%		50%	Thorium for U(IV), 1 mM fixed value for U(VI)
Neptunium		50%	50%		Thorium for Np(IV), neptunium for Np(V)
Plutonium	50%	50%			Americium/neodymium for Pu(III) and thorium for Pu(IV)
Americium	100%				Americium/neodymium
Curium	100%				Americium/neodymium

Table 3. Calculated Oxidation-state-specific solubility (M) of actinides in Salado (high magnesium) and Castile (high sodium chloride) brines (Reed et. al, 2011)

Actinide Oxidation State	Brine	^a PAVT 1999	^b PABC 2004	^c PABC 2009
An(III)	Salado	1.2x10 ⁻⁷	3.9x10 ⁻⁷	1.7x10 ⁻⁶
An(III)	Castile	1.3x10 ⁻⁸	2.9x10 ⁻⁷	1.5x10 ⁻⁶
An(IV)	Salado	1.3x10 ⁻⁸	5.6x10 ⁻⁸	5.6x10 ⁻⁸
An(IV)	Castile	4.1x10 ⁻⁹	6.8x10 ⁻⁸	6.8x10 ⁻⁸
^a Performance Assessment Verification Test - initial WIPP license application ^b Performance Assessment Baseline Calculation - 1 st recertification in 2004 ^c Performance Assessment Baseline Calculation - 2 nd recertification in 2009				

Investigations of High Ionic-Strength Redox Linkages

Research to understand the detailed mechanisms by which redox conditions are established and their impact on actinide speciation is ongoing within the WIPP project (Reed et.al, 2011). The two most important processes that will impact oxidation-state distribution are the effects of redox-active multivalent metals, such as iron or manganese, and the direct and indirect effects of microbial processes. The goal of this research effort is to quantify the degree of conservatism present in the current assumptions and move towards a more realistic but still conservative conceptual model for the WIPP site.

E_h Measurement in Brine Systems

The measurement of E_h, for reasons mentioned previously, is problematic in high ionic strength brine systems. In this context, these types of measurements, at best, provide qualitative but rarely quantitative data on the redox conditions in the brine experiment.

To investigate these qualitative relationships, E_h measurements were made on a series of plutonium solubility and redox speciation studies that contained excess reduced iron. All measurements were made in the nitrogen glovebox where the experiments were conducted (P_{O2} < 0.1 ppm). These experiments were not sampled frequently and were doubly sealed/isolated to minimize the effects of occasional elevated oxygen levels in the glovebox due to routine experiments and operations. An Orion epoxy sure-flow combination redox/ORP electrode (model 9678-BNWP) was used with the high ionic strength internal Ag/Cl reference solution provided by the manufacturer. This electrode was pre-conditioned in the glovebox for several hours. The manufacturer-supplied ORP standard was used to calibrate the electrode and frequent checks of the electrode response were made throughout the E_h measurement operations.

The results of the E_h measurements made are given in Table 4. Typical electrode equilibration times were 20-30 minutes. In the absence of iron and plutonium, the brines used (high magnesium GWB, and sodium chloride ERDA-6 – see Lucchini et.al 2007 for brine compositions), had a measured E_h of +464 ± 5 mV in the presence and absence of air.

In the presence of soluble/measurable amounts of dissolved iron species the E_h became negative, as expected, with a range of -100 mV to -220 mV. This seemed to qualitatively correlate with the measured concentration of Fe²⁺ in solution. Equilibration times under these conditions were ~ 20 minutes, slightly shorter than in the absence of Fe. Fe²⁺ and Fe³⁺ concentrations were measured using a modified method based on the FerroZene® complexation of Fe²⁺ (Pepper et al., 2008). Under the conditions of our experiments, approximately 1 mM carbonate was present in the brine (except experiment PuFeG7), so some solubilisation of Fe(III), as Fe³⁺, was possible and observed. These results were reproducible over the course of the five hours that samples were analyzed in the glovebox environment.

Table 4. *Qualitative Redox Indicators for Iron Interactions with Plutonium under Anoxic Conditions*

Experiment	Description	^a Oxidation State of Pu Solid	^b [Fe] _{total} in mM (%Fe ²⁺ in solution)	^c E _h Measured (± 3 mV)
PuFe23OX	ERDA-6 brine at pH ~9 with excess magnetite	~87% Pu(III), rest Pu(IV)	0.12 (25%)	-122 mV
PuFeCE8	ERDA-6 brine at pH ~8 with Fe coupon	~100 % Pu(III)	ND	ND
PuFeCE10	ERDA-6 brine at pH ~ 9.6 with Fe coupon	~100% Pu(III)	0.27 (100%)	ND
PuFeP	ERDA-6 brine at pH~9 with excess Fe powder	~100% Pu(III)	0.18 (100%)	-175 mV
PuFeC	ERDA-6 brine at pH ~ 9 with Fe coupon	~90% Pu(III), rest Pu(IV)	0.18 (58%)	-110 mV
PuFeG7	GWB brine at pH ~6.7 with Fe coupon	~ 100% Pu(III)	12.62 (97%)	-210 mV
a. Pu(III) content established by XANES analysis of solids b. Fe(II) content established by analysis using FerroZene® c. E _h measurement made using an Orion combination ORP electrode ND – not determined				

Our overall results in the presence of iron are consistent with what has been shown for low ionic strength systems (Christensen et.al., 2000; Holm and Curtiss, 1989) where somewhat good correlations and fast electrode response was seen when the Fe²⁺/Fe³⁺ couple set the redox potential and defined the electrode response. We are continuing to further quantify this response and explore lower concentration limits for the applicability of this technique.

Effect of Reduced Iron on Redox and Actinide Oxidation States

Long-term (~ 5.5 year) experiments to establish the oxidation state distribution of actinides in brine systems under a wide range of subsurface conditions are ongoing. In our investigations ²⁴²Pu, initially as PuO₂²⁺, was used to minimize radiolytic effects. In these brine systems, Pu(VI) is stable for years when no reducing agent is present (Reed et.al, 2007).

Two WIPP-relevant brines (Lucchini et.al., 2007), GWB as a high magnesium brine typical of MgO-reacted brine and ERDA-6 as a high sodium chloride brine typical of brine found in the far field, were used in these studies. The initial oxidation state was established using absorption spectrometry (Varian CARY 5000) and solids are prepared from these brines using established methods. Liquid scintillation counting (Beckman-Coulter LS 6500) and ICP-MS (Agilent) were used to determine total concentration. Aqueous iron chemistry was established using a combination of a FerroZene® colorimetric method and ICP-MS. XANES analysis, combined with anoxic dissolution and UV-VIS-NIR spectroscopy (Varian CARY 5000) were used to establish the oxidation state of the precipitated plutonium.

Iron reduction experiments were performed by adding iron and iron oxides to stable anoxic Pu(VI) solutions with different pH values. The reactivity of Fe^{2+} and Fe^{3+} towards various plutonium oxidation states was also established. At the end of the kinetic studies, samples of plutonium precipitates were recovered and analyzed by XANES. After equilibration for an additional 5.5 years, the solutions were analyzed to establish the iron speciation, plutonium speciation and E_h . Selected data for these experiments were shown in Table 4. Plutonium concentration trends are shown in Figure 1.

Initially, only Pu(IV) was evident in the XANES analysis (see Figure 2). This correlated with a plutonium concentration that was in the range of 2×10^{-9} M to as high as 1.5×10^{-7} M at the lower end of the pH range (pH = 7). These data agreed with the results obtained in a prior study after approximately two years when Pu-239 was the plutonium isotope. After ~5.8 years, these same solid samples were re-analyzed and found to be mostly Pu(III) with some Pu(IV). These results are summarized in Table 4. The observation of Pu(III) in the solid phase correlated with an increase in the plutonium solution concentrations from 1×10^{-8} M to 3×10^{-7} M. This is a slight elevation in concentration, by a factor of ~ 2 to 5, when compared to the earlier Pu(IV)-relevant data. This increased solubility is also consistent with the phase transformation to Pu(III) since the solubility of Pu(III) is expected to be somewhat higher than Pu(IV) – see Table 3.

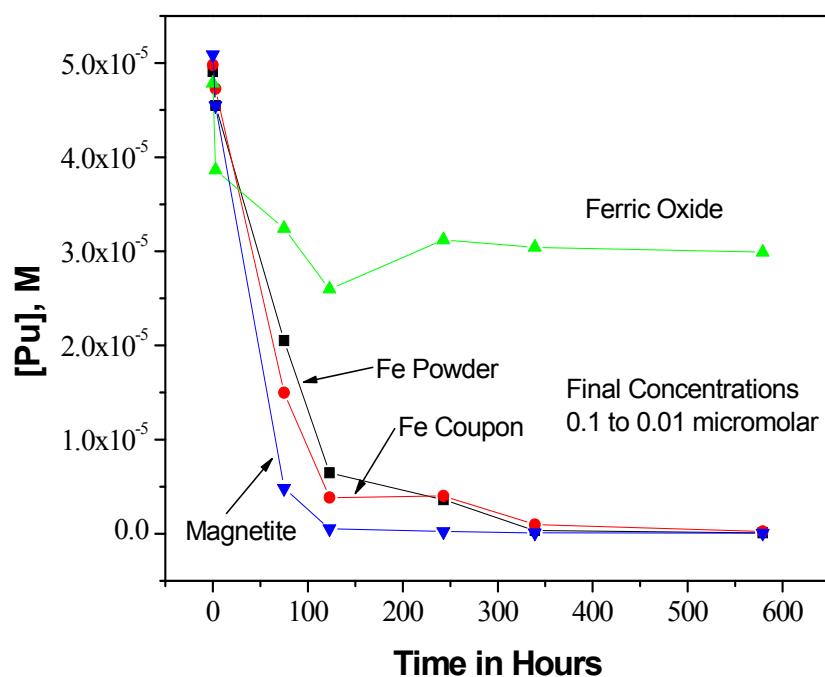


Figure 1. Concentration of Plutonium as a Function of Time after contact with Iron and Iron Oxide Phases in ERDA-6 Brine. Fe powder is experiment PuFeP, Fe coupon is experiment PuFeC, magnetite is experiment PuFe23OX, and ferric oxide is experiment PuFe3OX.

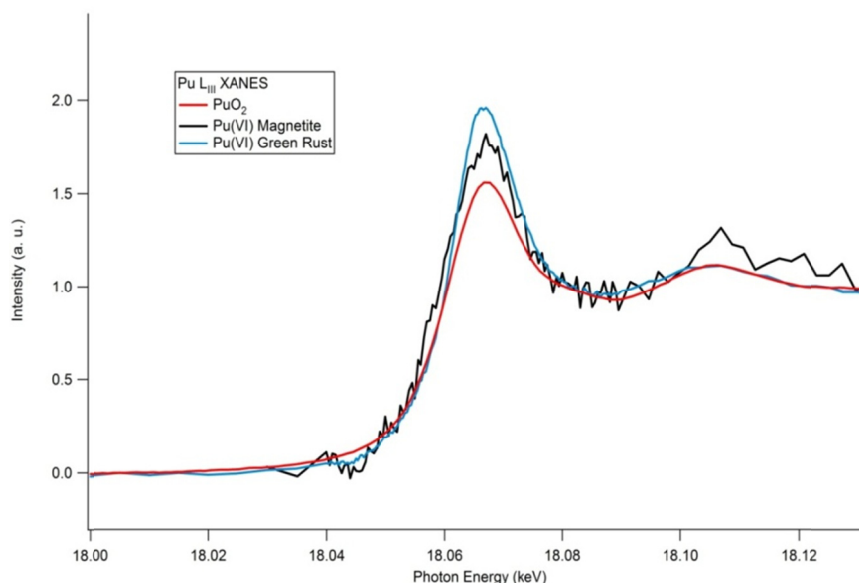


Figure 2. *XANES Analysis of Plutonium Precipitates in the Magnetite and Iron Reduction Experiments at 3 months. Pu(IV) phases were predominantly noted.*

The plutonium (III/IV) solids data show a qualitative correlation with the Fe(II)/Fe(III) ratio and measured E_h . Experiments with less negative E_h also had a greater amount of Fe(III) and Pu(IV) species present in the system. This adds to the linkages seen by others between the iron and plutonium chemistry in subsurface conditions. Although these specific experiments were performed in brine, they are consistent with the correlation between iron chemistry and other metals observed in low ionic strength groundwater (Masue-Slowey et.al, 2011; Holm and Curtiss, 1989; Christensen et.al, 2000). Although not discussed in this paper we have also demonstrated that U(VI) and Np(V) are reduced by zero-valent iron and Fe(II) aqueous/solid species and this also confirms the lower oxidation states expected in the WIPP for these actinides.

Influence of Halotolerant and Halophilic Microorganisms on Redox and Actinide Oxidation State

Microorganisms affect the redox behavior of multivalent actinides in two important ways: (1) indirectly, by helping impose reducing conditions in subsurface environments via the reduction of oxygen and by generating reducing agents, such as dissolved organic species and Fe^{2+} , and (2) directly, by enzymatic reduction, and in less common cases oxidation of multivalent actinides such as plutonium. This redox effect has been well demonstrated for bacteria typically found in low ionic-strength groundwater, soils, sediments, and porewaters (Rittmann et.al, 2002; Banaszak et.al, 1999; Reed et.al, 2007; Lovely, 1993; Caccavo et.al, 1992; Gorby and Lovley, 1992; Boukhalfa et.al, 2007; Francis and Gillow, 2008).

This potentially important microbial process has, however, not been extended to the halotolerant and halophilic *Bacteria* and *Archaea* that are typically present in high ionic-strength brine systems. In fact, little is known about the effects of these organisms on metal redox reactions, with the exception of marine sediments. It may be

that iron and other metals are only present as minor constituents in these systems and the concentration of sulfate too high for metals to be feasible terminal electron acceptors. We are addressing the lack of data concerning metal reduction in high ionic strength matrices and expect to show that some of the same processes that are known to occur at lower ionic strengths will also occur in brine systems. For the specific example of the WIPP, the nutrients present in the TRU waste (nitrates, organics, phosphates and sulfates) are expected to promote significant microbial growth and the potential effects of microbial growth are already factored into aspects of PA.

Our current emphasis is to investigate the impact of halotolerant and halophilic microorganisms on plutonium over a range of ionic strengths. The growth of many of these organisms during early repository history when oxygen is available will help create a reducing environment. Many of the extremely halophilic Archaea (ionic strengths greater than 2.5 M) are also efficient nitrate reducers; while, at lower ionic strengths (up to 2.5 M), many halotolerant and halophilic Bacteria may be capable of metal or sulfate reduction.

We have measured iron reduction in incubations of a mixed culture of halophilic Bacteria and Archaea (Figure 3). This incubation selected for specific organisms (Figure 3), and we are in the process of elucidating the mechanism for iron reduction. Thus far, separate incubations of the bacterial species alone have also yielded Fe^{2+} , albeit incomplete. The formation of Fe^{2+} in solution will actively reduce Pu(V/VI) down to Pu(III) . The demonstration of Fe(III) reduction also links, at least qualitatively, to what we have observed for soil bacteria.

We have also noted the enhanced reduction of Np(V) when added to Fe(III) incubations with halophilic microorganisms (see Figure 4). It is not however clear if this result is due to a direct enzymatic or co-metabolic mechanism due to the generation of reducing agents. The microbial effects on the oxidation state distribution of the multivalent actinides, particularly U, Pu and Np, continues to be the focus of ongoing studies.

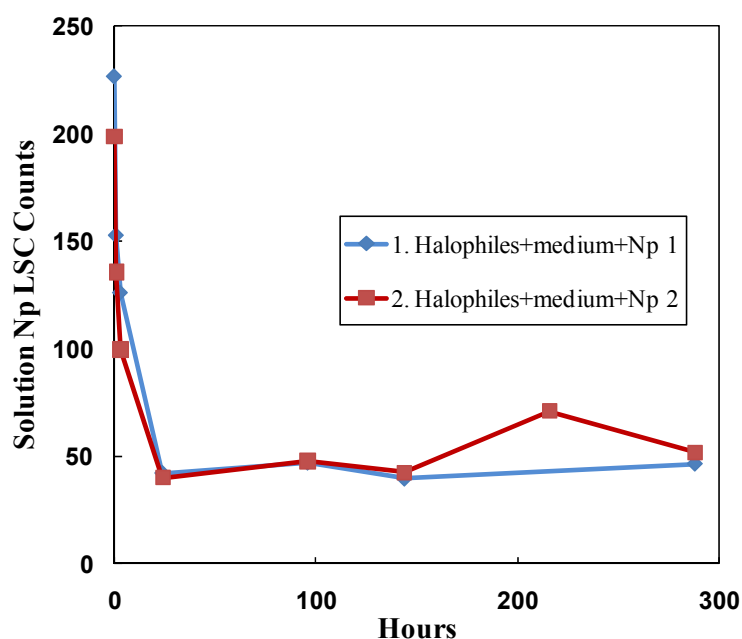


Figure 4. Bio-enhanced Np(V) Reduction Using Fe(III) High Ionic Strength Medium

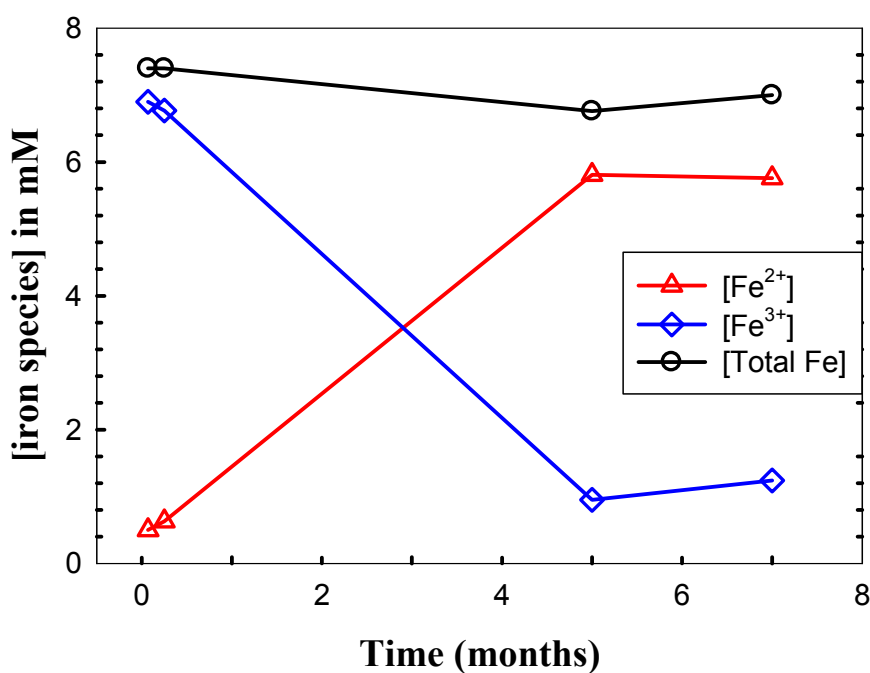
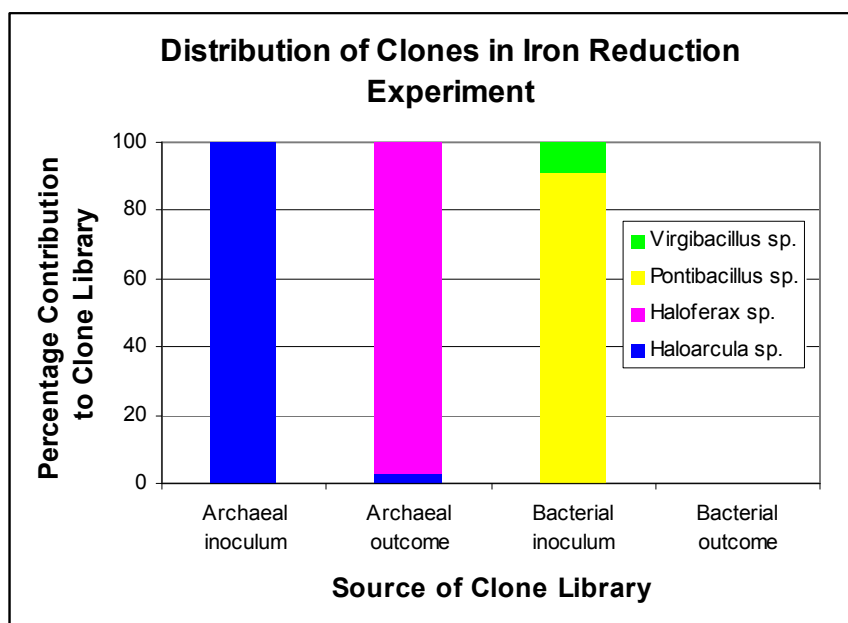


Figure 3. Top: Graph depicting the distribution of clones with two distinct libraries, Bacterial and Archaeal. Shows almost complete disappearance of *Haloarcula* sp. and complete disappearance of Bacterial species during the course of incubation, with selection for *Haloferax* sp.. Bottom: Results for iron analysis in incubation tube C of PZ-13 iron-reduction experiment. Levels of iron(III) decrease with a concomitant increase in iron(II). Total iron remains constant throughout the incubation period.

Summary and Conclusions

The factors that will define E_h in a brine system were discussed. WIPP assumptions, based on expert opinion, are being supported by ongoing site-relevant research even though little site relevant data existed at the time they were established.

E_h brine measurements, when performed with excess reduced iron in solution, qualitatively correlated with the Fe^{2+} content in the brine systems. Equilibration times were relatively rapid and effort to quantify this effect more rigorously is underway. This reduced iron is very reactive in brine across a wide pH range and is very effective in reducing multivalent actinides to their lowest possible oxidation state: U(IV), Pu(III) and Np(IV). These experimental results support the overall WIPP PA assumptions and establish them to be conservative with respect to overall solution concentration of mobile actinide species. The one important and key area that is not fully resolved is the long-term stability of the Pu(III) phases being observed and in particular the effects of radiolysis, the more repository-relevant condition, will have on the distribution of plutonium between Pu(III) and Pu(IV). It was already demonstrated that reduced iron is very effective in reducing Pu(V/VI) in radiolysis-affected systems (Reed et.al., 2007). This lower oxidation-state equilibration remains the focus of our ongoing research.

Lastly, progress is reported on establishing the effects of microbial growth, for the halotolerant and halophilic *Bacteria* and *Archaea*, typically found in high ionic strength brine systems. Oxygen consumption and Fe^{3+} reduction were observed. Bio-enhanced reduction of Np(V) was likely observed and there is an expectation that the Fe^{2+} formed will certainly lead to the reduction of high-valent plutonium. This work is expected to show that many microbial controls and effects that are well demonstrated for soil bacteria will also function for the microorganisms typically found at high ionic strength.

Future Directions of the Research

Research to understand the key subsurface processes that control and determine actinide redox reactions in the WIPP repository will continue. Near-term emphasis is on work to establish the key mechanisms of the reduced-iron plutonium interactions. Experiments to establish the long-term stability of reduced plutonium phases (both Pu(III) and Pu(IV)) are planned. The characterization of WIPP-indigenous microorganisms is ongoing with continued emphasis on halotolerant and halophilic microorganisms that biodegrade organic chelating agents and are important in the bioreduction of higher-valent actinides.

Acknowledgement

The authors wish to thank the Recosy project for the opportunity to participate as a presenter and contribute this paper to the third annual meeting; also some travel expenses were provided. The authors also wish to thank Dan Olive and professor Jeff Terry (IIT) for performing the XANES analysis on the plutonium precipitates. These analyses were performed at the Argonne National laboratory Advanced Photon source (APS). This work was supported by the Waste Isolation Pilot Plant program through

the Department of Energy Carlsbad Field Office. Some support was also received by the Environmental Remediation Science Program, DOE Office of Science.

References

- Banaszak, J.E., Rittmann, B.E., and Reed, D.T. (1999). Subsurface interactions of actinide species and microorganisms: Implications for the bioremediation of actinide-organic mixtures, *J. Radioanal. Nucl. Chem.*, 241: 385-435.
- Borkowski, M., Lucchini, J.F., Richmann, M.K., and Reed, D. T. (2009). Actinide (III) Solubility in WIPP Brine: Data Summary and Recommendations. Report LA-14360. Los Alamos. September 2009. LA-UR 09-03222.
- Boukhalfa, H., Icopini, G.A., Reilly, S.D., and Neu, M.P. (2007). Plutonium(IV) reduction by the metal-reducing bacteria *Geobacter metallireducens* GS15 and *Shewanella oneidensis* MR1, *Appl. Environ. Microbiol.*, 73: 5897–5903.
- Caccavo, F., Blakemore, R.P., and Lovley, D.R. (1992). A hydrogen-oxidizing, Fe(III) reducing microorganism from the Freat Bay Estuary, New Hampshire, *Appl. Environ. Microbiol.*, 58: 3211–3216.
- Capdevila, H., and Vitorge, P. (1990). Temperature and ionic strength influence on U(VI/V) and U(IV/III) redox potential in aqueous acidic and carbonate solutions, *J. Radioanal. Nucl. Chem.*, 143(2): 403-414.
- Christensen, T.H., Bjerg, P.L., Banwart, S.A., Jakobsen, R., Heron, G., Albrechtsen, H.J. (2000). Characterization of redox conditions in groundwater contaminant plumes, *J. Contam. Hydro.*, 45: 165-241.
- Degueldre, C., Rocchiccioli, F., Laube, A. (1999). Accelerated measurement of groundwater redox potential: method and application, *Analytica Chem.*, 396: 23-31.
- Francis, A.J., Dodge, C.J., and Gillow, J.B. (2008). Reductive dissolution of Pu(IV) by *Clostridium* sp. Under anaerobic conditions, *Environ. Sci. Technol.*, 42: 2355-2360.
- Gorby, Y.A., and Lovley, D.R. (1992). Enzymatic uranium precipitation, *Environ. Sci. Technol.*, 26: 205–207.
- Holm, T.R., and Curtiss, C.D. (1989). A comparison of Oxidation –Reduction Potentials Calculated From the As(V)/As(III) and Fe(III)/Fe(II) Couples with Measured Platinum-Electrode Potential in Groundwater, *J. Contam. Hydrology*, 5, 67-81.
- Kehew, A.E., Hughes, L.D., and Chowdhury, S.H. (2000). Aquifer Vulnerability Assessments: Are they Vulnerable to Misinterpretation and Misuse?, *Groundwater* 2000, 455-456.
- Lindberg, R.D., and Runnels, D.D., (1984). Groundwater Redox Reactions – An Analysis of Equilibrium State Applies to Eh Measurements and Geochemical Modeling, *Science*, 225, 925-927.
- Lovley, D.R. (1993). Dissimilatory metal reduction, *Annu. Rev. Microbiol.*, 47: 263–290.
- Lucchini, J.F., Borkowski, M., Richmann, M.K., and Reed, D. T. (2007). Solubility of Nd^{3+} and UO_2^{2+} in WIPP brine as oxidation-state invariant analogs for plutonium, *Journal of Alloys and Compounds*, Volumes 444-445 (2007) 506-511.

Masue-Slowley, Y., Kocar, B.D., Jofre, S.A.B., Mayer, K., and Fendorf, S. (2011). *Env.Sci. Tech.*, 45: 582-588.

Pepper, S.E., Borkowski, M., Richmann, M.K., and Reed, D.T. (2010). Determination of Ferrous and Ferric Iron in Aqueous Biological Solutions, *Analytical Chimica Acta*, 663, 172-177.

Reed, D.T., Lucchini, J.F., Aase, S.B., and Kropf, A.J. (2006). Reduction of Plutonium (VI) in Brine under Subsurface Conditions, *Radiochim Acta*, 94: 591-597.

Reed, D.T., Pepper, S.E., Richmann, M.K., Smith, G., Deo, R.P., and Rittmann, B.E. (2007) Subsurface bio-mediated reduction of higher-valent uranium and plutonium, *J. Alloys Compd.*, 376: 444-445.

Reed, D.T., Deo, R., and Rittmann, B.E. (2010). "Subsurface Interactions of Actinide Species and Microorganisms," Chapter 33 in *Chemistry of the Actinide and Transactinide Elements*, Elsevier Press, NY, NY.

Reed, D.T., Borkowski, M., Richmann, M.K., Lucchini, J.F., and Garner, J. (2011). Appendix SOTREM-2009, Actinide Chemistry Source Term, Los Alamos National Laboratory, Los Alamos, New Mexico.

Rittmann, B.E., Banaszak, J.E., and Reed, D.T. (2002). Reduction of Np(V) and precipitation of Np(IV) by an anaerobic microbial consortium, *Biodegradation*, 13 (5) 329–342.

Rolm, T.R. and Curtiss, C.D. (1989). A comparison of oxidation-reduction potentials calculated from the As(V)/As(III) and Fe(III)/Fe(II) couples with measured platinum-electrode potentials in groundwater, *J. Contam. Hydro.*, 5: 67-81.

Wiesner, A.D., Katz, L.E., and Chen, C.C. (2006). The impact of ionic strength and background electrolyte on pH measurements in metal ion adsorption experiments, *J. Colloid and Int. Science*, 301: 329-332.

TRAPPING OF RADIONUCLIDES/ACTINIDES IN THE CANISTER CORROSION PRODUCT MAGNETITE

Andreas Loida*, Volker Metz, Elke Bohnert, Bernhard Kienzler,
Nikolaus Müller, Dieter Schild, Eva Soballa

Karlsruhe Institute of Technology, Institut für Nukleare Entsorgung (KIT-INE), DE

*Corresponding author: Andreas.Loida@kit.edu

Abstract

Relevant reactions affecting the observed radionuclide concentrations released from spent nuclear fuel (SNF) are determined by redox phenomena. In order to investigate these reactions, the reductive trapping of radionuclides/actinides onto canister corrosion products was investigated. The system under investigation consists of magnetite that has been in contact with spent fuel for ten years immersed in 5 M NaCl solution. The experiment was terminated, the gas phase and the solution composition were analyzed. Now, emphasis was focused on characterizing the magnetite after termination of the experiment. By dissolution experiments using magnetite as fabricated and subsequent gas analysis, considerable amounts of CO₂ were found. This is an explanation for the unexpected high U concentrations in the solution after termination of the SNF-magnetite experiment. Moreover, the mineralogical phase composition of the reacted magnetite was investigated by XRD and the distribution of radioelements between the aqueous phase, the vessel wall and the magnetite was determined. Released amounts of Am, Pu and U were re-immobilized at 95%, 87% and 71% upon the surface of the magnetite. Due to radiolysis, a relatively high percentage of O₂ (5.4 vol.%) was found in the gas phase, which influences the reductive trapping of actinides and may interfere with sorption processes.

Introduction

The source term from spent nuclear fuel (SNF) dissolution is highly dependent on oxidative dissolution of the fuel matrix. The capacity of corroded canister iron phases to incorporate radionuclides is under investigation. A stable corrosion product of steel canister material under reducing conditions is magnetite. In the present study, it was intended to investigate the reductive trapping of actinides released from SNF onto the metallic corrosion products of the canister. The experiment (denoted as “K14Mt”) was running over roughly 10 years, which was designed to investigate the effect of magnetite on the overall corrosion behaviour of SNF in NaCl solution. The NaCl solution was sampled and analysed regularly during ~ 5 yrs. After another 5 yrs. period, this experiment was terminated and investigations of the gas phase, the solution composition and the solid material were performed. Unexpectedly, a rather high U concentration was measured ($\sim 1 \cdot 10^{-4}$ M), in association with a high CO₂ partial

pressure (0.8 vol. % in the gas phase). First analyses by optical microscopy (SNF and magnetite), SEM/EDS (magnetite), XPS (magnetite), and Raman spectroscopy were carried out. Relevant results are summarized in Loida et al. (2010).

To complete this study, emphasis was directed towards the characterization of the magnetite material. Main points of interest were (i) indications of phase alteration, and (ii) carbonate concentrations of the magnetite as fabricated. Additionally, the distribution of radionuclides released from the SNF sample during ~10 years of corrosion experiment over the magnetite, the container wall and the aqueous phase was determined.

Experimental

The corrosion experiment was performed with a pellet sized segment of high burnup SNF (50 MWd/kg U, linear power 260 W/m), 6.6 g fuel, and 10 mm in length together with commercially available magnetite (ALFA 012962, grain size ~ 5 µm). The SNF sample and magnetite were immersed simultaneously in 5 mol/L NaCl solution (initial volume 200 mL, under Ar-atmosphere) in a glass vessel. During the initial phase of the experiment, the leachant was replaced entirely by fresh solution for four times until total of 65 days. This procedure removed the "initial release fraction (IRF)", such as Cs and fission gases in the gap between fuel and cladding and on grain boundaries. Afterwards the experiment was continued without replacing the solution (static), lasting over 3562 days. The gas phase and solution were sampled at 78, 215, 349, 771, 1895 and 3562 days after start of the static phase. The analytic procedures are described by *Grambow et al. (1996)*. A detailed description of the entire experimental procedure is given by *Loida et al. (2003)*. After termination of the experiment, fractions of the gas phase, the NaCl solution and the magnetite were removed and analyzed. Various methods have been applied to study the solids: Optical microscopy, SEM/EDX, Raman spectroscopy, XPS and XRD. XRD measurements were performed using a Bruker D8 Advance diffractometer equipped with a Cu K_α radiation tube and Ni filters, working at a current of 25 mA and a voltage of 40 kV. Diffraction patterns were recorded from 2 to 100° 2θ with steps of 0.01° 2θ, 8 seconds counting time second and variable slit widths. Measured reflexes were compared to XRD patterns of relevant phases of the JCPDS database. Radionuclides retained upon the magnetite and on the vessel wall were determined by digestion/stripping the material in acid (HCl 30% or 5M HNO₃) and consecutive radiochemical analyses.

Results and discussion

Phase composition of the reacted magnetite by XRD

To verify the phase composition of the magnetite after the experiment a sample of this material (samples of some mg in weight, γ-dose rate < 0.5 µSv/h) was used for XRD measurements. Diffraction patterns of the untreated ALFA 012962 material as fabricated and the sample recovered from the leaching experiment show essentially the same reflexes. In both samples magnetite (Fe₃O₄) and hematite (α-Fe₂O₃) are detected as major phases (Figure 1). Though weak reflexes at 33.9°, 47.2° and 59.8° 2θ indicate

traces of an unidentified phase, but no reflexes of a Fe-carbonate mineral could be observed.

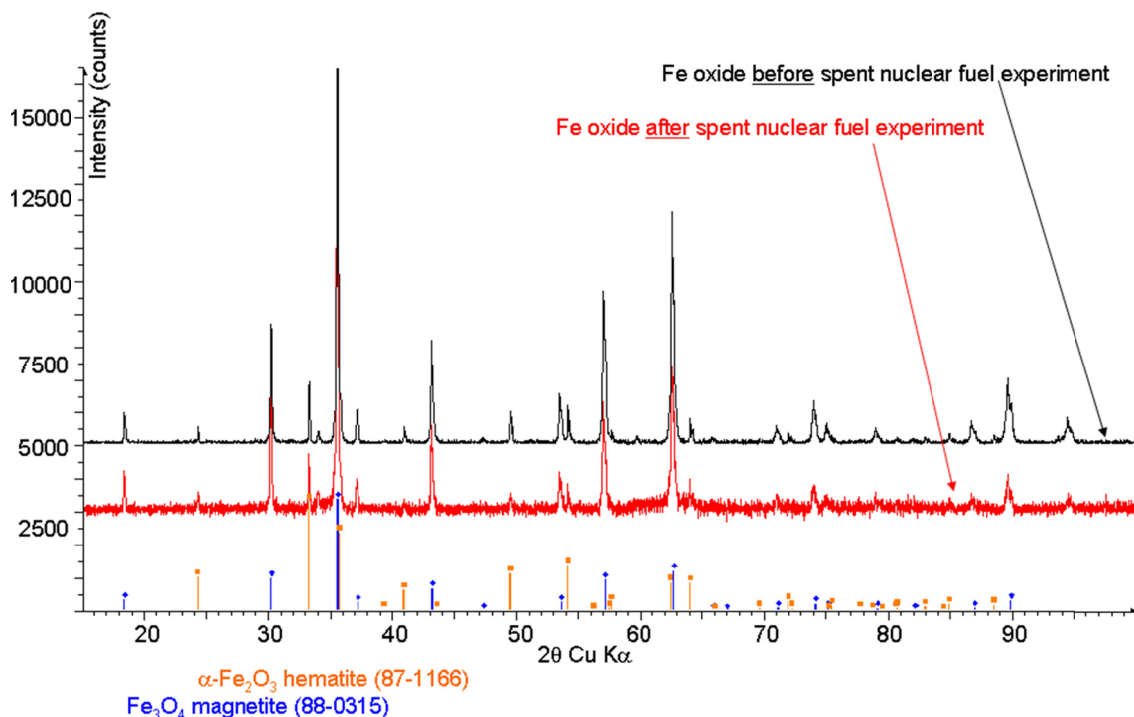


Figure 1: Diffraction patterns of the untreated ALFA 012962 material and after-recovered from the leaching experiment. For comparison reflexes of magnetite (Fe_3O_4 , JCPDS file #88-0315) and hematite ($\alpha\text{-Fe}_2\text{O}_3$, JCPDS file #87-1166) are shown

Phase composition of the reacted magnetite by Raman spectroscopy

Small samples of the reacted ALFA 012962 magnetite, as well as reference materials (hematite, goethite and magnetite) were analyzed by Raman spectroscopy. The spectra are shown in Figure 2. In the spectra denoted as “K14 S6 mt, area #1” and “K14 S6 mt, area #2” measured upon the corroded magnetite sample material after the experiment no magnetite, but only hematite was detected by Raman spectroscopy. It is known that magnetite may undergo a phase transformation by the high laser irradiation used in Raman spectroscopy (*de Faria et al. (1997)*). Therefore low laser energy was applied and magnetite spectra could be measured with the reference samples. Due to the fact that (a) magnetite was detected with the reference sample and (b) the black colour of the magnetite increased the surface sensitivity of Raman spectroscopy, it is concluded that hematite covers the surfaces of the sample K14 S6 mt.

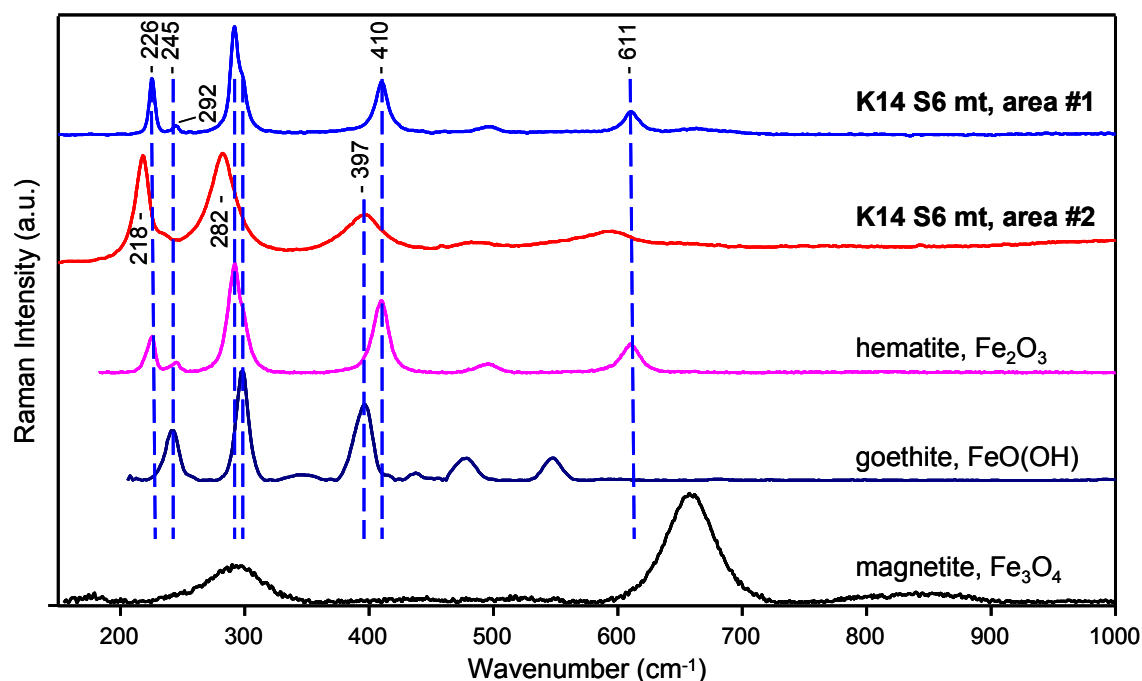


Figure 2: Raman spectra of the reacted ALFA 012962 magnetite samples and the reference minerals hematite, goethite and magnetite

Magnetite dissolution experiments

To find an explanation of the unexpected high CO₂ content of the gas phase encountered at the end of the SNF-magnetite corrosion experiment and eventually to identify the CO₂ source, magnetite dissolution experiments were carried out. An amount of 5 g magnetite as fabricated (ALFA 012962) was inserted in 30 ml HCl (30% ultrapure) under pure Ar atmosphere using a 250 mL autoclave. The gas phase was sampled after 74 days and replaced by Ar. After additional 31 days gas was sampled again. The gas was analyzed by mass spectrometry. The results are shown in Table 1. The fraction of Ar was found to decrease to 33 or 26.3 vol. %, whereas H₂ was formed up to percentages of 66.8 or 73.5 vol.%, respectively. The percentage of CO₂ was found to be 0.106 vol% after 74 d and 0.082 vol.% after 31 days, respectively. With regard to the measured N₂ contamination of 0.07 vol.% (air contamination over valves and fittings) the CO₂ percentage from air should not exceed $0.3 \cdot 10^{-4}$ vol%. Even in the case of a complete exchange of the Ar atmosphere by air the maximum possible amount of CO₂ would be about 0.03 vol.%, only. After the end of both reaction intervals the original magnetite was found to be completely dissolved.

The outcome of the magnetite dissolution experiments supports the assumption that the unexpected high CO₂ concentrations in the atmosphere of the long-term SNF-magnetite experiment result from a certain carbon/carbonate content of the magnetite. The relevant phase is a minor component and was not observed by XRD.

Table 1: Composition of the gas phase after dissolution of 5 g magnetite (ALFA 012962) in 30 mL HCl.

	1 st Interval 74 d Percentage	2 nd Interval 31 d Percentage
Ar	33.011	26.343
CO ₂	0.106	0.082
H ₂	66.803	73.504
N ₂	0.076	0.069
O ₂	0.004	0.002
Total	100.000	100.000

Radionuclide distribution

A further point of interest was the distribution of released radionuclides between the aqueous phase, the glass vessel wall and the magnetite. Radionuclides retained on the glass vessel wall were re-mobilized by stripping the vessel with HNO₃ followed by radiochemical analysis of the stripping solution. The measured distribution of elements in the aqueous phase (leachant), upon the glass vessel wall and upon the magnetite after the 3562 days experiment is shown in Table 2.

Table 2: Measured radionuclides in the leachant, upon the glass vessel wall and upon the magnetite after 3562 days co-dissolution of SNF and magnetite in 5 M NaCl solution in mol

	NaCl solution	Vessel wall	Magnetite	Total
Cs	$1.4 \cdot 10^{-06}$	$4.6 \cdot 10^{-10}$	$7.4 \cdot 10^{-08}$	$1.5 \cdot 10^{-06}$
Sr	$3.0 \cdot 10^{-07}$	$6.3 \cdot 10^{-11}$	$2.2 \cdot 10^{-09}$	$3.0 \cdot 10^{-07}$
Tc	$1.5 \cdot 10^{-07}$	$2.1 \cdot 10^{-11}$	$2.2 \cdot 10^{-09}$	$1.5 \cdot 10^{-07}$
Np	$2.3 \cdot 10^{-09}$	$1.3 \cdot 10^{-11}$	$1.4 \cdot 10^{-09}$	$3.7 \cdot 10^{-09}$
Am	$1.6 \cdot 10^{-09}$	$3.0 \cdot 10^{-11}$	$3.4 \cdot 10^{-08}$	$3.6 \cdot 10^{-08}$
Pu	$2.4 \cdot 10^{-09}$	$5.3 \cdot 10^{-10}$	$2.0 \cdot 10^{-08}$	$2.3 \cdot 10^{-08}$
U	$1.5 \cdot 10^{-05}$	$2.8 \cdot 10^{-07}$	$3.6 \cdot 10^{-05}$	$5.1 \cdot 10^{-05}$

Table 2 shows that the total amount of U found in the leachant, upon the glass vessel wall and on the magnetite after 3562 days was measured to the highest extent of $5.1 \cdot 10^{-5}$ mol. More than 70 % of this amount was re-immobilized upon the magnetite. The released Cs was determined to be $1.4 \cdot 10^{-6}$ mol, at which roughly 95% was found in the aqueous phase. Sr and Tc, both were released at similar amounts, i.e. $3.0 \cdot 10^{-7}$ or $1.5 \cdot 10^{-7}$ mol and in both cases about 98.7% were found in solution. The releases of Am and Pu were found to be $3.6 \cdot 10^{-8}$ or $2.3 \cdot 10^{-8}$ mol, from which about 95 % or 90% were retained upon the magnetite and the vessel wall. Np was released at $3.7 \cdot 10^{-9}$ mol, from which about 61 % were found in the aqueous phase and roughly 39 % upon the magnetite. The retention of radioelements upon the glass vessel wall does not play a significant role except for plutonium. Figure 3 shows the distribution of released radioelements between the aqueous phase, the glass vessel wall and the magnetite.

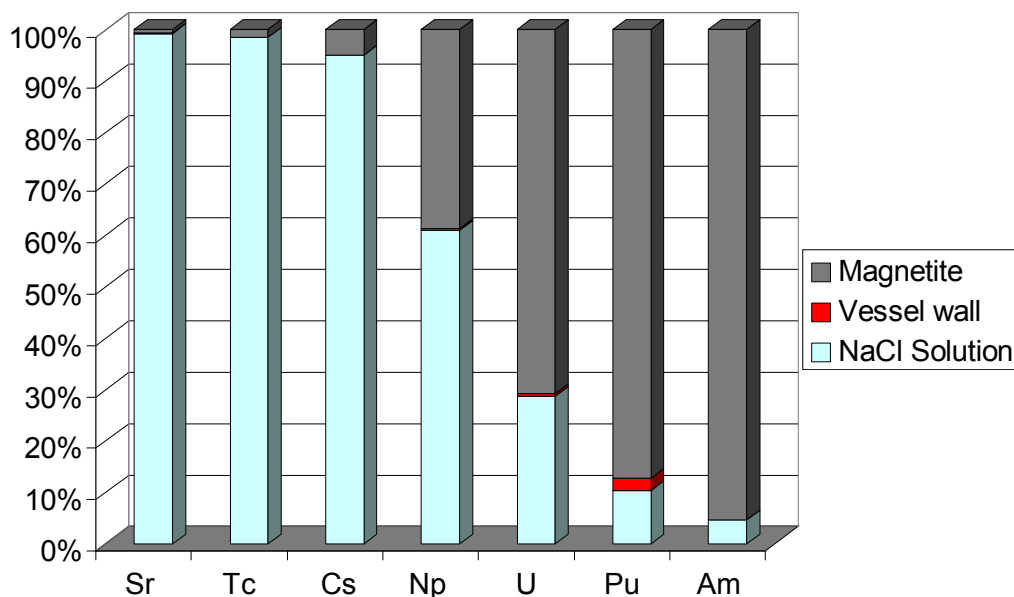


Figure 3: Distribution of released radionuclides between the aqueous phase, the magnetite and the glass vessel wall in terms of percentage

The related Kd values of Cs, Sr, Tc, Np, Am, Pu and U are compiled in Table 3. With respect to U a Kd value of 41.3 mL/g was found. This is a factor of about more than 10 higher as found in the frame of U (VI) sorption studies upon magnetite by *Missana et al. (2003)*, which is indicated as Kd (U VI) 4 mL/g.

Table 3: Kd values of radionuclides sorbed upon the magnetite after 3562 days co-dissolution of SNF and magnetite in 5 M NaCl solution

Nuclide	Kd (mL/g)
Cs	0.9
Sr	0.1
Tc	0.2
Np	10.5
Am	344.5
Pu	140.4
U	41.3

Concluding remarks

The gas composition in the SNF leaching experiment “K14Mt” changed significantly over almost 10 years observation period. Due to the unexpected elevated concentrations of CO₂ the U concentration in solution increased up to $\sim 1 \cdot 10^{-4}$ M. The considerable CO₂ content in the gas phase at the end of the corrosion experiment is related to the carbon / CO₂ content of the “Fe₃O₄” material used in the leaching experiment. The relevant

carbon-containing phases are of minor concentration in the ALFA 012962 magnetite and could not be detected by XRD and Raman spectroscopy.

In spite of the higher concentrations of radionuclides, in particular of U, due to the high CO₂ content, considerable amounts of radionuclides were retained upon the magnetite. In particular, with respect to Am, Pu, U and Np about 95, 87, 71 and 39 % of the total released amounts were found to be re-immobilized upon the magnetite ALFA 012962 (cf. Fig. 3).

Due to the Raman findings which is corroborated by XRD (Fig. 1) a hematite layer is present onto the surfaces of this material. Therefore, the trapping of the actinides cannot be attributed to reductive process alone, but sorption reactions may influence the retention, too. The ALFA 012962 magnetite plays a significant role in retaining the redox sensitive actinides.

Acknowledgement

The research leading to these results has received funding from the European Union's European Atomic Energy Community's (Euratom) Seventh Framework Programme FP7/2007-2011 under grant agreement n° 212287 (RECOSYproject)

References

- de Faria, D. L. A., Venaüncio S., Silva, M. T. de Oliveira, M.T. (1997), Raman Microspectroscopy of Some Iron Oxides and Oxyhydroxides, J. Raman Spectr., Vol. 28, 873-878
- Grambow, B., Loida, A., Dressler, P., Geckeis, H., Gago, J., Casas, I., de Pablo, J., Gimenez, J., Torrero, M.E., (1996), Long-term safety of radioactive waste disposal: Chemical reaction of fabricated and high burnup spent fuel with saline brines, Wissenschaftliche Berichte, Forschungszentrum Karlsruhe FZKA 5702,
- Loida, A., Bohnert, E., Kienzler, B., Müller, N., Plaschke, P., Schild, D., Soballa, E. (2010) Release and retention of radionuclides during 10 years corrosion of spent nuclear fuel (SNF) in presence of magnetite, 2nd Proceedings of the Annual Workshop 7th EC FP - Recosy CP, Larnaca (Cyprus) 16th – 19th March 2010, KIT Scientific Reports 7557, Karlsruher Institut für Technologie (KIT), Karlsruhe, Germany, pp.111-116
- Loida, A., Kienzler, B., Geckeis, H. (2003) Mobilization/Retention of Radionuclides during Co-dissolution of high burnup spent fuel and near field materials in salt brines, Mat. Res. Soc. Symp. Proc. Vol.757, pp. 433-439, Warrendale, PA, USA
- Missana, T., Garcia-Guthierres, M., Fernandez, V. (2002) Uranium (IV) sorption on colloidal magnetite under anoxic environment: Experimental study and surface complexation modelling, Geochimica et Cosmochimica Acta, Vol. 67, No 14, 2543 - 2550

POSTER ABSTRACTS

List of poster abstracts

Sorption and redox behavior of radionuclides in natural clay rocks. <i>N. L. Banik, C. M. Marquardt, J. Rothe, D. Schild, T. Schäfer.</i>	277
On the redox chemistry at the near field of repository, the influences of iron canister material and hydrogen <i>D. Cui, P. Carbol, K. Spahiu.</i>	278
Behaviour of Tc(VII) in aqueous solutions in the presence of iron oxides and microorganisms. <i>R. Druteikiene, B. Luksiene, D. Peciulyte, K. Mazeika, A. Gudelis, D. Baltrunas</i>	279
Effect of EDTA, ISA and Picolinic Acid on Redox Chemistry of Tc <i>N. Evans, R. Hallam, S. Jain, M. Felipe-Sotelo, N. Bryan.</i>	280
Uptake of Np(IV) by C-S-H phases and cement. An EXAFS study. <i>X. Gaona, R. Dähn, J. Tits, C. Scheinost E. Wieland.</i>	281
Redox potential measurements on unirradiated UO ₂ (s) dissolution experiments under alkaline conditions in the presence of dithionite <i>M. Grivé, V. Montoya, O. Riba, L. Duro.</i>	282
Agreement between measured Eh and quantification of actinide oxidation states - Progress Report <i>S. Holgersson.</i>	283
Tc(VII), U(VI) and Np(V) sorption/reduction kinetics under glacial melt water conditions: Comparison between batch and column migration experiments <i>F. Huber, P. Kunze, T. Schäfer.</i>	284
Actinide Partition in Humic Colloidal Ternary Systems. <i>R. Kay, L. Abrahamsen, N.D. Bryan, A. Stockdale.</i>	285
Interaction of iron bearing minerals with dithionite in Boda Claystone samples <i>K. Lázár, J. Megyeri, E. Bokori, Z. Máthé.</i>	286
Migration of uranyl ions in Boda Claystone samples <i>K. Lázár, J. Megyeri, Zs. Mácsik, E. Széles, Z. Máthé.</i>	286
Trapping of radionuclides/ actinides onto canister corrosion products. <i>A Loida, V. Metz, E. Bohnert, B. Kienzler, N. Müller, D. Schild, E. Soballa.</i>	287
Actinide redox chemistry in high salinity media: a LANL/ACRSP overview. <i>J.F. Lucchini, D. Reed, M. Richmann, J. Swanson, D. Ams, H. Khaing, M. Borkowski</i>	288

Investigation of redox behaviors of iron in aqueous solutions by combination of chemical speciation and Eh measurements. <i>J. Y. Oh, J. I. Yun.</i>	289
An Electrochemical Approach to Study the Reactivity of Pyrite with Soluble Iodine and Selenium Specie <i>M. Perdicakis, C. Malhomme, C. Bouchereau.</i>	289
Voltammetric characterization of Boda Albitic Claystone: Comparison with Mössbauer spectroscopy data <i>M. Perdicakis, Y. Xu, K. Lázár, Z. Máthé.</i>	290
Electrochemical investigations on doped and undoped UO ₂ spent fuel model surfaces <i>T. Petersmann, T. Gouder, A. Seibert, Th. Fanghänel.</i>	291
Redox measurements of iron systems from the intercomparison exercise. <i>O. Riba, M. Grivé.</i>	292
Oxygen scavenger capacity. <i>Rojo, F. Clarens, J. de Pablo.</i>	293
Complexation study of U(VI) with phenol by TRLFS. <i>C. Sabater, C. Walther, G. Geipel, M. Grivé, L. Duro.</i>	294
Formation of Fe(III)-hydroxo complexes in brines. <i>T. Scharge, B. P. Bischofer, S. Hagemann.</i>	295
The interaction of Fe(II) with clay minerals <i>D. Soltermann, D. Marques Fernandes, B. Baeyens, R. Dähn, M. H. Bradbury.</i>	296
Progress in the development of a fibre optical chemical sensor (FOCS) for the simultaneous determination of proton oxygen and chloride concentrations. <i>D. Steinbrück, E. Schmälzlin, M.U. Kumke.</i>	297

SORPTION AND REDOX BEHAVIOR OF RADIONUCLIDES IN NATURAL CLAY ROCKS

N. L. Banik, C.M. Marquardt, J. Rothe, D. Schild, T. Schäfer

Karlsruhe Institute of Technology (KIT), Institute for Nuclear Waste Disposal (INE),
D-76344 Eggenstein-Leopoldshafen, Karlsruhe, Germany

Abstract

Studies have been performed on the sorption and redox behavior of radionuclides (Np, Pu, Tc) on the natural clay rocks OPA and COx. The batch experiments were performed with artificial porewater at radionuclide concentrations between 3.0×10^{-4} and 1.0×10^{-8} M under argon atmosphere (+1% CO₂). The pH was pH 7.2 – 7.6 and the contact times were up to 1 year.

We observed that the sorption of the radionuclides increases with increasing clay amounts and with increasing contact time. More than 80 % of Np and Pu are sorbed on the clay whereas only 35 % of Tc is bound on OPA and COx after 4 months contact time. The preliminary K_d values for batch experiments of OPA and COx are calculated to be 6.33 and 5.53 mL/g for Pu, 5.50 and 5.35 mL/g for Np, 0.053 and 0.036 mL/g for Tc with a solid/liquid ratio of 10. The samples are characterized by EXAFS, UV-Vis, XPS, capillary electrophoresis, and liquid-liquid extraction. Preliminary results show that Np is sorbed on both solid phases in the form of Np(V), Pu is sorbed as Pu(IV), and Tc as Tc(VII) after 1 week contact time. The spectroscopic results of this study will be presented.

ON THE REDOX CHEMISTRY AT THE NEAR FIELD OF REPOSITORY, THE INFLUENCES OF IRON CANISTER MATERIAL AND HYDROGEN

Daqing Cui, Paul Carbol and Kastriot Spahiu

Studsvik, JRC-ITU and SKB

Abstract

During this 3rd year, our efforts were concentrated on the following two important aspects relevant to the redox chemistry at near field repository environment:

Np-Pu reductive immobilization by iron canister material

The results of Np(V)-Fe(0) redox experiment was reported as a manuscript and submitted for publication.

The Pu(VI) –Fe(0) redox experiment was restarted after adopting a method of oxidising Pu(IV) by fuming HClO₄ to Pu(VI) and then add it to a carbonate solution. At room temperature, oxidation reactions by ClO₄⁻ are generally kinetically slow and should not have significantly influence on the reducing capacity of Fe(0). To substantiate this statement a separate experiment was made to study the reaction of ClO₄⁻ with Fe(0).

Anyhow, to minimize the potential effect of excess ClO₄⁻ on the simulated near field reducing conditions, after oxidizing Pu(IV) to Pu(VI) and diluting it in a 2 mM HCO₃⁻ solution, KCl was added to precipitate most ClO₄⁻ left in the solution. The solubility of KClO₄ is 1.5 g/l. In a solution containing ppm-level of Pu(VI) most of the Pu was found to be immobilized on the iron surface and the oxidation state of the precipitated Pu on the iron surface will be analysed by XANES.

Mechanisms of the hydrogen influence on radionuclide migration by D/H isotope exchange method.

- It was observed that isotope exchange between D in D₂ gas (11 bar) and H in water solution does slowly occur with the presence of SIMFUEL pellet, (a spent fuel simulator containing UO₂ and noble metal fission product particles through the reaction $D_2 + H_2O \Rightarrow D_2O + H_2$, but not significant occurs in the blank experiment.
- The decrease of N₂/O₂ ratio in the gas mixture of air and D₂ in autoclave containing water solution and the SIMFUEL pellet, but not in blank experiment without SIMFUEL.
- The D/H ratio in water solution that interacted with a 11.3 bar gas mixture of D₂ + 0.14% O₂ with the presence of SIMFUEL pellet for 2 months was found to be (7157 dD per mil) 1270 ppm (isotopic ratio). It is about three times higher than the calculated value according to the O₂ added in the system. It proves that beside the deoxygenation reaction, $2D_2 + O_2 \Rightarrow 2D_2O$, there should be an isotope exchange reaction $D_2 + H_2O \Rightarrow D_2O + H_2$.

BEHAVIOUR OF Tc(VII) IN AQUEOUS SOLUTIONS IN THE PRESENCE OF IRON OXIDES AND MICROORGANISMS.

R. Druteikiene, B. Luksiene, D. Peculyte, K. Mazeika, A. Gudelis, D. Baltrunas

¹ Center for Physical Sciences and Technology, Savanoriu av. 231, Vilnius, Lithuania

² Institute of Botany of Nature Research Center, Zaliujų Ezerų 49., Vilnius, Lithuania

Abstract

The factors that influenced technetium (TcO_4^-) reduction, and sorption onto iron oxides, including pH, incubation time, humic acid, microbial activity, were examined. Batch experiments under ambient conditions were conducted. Bacteria and fungi for batch experiments of Tc sorption onto iron mineral were selected after tests under different conditions. Only some strains, isolated from the substrates, were screened based on their peculiarities: ability to reduce nitrate, H_2S formation, organic acid production and resistance to different pH values. Most attention was paid to bacteria and especially to facultative aerobes.

Results showed that after a short exposure period (48 hours) under alkaline conditions (pH 8-9) more than 75% of TcO_4^- were associated with Fe(II) oxide particles and removed from solution. The removal of Tc from solution may be controlled by reduction of Tc(VII) to Tc(IV) by biogenic Fe(II). Under these circumstances no pronounced effect of the sorption of technetium onto Fe(III) oxide was determined. After 15 days 99% of TcO_4^- remained in solution.

An investigation of technetium reduction and sorption onto iron oxides under the acidic (pH 3-5) and neutral (pH 6-7) suggested that the pH of solution had a very slight influence on the technetium sorption.

EFFECT OF EDTA, ISA AND PICOLINATE ON REDOX CHEMISTRY OF Tc

N. Evans¹, R. Hallam¹, S. Jain¹, M. Felipe-Sotelo¹ and N. Bryan².

¹Department of Chemistry, Loughborough University, Loughborough, Leicestershire,
LE11 3TU, UK

²Department of Chemistry, Manchester University, Manchester, M13 9PL, UK

Abstract

The electrochemical reduction of technetium from oxidation state VII to IV has been performed in the presence and absence of the anthropogenic ligands EDTA, picolinic acid, α -isosaccharinic acid (ISA) and gluconic acid. It has been observed that three of the ligands, EDTA, gluconate and picolinate prevent the reduction taking place, whereas the presence of ISA does not affect the formation of Tc(IV) species. In the presence of the three ligands technetium remains in solution and does not precipitate as TcO₂(am), despite the very reducing conditions present in the experiments. The mechanism causing this phenomenon is still under investigation, but it may involve the formation of a technetium complex(es) of intermediate oxidation state(s) such as Tc(V) and/or Tc(VI), as occurs in technetium pharmaceuticals.

UPTAKE OF Np(IV) BY C-S-H PHASES AND CEMENT: AN EXAFS STUDY

X. Gaona^{1,*}, R. Dähn¹, J. Tits¹, A. C. Scheinost^{2,3}, E. Wieland¹

¹Laboratory for Waste Management, Paul Scherrer Institut, Villigen PSI (Switzerland)

²Helmholtz-Zentrum Dresden-Rossendorf, Institute of Radiochemistry, Dresden (Germany)

³Rossendorf Beamline (ROBL) at ESRF, Grenoble (France)

*Current address: Institut für Nukleare Entsorgung, Karlsruhe Institute of Technology, Karlsruhe (Germany)

Abstract

In many nuclear waste disposal concepts cementitious materials are foreseen to be used for the immobilization of long-lived intermediate level wastes (ILW). ILW may contain significant amounts of neptunium-237, which is expected as Np(IV) under the reducing conditions developing after the closure of the repository. Predicting the release of Np(IV) from this environment requires a sufficiently detailed understanding of its interaction with the main sorbing components of cement. In this study, the uptake of Np(IV) by calcium silicate hydrates (C-S-H) and hardened cement paste (HCP) has been investigated using extended X-ray absorption spectroscopy (EXAFS).

Evaluation of EXAFS data from Np(IV)-doped C-S-H and HCP indicates the predominant incorporation of Np in the C-S-H structure throughout the complete sequence of cement degradation. Two species were identified, corresponding to Np(IV) in C-S-H with Ca:Si 1.65 (fresh cement) and 0.75 (highly degraded cement). The coordination environment of Np(IV) was found to depend on the Ca:Si ratio but not on pH, consistently with the aqueous speciation of Np(IV) in the pH range 10 – 13.3 (with predominance of Np(OH)₄(aq)). These results unequivocally show that C-S-H phases are responsible for Np(IV) immobilization in cementitious materials, whilst incorporation in the interlayer of the C-S-H structure is regarded as the predominant uptake mechanism.

REDOX POTENTIAL MEASUREMENTS ON UNIRRADIATED- UO₂(s) DISSOLUTION EXPERIMENTS UNDER ALKALINE CONDITIONS IN PRESENCE OF DITHIONITE.

M. Grivé¹, V. Montoya¹, O. Riba¹, L. Duro¹

¹Amphos 21, Passeig de Garcia i Fària, 49-51, 1-1, Barcelona (Spain)

Abstract

Concrete (cement) based barriers are considered in the High and Low and Intermediate Level Waste repositories (HLW and LILW). These materials do not only offer high mechanical capacity and low hydraulic conductivity but also radionuclide retention capacity by establishing alkaline and reducing conditions.

In the framework of the ReCosy project, Amphos 21 has studied the solubility of unirradiated-UO₂(s) at pH 10, 11 and 12, in presence of Na-dithionite as a reducing agent and using 0.1M NaClO₄ as electrolyte. Dithionite has been previously used in different UO₂(s) solubility studies described in the literature although in most of them redox potential measurements have not been performed. In this work, pH and Eh measurements have been performed inside the reactor and solutions have been periodically sampled to analyse the total uranium concentration after being filtered through a 0.22µm pore size filter. In general, the redox measurements, performed with conventional combined Pt electrode using Ag / AgCl as a reference, show higher redox potential values than the ones expected from the measured uranium concentrations.

AGREEMENT BETWEEN MEASURED EH AND QUANTIFICATION OF ACTINIDE OXIDATION STATES - PROGRESS REPORT

Stellan Holgersson

Chalmers University of Technology, Department of Chemical and Biological
Engineering- Nuclear Chemistry, Kemivägen 4, SE 41296 Göteborg, Sweden

Abstract

Within the RECOSY program, Chalmers University will investigate the agreement of redox measurements in the laboratory between an ordinary redox electrode (Pt/Ag/AgCl) and the speciation determinations of actinides by solvent extraction. The systems studied will be simple representatives of a final repository of radioactive waste in a granitic bedrock: so-called batch experiments with crushed rock and synthetic groundwater in inert-gas atmosphere where redox control will be made by Fe(II)/Fe(III). Not at least the recent results from the RECOSY Interlaboratory Comparison Exercise have shown the need for complementary redox determination methods.

This progress report accounts for the latest results with U(IV/VI) and Np(IV/V) reduction, separation and quantification. Two solvent extraction methods that uses β -diketones for actinide separation, reported in the literature, are studied. The method with thenoyltrifluoroacetone (TTA) extraction is suitable for trace amounts of tetravalent actinides and gives a maximal separation from other oxidation states at pH 0.6 [1], which is also confirmed in our work.

The alternative method that is tested in our work is extraction with another β -diketone dibenzoylmethane (DBM), where the extraction is claimed to take place in neutral pH, which would be an advantage by avoiding large pH adjustments. The method extracts hexavalent actinides at pH 7 and tetravalent actinides at pH 4 [2].

References

- [1] Bertrand, P.A. and Choppin, G.R.(1982): Separation of actinides in different oxidation states by solvent extraction. *Radiochim. Acta* 31, 135
- [2] Saito, A. and Choppin, G.R.(1983) Separation of actinides in different oxidation states from neutral solutions by solvent extraction. *Anal.Chem.* **55**, 2454,

Tc(VII), U(VI) AND Np(V) SORPTION/REDUCTION KINETICS UNDER GLACIAL MELT WATER CONDITIONS: COMPARISON BETWEEN BATCH AND COLUMN MIGRATION EXPERIMENTS

F. Huber, P. Kunze, T. Schäfer

Karlsruhe Institute of Technology (KIT), Institute for Nuclear Waste Disposal (INE), D-
76344 Eggenstein-Leopoldshafen, Karlsruhe, Germany

Abstract

Reduction kinetic experiments of Tc(VII), U(VI) and Np(V) were performed in natural groundwater from the Grimsel Test Site (GTS, Switzerland) in presence of fracture filling material ($V/m = 4$) simulating glacial melt water intrusion conditions (pH 9.6; ionic strength $\sim 1\text{mM}$). This groundwater was also used throughout the InterComparison Exercise (ICE) under the reference number NAT 3. The batch-type studies show a decreasing Eh(SHE) potential from +25mV to -70mV (pH 9.6 - 9.1) over the experimental duration of 7500h. Comparison with thermodynamic calculations reveal a stability of U(VI) species and no sorption could be observed, whereas the pe/pH conditions are close to the borderline of the $\text{TcO}_4^-/\text{TcO}_2(\text{s})$ transition. Observed slightly lower ^{99}Tc distribution coefficients for fracture filling material (FFM) from Grimsel compared to Äspö can be correlated to the FFM Fe(II) inventory. In the case of $^{237}\text{Np}(\text{V})$, a decrease in concentration after ~ 300 h can be explained by a slow reduction to Np(IV) and subsequent sorption to mineral surfaces in accordance with the evolution of pe/pH. The batch sorption/reduction data will be compared with distribution coefficients re-calculated from column migration studies on an over cored natural fracture from Äspö (Sweden) having the full 3D geometry reconstruction and connected porosity through computer tomography (CT) data.

ACTINIDE PARTITION IN HUMIC COLLOIDAL TERNARY SYSTEMS.

R. Kay⁽¹⁾, L. Abrahamsen^(1,#), N.D. Bryan⁽¹⁾, A. Stockdale⁽¹⁾

1: University of Manchester, School of Chemistry, Centre for Radiochemistry Research
- currently at U.K. National Nuclear Laboratory

Abstrat

Humic substances are naturally occurring organic ligands 'HA'. They are ubiquitous in the environment and will bind to virtually all metal ions strongly. It is essential to consider their effects on metal ion transport in the environment e.g. in safety case for a radioactive waste repository.

The humic ternary systems (HA + mineral + radio nuclide 'RN') are complex, therefore accurate modeling of these systems is difficult. The aim this work is to develop a simple mathematical model to describe the behaviour of actinides in the environment.

INTERACTION OF IRON BEARING MINERALS WITH DITHIONITE IN BODA CLAYSTONE SAMPLES

K. Lázár¹, J. Megyeri¹, E. Bokori¹, Z. Máthé²,

Institute of Isotopes, Hungarian Academy of Sciences (HU)
²Mecsekérc Environmental Plc. (HU)

Abstract

Characteristic response from iron bearing minerals in Boda Claystone samples was found by using sodium dithionite reductant solutions. Samples originated from different regions of Boda Claystone formation were exposed to the treatment, the changes in their $\text{Fe}^{2+} / \text{Fe}^{3+}$ components were monitored by Mössbauer spectroscopy. Fe^{2+} components of the original minerals were not affected by the treatment. The hematite phase almost disappeared and the ferric ions of the clay components were also reduced to ferrous state. The reduction is probably mediated by the liquid phase. The significant part of the formed ferrous ions is relocated in the solid phase as a new constituent.

MIGRATION OF URANYL IN BODA CLAYSTONE SAMPLES

K. Lázár¹, J. Megyeri¹, Zs. Mácsik¹, É. Széles¹, Z. Máthé²

¹ Institute of Isotopes, Hungarian Academy of Sciences (HU)
² Mecsekérc Environmental Plc. (HU)

Abstract

Migration of UO_2^{2+} through Boda Claystone borecore disc samples was studied by using saturated uranyl acetate solutions in break-through cells. LA-ICP-MS was used to analyse the distribution of uranium in the bore core discs stored in the cells for 400 days. $\text{Fe}^{2+}/\text{Fe}^{3+}$ ratios were monitored in the mineral components of clay before and after the experiments by Mössbauer spectroscopy. The strong accumulation of uranium in a few mm thick surface layer was not accompanied with any noticeable change in the $\text{Fe}^{2+} / \text{Fe}^{3+}$ ratio of minerals. Thus as for the accumulation of uranium under the recent conditions, sorption processes prevailed.

TRAPPING OF RADIONUCLIDES/ACTINIDES IN THE CANISTER CORROSION PRODUCTS

Andreas Loida, Volker Metz, Elke Bohnert, Bernhard Kienzler,
Nikolaus Müller, Dieter Schild, Eva Soballa

Karlsruhe Institute of Technology, Institut für Nukleare Entsorgung (KIT-INE), DE

Abstract

Spent fuel dissolution highly depend on oxidative dissolution. The capacity of corroded canister iron phases to incorporate radionuclides is not sufficiently understood. The source term for safety analysis use over-conservative assumptions.

The objectives of KIT-INE are the determination of trapping of redox sensitive radionuclides and actinides onto canister corrosion products by magnetite interacting with spent fuel for 10 years in sat. in NaCl solution. This work include investigation of gas phase, leachant, magnetite surface / bulk properties, trapping of U and Pu by XPS, Raman spectroscopy, XRD, SEM-EDX and Optical spectroscopy

ACTINIDE REDOX CHEMISTRY IN HIGH SALINITY MEDIA: A LANL/ACRSP OVERVIEW

Jean Francois Lucchini, Donald Reed, Michael Richmann, Juliet Swanson, David Ams,
Hnin Khaing and Marian Borkowski

Earth and Environmental Sciences Division, Los Alamos National Laboratory, Carlsbad
Operations, USA

Abstract

Actinide redox chemistry is a critical factor in establishing the concentration of actinides in brine for a salt-based nuclear waste repository. It is well known that the solubility of reduced actinides (III and IV oxidation states) is significantly lower than oxidized forms (V and/or VI). In this context, understanding the interactions of reduced metals and microbiological processes with actinides is very important to fully evaluate the conditions that will lead to lower-valent oxidation states for the actinides.

The Los Alamos National Laboratory (LANL) Actinide Chemistry and Repository Science Program (ACRSP) team has been investigating the fate of actinides in high salinity media as part of the ongoing recertification efforts of the Waste Isolation Pilot Plant (WIPP) repository. We experimentally demonstrated reduction of uranium and plutonium under WIPP-relevant conditions, using iron and/or selected bacteria. An overview of the ACRSP current research and recent results, with a special emphasis on the processes that control redox, will be featured in the presentation.

INVESTIGATION OF REDOX BEHAVIORS OF IRON IN AQUEOUS SOLUTIONS BY COMBINATION OF CHEMICAL SPECIATION AND Eh MEASUREMENTS

J. Y. Oh and J. I. Yun.

Dept. of Nuclear and Quantum Eng., KAIST, Daejeon 305-701, Korea

Abstract

Iron is not only redox sensitive but also redox controlling element and exists abundantly as nuclear waste container in the near-field of a repository. Redox behavior influencing migration of radionuclides can be affected by their geochemical reactions in groundwater. Redox potential measurements using redox electrodes provide high uncertainty problem. The objective of this study is to investigate redox behaviors of iron in aquatic system by chemical speciation and Eh measurements.

AN ELECTROCHEMICAL APPROACH TO STUDY THE REACTIVITY OF PYRITE WITH SOLUBLE IODINE AND SELENIUM SPECIES

Michel Perdicakis, Cindy Malhomme and Clément Bouchereau

CNRS, Université de Nancy, Laboratoire de Chimie Physique et Microbiologie pour
l'environnement (LCPME) F-54602 Villers-les-Nancy cedex, France

Abstract

In this work, by means of voltammetric and dielectric measurements performed with micrometric particles of pyrite that reacted with soluble species of iodine and selenium as well as with corrosion current and Scanning Reference Electrode Technique measurements, we investigated the reactivity of FeS₂ towards iodate, iodine, iodide, selenate and selenite. Solution aliquots sampled and analyzed during the measurements and the characterization of the pyrite surface with XPS spectrometry came to the completion of the electrochemical techniques.

VOLTAMMETRIC CHARACTERIZATION OF BODA ALBITIC CLAYSTONE: COMPARISON WITH MÖSSBAUER SPECTROSCOPY DATA

M. Perdicakis¹, Y. Xu¹, K. Lázár², Z. Máthé².

¹Laboratoire de Chimie Physique et Microbiologie pour l'Environnement, Nancy-
Université — CNRS F - 54602 Villers-lès-Nancy Cedex, France

²Institute of Isotopes, Hungarian Academy of Sciences. H - 1525 Budapest. P.O. Box
77, Hungary

Abstract

Redox processes may influence the migration of certain radionuclides that are able to change their valence, and as a consequence, to change the charge of the migrating species. When the central radionuclides are in the higher valence state, they are charged and are able to migrate in aqueous media. In contrast, these species are neutral in their reduced forms and may precipitate. In turn, the opposite process of the previous reduction should also proceed in the neighbouring media, e.g. in a host rock.

In several cases the Fe(II) oxidation is considered as the possible counterpart of the previously mentioned reductions. Boda Siltstone Formation (BSF) is considered as a perspective medium for disposal of nuclear waste in Hungary. In general, overwhelming part of the BSF was formed under strong oxidation conditions in highly alkaline media at arid/semi-arid conditions. Thus further oxidation can hardly be expected. In correspondence, dominant part of the iron is present as hematite. A previous study performed with Mössbauer spectroscopy in BSF samples showed that minor amounts of iron can exist in the ferrous form (and, in specific regions, exclusively in the ferrous state) in spite of the predominance of the oxidative conditions controlling the genesis of the formation.

The aim of this study was to characterize electrochemically two series of samples from the BSF, which have been previously characterized by Mössbauer spectroscopy, and to specify the redox status of iron.

ELECTROCHEMICAL INVESTIGATIONS ON DOPED AND UNDOPED UO₂ SPENT FUEL MODEL SURFACES

T. Petersmann, T. Gouder, A. Seibert, Th. Fanghänel.

European Commission, JRC, Institute for Transuranium Elements, Herrmann-von-Helmholtz-Platz 1, 76344 Eggenstein-Leopoldshafen (D)

Abstract

In order to understand spent nuclear fuel (SNF) corrosion, elucidation of the processes is indispensable. In this context, the impact of individual components on fuel corrosion has to be studied. In a first set of experiments, the reactivity of SNF model surfaces (UO₂ thin films with Pd or Mo) is investigated in cyclovoltammetric measurements.

Recently we showed that the corrosion of UO₂ in aqueous solution (under oxic conditions) is decreased when Pd is incorporated into the oxide matrix. The formation of secondary phases at the UO₂ surface containing the Pd disables this inhibiting effect of Pd.

In further gas adsorption experiments we have demonstrated, that exposure of molecular hydrogen to hyperstoichiometric UO_{2+x} does not result in reduction of the oxide. Only at Pd-doped UO_{2+x} surfaces is H₂ activated which leads to an oxide reduction.

Now the electrochemical studies are extended to a more reductive environment (Ar, Ar/H₂) to clarify the mechanism of SNF matrix reduction by H₂ in aqueous solution.

REDOX MEASUREMENTS OF IRON SYSTEMS FROM THE INTER-COMPARISON EXERCISE

O. Riba, M. Grivé

Amphos 21. Pg. Garcia i Fària, 49 – 51, 08019, Barcelona (Spain)

Abstract

The Intercomparison Exercise (ICE) was conducted within the EUROATOM FP7 Collaborative Project “Redox phenomena controlling systems” (CP ReCosy) with the aim to compare different redox determining methods.

Amphos performed redox measurements under controlled inert atmosphere of the different systems selected for the exercise using conventional combined Pt electrode. The study was focussed on the equilibration time of the measurements by taking periodic readings while the systems were continuously stirred. The Eh readings indicate good agreement with the measurements performed by other participants using similar methodology. Thermodynamic calculations indicate the redox potential of each system was controlled by an iron redox couple and highlighted the usefulness of equilibrium models to validate redox measurements.

OXYGEN SCAVENGER CAPACITY

Isabel Rojo, Frederic Clarens, Joan de Pablo

CTM (Fundació CTM Centre Tecnològic) (Partner 6)

Abstract

The oxygen scavenger capacity has been evaluated for four different minerals that can potentially interact with radionuclides coming from nuclear waste repositories: two natural iron sulphides, pyrrhotite and pyrite, and two fracture filling materials (FFM) from Äspö and Grimsel. Experiments were performed with an initial oxygen concentration of 10^{-3} M in 0.1M NaClO₄ media. The oxygen uptake capacity measured as rate of oxygen consumption follows the order: pyrrhotite > FFM Äspö >> pyrite > FFM Grimsel. However, the oxygen scavenger capacity of FFM Grimsel is negligible as its response is of the same order of the blank experiment (ionic medium).

In parallel, the mineral dissolution has been monitored. In the experiments with pyrrhotite and pyrite the aqueous concentrations of Fe_{total}/SO₄²⁻/S₂O₃²⁻ increase with time, the same behavior is observed for Ca²⁺/NH₄⁺/SO₄²⁻/Si/Al/trace metals in the Äspö FFM experiment. Due to electrolyte diffusion from the pH/redox electrodes used, in all experiments a linear increase of K⁺ concentration in solution has been observed.

Mineral changes have been characterized at the end of the experiments by XRD. New crystalline phases of α -S₈, biothite and goethite have been identified in the pyrrhotite experiment; and clinocllore in the final FFM Äspö solid. Other solids are being characterized.

COMPLEXATION STUDY OF U(VI) WITH PHENOL BY TRLFS

C. Sabater¹, C. Walther², G. Geipel³, M. Grivé¹, L. Duro¹

¹Amphos21, Pg. Garcia i Fària 49-51, 08019 Barcelona, Spain,

²Karlsruhe Institute of Technology, Institute of Nuclear Waste Disposal, P.O. box 3640,
76021 Karlsruhe, Germany

³Helmholtz Zentrum Dresden-Rossendorf, Institute of Radiochemistry, P.O. box
510119, 01314 Dresden; Germany

Abstract

As part of long term safety assessment of nuclear repositories, geochemical modelling calculations simulating the reactions which may occur between the host rock and fluids must be performed. In some cases, these host rocks may contain appreciable amounts (~ 1-10 % by weight) of organic carbon under the form of natural organic matter (NOM), which is essentially represented by kerogen. The need of an appropriate knowledge of the thermodynamic properties of the organic ligands resulting from the kerogen degradation with radionuclides has lead to the selection of phenol as one of the Low Molecular Weight (LMW) organic ligands representative of those oxygenated aromatic-rich, type-III kerogen degradation products.

The aim of the present work is to investigate the complexation capacity of phenol with U(VI) at acidic and alkaline pH.

Preliminary data suggest that non-fluorescent U(VI)-phenol complex/es may be form under acidic conditions for phenol/U(VI) ratios higher than 1. At high pH, an extensive study will be required in order to understand the effect of deprotonated phenol in the complexation proces. Further work to be developed in the present study will involved the estimation of the stoichiometry as well as the calculation of the stability constants of the U(VI)-phenol complex/es formed at different pH conditions.

FORMATION OF Fe(III)-HYDROXO COMPLEXES IN BRINES

Tina Scharge, Barbara P. Bischofer, and Sven Hagemann

Gesellschaft für Anlagen und Reaktorsicherheit (GRS) mbH (GER)

Abstract:

UV-spectra of saline samples including Fe(III) and various concentrations of chloride were measured at different pH values for a better understanding of the iron speciation in saline solutions. Fe(III)-chloro complexes were investigated at pH=1 and various HCl, NaCl and MgCl₂ concentrations from 0.01 – 9.6 mol/l chloride. pH titrations were conducted for detecting Fe(III)-hydroxo complexes. These investigations were carried out in simple Fe(ClO₄)₃ solutions without disturbing chloride and also with high constant NaCl and MgCl₂ concentrations. All experiments were conducted at 25°, 40°, and 60°C. One objective of these measurements was the identification of single species spectra for Fe(III)-chloro, hydroxo and possible mixed chlorohydroxo complexes. This could contribute to the analysis of complex UV-spectra of Fe(III)-samples.

THE INTERACTION OF Fe(II) WITH CLAY MINERALS

D. Soltermann , M. Marques Fernandes, B. Baeyens, R. Dähn, M. H. Bradbury

Laboratory for Waste Management, Paul Scherrer Institute, CH-5232, Villigen,
Switzerland

Abstract

In the safety case for high-level radioactive waste repositories, redox phenomena play an important role in radionuclide retention. Virtually all deep underground repository concepts contain large amounts of iron, and reducing conditions will prevail in the long-term. The presence of high ferrous iron (Fe(II)) concentrations in the interstitial porewaters in the near- and far-fields could have a significant influence on the sorption behaviour of radionuclides.

The overall objective of this project is to investigate, in a combined macroscopic (wet chemistry) and microscopic (surface analysis) approach, the influence of reducing conditions on the characteristics of representative clay minerals, particularly with respect to radionuclide retention in the presence of high aqueous Fe(II) concentrations. In the macroscopic approach an electrochemical method will be used to investigate the sorption of Fe(II) under different reaction conditions and under controlled reducing potential. In the microscopic part, the effect of reducing conditions on the structural characteristics of selected clay minerals will be investigated using spectroscopic methods (XAS, Moessbauer spectroscopy).

PROGRESS IN THE DEVELOPMENT OF A FIBRE OPTICAL CHEMICAL SENSOR (FOCS) FOR THE SIMULTANEOUS DETERMINATION OF PROTON, OXYGEN AND CHLORIDE CONCENTRATIONS

Dörte Steinbrück, Elmar Schmäzlin and Michael U. Kumke

Institute of Chemistry, University of Potsdam (GER)

Abstract

Multiparameter fiber-optical chemical sensing (FOCS) for the detection of oxygen, pH, and chloride is developed. In the course of setting up a multiparameter sensing based on luminescence decay time measurements, the sensors and the instrumentation were further optimized for the single parameters.

With respect to the determination of oxygen a novel luminescence probe was implemented in the sensor and its performance as a fiber-based as well as based on polystyrene beads was characterized in detail for both systems. The novel dye has an improved dynamic range in decay time change (gain factor of 10!) compared to the probe used in the previously established oxygen sensor. In the development of multiparameter FOCS the determination of pH and chloride was investigated with emphasis on a time-resolved detection scheme using frequency phase modulation spectroscopy.



ISSN 1869-9669
ISBN 978-3-86644-756-1

